

# CANADIAN THESES ON MICROFICHE

# THÈSES CANADIENNES SUR MICROFICHE



National Library of Canada  
Collections Development Branch

Canadian Theses on  
Microfiche Service

Ottawa, Canada  
K1A 0N4

Bibliothèque nationale du Canada  
Direction du développement des collections

Service des thèses canadiennes  
sur microfiche

## NOTICE

The quality of this microfiche is heavily dependent upon the quality of the original thesis submitted for microfilming. Every effort has been made to ensure the highest quality of reproduction possible.

If pages are missing, contact the university which granted the degree.

Some pages may have indistinct print especially if the original pages were typed with a poor typewriter ribbon or if the university sent us an inferior photocopy.

Previously copyrighted materials (journal articles, published tests, etc.) are not filmed.

Reproduction in full or in part of this film is governed by the Canadian Copyright Act, R.S.C. 1970, c. C-30. Please read the authorization forms which accompany this thesis.

**THIS DISSERTATION  
HAS BEEN MICROFILMED  
EXACTLY AS RECEIVED**

## AVIS

La qualité de cette microfiche dépend grandement de la qualité de la thèse soumise au microfilmage. Nous avons tout fait pour assurer une qualité supérieure de reproduction.

S'il manque des pages, veuillez communiquer avec l'université qui a conféré le grade.

La qualité d'impression de certaines pages peut laisser à désirer, surtout si les pages originales ont été dactylographiées à l'aide d'un ruban usé ou si l'université nous a fait parvenir une photocopie de qualité inférieure.

Les documents qui font déjà l'objet d'un droit d'auteur (articles de revue, examens publiés, etc.) ne sont pas microfilmés.

La reproduction, même partielle, de ce microfilm est soumise à la Loi canadienne sur le droit d'auteur, SRC 1970, c. C-30. Veuillez prendre connaissance des formules d'autorisation qui accompagnent cette thèse.

**LA THÈSE A ÉTÉ  
MICROFILMÉE TELLE QUE  
NOUS L'AVONS REÇUE**

**Canada**

0-316-19407-3



National Library of Canada

Bibliothèque nationale du Canada

59

Canadian Theses Division

Division des thèses canadiennes

Ottawa, Canada  
K1A 0N4

67315

**PERMISSION TO MICROFILM — AUTORISATION DE MICROFILMER**

• Please print or type — Écrire en lettres moulées ou dactylographier.

Full Name of Author — Nom complet de l'auteur

Judith Grace Shelling

Date of Birth — Date de naissance

30 Nov 83

Country of Birth — Lieu de naissance

CANADA

Permanent Address — Résidence fixe

Box 25  
Chermainus, B.C.  
V0R 1K0

Title of Thesis — Titre de la thèse

The Calcium and Lanthanide Binding Properties  
of Peptides and Calcium Binding Proteins

University — Université

The U. of Alberta

Degree for which thesis was presented — Grade pour lequel cette thèse fut présentée

Ph.D

Year this degree conferred — Année d'obtention de ce grade

1984

Name of Supervisor — Nom du directeur de thèse

Dr. Brian D. Sykes

Permission is hereby granted to the NATIONAL LIBRARY OF CANADA to microfilm this thesis and to lend or sell copies of the film.

L'autorisation est, par la présente, accordée à la BIBLIOTHÈQUE NATIONALE DU CANADA de microfilmer cette thèse et de prêter ou de vendre des exemplaires du film.

The author reserves other publication rights, and neither the thesis nor extensive extracts from it may be printed or otherwise reproduced without the author's written permission.

L'auteur se réserve les autres droits de publication; ni la thèse ni de longs extraits de celle-ci ne doivent être imprimés ou autrement reproduits sans l'autorisation écrite de l'auteur.

Date

23 March 84

Signature

THE UNIVERSITY OF ALBERTA

The Calcium and Lanthanide Binding Properties of Peptides  
and Calcium Binding Proteins

by

Judith Grace Shelling



A THESIS

SUBMITTED TO THE FACULTY OF GRADUATE STUDIES AND RESEARCH  
IN PARTIAL FULFILMENT OF THE REQUIREMENTS FOR THE DEGREE  
OF Doctor of Philosophy

Department of Biochemistry

EDMONTON, ALBERTA

Spring, 1984

THE UNIVERSITY OF ALBERTA

RELEASE FORM

NAME OF AUTHOR Judith Grace Shelling  
TITLE OF THESIS The Calcium and Lanthanide Binding Properties of Peptides and Calcium Binding Proteins

DEGREE FOR WHICH THESIS WAS PRESENTED Doctor of Philosophy  
YEAR THIS DEGREE GRANTED Spring, 1984

Permission is hereby granted to THE UNIVERSITY OF ALBERTA LIBRARY to reproduce single copies of this thesis and to lend or sell such copies for private, scholarly or scientific research purposes only.

The author reserves other publication rights, and neither the thesis nor extensive extracts from it may be printed or otherwise reproduced without the author's written permission.

(SIGNED) ... *Judith Grace Shelling* .....

PERMANENT ADDRESS:

..... Box 25 .....

..... Chemainus, B. C. ....

..... V0R 1K0 .....

DATED ... 12 March ..... 1984

THE UNIVERSITY OF ALBERTA  
FACULTY OF GRADUATE STUDIES AND RESEARCH

The undersigned certify that they have read, and recommend to the Faculty of Graduate Studies and Research, for acceptance, a thesis entitled The Calcium and Lanthanide Binding Properties of Peptides and Calcium Binding Proteins submitted by Judith Grace Shelling in partial fulfilment of the requirements for the degree of Doctor of Philosophy.

..... *Brian D. Lyles* .....  
Supervisor

..... *Cyril M. Kay* .....  
..... *Dallas Rabe* .....  
..... *Robert Stodje* .....

..... *Robert G. Bryant* .....  
External Examiner

12 March 1984  
Date.....

Dedication

To my parents, Lou and Grace Shelling, for their constant encouragement and support,

and

to Matthew, who has waited so long because this was important to me;

I have never loved you more, and I can never thank you enough.

### Abstract

Proton nuclear magnetic resonance has been employed to study the binding of  $N^{\alpha}$ -Acetyl-L-aspartic acid and  $N^{\alpha}$ -Acetyl-L-aspartyl-L-glycyl-L-aspartylamide to the series of six lanthanide ions  $Dy^{3+}$  through  $Lu^{3+}$ . Values for the dissociation constants and the maximum lanthanide-induced shifts were obtained and the shifts were separated into contact and dipolar terms. The results indicate the contact shifts in  $^1H$  NMR are not always negligible, and that  $Yb^{3+}$  appears to be the best calcium analogue for structural studies which employ lanthanide-induced shifts.

The binding of  $Ca^{2+}$ ,  $La^{3+}$ ,  $Gd^{3+}$  and  $Yb^{3+}$  to the DTNB light chains of rabbit skeletal myosin was studied using far ultraviolet circular dichroism. The changes in ellipticity upon metal binding were different for all three lanthanides, with only lanthanum displaying an effect which was similar to that shown by calcium.

The effect of  $Ca^{2+}$  binding on the proton nuclear magnetic resonance spectrum of brain specific S100b calcium binding protein has been examined at two pH values, 8.5 and 7.5. At pH 8.5, S100b protein binds two  $Ca^{2+}$  per monomer with  $K_d$  values of  $6 \times 10^{-5}$  M and  $2 \times 10^{-4}$  M, whereas at pH 7.5 the protein binds only one  $Ca^{2+}$  per monomer with  $K_d$   $2 \times 10^{-4}$  M. In the absence of  $Ca^{2+}$ , S100b undergoes a conformational change when the protein is titrated from pH 8.6 to 6.0. Addition of  $Ca^{2+}$  perturbed the environment of tyrosine

and phenylalanine residues, and studies at alkaline pH and high temperatures suggest that the protein is more stable in the presence of  $\text{Ca}^{2+}$ . The single tyrosine residue in the protein ionizes only after the protein is denatured by exposure to high pH.

Proton nuclear magnetic resonance has been employed to study the environment of several proton nuclei (primarily those arising from aromatic residues) of the porcine intestinal calcium binding protein. An assignment for the single tyrosine (tyr 16) residue has been made on the basis of laser photochemical induced dynamic nuclear polarization (CIDNP) and homonuclear decoupling experiments. pH titration studies have shown that the tyrosine  $\text{pK}_a$  is unusually high in the apo protein, and increases even further upon the addition of calcium. The observation of a CIDNP effect with this single tyrosine in both the presence and absence of calcium indicates that this tyrosine is solvent accessible and therefore exposed on the surface of the molecule. The protein was  $K_{d1} = K_{d2} = 1 \times 10^{-7}$  M. In the presence of calcium, the protein was observed to bind one mole equivalent of ytterbium with a  $K_d\text{-Yb}^{3+}/K_d\text{-Ca}^{2+} \leq 0.18$ , and the lanthanide-induced shifts were very broad at room temperature. The observed effects of increasing temperature and KCl concentration upon the LIS supports the proposal that these resonances were broadened due to their close proximity to the ytterbium ion in the metal binding sites of ICaBP. Two mole equivalents of lutetium bound to the apo protein in a



sequential manner, with  $K_{d1} \leq 10^{-6}$  M and  $K_{d2} = 2 \times 10^{-6}$  M. The binding of the second  $\text{Lu}^{3+}$  equivalent had little effect on the proton-nuclear magnetic resonance spectrum; and the presence of excess  $\text{Lu}^{3+}$  resulted in aggregation.

### Acknowledgments

I cannot begin to express my gratitude to my supervisor, Dr. B. D. Sykes, who spent many evenings and mornings pouring over my spectral results, derivations, manuscripts, and this thesis, and who was always ready to lend a helping hand with instrumental problems and in the determination of appropriate experimental conditions. He was a constant source of inspiration, ideas, foresight, understanding, and enthusiasm, and he was an indispensable aide in writing this thesis.

Also many thanks to Dr. C. M. Kay, Dr. R. S. Hodges, and Dr. T. Hofmann for their constant moral and scientific support and helpful insights into my research. Many thanks in this area also go out to Dr. R. Mani, J. O'Neil, Dr. D. Scraba, Dr. M. James, Dr. W. Bridger, and Dr. J. Takats.

I can't begin to thank all of the members in my lab group who have helped in my tenure here; Heather Dettman, John Shriver, Brian Edwards, Lana Lee, Fred Brauer, Jean-Robert Brisson, John Baldo, Gillian Henry, Tom Williams, and David Corson. Special thanks to Gerry McQuaid for maintaining the 270 MHz NMR spectrometer and for increasing my knowledge of excellent literature, and to Heather Dettman for organizing those wonderful hiking and skiing trips to the mountains, which were a welcome diversion from weekends in the lab. Because of my encounters with these people, I finally learned how to cook, and I'll never forget all of

those wonderful cooperative dinners!

There is also many thanks to the supportive graduate students and post doctoral fellows with whom I have had enlightening discussions about scientific and other subjects; Jean Gariépy, Tania Watts, Paul Cachia, Robert Devine, Murray Ratcliffe, Ole Hindsgaul, Max Hincke, Tanya Watts, Brian McDonough, Fran Legget, Janice McDonald, Irene Fecycz, and the many others. Special thanks to Clive Sanders and Ruthven Lewis for their constant support and encouragement throughout my graduate career.

We are indebted to Dr. W. D. McCubbin, K. Oikawa, Dr. W. Anderson, D. Bacon, Dr. J. Pearlstone, and Dr. M. Hincke for helpful discussions. The crystal structure of the porcine ICaBP was plotted with the help of Mr. R. Reed and Mr. M. Fuginaga, who were both helpful and informative. Many thanks to Perry d'Obrenan for an excellent job on many of the figures contained in this thesis and for those used for publications. We also thank the following people for competent technical assistance: K. Oikawa for the CD spectra, M. Natriss for amino acid analysis, and Dr. R. Audette (Alberta Agriculture Toxicology Laboratory) for atomic absorption spectrophotometric results. The porcine ICaBP was prepared by Ms. M. Kawakami and Mr. J. D. J. O'Neil and our collaboration was made more fruitful through our discussions with both J. O'Neil and Dr. T. Hofmann. The bovine brain S100b protein was isolated by Dr. R. S. Mani and this

collaboration was enriched by discussions with Dr. R. S. Mani and Dr. C. M. Kay. The synthesis of Ac-DGD-amide was carried out by Ms. Michelle Bjornson, Dr. A. Taneja, and Dr. R. Reid. Discussions with these three people, and with Dr. R. S. Hodges, aided greatly in the results achieved in this collaboration. A special thankyou to Michelle Bjornson who, as a summer student in our lab, managed to produce excellent results for the Ac-DGD-amide titrations with a minimal amount of previous experience and a maximal amount of enthusiasm, despite my supervision!

My work was supported by the Medical Research Council of Canada Group on Protein Structure and Function, The University of Alberta in the form of a Fellowship and a Teaching Assistantship, and the Alberta Heritage Fund for Medical Research in the form of a Studentship.

## List of Abbreviations and Symbols

Ac-Asp	N <sup>α</sup> -Acetyl-L-aspartic acid
Ac-DGD-amide	N <sup>α</sup> -Acetyl-L-aspartyl-L-glycyl-L-aspartyl-L-amide
ADP	adenosine diphosphate
ATP	adenosine triphosphate
ATPase	adenosine triphosphatase
ave	average
calm	calmodulin
CaBP	calcium binding protein(s)
CIDNP	laser photochemical induced dynamic nuclear polarization
cm	centimeters
CD	circular dichroism
DEAE	diethyl aminoethyl
deg	degree(s)
dmole	decimole
DSS	sodium 2,2-dimethyl-2-silapentane-5-sulfonate
DTNB	5,5'-dithiobis-(2-nitrobenzoic acid)
EDTA	ethylenediaminetetraacetic acid
ESR	electron spin resonance
FMN	flavin mononucleotide
<sup>1</sup> H	proton
H <sub>0</sub>	external magnetic field
Hz	hertz, or cycles·sec <sup>-1</sup>

MHz	megahertz
HMM	heavy meromyosin
ICaBP	intestinal calcium binding protein
[L] <sub>0</sub>	the total ligand concentration.
LC	light chain
LIS	lanthanide-induced shift(s)
LMM	light meromyosin
LSR	lanthanide-shifted resonance(s)
[M] <sub>0</sub>	the total metal ion concentration
NES	(2[N-Morpholino]ethane) sulfonic acid
ml	millilitre
mM	millimolar
MOPS	3-(N-morpholino)propanesulfonic acid
MRW	mean residue weight
nm	nanometres
nmoles	nanomoles
N	Avagadro's number
NMR	nuclear magnetic resonance
parv	parvalbumin
Pi	inorganic phosphate
pCa	$-\log[Ca^{2+}]$
pH	$-\log[H^+]$
pD	pH observed in D <sub>2</sub> O or deuterated buffer
ppm	parts per million

PAGE	polyacrylamide gel electrophoresis
Pipes	piperazine-N,N'-bis[2-ethane sulfonic acid]
rf	radio frequency
Rf	(the distance travelled by a protein sample on SDS PAGE)/(the distance travelled by the tracer dye in the same sample)
SDS	sodium dodecyl sulphate
sec	second(s)
S1	heavy meromyosin subfragment one
S100b	bovine brain S100b protein
S2	heavy meromyosin subfragment two
STI	soybean trypsin inhibitor
Tm	tropomyosin
cTm	cardiac tropomyosin
Tn	troponin
TnC	troponin C
Tris	tris(hydroxymethyl)aminomethane
$\mu$ l	microlitre
$\mu$ M	micromolar
UV	ultraviolet
kDalton	kilodalton
$\delta$	chemical shift in ppm
$\tau_R$	rotational correlation (tumbling) time
$\tau_s$	electron correlation time
$T_{1\rho}$	electron spin relaxation time
$\nu$	frequency

$\nu_M$	frequency in the absence of a metal ion
$\Delta$	frequency in the presence of a metal ion
$\nu^{dia}$	frequency difference
$\nu^{para}$	frequency in the presence of a diamagnetic metal ion
$\lambda$	frequency in the presence of a paramagnetic metal ion
$\mu_p$	wavelength in nanometres
$\chi$	paramagnetic moment
$\Delta_m^{d,i}$	magnetic susceptibility per molecule
$\Delta_m^{c,i}$	the dipolar shift of nucleus $i$ in the presence of lanthanide $m$
$\Delta_m^{obs,i}$	the contact shift of nucleus $i$ in the presence of lanthanide $m$
$r_{im}$	$\nu^{para} - \nu^{dia}$
	the distance between nucleus $i$ and the metal ion $m$ .



# Table of Contents

Chapter	Page
I. INTRODUCTION .....	1
A. The Homologous Calcium Binding Sites of Carp Muscle Parvalbumin and the Calcium Binding Proteins. ....	1
B. The <sup>1</sup> H NMR spectra of Calcium Binding Proteins in the Presence and Absence of Metal Ions .....	13
C. The History and Objectives of This Project ....	15
II. NMR THEORY AND METHODOLOGY .....	22
A. The Magnetic Properties of Chemical Substances .....	22
Diamagnetism .....	22
Paramagnetism .....	22
Magnetic Susceptibility .....	23
B. The General Properties of the Lanthanides and Their Usefulness as Structural Probes .....	24
The Chemistry of the Lanthanides .....	24
Lanthanide Ions as Calcium Probes .....	28
NMR Studies of Lanthanide Complexes .....	28
Diamagnetic Shifts .....	31
Lanthanide Induced Shifts .....	31
C. Chemical Exchange .....	39
Slow Exchange Limit .....	43
Fast Exchange Limit .....	43
The Effect of Chemical Exchange on the NMR Spectrum .....	44
D. Laser Photochemical Induced Dynamic Nuclear Polarization - CIDNP .....	44
E. Spin Decoupling .....	46

III. EXPERIMENTAL PROCEDURES .....	48
A. Minimization of Metal Ion Contamination .....	48
Preparation of Plasticized Glassware .....	48
Dithizone Treatment .....	48
Chelex Treatment .....	49
B. Preparation of the Proteins and Peptides .....	49
Preparation of the Peptides .....	49
Preparation of the DTNB Light Chains of Rabbit Skeletal Muscle .....	50
Preparation of Bovine Brain S100b .....	51
Preparation of Porcine Intestinal Calcium Binding Protein .....	51
C. Preparation of Stock Metal Ion Solutions .....	53
Calcium Stock Solutions .....	53
Lanthanide Stock Solutions .....	54
D. The Determination of $Ca^{+2}$ and Lanthanide Con- centrations .....	57
Calcium Titrations .....	57
Lanthanide Titrations .....	57
E. pH Measurements .....	57
F. Amino Acid Analysis .....	58
G. SDS Polyacrylamide Gel Electrophoresis .....	59
H. Ultraviolet Spectrophotometry .....	60
I. Circular Dichroism .....	61
Sample Preparation .....	61
Data Acquisition Parameters .....	61
J. Nuclear Magnetic Resonance .....	62
Sample Preparation .....	62

Acquisition Parameters .....	66
K. Calculations and Theoretical Determinations ...	68
Determination of $\alpha$ -Helix; $\beta$ -Sheet, and $\beta$ - Turn Content for Rabbit Skeletal DTNB, Light Chain .....	68
L. Laser Photochemical Induced Dynamic Nuclear Polarization - CIDNP .....	69
IV. CONTACT AND DIPOLAR CONTRIBUTIONS TO LANTHANIDE INDUCED NMR SHIFTS OF AMINO ACID AND PEPTIDE MODELS FOR CALCIUM BINDING SITES IN PROTEINS .....	71
A. Introduction .....	71
B. Theory .....	73
C. Results .....	75
D. Discussion .....	83
E. Conclusions .....	96
V. THE INTERACTION OF THE DTNB LIGHT CHAIN OF RABBIT SKELETAL MYOSIN WITH LANTHANIDE IONS .....	98
A. Introduction .....	98
B. Results .....	112
C. Discussion .....	121
VI. <sup>1</sup> H NUCLEAR MAGNETIC RESONANCE STUDIES OF BOVINE BRAIN S100b PROTEIN .....	126
A. Introduction .....	126
B. Results .....	134
C. Discussion .....	152
VII. <sup>1</sup> H NUCLEAR MAGNETIC RESONANCE STUDIES OF PORCINE INTESTINAL CALCIUM BINDING PROTEIN: TYROSINE RESONANCE ASSIGNMENTS .....	157
A. Introduction .....	157
B. Results .....	159
C. Discussion .....	175

VIII. THE DETERMINATION OF THE  $K_d$  OF PORCINE iCaBP FOR CALCIUM IN THE PRESENCE OF EDTA AND ANALYSIS OF THE RESULTS TO DETERMINE IF THE  $Ca^{2+}$  SITES ARE COOPERATIVE .....182

    A. Introduction .....182

    B. Results .....186

    C. Discussion .....197

IX.  $^1H$  NUCLEAR MAGNETIC RESONANCE STUDIES OF THE INTERACTION OF LANTHANIDE IONS WITH PORCINE INTESTINAL CALCIUM BINDING PROTEIN .....198

    A. Introduction .....198

    B. Results .....201

    C. Discussion .....220

CONCLUDING DISCUSSION .....225

    A. Highlights of the Studies on CaBP and Peptides .....225

    B. Possible Future Studies .....227

BIBLIOGRAPHY .....231

## List of Tables

Table		Page
I.1	One and Three letter Symbols for The Amino Acids.....	7
I.2	The Dissociation Constants and $Ca^{+2}/Mg^{+2}$ Specificities of The Representative Calcium Binding Proteins.....	12
II.1	Electronic Configuration and Effective Ionic Radii for $Y^{+3}$ , $Ca^{+2}$ , and the Tri-positive Lanthanide Ions.....	26
IV.1	The Contact and Dipolar Shift Parameters for the Analysis of LIS.....	76
IV.2	The $\Delta_m^{obs.1}$ and $K_s$ Parameters for the Peptides.....	78
IV.3	Calculated Values for the Slopes and Intercepts of the Plots of $\Delta_m^{obs.1}/\langle S_z \rangle_m$ versus $D_{1m}/\langle S_z \rangle_m$ .....	84
IV.4	The Calculated Contact and Dipolar Values for Ac-Asp.....	85
IV.5	The Calculated Contact and Dipolar Values for the LM Species of Ac-DGD-amide.....	86
IV.6	The Calculated Contact and Dipolar Values for the LM <sub>2</sub> Species of Ac-DGD-amide.....	87
V.1	Amino acid analysis of the isolated DTNB LC.....	113
IX.1	The Chemical Shift Values of the Lanthanide-Shifted Resonances of $Yb^{+3}$ -Substituted Porcine ICaBP as a Function of Temperature.....	210
IX.2	The Observed Linewidths and Calculated Distances for the LSR of $Yb^{+3}$ -substituted Porcine ICaBP.....	211

## List of Figures

Figure		Page
I.1	An $\alpha$ -carbon stereo drawing of the X-ray crystal structure of carp parvalbumin.....	4
I.2	Two and three dimensional representations of a model calcium binding site.....	5
I.3	Representative amino acid sequences from the six families of proteins containing the EF hand structure.....	8
I.4	A 270 MHz $^1\text{H}$ NMR spectrum of porcine ICaBP showing both the commonly occurring and upfield-shifted chemical shifts of the aromatic and methyl residues.....	14
II.1	The qualitative picture of the effect of magnetic anisotropy on the internal field experienced by nucleus $j$ near the principal axis of the susceptibility tensor.....	34
II.2	The three values $r$ , $\theta$ and $\phi$ define the spherical coordinates of nucleus $j$ in the principle axis system of the magnetic susceptibility tensor of a paramagnetic ion.....	37
II.3	Contour maps of the dipolar shifts of $\text{Yb}(\text{HBPz}_3)_3$ and of $\text{Yb}^{3+}$ bound to the EF site of carp parvalbumin.....	40
II.4	Theoretical spectra for slow, intermediate, and fast exchange.....	42
IV.1	The spectra of $\text{N}^{\alpha}$ -Ac-Asp in the absence and presence of $\text{Er}^{3+}$ .....	79
IV.2	Plots of the absolute values of $(\delta_{\text{obs}} - \delta_0)$ vs $[\text{M}]_0/[\text{L}]_0$ for the $\alpha\text{CH}$ proton of Ac-asp with $\text{Yb}^{3+}$ and for the $\beta\text{B}$ protons of Ac-DGD-amide with $\text{Dy}^{3+}$ .....	80
IV.3	Plots of $\Delta_m^{\text{obs}}/ \langle S_z \rangle_m$ vs $D_{1m}/ \langle S_z \rangle_m$ for the four observable $^1\text{H}$ NMR resonances of Ac-Asp.....	82
IV.4	Plots of $\Delta_m^{\text{obs}}/ \langle S_z \rangle_m$ vs $D_{1m}/ \langle S_z \rangle_m$ for the four observable $^1\text{H}$ NMR resonances of the LM species of Ac-DGD-amide.....	88

Figure		Page
IV.5	Plots of $\Delta_m^{obs.}/\langle S_z \rangle_m$ VS $D_m/\langle S_z \rangle_m$ for the four observable $^1H$ NMR resonances of the $LM_2$ species of Ac-DGD-amide.....	89
V.1	Schematic diagram of a myosin molecule and the subfragments resulting from the enzymatic cleavage of myosin.....	100
V.2	Proposed mechanism for the generation of force by the interaction of the S1 units of a myosin filament with the actin filament.....	101
V.3	A Plot of $10^{-3}$ x molecular weight VS Rf for one of the SDS gels of the DTNB LC, using cTm, STI, and lysozyme as standards.....	114
V.4	The UV spectrum of the DTNB LC.....	115
V.5	A Plot of $10^{-4}$ x $[\theta]$ in $deg \cdot cm^2 \cdot dmole^{-1}$ VS wavelength in nanometers for the DTNB LC.....	116
V.6	A plot of $10^{-3}$ x $[\theta]$ in $deg \cdot cm^2 \cdot dmole^{-1}$ VS pCa for the $Ca^{+2}$ titration of the DTNB LC.....	118
V.7	$^1H$ NMR spectra of the apo- and $Ca^{+2}$ -saturated forms of the DTNB LC.....	120
VI.1	The UV spectrum of S100b in 0.1M Tris-HCl, pH 7.5.....	132
VI.2	The complete 270 MHz $^1H$ NMR spectra of apo- and calcium-saturated S100b at pH 7.5.....	135
VI.3	Titration of apo S100b with calcium at pH 7.5, followed by the addition of KCl.....	137
VI.4	The plot of the intensity of the 7.33 ppm phenylalanine resonance at pH 7.5 as a function of $[Ca^{+2}]_0/[S100b]_0$ .....	139
VI.5	Titration of apo S100b with KCl at pH 7.5, followed by the addition of calcium.....	140
VI.6	The pH titration of the histidine residues of apo S100b.....	141

Figure		Page
VI.7	The plot of the chemical shift of two of the histidine resonances of apo S100b as a function of increasing pH.....	143
VI.8	The pH titration of the histidine residues of calcium-saturated S100b.....	144
VI.9	The plot of the chemical shift of two of the histidine resonances of calcium-saturated S100b as a function of increasing pH.....	146
VI.10	Titration of apo S100b with calcium at pH 8.23.....	147
VI.11	The plot of the intensity of the phenylalanine resonance at 7.35 ppm at pH 8.23 as a function of $[Ca^{+2}]_0/[S100b]_0$ .....	148
VI.12	The alkaline pH titration of S100b in the absence of calcium.....	149
VI.13	The alkaline pH titration of S100b in the presence of calcium.....	150
VII.1	A protein backbone stereo drawing of the X-ray crystal structure of the minor A form of bovine ICaBP.....	158
VII.2	The UV spectrum of porcine ICaBP.....	160
VII.3	The complete 270 MHz $^1H$ -NMR spectrum of the apo ICaBP.....	161
VII.4	$^1H$ NMR laser photo CIDNP spectra for apo and calcium-saturated ICaBP.....	163
VII.5	$^1H$ NMR homonuclear decoupling spectra for apo and calcium-saturated ICaBP.....	165
VII.6	The pH titration of ICaBP in the presence of excess EDTA.....	167
VII.7	The plot of chemical shift of the phenylalanine and tyrosine resonances of apo porcine ICaBP as a function of increasing pH.....	168
VII.8	The pH titration of ICaBP in the presence of excess calcium.....	169



Figure	Page
VII.9	The titration of apo porcine ICaBP with $\text{Ca}^{2+}$ .....171
VII.10	A plot of the intensity of the 7.16 ppm resonance of phenylalanine as a function of $[\text{Ca}^{2+}]_0/[\text{ICaBP}]_0$ .....172
VII.11	The CD spectra of ICaBP in the presence of excess EDTA and $\text{Ca}^{2+}$ .....174
VIII.1	A plot of the area under the 2.54 ppm resonance of EDTA vs $[\text{Ca}^{2+}]_0/[\text{EDTA}]_0$ .....183
VIII.2	The complete 270 MHz spectrum of EDTA in the presence of calcium.....187
VIII.3	The titration of porcine ICaBP with $\text{Ca}^{2+}$ in the presence of EDTA.....189
VIII.4	A plot of $[\text{A}_c^{\text{max}}/\text{A}_c^{\text{obs}}] - 1$ vs $[\text{A}_p^{\text{max}}/\text{A}_p^{\text{obs}}] - 1$ for the titration of ICaBP in the presence of EDTA.....192
VIII.5	The plot of $\log [(\text{A}_c^{\text{max}}/\text{A}_c^{\text{obs}}) - 1]$ vs $\log [(\text{A}_p^{\text{max}}/\text{A}_p^{\text{obs}}) - 1]$ for the titration of porcine ICaBP with calcium in the presence of EDTA.....194
IX.1	The complete 270 MHz $^1\text{H}$ NMR spectra of initially $\text{Ca}^{2+}$ -saturated porcine ICaBP in the presence of excess $\text{Yb}^{3+}$ .....202
IX.2	The titration of $\text{Yb}^{3+}$ -substituted ICaBP with KCl.....205
IX.3	The effect of increasing temperature on the LIS of $\text{Yb}^{3+}$ -substituted porcine ICaBP.....208
IX.4	A plot of the chemical shift of the lanthanide-shifted resonances of calcium-substituted porcine ICaBP as a function of $1/T^3$ .....212
IX.5	The titration of $\text{Ca}^{2+}$ -saturated ICaBP with $\text{Yb}^{3+}$ .....214
IX.6	The plot of the intensity of the lanthanide-shifted resonance at 19.9 ppm vs $[\text{Yb}^{3+}]_0/[\text{Ca}^{2+}\text{-saturated ICaBP}]_0$ .....216
IX.7	The titration of apo ICaBP with $\text{Lu}^{3+}$ .....217

Figure		Page
IX.8	A plot of the intensity of the resonance at 7.17 ppm resonance of phenylalanine as a function of $[Lu^{3+}]_0/[ICaBP]_0$ .....	218
IX.9	A plot of the change in area under the phenylalanine resonance at 7.01 ppm versus $[Lu^{3+}]_0/[ICaBP]_0$ .....	219

## I. INTRODUCTION

### A. The Homologous Calcium Binding Sites of Carp Muscle Parvalbumin and the Calcium Binding Proteins.

Calcium plays a dominant role in the control of many biological processes (1,2). There are close to 100 proteins which have one or more calcium binding sites and the effect that calcium binding exerts on these proteins is specific to the type of protein involved (1). The calcium binding proteins have been loosely divided into the following five classes (3);

- 1) Enzymes which bind calcium in their active site such that the metal ion is directly involved in catalysis,
- 2) Enzymes which are activated by the addition of calcium ions,
- 3) Proteins which modulate the activity of other proteins and enzymes via calcium binding,
- 4) Proteins which employ  $\gamma$ -carboxy-glutamic acid in  $\text{Ca}^{2+}$  coordination, and
- 5) Proteins which bind calcium rather specifically, but for which a physiological function has not been determined.

X-ray crystallographic studies of the calcium binding proteins (CaBP) thermolysin (4), carp parvalbumin (5), bovine  $\beta$ -trypsin (6), bovine pancreatic phospholipase  $\text{A}_2$  (7), and porcine intestinal calcium binding protein (iCaBP) (8)

have been carried out and published in the literature. The structures of these proteins, despite their varied biological functions, have several common features (3,9):

- 1) Only oxygen atoms were observed to be coordinated to the metal ion;
- 2) These liganding oxygens were contributed by either the carboxylic acid side chains of aspartic acid and glutamic acid residues, the non-ionic side chains of asparagine and glutamine residues, the hydroxyl groups of serine and threonine, peptide backbone carbonyl groups, or bound water molecules;
- 3) The preferred coordination number was 6, with the ligands in the binding site adopting an octahedral geometry around the cation.

The discussions and experiments presented in the following text will centre on proteins from classes 3 and 5. Class 3 encompasses the so-called "modulator" proteins as they modulate the activity of other proteins and enzymes. The best known examples of this class are troponin C (TnC) and calmodulin, and some of their properties and characteristics will be presented, although no experimental work was done on these systems directly. The discussion of class 5 proteins will include carp parvalbumin, the DTNB light chain of rabbit skeletal muscle (DTNB LC), porcine intestinal calcium binding protein (ICaBP), and bovine brain S100b (S100b), with all but parvalbumin being directly studied in

this project.

The determinations of the primary sequence (10) and the X-ray crystal structure (11), (Figure I.1) of carp parvalbumin permitted a detailed analysis of its two calcium binding sites. Parvalbumin has six  $\alpha$ -helices which are labelled *A* through *F*. Both calcium binding sites are homologous in their sequence and in their three dimensional structures. Each binding site is composed of a linear sequence of 30 to 35 amino acids. They can be visually described as having a *helix-loop-helix* arrangement where two helices flank a 12 residue calcium binding loop, as shown in Figure I.2A. In parvalbumin, the two pairs of helices involved are the CD and EF helices, where the N- and C-terminal  $\alpha$ -helical regions are approximately perpendicular to each other. The orientation of these two helices about the binding site can be represented by the index and thumb of the right hand, as shown in Figure I.2B. Kretsinger and Nockolds (11) suggested the term *EF hand* to depict these sites, arising from the structure of the second calcium binding site of carp parvalbumin, which is flanked by helices *E* and *F*.

Many proteins (1, 13-15), collectively referred to as calcium binding proteins (CaBP), have one or more metal binding sites which are homologous to the CD and EF calcium binding sites of carp muscle parvalbumin. At the present time, six families of EF hand proteins have been established; parvalbumins, TnC's, calmodulins, myosin light

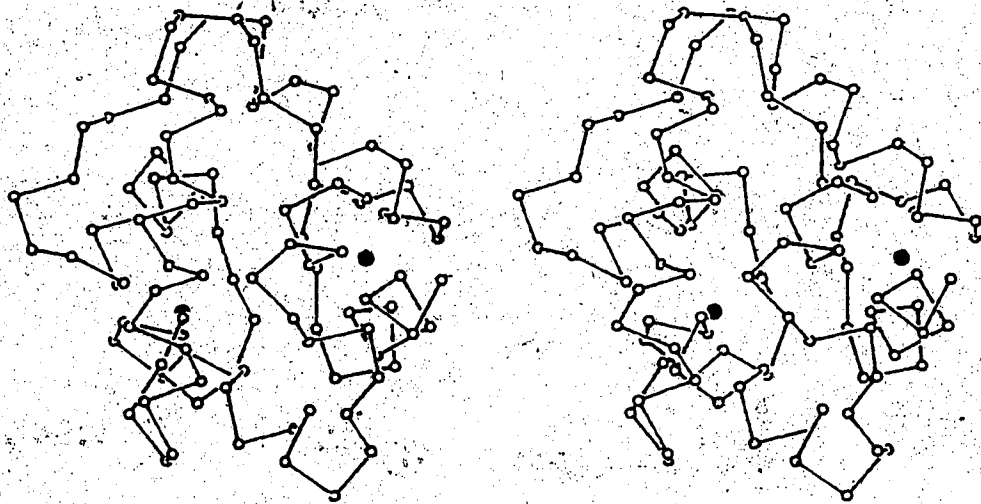


Figure 1.1 An  $\alpha$ -carbon stereo drawing of the X-ray crystal structure of carp parvalbumin,  $pI = 4.25$ . The CD calcium binding domain (shown on the left side of the stereodrawing) consists of the C helix, the CD calcium binding loop, and the D helix. The EF calcium binding domain (shown on the right side of the stereodrawing) consists of the E helix, the EF calcium binding loop, and the F helix. Atomic coordinates available from the Brookhaven Protein Data Bank were used to prepare this figure, which was taken from Reference 12 (Figure 2) with permission.

B

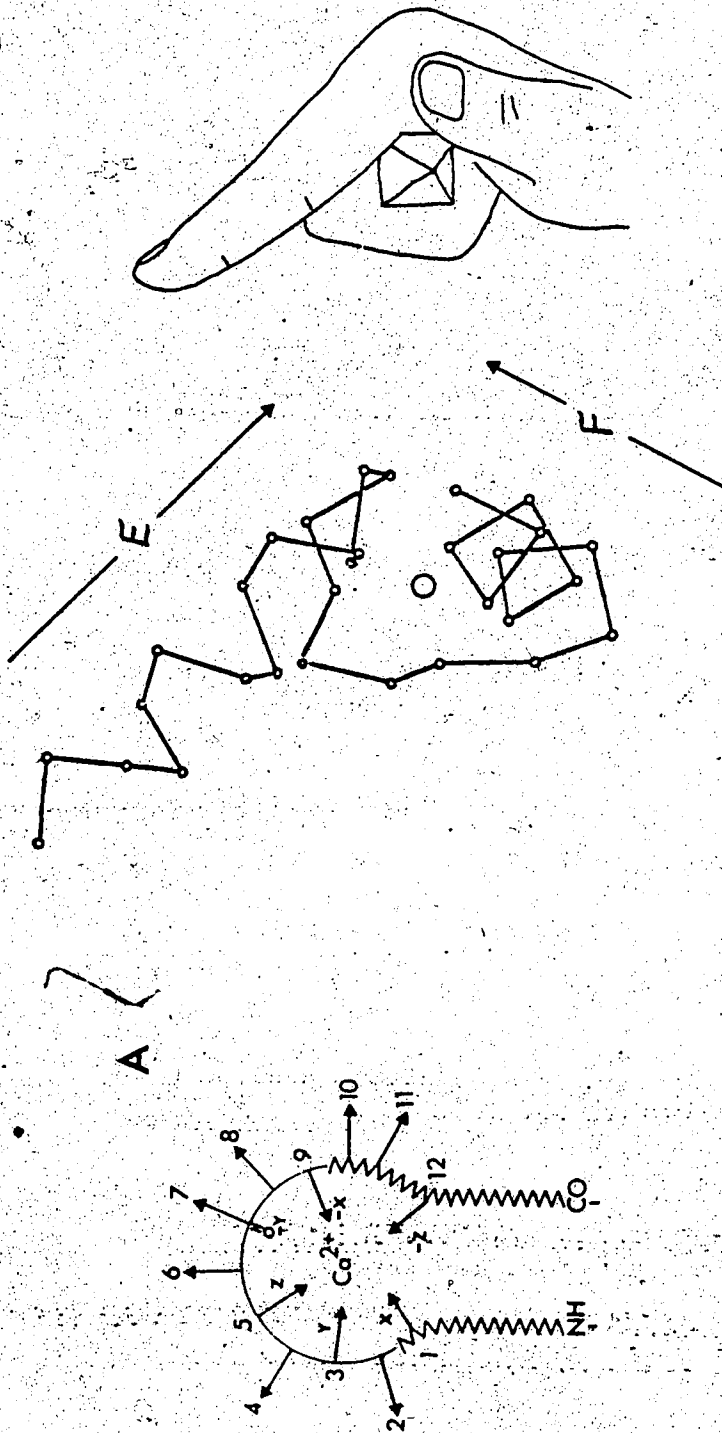


Figure 1.2 Two and Three Dimensional Representations of a Model Calcium Binding Site.  
A. A two dimensional representation of a helix-loop-helix site. The jagged lines indicate the N- and C-terminal helical region; taken from Reference 9, Figure 1.10A, with permission.  
B. A three dimensional representation of the EF hand of carp parvalbumin. It consists of three elements: the E alpha helix which is represented by the right forefinger; the EF calcium binding loop, which is represented by the curled middle finger; and the F alpha helix, which is represented by the thumb. The arrows indicate the direction of the carboxyl terminus of the protein. This figure was taken from Reference 12 (Figure 3) with permission, and was originally adapted from reference 10.

chains, intestinal calcium binding proteins, and the brain specific S100 proteins (16). In all of these proteins the metal binding loop is wrapped around the  $Ca^{2+}$  ion in such a way that the ligand sites are filled in the order X, Y, Z, -Y, -X, -Z. The -Y ligand in such sites is always a carbonyl oxygen from the protein backbone, whereas all of the other ligands are amino acid side chains or water molecules (1,17). It is obvious that the arrangement of the coordinating ligands provides for a regular and easily recognizable amino acid sequence and Figure I.3 shows some representative examples of these sequences, the sources of these sequences were carp parvalbumin (4.25 isozyme), (10); rabbit skeletal TnC, (18); porcine ICaBP, (19); skeletal DTNB light chain, (18,14); bovine brain calmodulin, (20); bovine brain S100b, (21). The single letter amino acid symbols have been tabulated in Table I.1. The homologous binding site regions of these molecules will hereafter be distinguished in the text on the basis of their alignment with skeletal TnC. In this system the calcium binding sites of TnC are numbered in sequence as I, II, III, and IV, starting from the N-terminus. The six proteins contained in Figure I.3, and the numbers of their functional binding sites are carp parvalbumin (III,IV), rabbit skeletal TnC (I-IV), porcine intestinal calcium binding protein (III,IV), bovine brain calmodulin (I-IV), rabbit skeletal DTNB LC (I) and bovine brain S100b (III,IV). The properties of these different proteins can vary according to the species and/or tissue type from which



Table I.1

One and Three Letter Symbols for The Amino Acids

One Letter Symbol	Amino Acid	Three Letter Symbol
A	alanine	ala
B	asn + asp	asx
C	cysteine	cys
D	aspartic acid	asp
E	glutamic acid	glu
F	phenylalanine	phe
G	glycine	gly
H	histidine	his
I	isoleucine	ile
K	lysine	lys
L	leucine	leu
M	methionine	met
N	asparagine	asn
P	proline	pro
Q	glutamine	glu
R	arginine	arg
S	serine	ser
T	threonine	thr
V	valine	val
W	tryptophan	trp
Y	tyrosine	tyr
Z	gln + glu	glx

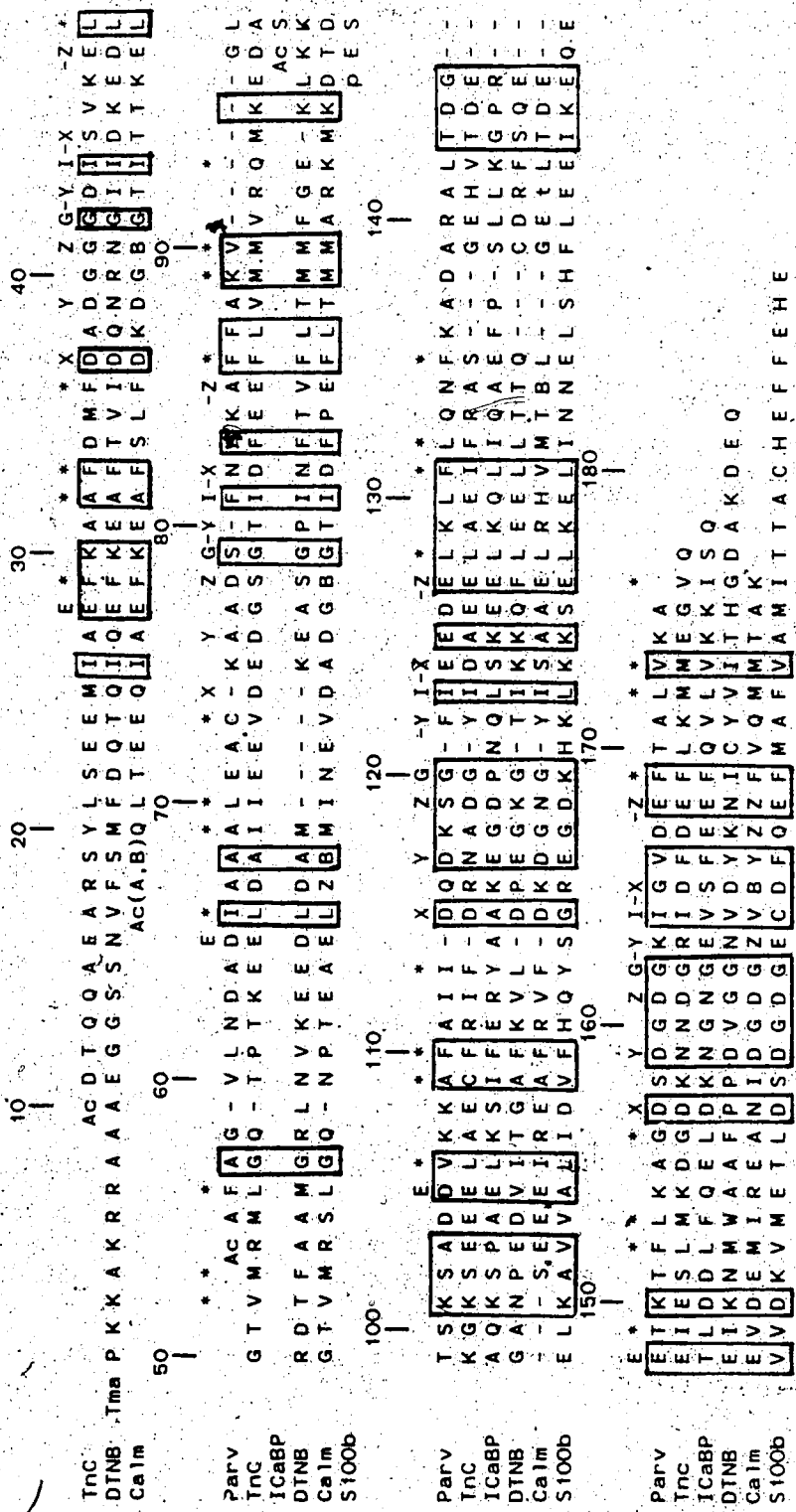


Figure 1.3 Representative Amino Acid Sequences from the Six Families of Proteins containing the EF Hand Structure. The sequences are aligned by the correspondence of their helix-loop-helix regions to those of skeletal Tnc. The two Ca<sup>2+</sup> binding sites of S100b and ICaBP were aligned arbitrarily with site III and IV of Tnc. The letters in the EF hand "test sequence" X, Y, Z, -Y, -X, and -Z refer to the vertices of the calcium coordination octahedron. All of these vertices in the EF hand of parvalbumin have oxygen atoms (D, N, E, Q, S, T) as a calcium ligand except -Y whose vertex is provided by a backbone carbonyl. The symbol ' corresponds to a hydrophobic (L, I, V, F, M) residue in the EF hand. The boxed areas indicate where the alignment shown has resulted in three or more homologous amino acid residues. The position of the deletion in the sequence of ICaBP at residue position 138 is arbitrary and varies according to the reference used; the sequence references are given in the text and the labelling method is a modification of that used in Reference 22. Other symbols employed are: tma, trimethyl alanine; t, trimethyl lysine; p, pyroglutamic acid. The sequence numbers are arbitrary.

they are isolated, so the following text will confine itself to the sources specified above, unless otherwise stated.

The existence of these proteins and their highly homologous binding sites can be explained by their evolution from an ancestral gene which coded for a 40 amino acid long Ca<sup>2+</sup> binding domain (16,23). It is thought that this domain underwent two successive gene duplications to produce a four domain protein where domain I was genetically closer to domain III, and II to IV. Gene deletions and mutations are thought to have led to proteins with altered EF hands such as (9)(Figure 1.3):

- 1) defunct and deleted sites in the DTNB LC (III,IV) and parvalbumin (II);
- 2) distorted sites through insertion or deletion of residues as in the case of the DTNB LC (II), S100b (III), and ICaBP (III);
- 3) substitutions generating high affinity Ca<sup>2+</sup> binding sites such as sites III and IV of TnC and the CD (III) and EF (IV) sites of parvalbumin.

Due to the importance of the EF hand arrangement in determining the calcium binding sites of these proteins, many studies have tried to clarify the high calcium affinity of this structural arrangement. Three contributing factors have been identified to date (3, and references therein).

- 1) Numerous studies with proteolytic, chemically cleaved, and synthetic peptides which represented

parts of either parvalbumin, skeletal TnC, or calmodulin have indicated that the placement of amino acids according to the right sequences is not, in itself, a sufficient condition for  $\text{Ca}^{+2}$  binding. Such a sequence is, however, required since parvalbumin and cardiac TnC each contain one site with amino acid substitutions which are thought to have the right structure but which will not bind calcium. Also, the myosin light chains (A1, A2, DTNB) have four homologous EF hand-like loops but only the DTNB LC binds  $\text{Ca}^{+2}$ , and it only binds one mole of metal ion per mole of LC. It is therefore apparent that other features must play a role in determining the calcium affinity of such sites.

- 2) When peptide fragments with the helix-loop-helix arrangement were studied, moderate calcium affinity was commonly found while no appreciable  $\text{Ca}^{+2}$  was bound by the isolated 12 residue peptide. In addition, Chou and Fasman type calculations have suggested that  $\beta$ -turns in the  $\text{Ca}^{+2}$  loop contribute to the  $\text{Ca}^{+2}$  affinity, (24). These studies, as well as more recent interpretations based on sequence analysis (241), indicate that the helices directly contribute to the binding of calcium, and this could explain why no direct relation exists between the binding strength of the site and the number of ligands (1).
- 3) Only proteolytic fragments containing two EF binding

sites closely resemble the native proteins with respect to  $\text{Ca}^{+2}$  binding. Thus the structural relation between these two sites is important in addition to the specific amino acid sequence and the helices flanking the calcium binding loop. For example, chemical modification of the single arg-75 residue in parvalbumin results in the loss of the calcium binding affinity of the protein (25). This residue is more than 20 Å from the  $\text{Ca}^{+2}$  binding site but it is involved in a salt linkage with glutamic acid residue 81; it is this linkage which is responsible for preserving the relationship between the two calcium binding loops.

The binding sites of CaBP are not always specific for  $\text{Ca}^{+2}$ , but many also bind  $\text{Mg}^{+2}$  and other divalent metal ions as well. This is an important point as most cells contain specialized pumps which utilize ATP to actively excrete  $\text{Ca}^{+2}$  from the inside of the cell. Under normal conditions, the intracellular  $\text{Ca}^{+2}$  levels are kept as low as  $10^{-7}$  to  $10^{-8}$  M, whereas the extracellular calcium levels are usually in the order of  $10^{-3}$  M (1,3). Thus a non-specific binding site will be saturated with  $\text{Mg}^{+2}$  under normal (unstimulated) conditions. A summary of the  $\text{Ca}^{+2}$  and  $\text{Mg}^{+2}$  binding characteristics of the six representative proteins is given in Table I.2.

Table 1.2

The Dissociation Constants and  $\text{Ca}^{2+}/\text{Mg}^{2+}$  Specificities of the Representative Calcium Binding Proteins

Protein	$\text{Ca}^{2+}$ specific	$K_{Ca}$ (M)	non-specific	$M^{2+}$	$K_d$ (M)
parv <sup>a</sup>	0		2	Ca Mg	$4 \times 10^{-9}$ $7 \times 10^{-5}$
TnC <sup>b</sup>	2	$3 \times 10^{-6}$	2	Ca Mg	$5 \times 10^{-8}$ $2 \times 10^{-4}$
ICaBP <sup>c</sup>	0		2 2	Ca Mg	$5 \times 10^{-7}$ very weak
DTNB <sup>d</sup>	0		1 $\geq 1$	Ca Mg <sup>o</sup> Ca	$6 \times 10^{-6}$ $1 \times 10^{-3}$ $1 \times 10^{-4}$
calm <sup>e</sup>	0		3 1	Ca Mg Ca Mg	$2 \times 10^{-7}$ $1 \times 10^{-4}$ $1 \times 10^{-6}$ $2 \times 10^{-5}$
S100b <sup>f</sup>	2	$6 \times 10^{-5}$ $2 \times 10^{-4}$			

<sup>a</sup>Reference 37.

<sup>b</sup>Reference 38. The values given are for isolated TnC, where sites I and II are the  $\text{Ca}^{2+}$  specific sites.

<sup>c</sup>Reference 39.

<sup>d</sup>Reference 40: value given is for the isolated LC.

<sup>e</sup>Reference 41.

<sup>f</sup>Reference 27.

ND - not determined

## B. The $^1\text{H}$ NMR spectra of Calcium Binding Proteins in the Presence and Absence of Metal Ions

NMR spectroscopy has been used extensively to study CaBP including  $^1\text{H}$  (26-32),  $^{19}\text{F}$  (32,33), and  $^{13}\text{C}$  (34) NMR studies of the protein, and  $^{23}\text{Na}$  (3,35),  $^{45}\text{Ca}$  (3,36), and  $^{113}\text{Cd}$  (3,42) NMR studies of the bound metals. This brief discussion will highlight some of the  $^1\text{H}$  NMR spectral characteristics of CaBP. Such studies have been carried out on calmodulin (29,31,43), parvalbumin (44), TnC (28,29,32), the alkali and DTNB light chains (45), ICaBP (26), and S100b (27).  $^1\text{H}$  NMR can be used to study the solution conformation of CaBP's, in that both large conformational changes as well as much more subtle changes in the environment of specific amino acid residues is reflected by the perturbation of the proton resonances of the protein. All of these proteins, except the DTNB LC, exhibit unique high field phenylalanine resonances in the range of ca. 6-7 ppm for the apo protein. Similarly, all except the DTNB LC display several upfield shifted methyl resonances in the range of ca. -0.5 to +0.5 ppm for the apoprotein, as indicated in Figure 1.4 for ICaBP. The high field methyl groups are thought to be the result of ring current effects arising from the close proximity of these nuclei to aromatic residues (46). The lack of these resonances in the DTNB LC spectrum is thus unusual, but this particular calcium binding site, when  $\text{Mn}^{2+}$  is substituted for  $\text{Ca}^{2+}$ , has an ESR spectrum which is very different from those of the other proteins studied (47). These two

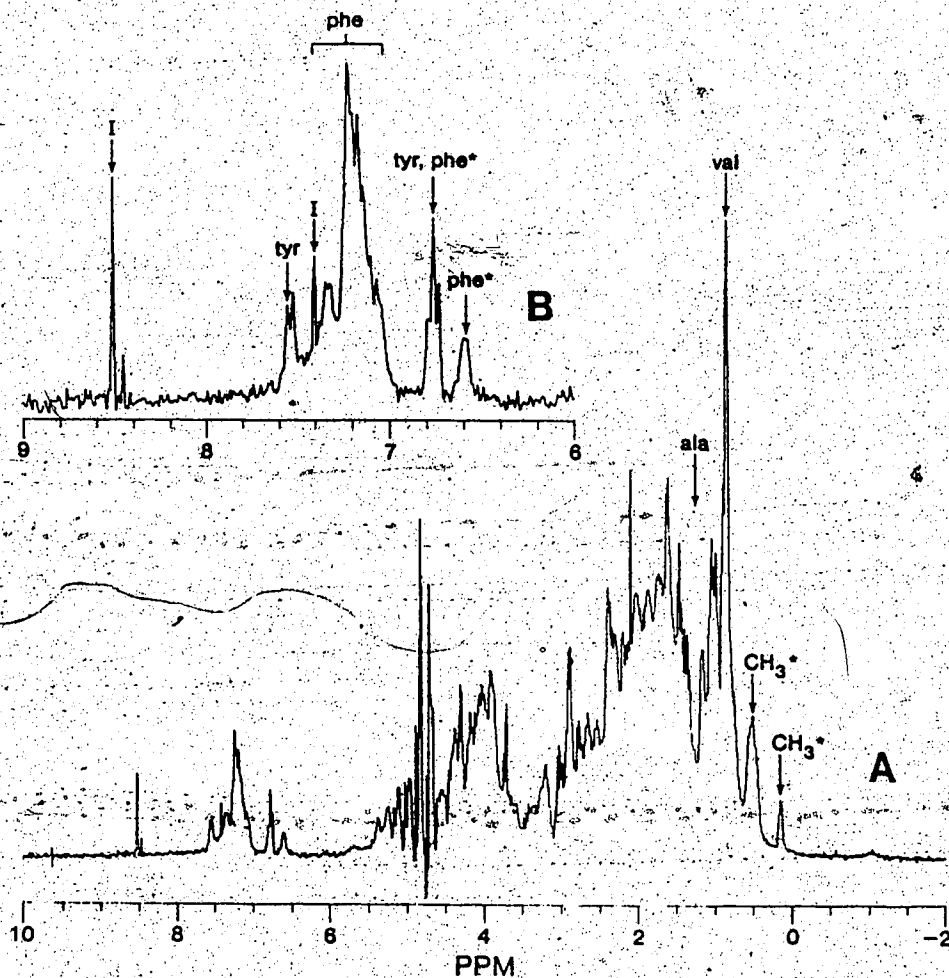


Figure 1.4 A. A 270 MHz  $^1\text{H}$  NMR spectrum of porcine ICaBP showing both the commonly occurring and the upfield shifted chemical shifts of the aromatic and methyl residues (see Figure VII.3 and accompanying text for details). The protein has five phenylalanines, one tyrosine, and no histidine or tryptophan. The methyl resonances of alanine and valine in 50 mM  $\text{K}_2\text{HPO}_4$ , pH 7.0 are indicated by arrows, as are the upfield shifted  $\text{CH}_3$  groups. The inset B shows the expanded spectrum of the aromatic region where the upfield shifted phenylalanines and the assigned tyrosine resonances are indicated with arrows. The symbols are: \*, upfield shifted resonance; I, imidazole buffer resonance; adapted from Reference 26.



types of resonances, along with the rest of the aromatic resonances, are shifted away from the bulk of the spectrum, which arises from the protons of the aliphatic residues. Because there are relatively few of these resonances and they have unique shifts, it is much easier to both assign these resonances to a particular type of amino acid and to observe defined variations in these resonances as the system is perturbed. Therefore, a great deal of attention in the studies cited above entails the effect of metal ion addition and other perturbations on these resonances.

The presence of upfield shifted phenylalanine resonances in the aromatic region and upfield shifted methyl groups in the aliphatic region in the apo protein indicates that a well-defined tertiary structure exists even in the absence of  $\text{Ca}^{+2}$ . This supports the CD results for these proteins which show a high degree of  $\alpha$ -helical content.

### C. The History and Objectives of This Project

The initial objective of this project was to obtain a  $\text{Ca}^{+2}$  binding protein which had only one high affinity calcium binding site, and to study the structure of this binding site using nuclear magnetic resonance as the primary tool. As with all projects, the course which is plotted originally must be modified to accommodate the results which are achieved as one attempts to follow that course. The original intention was to probe the light chains of myosin,

specifically the DTNB LC of rabbit skeletal myosin and the EDTA light chain of scallop myosin. These light chains have only a single  $\text{Ca}^{2+}$  binding site and thus are a simpler system than parvalbumin, which had already been extensively studied in our lab by Dr. Lana Lee. The EDTA light chain, however, lacked any aromatic residues other than phenylalanine (48) and would have been a more difficult system to probe with  $^1\text{H}$  NMR since it is the aromatic groups which are most often used to identify calcium binding effects, particularly tyrosines. To complicate matters further, the isolated EDTA light chain does not bind calcium (49) and we would have been forced to look at either myosin as a whole or a fragment thereof. Unfortunately, there are distinct handicaps to be dealt with when one employs  $^1\text{H}$  NMR to study high molecular weight species. For all of the above reasons, we thought that this system would be, at that time, too difficult to handle using this particular technique.

The focus of our attention then shifted to the DTNB LC of rabbit skeletal muscle. This protein has one high affinity site for calcium and binds metal ions in the isolated state, as well as in the native myosin molecule (see Chapter V). The ultimate goal of this project was to attempt to do a structural analysis of the binding site using the LIS of  $\text{Yb}^{3+}$ , as had been carried out on parvalbumin by Dr. L. Lee and Dr. B. D. Sykes; the only difference would have been that the known X-ray crystal structure of parvalbumin was used in interpreting the data in the latter analysis, while

no such structure was available for the DTNB LC. Previous workers have calculated theoretical binding site structures for TnC and calmodulin on the basis of the structure of parvalbumin, and this approach would also have been used by ourselves to aid in the data analysis. Due to the increasing number of reports in the literature indicating that a lanthanide ion cannot always functionally replace a calcium ion, we began by choosing three lanthanides which covered both the ends and the middle of the series and used CD to determine their effects on the overall conformation of the molecule compared with calcium. The difference in the CD effects which we observed, the fact that we had difficulty in obtaining a  $10^{-6}$  M association constant for the isolated LC, and our inability to see any spectral differences in the  $^1\text{H}$  NMR spectra upon the addition of  $\text{Yb}^{3+}$  led us to think about using the LC in its native state, *i.e.* while it was still associated with myosin. Because of the large molecular weight of myosin, direct  $^1\text{H}$  NMR studies on that species were out of the question so we attempted to prepare HMM S1 using papain. S1 is much smaller than myosin, and yet retains all of its biological properties and functions. There was also the added attraction that we could monitor the ATPase activity of this fragment and thus have an independent means of assessing the effects of the lanthanide ions. We prepared this subfragment using papain, but the ATPase was quite low (*i.e.* 50 to 60 % that of myosin). SDS PAGE indicated that the protein had been extensively nicked during the cleavage.

as had been observed by others (50,51). S1 prepared with chymotrypsin was also nicked. The addition of  $\text{Yb}^{3+}$  to the S1 subfragment prepared with papain led to precipitation of the protein so this entire segment of the work was abandoned.

We then decided to look more closely at the nature of the lanthanide-amino acid side chain interaction itself and initiated a series of studies on small peptides, both as purchased and those synthesized in collaboration with Dr. R. S. Hodges, The University of Alberta. The objective here was to look at the binding of small ligands, which mimicked the  $\text{Ca}^{2+}$  binding sites, and to look at their structural characteristics when bound to lanthanide ions. We were particularly interested in determining the magnitude of the contact interaction of the LIS, which are assumed to be negligible in  $^1\text{H}$  NMR spectra. This segment of the project was completed successfully, with the help of Dr. Ron Reid, Dr. Ashok Taneja, and Ms. Michelle Bjornson, and gave us some surprising results which should prove to be beneficial to those using the LIS of lanthanide ions to probe the structures of calcium binding sites.

During this time we also began a fruitful collaboration with Dr. Theo Hofmann and Mr. Joseph D. J. O'Neil at The University of Toronto. From them we obtained some purified ICaBP, which was thought, at that time, to have a single  $\text{Ca}^{2+}$  binding site. We received the protein in a calcium-saturated state and our preliminary work involved adding

$\text{Yb}^{3+}$  to this state. LIS were immediately apparent, and this form of the protein bound one mole equivalent of  $\text{Yb}^{3+}$ . We looked at both the effects of salt and temperature on these shifts. The temperature dependency was very odd so we decided to prepare the apo-protein and do some calcium binding studies on it first, before proceeding with further lanthanide work. Initially there was some problem in obtaining a metal free protein, particularly when it became apparent that EDTA had a tendency to stick to the protein during desalting on sephadex columns; large columns and high salt concentrations were necessary to remove the EDTA completely. We made use of this contaminant EDTA to obtain a dissociation constant for the binding of calcium to the protein; this  $K_d$  was relative to the known  $\text{Ca}^{2+}$  dissociation constant of EDTA. These studies led us to make some conclusions about the nature of the mode of calcium binding by the protein, with respect to whether it displayed cooperativity. Even when we initially did manage to get rid of the EDTA contamination, this protein was found to contain some metal ion contamination in the initial studies which we carried out. This problem was finally solved by pretreatment of all of the desalting column buffers and the deuterated NMR sample buffer with chelex-100 resin. Prior to this time, the deuterated NMR buffers in the lab which were used for these types of studies had been pre-treated with dithizone, which has a high affinity for lanthanides and transition metals but not for  $\text{Ca}^{2+}$  and  $\text{Mg}^{2+}$ .

The addition of  $\text{Ca}^{+2}$  to ICaBP led to spectral changes consistent with the binding of two metal ions. This was later verified by our collaborators so now we were looking at a protein which bound two moles of  $\text{Ca}^{+2}$  rather than one. There were distinct differences between the apo- and  $\text{Ca}^{+2}$ -saturated spectra, indicating that the conformation of the protein changed upon calcium ion addition. The resonances of the single tyrosine residue of ICaBP were identified in both states by pH and CIDNP studies. The CIDNP studies also revealed information on the degree of exposure of this tyrosine in both states. We later returned to look at the temperature effects anew, armed with a better understanding of the calcium binding mode of the protein. We titrated the apo protein with  $\text{Lu}^{+3}$  and found that this form of the protein bound two equivalents of lanthanide. From these results, and the  $\text{Yb}^{+3}$  data mentioned above, we were able to determine that, while the apo form of ICaBP bound two lanthanide ions, in the presence of a saturating concentration of calcium only one lanthanide ion was coordinated.

We also began a collaboration on a totally different kind of CaBP, the bovine brain S100b protein, with Dr. R. S. Mani and Dr. C. Kay at The University of Alberta. This protein exists as a dimer in solution and each monomer binds one or two  $\text{Ca}^{+2}$  ions, depending upon the pH. The apo- and  $\text{Ca}^{+2}$ -saturated spectra were different, both at pH 7.5 and at pH 8.5, indicating that conformational changes were taking place upon calcium ion addition at both pH values. The

effect of  $\text{Ca}^{2+}$  at pH 7.5 was found to be partially reversed by the addition of  $\text{K}^+$ . The apo spectra at pH 7.5 and pH 8.5 differed as well, indicating a change in conformation of the protein as a function of pH. This was later verified by a pH titration of both the apo- and calcium-saturated forms of S100b. The single tyrosine residue ionized only at high pH, where the  $^1\text{H}$  NMR spectra indicated that the protein was denaturing.

Further work is anticipated on both ICaBP and S100b.

## II. NMR THEORY AND METHODOLOGY

### A. The Magnetic Properties of Chemical Substances

This section is intended to be a brief and simple review of some of the magnetic properties of the elements and will emphasize those features which are relevant to the studies undertaken in this work.

#### Diamagnetism

All molecules contain at least some if not all of their electrons in closed shells, where the electron spin moments and orbital angular moments of individual electrons balance one another out so that there is no net magnetic moment (52,53). However, when an atom or molecule is placed in a magnetic field, a small magnetic moment is induced which is directly proportional to the strength of the applied field. For diamagnetic materials, the electron spin moment is zero, and it is a small net orbital moment which is set up in opposition to the applied field, the magnitude of which depends on the size and shapes of the orbitals in the closed shells (52).

#### Paramagnetism

A paramagnetic substance has unpaired electrons, for which the electron spin moments and orbital angular moments do not cancel out, resulting in a net permanent moment (52). Normally these moments are randomly oriented, such that the



net moment of a sample is zero. However, in the presence of an external magnetic field  $H_0$ , these moments become aligned with  $H_0$  and a net magnetic moment is induced. An atom with a permanent magnetic moment will still have diamagnetic behaviour working in opposition to that paramagnetism when placed in a magnetic field, providing that the atom has one or more closed shells of electrons.

### Magnetic Susceptibility

The magnetic field patterns around a current-carrying conductor can be represented by lines which are called the magnetic flux (54). When a substance is placed in the magnetic field, the moments which are induced in that substance alter the flux within it. The susceptibility of a diamagnetic substance is negative because the flux from the induced dipoles cancel out some of the flux due to the applied field. For paramagnetic substances, the flux is greater within the substance than it would be in the rest of the field so paramagnetic molecules have positive susceptibilities (52,55). Susceptibility is thus a measure of the magnitude of the diamagnetic and paramagnetic moments which are induced in the presence of the external magnetic field.

Magnetic susceptibility is a tensor quantity which has three principle axes, these three axes are taken as the principle axes of a cartesian coordinate system, where the principle molecular magnetic susceptibilities are  $\chi_x$ ,  $\chi_y$ , and  $\chi_z$ . The magnetic susceptibility tensor can have three

types of symmetry.

SYMMETRY

PRINCIPAL AXIS

spherical

$$\chi_x = \chi_y = \chi_z$$

axial

$$\chi_x = \chi_y \neq \chi_z$$

non-axial

$$\chi_x \neq \chi_y \neq \chi_z$$

For spherical symmetry, the magnitude of the paramagnetic moment will be independent of the orientation of the susceptibility axis with respect to  $H_0$  because  $\mu_x = \mu_y = \mu_z$ ; this is an *isotropic* magnetic moment. For axial and non-axial symmetry, however, this will not be the case and the magnitude of the moment will be dependent upon the orientation of the susceptibility axis with respect to  $H_0$ ; this type of magnetic moment is *anisotropic*.

## B. The General Properties of the Lanthanides and Their Usefulness as Structural Probes

### The Chemistry of the Lanthanides

The transition elements may be strictly defined as those which, as elements, have partially filled  $d$  or  $f$  shells, and the lanthanides fall into this broad category. The first element in the lanthanide series is lanthanum which has an electron configuration in the ground state of  $[\text{Xe}]6s^2 5d$ . Because the  $4f$  shells become slightly more stable

than the  $5d$  shells upon the addition of electrons, the  $4f$  shells fill first. The fourteen elements following lanthanum in the periodic table are formed by the successive addition of 14 electrons to these empty shells until one reaches lutetium for which the  $f$  shells are completely filled with an electron configuration of  $[\text{Xe}]4f^{14}5d^06s^2$  (56). The 15 elements La through Lu have very similar chemical and physical properties so that all of these elements are combined into the classification *lanthanides*. Yttrium also has very similar properties and it is often found grouped with the lanthanides in the literature (56).

The subtle differences and trends that are encountered along the series are primarily due to the changes in the ionic radii of the cations, which are generally present as the  $M^{3+}$  state (Table II.1). As one proceeds through the lanthanide series, the nuclear charge and the number of  $4f$  electrons increases by one each step. The shielding of one  $4f$  electron by another is quite imperfect (much more so than with the  $d$  electrons) owing to the shapes of the orbitals, so that at each increase of a single electron the effective nuclear charge experienced by each  $4f$  electron increases, resulting in a reduction in size of the entire  $4f$  shell. The accumulation of these successive contractions is the total lanthanide contraction and can be easily observed in Table II.1.

Table II.1

Electronic Configuration and Effective Ionic Radii for  $Y^{+3}$ ,  $Ca^{+2}$ , and the Tripositive Lanthanide Ions

Element	Symbol	Electronic Configuration ( $M^{+3}$ )	Ionic Radii $M^{+3}$
Calcium	Ca	[K]	1.000 <sup>b</sup>
Yttrium	Y	[Ar]	0.900
Lanthanum	La	[Xe]	1.032
Cerium	Ce	4f <sup>1c</sup>	1.010
Praseodymium	Pr	4f <sup>2</sup>	0.990
Neodymium	Nd	4f <sup>3</sup>	0.983
Promethium	Pm	4f <sup>4</sup>	0.970
Samarium	Sm	4f <sup>5</sup>	0.958
Europium	Eu	4f <sup>6</sup>	0.947
Gadolinium	Gd	4f <sup>7</sup>	0.938
Terbium	Tb	4f <sup>8</sup>	0.923
Dysprosium	Dy	4f <sup>9</sup>	0.912
Holmium	Ho	4f <sup>10</sup>	0.901
Erbium	Er	4f <sup>11</sup>	0.890
Thulium	Tm	4f <sup>12</sup>	0.880
Ytterbium	Yb	4f <sup>13</sup>	0.868
Lutetium	Lu	4f <sup>14</sup>	0.861

<sup>a</sup>For a coordination number of 6, from Ref. 57.

<sup>b</sup>Radii for the  $M^{+3}$  ion.

<sup>c</sup>Only those with electrons outside the closed rare gas shell are indicated.

Plots of stability constants and ionization potentials (58) as well as other properties (56, 58, 59) of small molecule lanthanide complexes against atomic number frequently show inflections at or near  $Gd^{3+}$ , the lanthanide with the  $4f^7$  configuration. The fact that this inflection does not always occur exactly at gadolinium for all of these complexes has resulted in the view that these "breaks" are the result of structural changes (60, 61) associated with the change in size of the tripositive ion. There is support for this view in various studies where several small molecule complexes of the heavier lanthanide ions were shown to adopt structures having lower coordination numbers than the corresponding lighter lanthanide complexes (60, 62, 63, 242).

The majority of lanthanide complexes isolated involved oxygen donor ligands or mixed oxygen-nitrogen chelate ligands which are commonly anionic and multidentate as typified by  $\beta$ -diketonate (i.e. acetyl acetonate), dicarboxylate (i.e. citrate); and amine-carboxylate ligands (i.e. EDTA) (58). For a complex to be stable in aqueous media, the ligand must compete successfully with  $H_2O$ , which is a good ligand towards lanthanide ions and is available in great abundance, and also  $OH^-$  which forms insoluble hydroxides (64, 65) (i.e. upon dissolution in aqueous media, the lanthanides undergo extensive hydrolysis, which is evidenced by a significant decrease in the pH of an unbuffered solution).

## Lanthanide Ions as Calcium Probes

Lanthanide ions are the simplest cations which have useful physical properties and a chemistry closely allied to that of  $\text{Ca}^{+2}$ . The chemistry of these highly electropositive elements is largely ionic and is determined by the size of the  $\text{M}^{+3}$  ion (58). Because of this, lanthanide complexes closely resemble the complexes of the group IIA alkaline earth cations, which includes  $\text{Ca}^{+2}$  and  $\text{Mg}^{+2}$ . The interaction between metal ion and ligand is electrostatic and all of the lanthanide ions present the same empty 6s and 6p valence shell to coordinating ligands. The partially filled 4f shell lies deeper in the atom and takes effectively no part in covalent bond formation. Thus the influence of the ligand field on the 4f orbitals is very much smaller than in the d-block complexes where ligand field stabilization energies contribute significantly to the stability of complexes (66). The lanthanides from  $\text{Ce}^{+3}$  to  $\text{Yb}^{+3}$  are paramagnetic and it is this property which is very useful for structural studies using NMR, as will be outlined shortly. In order to carry out biochemically relevant studies on the CaBP's, one needs to use a metal ion which is similar to calcium in size, mode of binding, and functionality. Lanthanide metal ions can fulfill these requirements (Table II.1) (58,67-70).

## NMR Studies of Lanthanide Complexes

There have been many studies on both chemical (58,71-73) and biochemical (58,69,70,73-82) molecules which

have shown that structural information can be obtained from the NMR spectra of nuclei on metal binding ligands, including proteins, when a paramagnetic metal is used in place of the physiologically relevant diamagnetic metals. In these studies one is observing the effects of the unpaired electron upon those ligand nuclei which coordinate directly to the metal ion or which are brought into close proximity to the metal ion through coordination. This is manifested in the form of large changes in the chemical shifts and/or broadening of the resonances of these nuclei.

In studies on biochemical systems, the lanthanides have been used as NMR probes of the structure of small organic molecules, as well as proteins. Hinckley (83) first reported the use of lanthanide tris  $\beta$ -diketonates as shift reagents in organic solvents, to simplify the spectral analysis of cholesterol. The use of lanthanides as "shift reagents" often results in the resolution of previously overlapping peaks. In 1971, the first studies on the use of lanthanide tripositive ions in the determination of the structure of AMP in aqueous solution was reported (84-86) and this work has been extended to cyclic mononucleotides (87), dinucleotides (88), ATP (89), and ribonucleotides (90). The analysis for flexible molecules results in the determination of a series of geometries of the nucleotide which are compatible with the observed lanthanide induced NMR shifts.

The Oxford Enzyme Group first proposed that perturbations induced by lanthanide ions could be used to probe the structure of a protein (91-95). The early studies were based upon the binding of the broadening probe  $Gd^{3+}$  to a site on the enzyme lysozyme (91,92).  $Gd^{3+}$  induces no dipolar shifts (as will be discussed later) but it does induce nuclear relaxation which manifests itself in the form of broadening of the resonances of nearby nuclei; the extent of this broadening is dependent upon the distance of the nuclei from the paramagnetic centre. When  $Gd^{3+}$  was added to lysozyme, it bound to a site on the protein, thereby broadening certain resonances. By comparing the affected resonances and the calculated distances with the X-ray crystallographic structure of the protein, some assignments of resonances to specific protein residues were made.

In addition to the broadening studies, NMR shifts of lysozyme induced by lanthanides other than  $Gd^{3+}$  were used to determine geometrical information (78,95). From these studies the position of the metal ion in the protein, the magnitude of the principal elements of the magnetic susceptibility tensor of the metal, and the direction of the magnetic susceptibility tensor were determined. In addition, Lee and Sykes (76,77,96-100) have studied the lanthanide induced shifts and linebroadenings for  $Yb^{3+}$  substituted parvalbumin; these studies led to the determination of the orientation and principle elements of the magnetic susceptibility tensor of  $Yb^{3+}$  bound in the EF calcium binding site



of parvalbumin, and the three dimensional structure of the surrounding amino acid residues. Further work has demonstrated that these techniques can be extended to proteins which do not normally bind metal ions (101-103). By chemical modification, specific metal binding sites on bovine pancreatic trypsin inhibitor were introduced to probe its protein conformation. Other studies involving the use of lanthanide induced shifts to probe molecular structure include work on amino acids (74, 104-106), peptides (106, 107), and testosterone (108).

#### Diamagnetic Shifts

Diamagnetic shifts are the changes in the chemical shifts of a molecule due to the interaction of its nuclei with a diamagnetic metal ion, such as  $\text{Ca}^{+2}$ ,  $\text{Mg}^{+2}$ , or the diamagnetic lanthanides  $\text{La}^{+3}$  and  $\text{Lu}^{+3}$ . These shifts arise from perturbations in the environments of the affected residues due to the binding of metal ions, as a result of local changes in structure or overall conformational changes in the molecule. The chemical shifts of such residues typically span the -1 to 10 ppm region of the  $^1\text{H}$  NMR spectrum in both the presence and absence of metal ions.

#### Lanthanide Induced Shifts

LIS are the change in chemical shifts for the nuclei which are brought about by the interaction of these nuclei with the paramagnetic moment of a lanthanide ion. These

interactions typically shift the  $^1\text{H}$  NMR resonances of nuclei in the vicinity of the metal ion to positions outside the envelope of the diamagnetic spectrum. There are two distinct types of interactions which occur that each contribute separately to the observed value of the LIS (109-111). One is called the *contact* or *Fermi* interaction which is an interaction that depends upon the probability of the electron being located at the nucleus; this interaction is *isotropic*. Contact shifts are caused by movement of the unpaired electron spin density away from the metal cation to the ligand by covalent bond formation; this mechanism operates through the metal cation co-ordinating bond and so depends upon the degree of covalency in this bond. To interact in such a manner, the ligand nucleus observed must generally be either directly bonded to the metal centre or involved in a bonding system through which the electron could be delocalized, such as a conjugated system. The magnitude of the contact shift is dependent upon the lanthanide being observed, and the expression for this shift is

$$\Delta_m^{c,i} = A_m^i \langle S_z \rangle_m$$

where  $\Delta_m^{c,i}$  is the observed contact shift for nucleus  $i$  and lanthanide  $m$ ,  $A_m^i$  is the hyperfine coupling constant between the nucleus  $i$  and the unpaired electron spin of the lanthanide  $m$ , and  $\langle S_z \rangle_m$  is the projection of the total electron spin magnetization for the lanthanide ion  $m$  in the direction

of  $H_0$ . Values for  $\langle S_z \rangle_m$  have been determined experimentally for each of the lanthanides (112). This type of interaction, although independent of the orientation of the molecule to the external field, is dependent upon the structure of the metal-chelate complex. Also, because the lanthanides form complexes by electrostatic interaction, this precludes the operation of a contact mechanism of the same order of magnitude as found with the first row transition block metal complexes but, with even as little as 1% covalency, contact shifts should be observed (66).

The second type of interaction is called the *pseudoccontact* or *dipolar* interaction, and this interaction is *anisotropic*. The only trivalent lanthanide ions which do not display this type of shift are La and Lu, which are diamagnetic, and the paramagnetic lanthanide Gd ( $f^7$ ) because it has an isotropic ligand field arising from the presence of one electron in each of its seven  $f$  orbitals. An intuitive look at the dipolar interaction (113) deals with the case of the axially symmetric system, where  $\chi_x = \chi_y \neq \chi_z$ , where one can represent the susceptibility tensor by an ellipsoid of revolution (Figure II.1). The induced paramagnetic moment produces a dipole field acting at the nucleus  $i$  ( $N_i$ ). This dipole field will not average to zero over molecular orientation (*i.e.* rapid tumbling) because the magnitude of  $\mu_p$  itself depends upon the molecular orientation relative to  $H_0$  (110). Figure II.1 shows two possible orientations of the molecular susceptibility tensor for an axially symmetric system. The

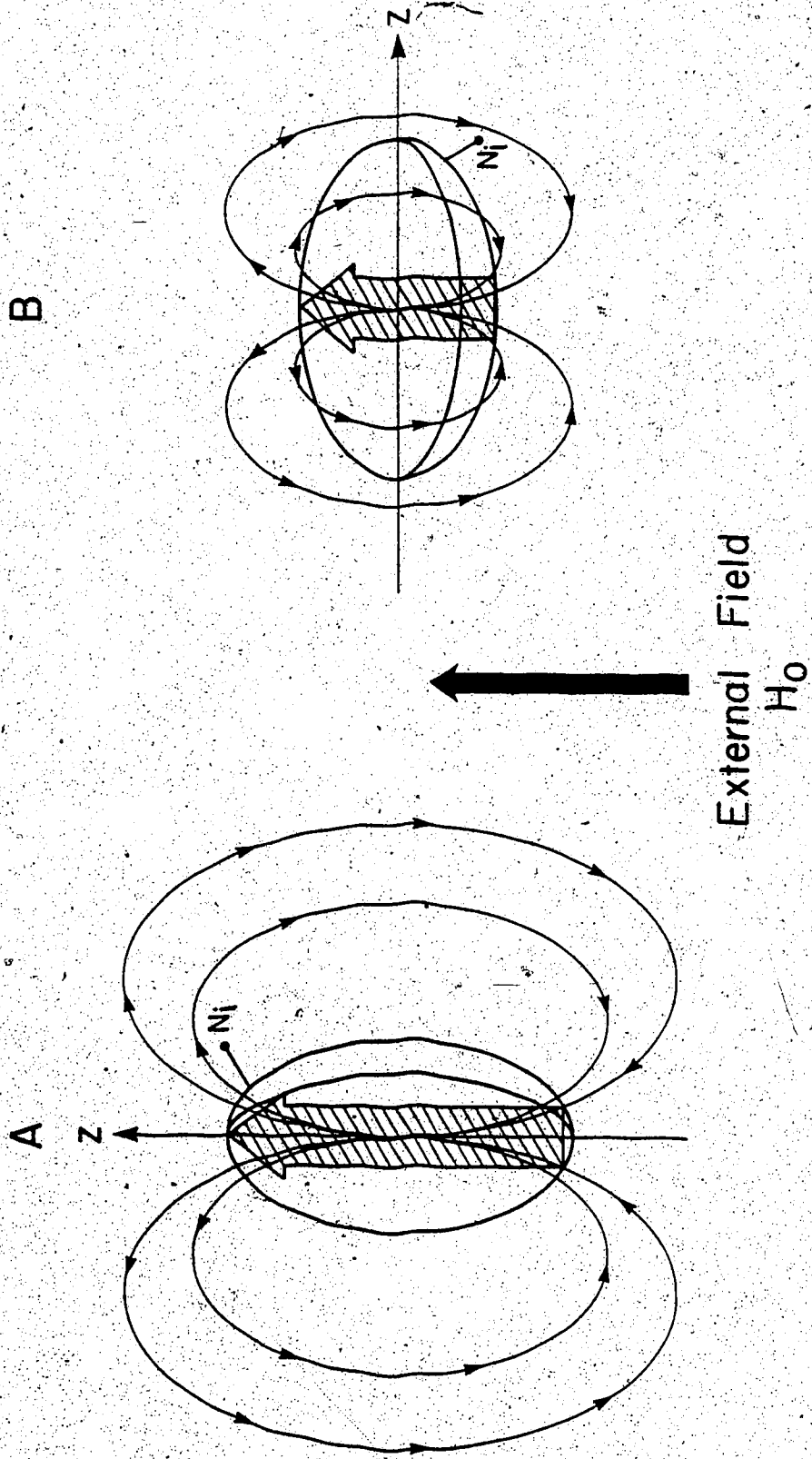


Figure II.1. A qualitative picture of the effect of magnetic anisotropy ( $\chi_{ij} \gg \chi_L$ ) on the internal field experienced by nucleus  $i$  ( $N_i$ ) near the principal axis of the susceptibility tensor ( $z$ ) adapted from reference 113, figure 4-4.

A. The symmetry axis  $z$  is parallel to  $H_0$ .

B. The symmetry axis  $z$  is perpendicular to  $H_0$ .

symmetry axis  $z$  defines the parallel direction, ( $\chi_z = \chi_{\parallel}$ ;  $\chi_x = \chi_y = \chi_{\perp}$ ) and the magnitudes of the induced moments, which are parallel to the applied field for paramagnetic substances, are indicated by the large arrows along with their associated flux lines. In the present example  $\chi_{\parallel} > \chi_{\perp}$  so that  $\mu_{\parallel} > \mu_{\perp}$ . When the symmetry axis of the molecule is parallel to the applied field (Figure II.1A), the internal magnetic field at  $N_i$  reinforces the external field and would cause  $N_i$  to come to resonance at lower applied field (downfield shift). This is analogous to the more familiar "ring current effect" observed for benzene, which causes aromatic protons to resonate at lower applied fields than aliphatic protons. When, in the course of tumbling, the molecular symmetry axis becomes perpendicular to the applied field (Figure II.1B), the nucleus  $N_i$  will experience a smaller internal field which opposes the external one (upfield shift). In the present example, when an average over all possible orientations is taken, the situation of Figure II.1A will dominate and a net downfield dipolar shift will result.

The general equation for the dipolar shift of nucleus  $i$  in an axially symmetric system is

$$\Delta_m^{d,i} = \left( \frac{1}{3N} \right) \left[ \chi_{\parallel} - \chi_{\perp} \right] \left\langle \frac{3\cos^2\theta_i - 1}{r_{im}^3} \right\rangle_{ave}$$

In the ensuing discussions and results, a negative value for a LIS represents a shift to lower frequency (upfield) in the presence of lanthanide ions. (i.e.  $\Delta_m^{obs,i} = \nu^{para} - \nu^{dia}$ ).

where  $\Delta_m^d$  is the dipolar component of the LIS of nucleus  $i$ ,  $r_{i,m}$  is the distance of nucleus  $i$  from the central ion  $m$ , and  $\theta_i$  is the angle between  $r_{i,m}$  and the principle axis of symmetry  $Z$ , as defined in Figure II.2. When the frequencies of rotation and/or translational motion of the residues are high compared with the frequencies of interest in the resonance, it is the time average of these frequencies which is observed, as indicated by the *ave* notation (114). In addition to this type of averaging, when the molecule is tumbling rapidly in solution there is also averaging over all of the possible orientations of the lanthanide complex with respect to  $H_0$ , as outlined previously (110).

The net result of this equation can be visualized with the aid of Figure II.1 (113). If the nucleus  $N_i$  had been located near the equator of the ellipsoid, it can be readily seen that an upfield shift would result. Thus, for axially symmetric systems, with  $\chi_{11} > \chi_{11}$ , a nucleus lying within cones coaxial with the principal axis of half angle  $\theta = 54.7^\circ$  will experience downfield shifts, while those lying to the equatorial region would experience upfield dipolar nuclear resonance displacements.

With this more simple system in mind, we will now outline the more general case for lanthanide complexes, which is that of the presence of an susceptibility tensor which does not have axial symmetry  $\chi_x \neq \chi_y \neq \chi_z$ . The terms in this relationship are

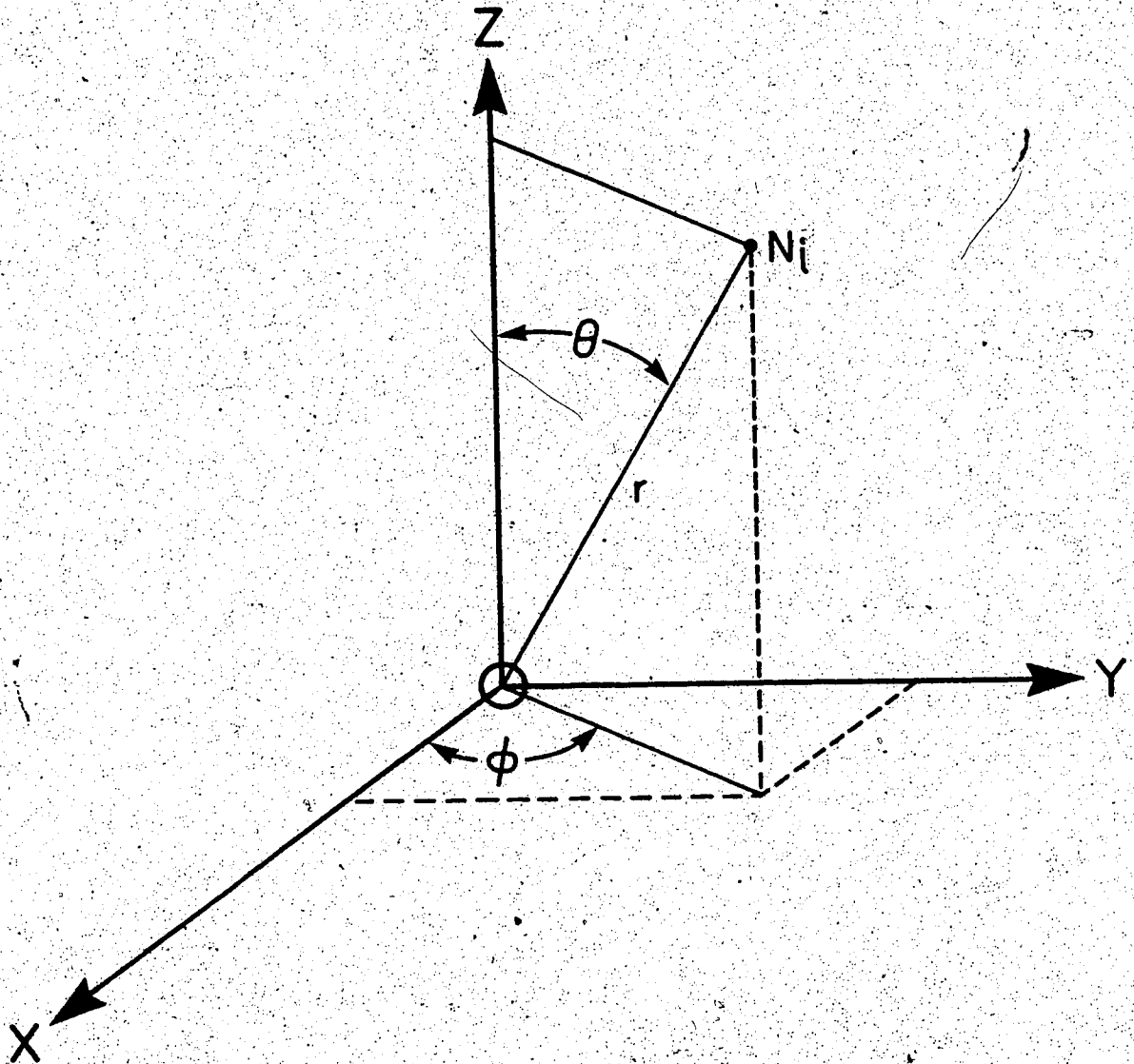


Figure II.2 The three values  $r$ ,  $\theta$ , and  $\phi$  define the spherical coordinates of nucleus  $i$  ( $N_i$ ) in the principal axis system of the magnetic susceptibility tensor of a paramagnetic ion ( $O$ ). The length of the vector  $ON_i$  is  $r$ : adapted from reference 113, Figure 4-5.

$$\Delta_m^{d,i} = D_{1m}G_1 + D_{2m}G_2$$

where, for the case of a molecule tumbling freely in solution, (i.e.  $1/\tau_R \gg$  the linewidth of the resonance and where  $T_{1e} \ll \tau_R$ ), one has

$$D_{1m} = \left( \frac{1}{3N} \right) \left[ x_z - \frac{1}{2}(x_x + x_y) \right]$$

and

$$D_{2m} = \left( \frac{1}{2N} \right) \left[ x_z - x_y \right]$$

where  $T_{1e}$  is the electron spin-lattice relaxation time,  $\tau_R$  is the correlation time for molecular tumbling in solution, and  $N$  is Avogadro's number (113). The geometric factors  $G_1$  and  $G_2$  are defined as

$$G_1 = \left\langle \frac{3\cos^2\theta_1 - 1}{r_{1m}^3} \right\rangle_{\text{ave}}$$

and

$$G_2 = \left\langle \frac{\sin^2\theta_1 \cos 2\phi_1}{r_{1m}^3} \right\rangle_{\text{ave}}$$

where  $\phi_1$  is the angle between the projection of  $r_{1m}$  on the  $xy$  plane and the  $x$  axis, as defined in Figure II.2. It is



readily apparent that if  $x_x = x_y$ , in the case above, then the  $D_{2m}$  component of the equations above is nullified and one has an equation with only a single term (axial symmetry). For a spherically symmetric system, there will be no dipolar shift as  $D_{1m}$  and  $D_{2m}$  are both nullified. The sign of the shift is a function of the size of the angles  $\theta_1$  and  $\phi_1$ , while the magnitude of the dipolar shift is inversely proportional to the cube of the vector  $r_{1m}$  (111, 113). Theoretical contour plots can be generated for all of the possible combinations of these three variables, and the structure of the molecule can then be determined from the observed LIS of each observed nucleus, after correction for the contributions of the contact shift and the diamagnetic shift. Figure II.3 shows a two dimensional representation of several of the contour plots derived for Tris[hydridotris(pyrazol-1-yl)borato]ytterbium(III) [Yb(HBPz<sub>3</sub>)<sub>3</sub>] and a three dimensional representation of the 14 ppm contour of Yb<sup>3+</sup>-substituted parvalbumin.

### C. Chemical Exchange

The following text will briefly define the terms slow and fast exchange, and explain the effect of exchange rates on <sup>1</sup>H NMR spectra. Let us consider a single nucleus which has two possible environments. For example, a nucleus within the metal binding site of a protein (H<sub>p</sub>) will experience two distinct environments if the concentration of metal ion is non-saturating, the environment of the apoprotein and the

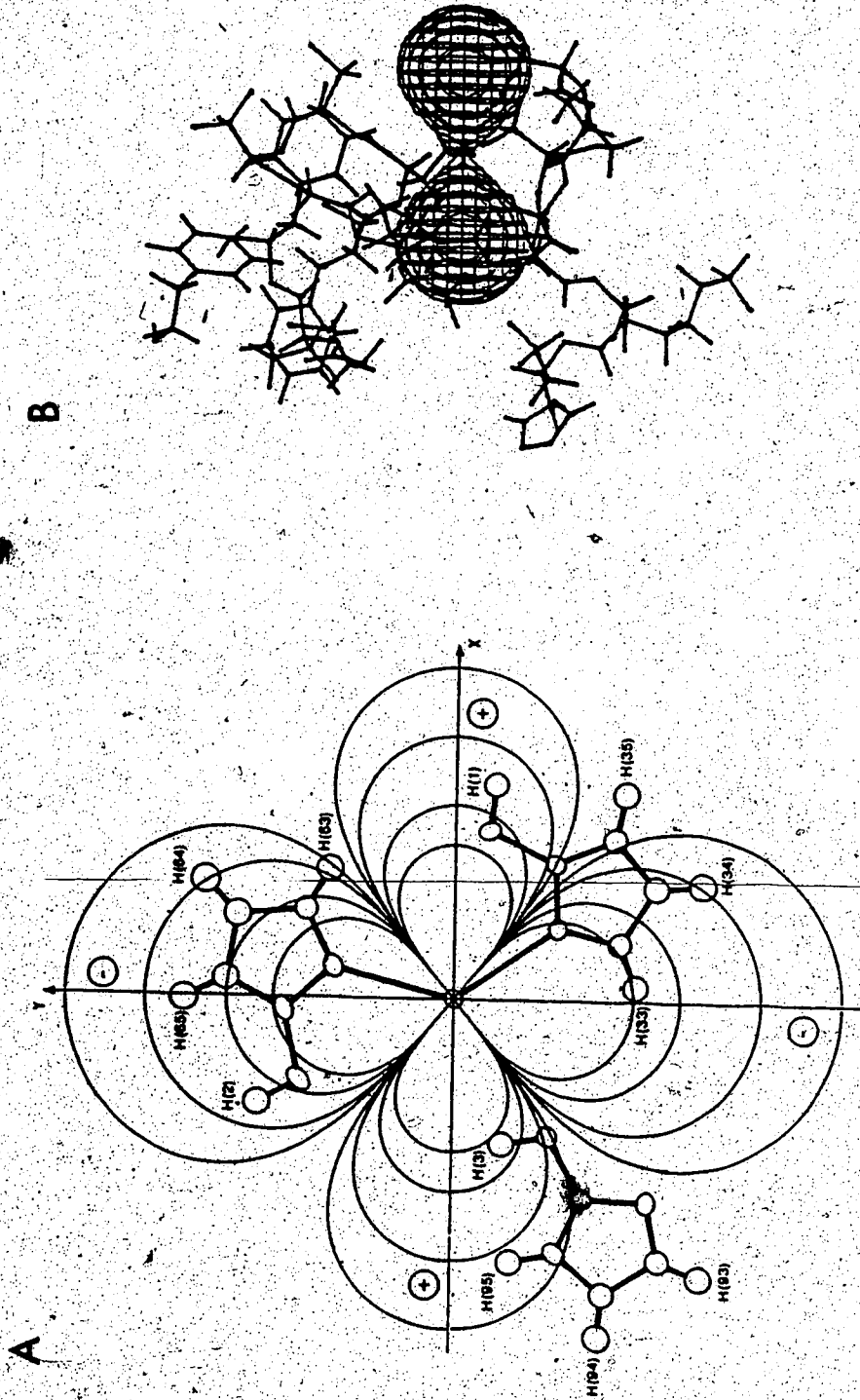
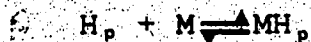


Figure 11-3. Contour maps of the dipolar shifts of Yb(HBPz), and of Yb' bound to the EF site of carp parvalbumin. A. A two dimensional contour map of Yb(HBPz). The contours are, in order of increasing size,  $\pm 100$ ,  $\pm 50$ ,  $\pm 20$ , and  $\pm 10$  ppm; from reference 71, with permission. B. The orientation of the 27 ppm paramagnetic chemical shift contour surface for Yb', found to the EF site of carp parvalbumin; from reference 100, with permission.

environment of the metal-bound protein, as indicated below:



These environments may differ because there is a conformational change upon metal binding, because the metal bound is paramagnetic, or for other reasons. The resonant nucleus jumps between the two environments, *A* (apo protein) and *M* (protein-metal complex). The complex tumbles with a rotational correlation time  $\tau_R$ , and the mean lifetimes of the nucleus in the respective environments are  $\tau_A$  and  $\tau_M$ .

A given nucleus which is perturbed by the binding of a metal to the protein will have two resonance frequencies  $\nu_A$  and  $\nu_M$ , corresponding to the *A* and *M* states of the protein respectively. Consider a coordinate system that rotates about  $H_0$ , in the same direction in which the nuclear moments precess (243), at a frequency

$$\nu_0 = 1/2(\nu_A + \nu_M).$$

In this rotating coordinate system a nucleus at site *A* precesses at  $(\nu_A - \nu_0)$ , whereas a nucleus at site *M* precesses at  $(\nu_0 - \nu_M)$ : the nucleus at site *M* in this rotating frame then appears to be precessing in a direction opposite to that of the nucleus in site *A* (116). A theoretical series of spectra have been computed and are shown in Figure II.4.

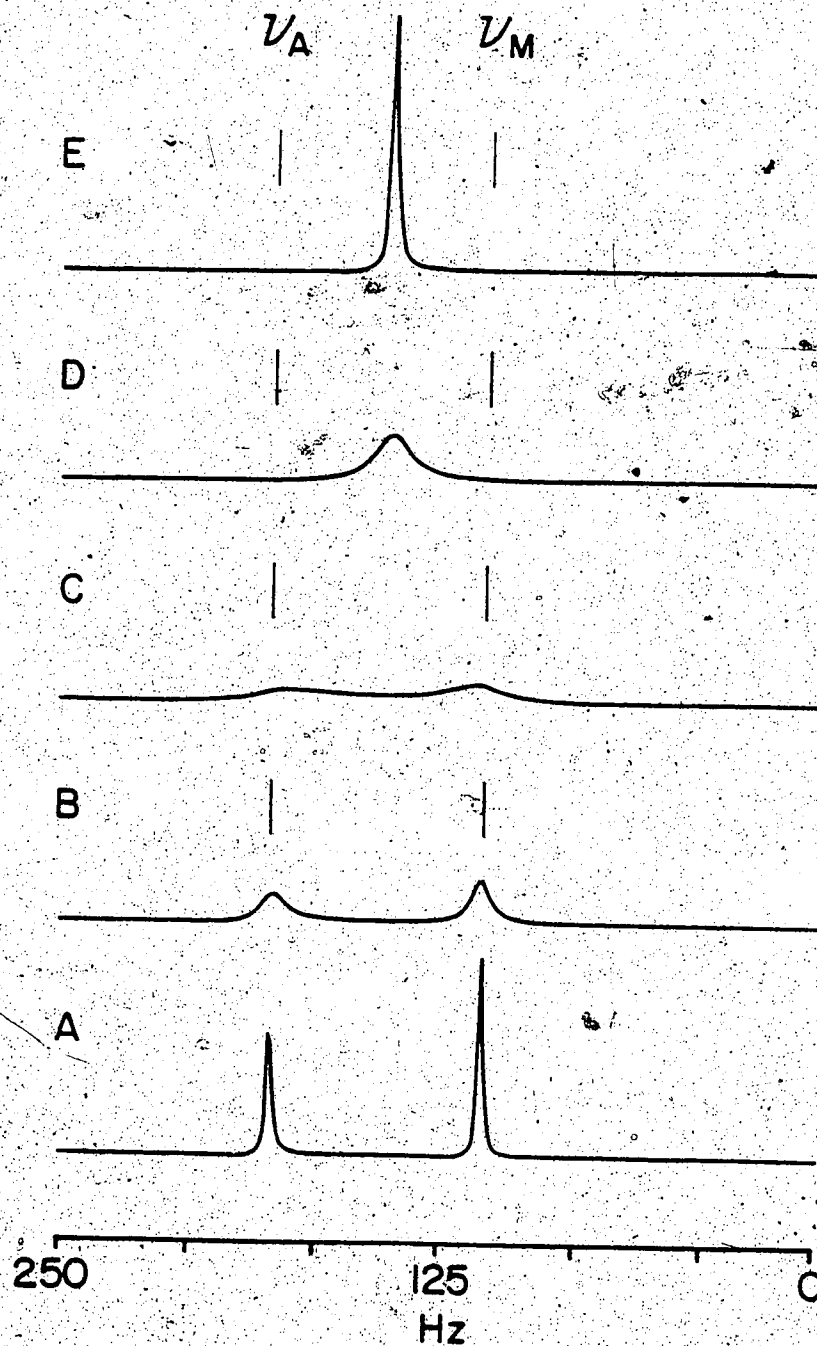


Figure II.4 Theoretical spectra for slow, intermediate, and fast exchange. The fraction of the nuclei in environment A was 0.45,  $\tau_A$  was  $10^{-3}$  sec,  $\tau_M$  was  $10^{-1}$  sec,  $\nu_A$  was 180 Hz, and  $\nu_M$  was 110 Hz. The rate constant varied in the series as: A, 5; B, 25; C, 70; D, 500; and E, 3000  $\text{sec}^{-1}$ .

### Slow Exchange Limit

When the rate of chemical exchange between these two environments is slow, then a given nucleus exists in either state for a period of time long enough that it can precess many times before it moves into the other state. The net result is that interaction with the applied field occurs for both state  $A$  and state  $M$ , and a single resonance line appears at each of  $\nu_A$  and  $\nu_M$  (Figure II.4A). This is the situation observed for proteins when the metal binding is tight and specific; the spectrum in the presence of metal ions consists of two resonances, one corresponding to the ligand nuclei in the absence of metal ions ( $\nu_A$ ) and the other resonance to the nuclei in the protein-metal complex ( $\nu_M$ ). Note that in Figure II.4A the intensity of the resonances reflects the fraction of nuclei in each of the two environments.

### Fast Exchange Limit

When the exchange rate between the two sites is fast, then, in the rotating frame, the nucleus remains stationary while in the laboratory frame it appears to be precessing at the frequency with which the coordinate system rotates. Thus one observes a single resonance at  $\nu_0$ , even though no nucleus actually precesses at that frequency.

### The Effect of Chemical Exchange on the NMR Spectrum

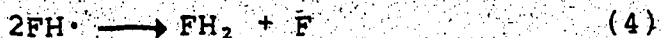
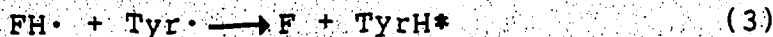
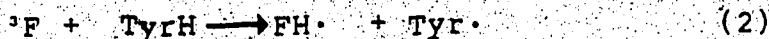
The series of theoretical spectra shown in Figure II.4 show the transition in the spectral characteristics as one goes from the slow exchange limit, through intermediate exchange limits, to the fast exchange limit. The two sharp resonances in the extreme of the slow exchange limit (A) are seen to broaden and move together as the exchange rate increases towards the intermediate range (B to C) and finally these broad lines coalesce into a single peak (D). As the rate increases further, this line sharpens up until it appears as a narrow singlet in the extreme of the fast exchange limit (E). The terms slow and fast exchange are frequently encountered in relation to chemical shifts and/or nuclear relaxation times (115,116), and the interpretation of NMR results must always take into account the existing exchange rates.

### D. Laser Photochemical Induced Dynamic Nuclear Polarization

#### - CIDNP

This effect is generated by the cyclic reaction of a photo-excited dye with certain amino acid residues which are accessible to the dye. Polarisation has been observed with tyrosine, histidine, and tryptophan (117). The polarisation of tyrosine in the presence of a flavin dye arises from the reversible hydrogen atom transfer from the phenolic OH of tyrosine (TyrH) to the photo-excited dye (F)(117). The flavin triplet is the reactive intermediate; the reactions can

be written as follows:



CIDNP (indicated by \*) is generated in a spin-selective recombination of a radical pair, as indicated in reaction (3). Reactions (1) to (3) constitute a cyclic process such that almost no net reaction occurs, although reaction (4) causes some bleaching of the dye.

The FID is first acquired on a solution containing the protein, and a dye in low concentration; this is termed the "dark" spectrum. The dye is then irradiated by an argon laser and a FID is acquired on the irradiated sample; this is termed the "light" spectrum. Alternating "light" and "dark" free induction decays are collected in a series of acquisitions, and then all of the "dark" FID's are added together and all of the "light" FID's are added together. The total "dark" spectrum is then subtracted from the total "light" spectrum to generate the pure CIDNP spectrum. The sign of this difference spectrum (absorption or emission) is a function of the nature of the radicals involved and can be

predicted (118).

The amino acid side chain must be accessible to the dye, and therefore to the solvent, for a CIDNP effect to be observed. This method thus distinguishes between exposed and buried groups and yields valuable information on the solution structure of proteins. In addition, it does not perturb the system in any way as there is essentially no net reaction, which is a distinct advantage for any technique.

#### E. Spin Decoupling

In order to simply explain the theory behind this technique, we will take tyrosine as a sample case, and focus on the 2,3 proton pair. A proton has a nuclear spin of  $1/2$  which allows it to have two spin states in the presence of an applied magnetic field. The spin states of protons on adjacent carbon atoms can interact, and it is these interactions which produce the multiplet nature of the resonances observed with NMR. The number of lines in a multiplet follows the  $n + 1$  rule where  $n$  is the number of adjacent protons. Both the 2 and 3 protons in tyrosine are adjacent to a single proton (3 and 2 respectively) and they appear as a doublet (2 lines) in a typical spectrum. In essence, the proton 3 can "feel" the two spin states of the proton 2 and interacts with each state in a different manner; proton 3 is said to be "spin-coupled" to proton 2.



If a rf field is applied directly at the spectral frequency of the resonance of proton 2, it absorbs this energy and its two spin states will rapidly interconvert. This results in both the loss of the resonance of proton 2, and the collapse of the doublet resonance of proton 3 to a singlet (one line) as proton 3 can no longer "feel" the two unique spin states of proton 2; proton 3 is said to be "spin-decoupled." Structure elucidation by this technique involves the irradiation of one proton resonance and the observation of the collapse of multiplet structure for the other resonances in the spectrum to which the irradiated proton is spin-coupled.

### III. EXPERIMENTAL PROCEDURES

#### A. Minimization of Metal Ion Contamination

##### Preparation of Plasticized Glassware

The items to be treated were soaked in 2% dimethyldichlorosilane (Sigma,  $[\text{CH}_3]_2[\text{Cl}]_2\text{silane}$ ) for 15 minutes and then soaked in a large volume of double distilled water. The items were then removed and washed extensively with double distilled water and dried at room temperature prior to use. Collection and storage of metal-free  $\text{D}_2\text{O}$ , buffer, and protein solutions in treated glassware showed none of the trace metal ions contamination which was evident with the similar use of plastic containers.

##### Dithizone Treatment

About 20 ml of solution was placed in a 30 ml separating funnel which had been washed well with double distilled water, followed by spectral grade  $\text{CCl}_4$ . The solution was then extracted 3 to 4 times with 5 ml of 0.001% dithizone in  $\text{CCl}_4$ , until the last two organic extraction phases remained green. The dithizone solution was dark green and was stored in the dark at  $4^\circ\text{C}$ . Up to 20 micromolar metal ion contamination has been observed in the treated solutions.

### Chelex Treatment

Approximately 1 ml of Chelex-100 (Bio-Rad) was measured out in double distilled water and then filtered on a buchner funnel for one hour over bench vacuum. Then 2 ml of D<sub>2</sub>O were added to the chelex and the capped vial was left overnight at room temperature. The suspension was filtered for about 10 sec on a buchner funnel and two more mls of D<sub>2</sub>O were added. This suspension was left sitting overnight at room temperature or at 37°C for one hour. The last step was then repeated. The resulting suspension was agitated and 200  $\mu$ l was removed and filtered for about 10 seconds on a buchner funnel before it was added to 10 ml of D<sub>2</sub>O or deuterated buffer. The resulting solution was left overnight at room temperature prior to use.

### B. Preparation of the Proteins and Peptides

#### Preparation of the Peptides

##### N<sup>α</sup>-Acetyl-L-Aspartic Acid

Ac-Asp was purchased from Sigma and was used without further purification.

##### N<sup>α</sup>-Acetyl-L-Aspartyl-L-Glycyl-L-Aspartylamide

Ac-DGD-amide was synthesized by stepwise solid-phase peptide synthesis on a Beckman 990 peptide synthesizer. All amino acids were protected at the  $\alpha$ -amino position with Boc-groups and the aspartic acid

side chain was protected with a benzyl group. The program used for the attachment of each amino acid, the picrate monitoring method, the acetylation procedure for the N-terminus of the peptide, and the HF peptide cleavage conditions were as previously described (119). The C-terminal amide was obtained directly by HF cleavage of the peptide from a benzhydrylamine polystyrene, 2% divinylbenzene support (Protein Research Foundation, Japan). The purity of the cleaved product was verified by high voltage paper electrophoresis at pH 6.5 prior to acetylation of the N-terminus when ninhydrin detection was possible. The N<sup>α</sup>-acetylated product showed a single sharp peak on high pressure liquid chromatography (HPLC) on a SynChropak RP-P reverse-phase column (4.1 mm X 25 cm) in 0.1% trifluoroacetic acid/H<sub>2</sub>O. The composition and concentration of the pure peptide stock solution was verified by amino acid analysis: Asp (2.05), Gly (0.95). The <sup>1</sup>H NMR spectrum was consistent with the given structure.

#### **Preparation of the DTNB Light Chains of Rabbit Skeletal Muscle**

Myosin was prepared from frozen rabbit muscle (Pel-Freez Biologicals, Inc.) by the method of Weeds and Hartley (120); in some preparations batchwise treatment with DEAE-sephadex A-50 was used to remove ribonucleoprotein. The resulting myosin solution (10-15 mg/ml) was dialyzed against

0.5M KCl, 10 mM EDTA, 5mM EGTA, pH 8.5 and then against the same buffer without EGTA. The DTNB light chains were then isolated according to the method of Weeds and Lowey (121). The lyophilized residue was dialyzed against 0.5M KCl, 10 mM EDTA, pH 7.8 (122) until all of the excess DTNB was gone, and then dialyzed exhaustively against the same buffer plus 10 mM 2-mercaptoethanol to unblock the thiols of the light chains. The entire preparation was carried out at 4°C and the protein was stored at 0°C in the lyophilized form. The buffers were prepared by weight of their constituents and were not pre-treated prior to use.

#### Preparation of Bovine Brain S100b

S100b protein was prepared and purified by Dr. R. Mani (Department of Biochemistry, University of Alberta) from bovine brain as previously described (123,124). S100b protein used in the present study was homogeneous according to previous criteria (123,124), including PAGE in the presence and absence of SDS, and the absence of tyryptophan, as revealed by ultraviolet absorption and derivative spectra.

#### Preparation of Porcine Intestinal Calcium Binding Protein

Porcine intestinal CaBP was purified from the mucosa of the duodenum and the jejunum by Ms. M. Kawakami and Mr. J. D. J. O'Neil (The University of Toronto) as described previously (124,125). It was of high purity as judged by the absence of histidine, half cystine, methionine, and

tryptophan upon amino acid analysis. The protein, as isolated, was judged to be calcium-saturated by comparison of its  $^1\text{H}$  NMR spectrum with that of the desalted protein after addition of excess calcium, and especially by the presence of non-exchangeable NH resonances even after the protein was dissolved in  $\text{D}_2\text{O}$  for several days; these resonances disappear when the apo protein is dissolved in  $\text{D}_2\text{O}$ . The protein was desalted using the following procedure. 1) A four ml solution of 2 mg/ml of ICaBP was made up in 10 mM Tris, 150 mM NaCl, 10 mM EDTA, pH 8.5 and let set a minimum of one hour at  $4^\circ\text{C}$ . It was then passed down a G-25 medium Sephadex column (34 X 2.2 cm; Pharmacia) over Chelex (2 X 2.2 cm; Bio-Rad, 100-200 mesh) in the same buffer without EDTA (125); the flow rate was c.a. 0.7 ml/min and the Tris buffer used was pretreated by running it down a chelex 100 column (25 X 4.5 cm; 100-200 mesh). The eluted protein was then freeze dried and made up to 4ml with double distilled, demineralized water. This sample was immediately passed down a G-25 medium (16 X 1.5 cm) over G-25 course (69 X 1.5 cm) over chelex (7 X 1.5 cm) column in the same water; the flow rate was c.a. 0.2-0.6 ml/min. All of the columns used for desalting were run at  $4^\circ\text{C}$ . The eluted protein (referred to as the apo protein hereafter) was then freeze dried and lyophilized once from  $\text{D}_2\text{O}$ .

## C. Preparation of Stock Metal Ion Solutions

### Calcium Stock Solutions

#### Rabbit Skeletal DTNB Light Chains

To allow for a greater range of added calcium in this particular titration, three calcium stock solutions (0.9 M, 0.11 M, and 0.06 M) were prepared from  $\text{CaCl}_2$  directly as purchased (Merck, Sharpe, and Dohme) and the final concentrations were determined by titration with EDTA (126) in 0.1M NaOH, using murexide as the indicator.

#### Bovine Brain S100b

Stock calcium solutions were prepared from anhydrous  $\text{CaCl}_2$  by weight in the same buffer as the protein samples. The final concentrations were determined by titration with EDTA (126) in 0.1 M NaOH, using murexide as the indicator, and by atomic absorption spectrophotometry. The total volume change over the  $\text{Ca}^{2+}/\text{K}^+$  titrations was 4%.

#### Porcine Intestinal Calcium Binding Protein

Stock calcium solutions were prepared from  $\text{CaCl}_2$  (anhydrous) or  $\text{CaCl}_2 \cdot 2\text{H}_2\text{O}$  by weight and the final concentrations were determined by titration with EDTA (126) in 0.1 M NaOH, using murexide as the indicator, and by atomic absorption spectrophotometry. The

solutions were made up in the same buffer as the protein, treated with dithizone or chelex, and the pH was readjusted to the original buffer pH. The final calcium ion concentrations in the sample were determined from the atomic absorption results for the standard calcium solution used for the titration. The result was 35.1 ppm (35.0 mM). The results for the  $^1\text{H}$  NMR sample itself after titration were slightly low ( $\approx 19\%$ ), possibly due to protein interference. The total volume change over the calcium titration was 2%.

#### Lanthanide Stock Solutions

##### Peptide Titrations

The stock solutions used in the Ac-Asp titrations were made up from the lanthanide chlorides (Alpha Inorganics) directly by the addition of ca. 1 ml of  $\text{D}_2\text{O}$ . The  $\text{Er}^{3+}$  and  $\text{Dy}^{3+}$  solutions did not dissolve readily so the pH was increased slowly until dissolution occurred. The resulting clear solutions were made up to a final volume of 2 ml, the pH was adjusted to 6.5, and the solutions were filtered through cotton wool. The final concentrations of each stock solution were determined by titration with EDTA (126) in pH 6.0 MES buffer, using xylenol orange as the indicator and were ca. 250 mM (except for  $\text{YbCl}_3$ , which was 22 mM).



The stock solutions for the Ac-DGD-amide titrations were made from the lanthanide oxides (Alpha Inorganics) via treatment with hot HCl in double distilled H<sub>2</sub>O. The dissolved oxide solution was filtered through a millipore filter, dithionated, and rotovapped to dryness. The residue was lyophilized from D<sub>2</sub>O overnight and then made up to volume in 30 mM imidazole-d<sub>4</sub>, 20 mM KCl, pH 6.5 buffer which had been previously dithionated. The pH was adjusted to ca. 5.8, the solution was filtered again, and the final lanthanide concentration was determined as outlined above.

The only problem with these studies was that there was a great deal of water present in some of the samples, resulting in a large HDO resonance in the <sup>1</sup>H NMR spectra; the size of this resonance increased as the sample was titrated with the lanthanide and this HDO resonance obscured several of the LSR in the resulting spectra. It was apparent that lyophilization of the lanthanide standards, prior to their being made up again in D<sub>2</sub>O, was not effective in removing the water coordinated to them; the lanthanide chlorides are very hygroscopic and pick up water readily. Towards the end of this project (the Lu<sup>3+</sup> titration of Ac-DGD-amide), it was found that heating the lanthanide chlorides overnight under vacuum (pump) at high temperature (80° C) was a much more efficient and a much easier (due to the tendency of the stock solutions to bump when they were lyophilized)

method of drying them.

#### Rabbit Skeletal DTNB Light Chains

The  $\text{LaCl}_3$  stock solution was made up in double distilled water, the other lanthanide stock solutions were made up in the CD buffer; they were all ca. 1 M in concentration. All the lanthanide stock solutions were prepared directly from the chlorides as purchased (Alpha Inorganics) and their concentrations were determined by titration with EDTA (126) in 0.1M MES, pH 6.0 using xylenol orange as the indicator.

#### Porcine Intestinal Calcium Binding Protein

Stock  $\text{YbCl}_3$  (Alpha Division) solutions were prepared by weight and the final concentrations were determined by titration with EDTA (126) in 0.1M MES, pH 6.0 using xylenol orange as the indicator. The solutions were made up in the same buffer as the protein, treated with dithizone, and the pH was readjusted to a final pH of 6.5.

#### EDTA Binding Studies

Stock calcium solutions were prepared from anhydrous  $\text{CaCl}_2$  by weight in the same buffer as the protein samples. The final concentrations were determined by titration with EDTA (126) in 0.1 M NaOH, using murexide as the indicator, and by atomic absorption spectrophotometry.

## D. The Determination of $\text{Ca}^{2+}$ and Lanthanide Concentrations

### Calcium Titrations

To 1 ml of double distilled water was added 25  $\mu\text{l}$  of a 0.1 M neutral stock solution, with stirring. Immediately prior to titration, 11  $\mu\text{l}$  of 1.0 M NaOH was added, followed by one drop of a stock solution of murexide (a fresh solution of 2 mg of murexide in 10 ml double distilled water). The resulting solution was immediately titrated from red to violet, with stirring. The pH of the solution after the addition of NaOH should be 13. The titrant solution was 30 mM EDTA (126) in double distilled water.

### Lanthanide Titrations

To one ml of 100 mM MES, pH 6.0 is added 5  $\mu\text{l}$  of a 1.0 M lanthanide stock solution, with stirring. Then 1 drop of 0.05% xylenol orange is added and the resulting solution titrated with 100 mM MES, 30 mM EDTA (126), pH 6.0.

### E. pH Measurements

The pH measurements were made with an Ingold microelectrode (model 6030-04) or a Radiometer electrode (model GK2321C) attached to a Beckman Expandomatic SS-2 or a radiometer PHM62 pH meter; the pH values quoted are those observed and are not corrected for the deuterium isotope effect on the glass electrode (these values are cited as pH or pD). Electrode standardization was achieved prior to each

measurement using Fisher standard buffers 4, 7, and 10. pH adjustments were made by the addition of small aliquots of DCl and/or chelexed NaOD. The sample pH was measured immediately prior to acquisition, and the samples were equilibrated 10 to 15 minutes prior to acquisition. Values above pH 11 were not corrected for Na<sup>+</sup> interference and thus cannot be considered more accurate than  $\pm 0.2$  pH units (127). pH adjustments were made by addition of small volumes of di-thionized DCl and/or chelexed NaOD (0.5M). The sample pH was measured immediately prior to the accumulation of spectra. The total volume change during the pH titrations of ICaBP was 12%. The total volume change over the S100b titrations was 11-20 %, primarily due to loss of sample on the electrode. The pH values for the extraction and reaction buffers employed to prepare the DTNB LC are cited at 4°C. The electrode was soaked in saturated KCl at this same temperature for 15 to 20 minutes prior to the pH measurements. The double distilled water used to wash the electrode, the HCl and KOH solutions used to adjust the pH, and the buffer being adjusted were all cooled to this same temperature prior to adjustment.

#### F. Amino Acid Analysis

A small aliquot of protein solution was lyophilized in a test tube which had been fired by heating at 150°C for more than five hours. (A small aliquot of norleucine standard was first added to the protein solution in the DTNB LC

determinations). Then 6N HCl-1% phenol was added, the tube was vacuum sealed and then heated for 24 hours at 110° C. The seal was broken, the HCl was pumped off, and amino acid analysis was performed as usual. The results for each DTNB LC sample were normalized by the norleucine content and the concentrations determined using the known amino acid content of the DTNB LC. Four separate aliquots of this sample were run, along with two standard solutions. The amino acid contents of the DTNB LC were determined by taking the total nmoles in the output and dividing them by the total number of amino acids in the DTNB LC. This gave the average number of nmoles/amino acid. The number of nmoles in the output for any one amino acid was then divided by this number to yield the amount of that particular amino acid.

#### G. SDS Polyacrylamide Gel Electrophoresis

The procedure adopted for SDS polyacrylamide gel electrophoresis has been cited in the literature (128). Protein samples with concentrations ranging from 0.5 to 1 mg/ml were made up in 50mM sodium phosphate buffer at pH 7, and then dialysed against this same buffer. After dialysis, SDS and 2-mercaptoethanol were added to the solutions to a final concentration of 1%, and they were heated at 37°C overnight (or at 50-60°C for one hour). After cooling, one drop of 0.5% bromophenol blue in 0.1M phosphate buffer and one drop of 80% glycerol were added. Then 10 to 60  $\mu$ l of the resulting solution were applied to a 10%, 100 mm vertical slab gel

(Bio-Rad apparatus) and run at 50 mA (40V) for several hours. The gels were fixed for a minimum of 30 minutes in 50% methanol, 10% acetic acid and stained for one hour in 0.5% Commassie Brilliant Blue, dissolved in the same solvent. The gels were destained in three steps, the first was for 15 to 20 minutes in the methanol:acetic acid solution above, and then destained overnight in 10% methanol, 10% acetic acid, and once again in a fresh aliquot of this latter solution until the gels were clear. The three standard proteins were cardiac tropomyosin, soybean trypsin inhibitor, and lysozyme. The Rf values for each of the four proteins were determined using densitometry.

#### H. Ultraviolet Spectrophotometry

Protein concentrations were routinely determined using cell with a path length of 1 cm. The following extinction coefficients were employed: myosin,  $\epsilon_{280}^{1\%} = 5.6$  in 0.5M KCl (120, 121); DTNB LC,  $\epsilon_{280}^{1\%} = 5.0$  in 0.5 M KCl (122); S100b,  $\epsilon_{278}^{1\%} = 2.4$  (123); ICaBP,  $\epsilon_{280}^{1\%} = 0.170$  and  $\epsilon_{278}^{1\%} = 0.190$  ml·mg<sup>-1</sup>·cm<sup>-1</sup> (26). The UV spectra of S100b and the DTNB LC were obtained on a Cary 118C recording spectrophotometer, while those the ICaBP protein were obtained on a Cary 14 recording spectrophotometer.

## I. Circular Dichroism

### Sample Preparation

#### Rabbit Skeletal DTNB Light Chains

For the CD spectra, the lyophilized protein was dialyzed at 4°C against 100 mM MOPS, 0.1M KCl, 1mM EDTA, 10 mM  $\beta$ -mercaptoethanol, pH 7.25, and then against 100 mM MOPS, 50 mM KCl, 1 mM EGTA, pH 7.25 until equilibrated. The protein concentrations were 48 to 61  $\mu$ M, and were verified by amino acid analysis.

### Data Acquisition Parameters

#### Rabbit Skeletal DTNB Light Chains

The CD spectra were measured at room temperature on a Cary Model 60 spectropolarimeter with a CD accessory. The results are expressed as molar ellipticity ( $[\theta]$ ) in  $\text{deg}\cdot\text{cm}^2\cdot\text{dmol}^{-1}$  calculated using the equation  $[\theta] = \frac{\theta \cdot \text{MRW}}{10 \cdot c \cdot l}$  where MRW is the mean residue weight (based on a molecular weight of 19,000 and a sequence of 169 amino acids for the DTNB light chain)  $\theta$  is the observed ellipticity, in degrees,  $l$  is the path length = 0.0501 cm, and  $c$  is the concentration of the protein in grams/ml. The experiments were carried out at room temperature and the sample volumes were 750 to 850  $\mu$ l.

### Porcine Intestinal Calcium Binding Protein

The CD spectra were measured at room temperature on a J-500 spectropolarimeter (Japan Spectroscopic Co.) equipped with a built-in data processor. The spectra were signal averaged eight times to reduce noise. The results are expressed as molar ellipticity ( $[\theta]$ ) in  $\text{deg}\cdot\text{cm}^2\cdot\text{dmole}^{-1}$  calculated using the equation  $[\theta] = \frac{100\cdot\theta}{c\cdot l}$  where  $c$  is the molar protein concentration,  $l$  is the path length in centimetres, and  $\theta$  is the observed ellipticity in degrees.

## J. Nuclear Magnetic Resonance

### Sample Preparation

#### Peptide Samples

##### *N<sup>α</sup>-Acetyl-L-Aspartic Acid*

A stock solution of Ac-Asp was prepared in  $\text{D}_2\text{O}$  and the pH adjusted to 6.50 with NaOD. Suitable dilutions of this stock were used to give a final sample concentration of 2 mM peptide in  $\text{D}_2\text{O}$ ; the final sample volume was 500  $\mu\text{l}$ . Each sample was made up to 0.5 mM DSS and the final pH was 6.5 prior to titration.

##### *N<sup>α</sup>-Acetyl-L-Aspartyl-L-Glycyl-L-Aspartylamide*



Aliquots of a stock solution of Ac-DGD-amide in  $D_2O$ , whose concentration was determined by amino acid analysis, were diluted in separate vials such that the final peptide concentration would be ca. 2 mM. The diluted samples were lyophilized and made up to volume in 30 mM imidazole-d, (Merck Sharp and Dohme), 20 mM KCl, pH 6.5 buffer in  $D_2O$  which had been previously treated with dithizone; the exact concentration of each sample was determined by amino acid analysis, and the sample volume ranged from 350 to 400  $\mu$ l.

#### Protein Samples

##### Rabbit Skeletal DTNB Light Chain

For the NMR spectra, the sample was dialyzed against 10 mM Tris, 0.1M KCl, 1 mM EDTA, 10 mM 2-mercaptoethanol, pH 7.5, and then again against 10 mM Tris, 60 mM KCl, pH 7.5. The dialysate was lyophilized, made up to 250  $\mu$ l with distilled water, and dialyzed again against 10 mM Tris, 50 mM KCl, pH 7.5. The final sample volume was determined by measuring the height of this sample in a 5mm NMR tube, then the sample was quantitatively removed and lyophilized. Two ml of  $D_2O$  were added to the dried protein and it was lyophilized once more. This freeze-dried protein was made up to volume in  $D_2O$  in the same NMR tube mentioned above and was left

standing overnight at 4°C; the final pD of the sample, measured immediately prior to acquisition, was 7.8 and did not change over the course of the calcium titration.

#### Bovine Brain S100b

The protein solutions were dialyzed against 10 mM Tris, pH 7.5 or 8.5 in the presence of EDTA, and then subjected to exhaustive dialysis against the same buffer in the absence of EDTA (5). The solution was then lyophilized to dryness, and lyophilized once again from 1-2 mls of dithionated D<sub>2</sub>O. The sample was then made up to volume with dithionated D<sub>2</sub>O; protein concentrations were 0.1 to 0.5 mM.

#### Porcine ICaBP

The protein solutions were made up to volume in 30 mM imidazole-d. (Merck Sharp and Dohme), 20 mM KCl, pH 6.5; the concentration of ICaBP was ca. 0.5 mM. The only exception was for the CIDNP experiments for which the buffer was 10 mM Tris, 40 mM KCl, pH 7.5, where the concentration of ICaBP was ca. 0.6 mM. Both NMR buffers were pretreated with dithione to remove contaminating metal ions. The concentration of the sample used in the calcium titration was determined by UV spectrophotometry and verified by amino acid analysis. A typical sample size was 350 μL.

The initial experiments performed on this protein were those involving the addition of  $\text{Yb}^{3+}$  to the protein. In these experiments we took the protein as received and dialyzed it against  $\text{H}_2\text{O}$ . It was then freeze-dried and made up to volume in the buffer outlined above. The  $^1\text{H}$  NMR spectra of these samples prior to the addition of  $\text{Yb}^{3+}$  indicated that the protein was calcium-saturated and that there was some imidazole present.

#### Standard Molecules

##### EDTA

A suitable quantity of  $\text{Na}_2\text{EDTA}$  was weighed out and placed in a preheated plasticized vial. The sample was then heated at  $80^\circ\text{C}$  overnight under a bench vacuum. The sample was removed, covered with a filter paper, and allowed to cool in a dessicator over drierite. The cooled sample was capped and reweighed to obtain a final determination of the solid EDTA content. The resulting solid was made up to volume in chelexed buffer. The loss in weight of the EDTA after heat treatment was 16 to 19%. This procedure is a modification of that employed to prepare the EDTA standards used to titrate the stock metal ion solutions (126).

### Acquisition Parameters

The NMR spectra were obtained using a Bruker HXS-270 NMR spectrometer operating in the Fourier transform mode and equipped with quadrature detection. The ambient temperature for the samples was 299°K, unless otherwise stated, and all of the samples were equilibrated 10-15 minutes prior to acquisition. The H<sub>2</sub>O resonance was suppressed with homonuclear decoupling. Chemical shift values are relative to the major resonance of DSS as an internal or external standard.

### Peptide Studies

The parameters used for the Ac-Asp spectra were 4K data points (8K for Lu<sup>3+</sup>); sweep width ±1000 (Lu<sup>3+</sup>), ±3164 (Yb<sup>3+</sup>), ±8064 (Tm<sup>3+</sup>, Er<sup>3+</sup>, Ho<sup>3+</sup>), ±25,000 (Dy<sup>3+</sup>); 7 μsec pulse (ca. 70°). The delay times between acquisitions were 250 μsec (Yb<sup>3+</sup>, Lu<sup>3+</sup>), 100 msec (Dy<sup>3+</sup>), and 500 msec (Tm<sup>3+</sup>, Er<sup>3+</sup>, Ho<sup>3+</sup>). The parameters for the Ac-DGD-amide spectra were 4K data points (8K for Lu<sup>3+</sup>); sweep width ±1000 (Lu<sup>3+</sup>), ±3166 (Yb<sup>3+</sup>), ±6329 (Ho<sup>3+</sup>, Tm<sup>3+</sup>, Er<sup>3+</sup>), ±15,152 (Dy<sup>3+</sup>); filter width=2x sweep width (Butterworth); 8 μsec pulse (ca. 80°). The delay time between acquisitions was 250 μsec for all of the titrations. DSS was used as an internal standard.

### DTNB LC Studies

The acquisition parameters were 4K data points, sweep width ±2300 Hz, filter width 2500 Hz (Butterworth), and 8 μsec pulse length (ca. 80°). DSS was used

as an internal standard.

#### 9100b Studies

The parameters used for the spectra were typically 4K data points, sweep width  $\pm 2300$  Hz, filter width 5000 Hz (Bessel), 8  $\mu$ sec rf pulse ( $80^\circ$ ). The HDO resonance, was suppressed with homonuclear decoupling. Chemical shift values are relative to the major resonance of DSS, which was measured separately. During the pH titration (pH 5.6 to 8.5), the histidine resonances were isolated from the rest of the spectrum using the Hahn Spin Echo Pulse Sequence (129).

#### ICABP Studies

The decoupling experiment for the calcium-saturated protein was carried out at 333°K. The parameters used for the spectra were typically 4K data points, sweep width  $\pm 2300$  Hz, filter width 2500 Hz (Butterworth) or 5000 Hz (Bessel), 8  $\mu$ sec pulse ( $\approx 80^\circ$ ). For the ytterbium spectra, the sweep widths were typically changed to  $\pm 20,000$  Hz and the filter width to 40,000 Hz, and the pulse width to 7  $\mu$ sec ( $\approx 70^\circ$ ). The pulse response of the Bessel filters in the spectra of the ytterbium-substituted protein produced a rolling baseline which made presentation of the very broad lanthanide-shifted resonances difficult. Consequently, a baseline correction was made to these spectra by fitting the baseline to a polynomial of the type

$$y = A + T(x) + W(x)^2 + U(x)^3$$

and subtracting this from the spectrum. Chemical shift values are relative to the major resonance of DSS, which was measured separately under identical conditions (30 mM imidazole-d<sub>4</sub>, 20 mM KCl, pH 6.5). For the spectra which are resolution enhanced, the FID was apodized by double exponential multiplication (DM = 4.0).

#### EDTA Studies

The parameters used for the spectra of EDTA were typically 4K data points, sweep width ±2300 Hz, filter width 2500 Hz (Butterworth), 8 μsec pulse (=80°). Chemical shift values are relative to the major resonance of DSS, which was measured separately in 30 mM imidazole-d<sub>4</sub>, 20 mM KCl, pH 6.5.

### K. Calculations and Theoretical Determinations

#### Determination of α-Helix, β-Sheet, and β-Turn Content for Rabbit Skeletal DTNB Light Chain

##### Theoretical

The sequence of the protein was analysed in four residue segments contents using published probability parameters (130). The resulting averaged probabilities for each of the three possible structural types were plotted. The portions of the sequence which showed the

highest probabilities of each of the three types were then analyzed carefully for single residues and/or linear sequences which showed  $\beta$ -sheet,  $\beta$ -turn, and helix-breaker sequences. Any segments which had significant breaking capacity were then eliminated, and the remaining sequence regions became the maximum theoretical determinations for  $\alpha$ -helix. These same regions were then analyzed in the same manner using hydrophobic probability parameters (132) in order to better define the helix boundaries, and to obtain a minimum theoretical  $\alpha$ -helix content.

#### Observed

The observed %  $\alpha$ -helix values were determined by CD using from the known ellipticities at 210, 215, and 220 nm and published values for the  $\alpha$ -helix,  $\beta$ -sheet, and  $\beta$ -turn ellipticities at these wavelengths (132). We assumed that the fractions of all three types of these structures added up to 1, solved two simultaneous equations for each possible pair of wavelengths, and averaged the three resulting determinations.

#### L. Laser Photochemical Induced Dynamic Nuclear Polarization

##### - CIDNP

Laser photo CIDNP experiments were performed by utilizing a Spectra Physics, Model 164 argon ion laser operating at 3.2 W in the multiline mode; 10 mm o.d. flat-bottomed NMR tubes were used. The sample was irradiated for 1s, the laser

beam being directed into the bottom of the sample via a computer-controlled shutter and mirror (29). The buffer was 10 mM Tris-HCl, pH 7.5. The [FMN]<sub>0</sub> for the apo protein was 0.19 mM and it was 0.39 mM for the calcium-saturated protein experiment. The sample volume was 1.2 ml. The [S100b]<sub>0</sub> was ≈0.4 mM, and the [ICaBP]<sub>0</sub> was 0.57 mM. The [Ca<sup>2+</sup>]<sub>0</sub>/[protein]<sub>0</sub> was 9.17 and 4.91 respectively for the CIDNP experiments on the calcium-saturated proteins.



#### IV. CONTACT AND DIPOLAR CONTRIBUTIONS TO LANTHANIDE INDUCED NMR SHIFTS OF AMINO ACID AND PEPTIDE MODELS FOR CALCIUM BINDING SITES IN PROTEINS

##### A. Introduction

As outlined in Chapter II, the interpretation of lanthanide induced shifts in terms of the structure of the metal-ligand complex relies on the separation of the LIS into its two components. One component is the *contact* interaction (110-112), which involves electron delocalization through chemical bonds and thus gives no easily interpreted structural information. The second component is the *dipolar* interaction which is a "through-space" interaction, that depends upon the orientation of the nucleus with respect to the metal. The form of the dependence of the dipolar shift on the geometry of the nuclei in the metal complex is known (109-111, Chapter II) and can therefore be used to determine the three dimensional structure of residues in close proximity to the bound metal.

Several methods have been proposed for the separation of contact and dipolar shifts (84, 133-135) but most of them rely on the lanthanide-ligand complex observed being axially symmetric, which is not true for CaBP, or proteins in general (77, 78, 100, 102, 136). We show herein that, under certain conditions, the dipolar component of the LIS can be extracted from the total shift without prior knowledge of the symmetry of the complex or the orientation of the principle

axis system of the magnetic susceptibility tensor. The separation of the contact and dipolar components of the LIS in this study required the use of several lanthanide ions. When one is examining nuclei which are very close to or within the metal binding site of a protein or peptide, contact interactions can become significant. The lanthanide ions in the second half of the series ( $Dy^{3+}$  to  $Lu^{3+}$ ) were chosen because they theoretically should include those lanthanides which produce the largest dipolar shifts (109,137), the smallest contact/dipolar shift ratios (137), and for which the absolute value of the contact shift is small (112,137). An additional consideration in such studies, since one is observing nuclei which are in close proximity to the metal centre, is that the paramagnetic metal ion will result in the broadening of these resonances (97), as well as shifting. The lanthanide ions in the second half of the series generally display relatively greater amounts of line broadening than those in the first half of the series (96,138), but not so severe that most data can not be readily analyzed (99).

The calcium binding proteins use aspartic acid, asparagine, glutamic acid, glutamine, serine, threonine, and peptide backbone carbonyl groups as the primary liganding groups within their highly homologous binding sites (1). For this reason, we have chosen to study the binding of lanthanides to the blocked amino acid Ac-Asp and the blocked model peptide Ac-DGD-amide, in order to evaluate the

relative magnitudes of the contact and dipolar components of the observed LIS in calcium binding peptides and proteins, and to determine which lanthanide studied is the best calcium analogue for the study of the structure of calcium binding sites.

### B. Theory

The chemical shifts induced by a lanthanide ion (excluding  $\text{La}^{3+}$  and  $\text{Lu}^{3+}$  which are diamagnetic and are used as controls, and  $\text{Gd}^{3+}$  for which the magnetic susceptibility tensor is isotropic) are composed of two sources: the contact shift and the dipolar shift. The magnitude and direction of these shifts are dependent upon which lanthanide metal ion is used and which type of nucleus is being observed. The total paramagnetic shift is given by (135).

$$\Delta_m^{\text{obs},i} = A_m^i \langle S_z \rangle_m + G_1^i D_{1m} + G_2^i D_{2m} \quad (1)$$

where  $\Delta_m^{\text{obs},i}$  is the observed LIS for a nucleus  $i$  and lanthanide  $m$ ,  $A_m^i$  is the hyperfine coupling constant between the nucleus  $i$  and the unpaired electron spin,  $\langle S_z \rangle_m$  is the projection of the total electron spin magnetization for the lanthanide  $m$  in the direction of the external magnetic field,  $D_{1m}$  and  $D_{2m}$  are values derived from the magnetic susceptibility tensor of the bound lanthanide  $m$  (109, 136, 139), and  $G_1^i$  and  $G_2^i$  are the geometric factors

$$G_1^i = \frac{3\cos^2\theta_i - 1}{r_{im}^3}$$

and

$$G_2^i = \frac{\sin^2\theta_i \cos 2\phi_i}{r_{im}^3}$$

where  $r_{im}$  is the distance of nucleus  $i$  from the central ion  $m$ ,  $\theta_i$  is the angle between  $r_{im}$  and the principle axis of symmetry, and  $\phi_i$  is the angle between the projection of  $r_{im}$  on the  $xy$  plane and the  $x$  axis (Figure II.2). Assuming that  $^1\text{H}$  NMR shifts are primarily dipolar in origin, a graphical solution to equation 1 may be obtained by rearranging it in a suitable manner (133, 135) to give

$$\frac{\Delta_m^{\text{obs}, i}}{\langle S_z \rangle_m} = A_m^i + \frac{D_{1m} G_1^i}{\langle S_z \rangle_m} \left[ 1 + \frac{D_{2m}}{D_{1m}} \left( \frac{G_2^i}{G_1^i} \right) \right] \quad (2)$$

For the series of the five lanthanides from  $\text{Dy}^{3+}$  to  $\text{Yb}^{3+}$ , the theoretical values of  $D_{2m}/D_{1m}$  range from -0.64 to +0.56 (135). In addition, previous work has pointed out that the angular factors for small ligands are often such that  $|G_2^i/G_1^i|$  is small (e.g. if  $0 \leq \theta_i \leq 40^\circ$ ,  $1.3 \leq 3\cos^2\theta_i - 1 \leq 2.0$  and  $0 \leq \sin^2\theta_i \leq 0.4$ ) (102). Thus, although lanthanide complexes are often devoid of axial symmetry, we have analyzed our data for the two ligands Ac-Asp and Ac-DGD-amide under the assumption that these two factors combine to make the

non-axial term in equation 2 small, such that we can extract the dipolar component of the LIS from the observed total shift without prior knowledge of the symmetry of the complex or the orientation of the principal axis system of the magnetic susceptibility tensor. For each nucleus  $i$ ,  $\nu_m^{obs} / \langle S_z \rangle_m$  is plotted versus  $D_{i,m} / \langle S_z \rangle_m$  for a series of lanthanide metals using theoretical values of  $\langle S_z \rangle_m$  and  $D_{i,m}$  (Table IV.1) (135). This plot should yield a straight line with a slope of  $G_i$  and an intercept  $A_m$  if the theoretical numbers are valid and if the assumption outlined above is correct. Also, since one is observing a series of lanthanide ions bound to the same ligand, all of the resulting complexes must be isostructural. Only under these conditions does one have a constant orientation of the magnetic susceptibility tensor and constant values for the hyperfine coupling constant over the series of metal ions employed (135).

### C. Results

*N*<sup>α</sup>-Acetyl-L-Aspartic Acid; Ac-Asp was titrated with five paramagnetic lanthanides from the heavy end of the lanthanide series ( $Dy^{3+}$  to  $Yb^{3+}$ ) and with the diamagnetic lanthanide  $Lu^{3+}$ . The <sup>1</sup>H NMR spectra of the N-acetyl CH<sub>3</sub> protons, the αCH proton, and the two βCH<sub>2</sub> protons were all in the NMR fast exchange limit in the presence of the lanthanides, as evidenced by the fact that only one exchange averaged resonance was observed for each nucleus. The βCH<sub>2</sub> protons titrated as two distinct resonances, and were

Table IV.1

The Contact and Dipolar Parameters for the Analysis of LIS<sup>a</sup>

Ln <sup>b</sup>	$\langle S_z \rangle_m$	D <sub>1m</sub>	D <sub>2m</sub>
Yb	2.587 <sup>b</sup>	22 <sup>c</sup>	4.65 <sup>d</sup>
Tm	8.208	53	-33.97
Er	15.374	33	-3.77
Ho	22.545	-39	-13.64
Dy	31.818	-100	-55.73

<sup>a</sup>Table IV.1 taken from Ref. 135.<sup>b</sup>In units of  $\beta H_0/3kT$ , from Ref. 112.<sup>c</sup>Scaled to the value of Dy, from Ref. 109, 136.<sup>d</sup>Scaled to D = -100 for Dy, from Ref. 135.

arbitrarily designated the terms  $\beta A$  and  $\beta B$ ;  $\beta A$  was assigned to the  $\beta$  resonance which displayed the larger LIS, as outlined in Figure IV.1. The resonances were broadened and shifted in the presence of the lanthanide ion and the magnitude of the LIS increased as a function of increasing concentration of lanthanide until the ligand was saturated. The overlapping  $\beta CH_2$  resonances were resolved into  $\beta A$  and  $\beta B$  in the presence of lanthanide. A typical plot of the observed chemical shift of the  $\alpha CH$  proton as a function of the  $[M]_0/[L]_0$  ratio is shown in Figure IV.2A. The chemical shift titration curves all fit to theoretical curves assuming a metal to ligand stoichiometry of 1:1. Values for the dissociation constant  $K_d$  and the paramagnetic chemical shift ( $\Delta_m^{obs.}$ ) of each nucleus in the  $Ln^{3+}$ -(Ac-Asp) complex were determined by non-linear least squares curve fitting procedures. These values are listed in Table IV.2.

*N<sup>o</sup>-Acetyl-L-Aspartyl-L-glycyl-L-Aspartylamide*: Ac-DGD-amide was titrated with the same six lanthanide ions ( $Dy^{3+}$  to  $Lu^{3+}$ ) and again the NMR spectra of all four observable shifting aspartic acid protons were in the NMR fast exchange limit. The acetyl  $CH_3$  protons were observed as a distinct resonance, but the two  $\alpha CH$  protons titrated as a single resonance and the four  $\beta CH_2$  protons migrated as two distinct resonances. These two resonances were designated  $\beta A$  and  $\beta B$ ;

The paramagnetic shift values used in the analyses were obtained by subtracting the chemical shifts determined for the diamagnetic lanthanide  $Lu^{3+}$  from the chemical shifts determined for each of the other lanthanides.

Table IV.2

The  $\Delta_m^{obs.}$  and  $K_d$  Parameters for the Peptides

Ligand	Ln <sup>3+</sup>	$K_d^a$ (mM)	$\Delta_m^{obs.}$ (ppm)			
			$\alpha$ CH	acetyl	$\beta$ A	$\beta$ B
Ac-Asp	Yb	0.30	-3.1	+0.4	-10.7	-8.9
	Tm	0.21	+19.1	+3.8	-15.9	-10.3
	Er	0.23	+3.5	+1.2	-10.5	-7.7
	Ho	0.17	+13.9	-0.6	+26.6	+23.3
	Dy	0.15	-- <sup>b</sup>	-- <sup>b</sup>	+68.8	+62.0
Ac-DGD- amide (LM)	Yb	0.21 <sup>c</sup>	-3.1	+0.6	-5.9	-0.7
	Tm	--	-3.8	+1.3	-9.4	-0.7
	Er	--	-- <sup>b</sup>	+0.5	-2.9	0.0
	Ho	--	+5.5	-0.9	+11.5	+5.6
	Dy	0.15	+14.0	-1.8	+26.4	+15.6
Ac-DGD- amide (LM <sub>2</sub> )	Yb	7.45 <sup>c</sup>	-3.9	+0.7	-7.7	-1.2
	Tm	--	-4.7	+1.9	-13.1	-- <sup>b</sup>
	Er	--	-- <sup>b</sup>	+0.8	-5.5	0.0
	Ho	--	+9.1	-1.6	+20.1	+10.2
	Dy	7.58	+21.1	-2.5	+41.9	+23.3

<sup>a</sup>  $K_d$  represents the average value for all observable protons for a given lanthanide ion.

<sup>b</sup> This data could not be determined due to overlap with the HDQ resonance.

<sup>c</sup> Value observed for a single proton.



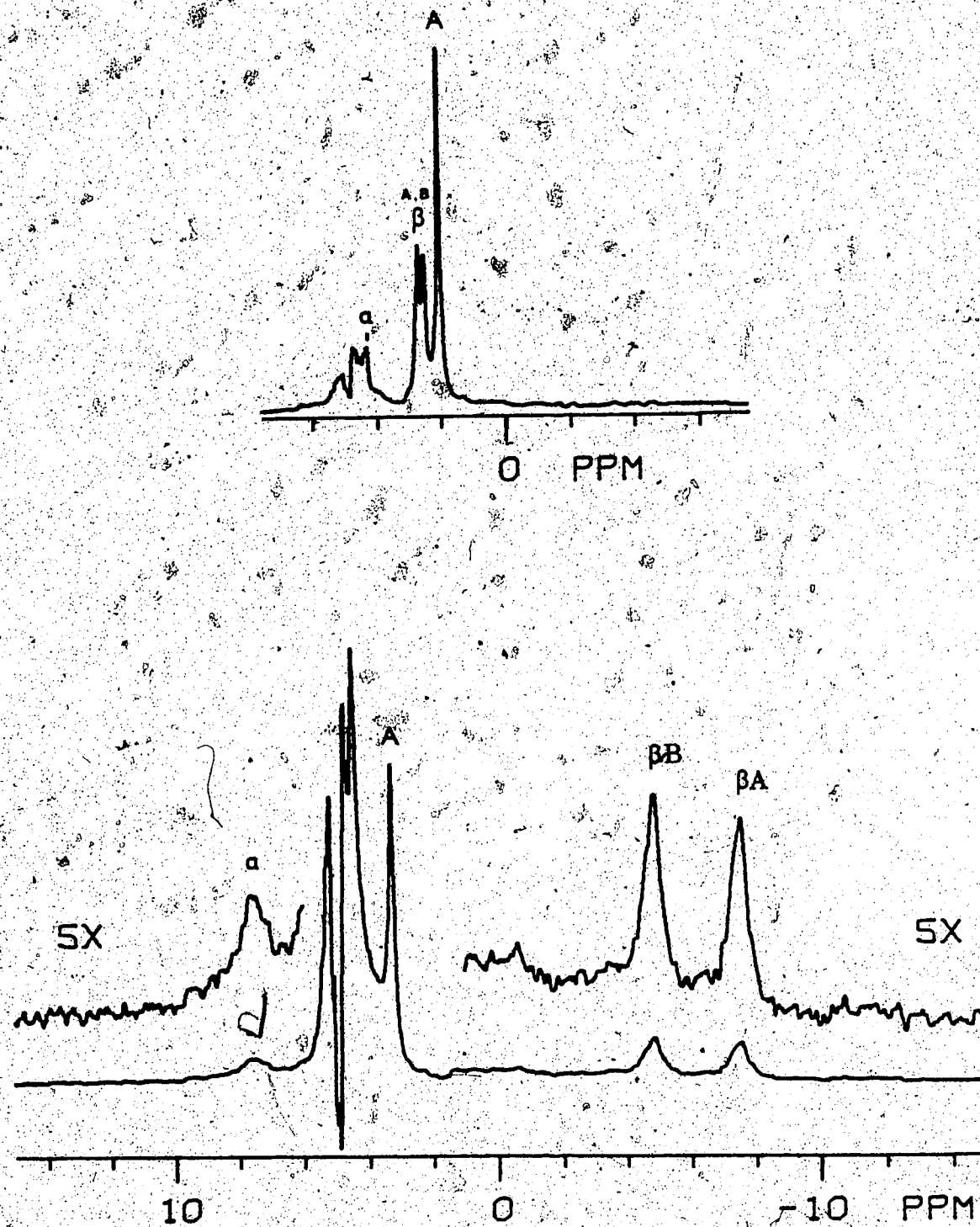


Figure IV.1. The <sup>1</sup>H NMR spectra of N<sup>α</sup>-Ac-Asp in the presence and absence of Er<sup>3+</sup>. The sample was 2 mM N<sup>α</sup>-Ac-Asp in D<sub>2</sub>O, pH 6.5. The symbols denote the following proton resonances: A, acetyl; α, αCH; β, BA, and BB, βCH<sub>2</sub>.  
 A. The spectrum in the absence of Er<sup>3+</sup>.  
 B. The spectrum in the presence of Er<sup>3+</sup>. The [Er<sup>3+</sup>]<sub>0</sub>/[amino acid]<sub>0</sub> ratio was 11.33.

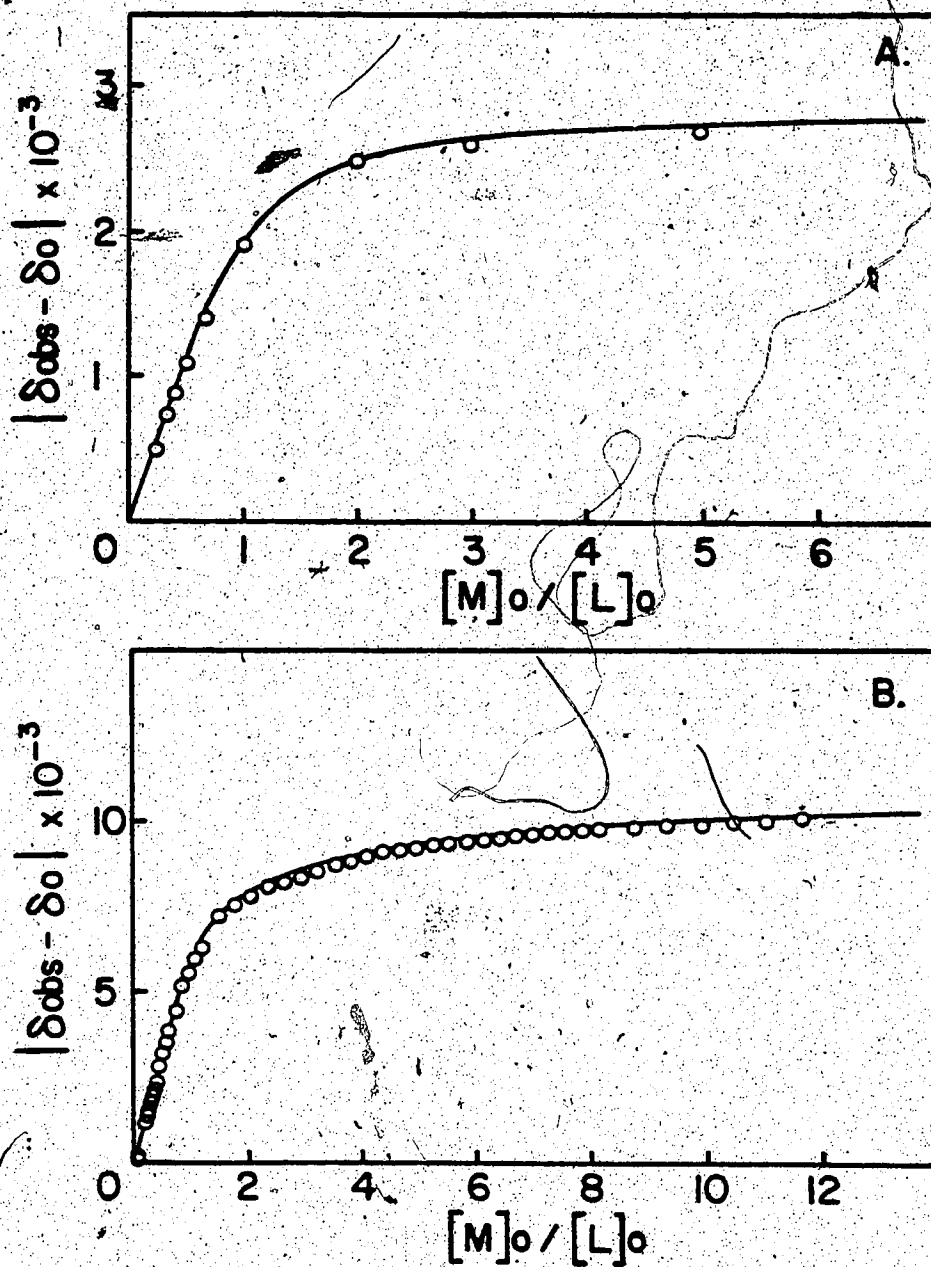


Figure IV.2 Plots of the absolute value of  $(\delta_{obs} - \delta_0)$  vs  $[M]_0/[L]_0$ , where  $\delta_{obs}$  is the observed LIS in ppm,  $\delta_0$  is the shift of the proton in the apoprotein, and  $[M]_0$  and  $[L]_0$  are the total lanthanide and peptide concentrations respectively.

A.  $^1H$  NMR chemical shift data for the titration of the  $\alpha$ CH proton of Ac-Asp with  $Yb^{3+}$ . The plotted curve is the best fit, assuming a metal:ligand stoichiometry of 1:1.

B.  $^1H$  NMR chemical shift data for the titration of the  $\beta$ B protons of Ac-DGD-amide with  $Dy^{3+}$ . The plotted curve is the best fit, assuming a final metal:ligand stoichiometry of 2:1.

$\beta$ A was assigned to the  $\beta$  resonance which displayed the larger LIS. The  $\alpha$ CH<sub>2</sub> protons of the glycine residue were not affected by the addition of lanthanide. A typical plot of the observed chemical shift as a function of  $[M]_0/[L]_0$  is shown in Figure IV.2B for one of the two observable  $\beta$ CH<sub>2</sub> resonances of aspartic acid. In these studies, the chemical shift titration data all fit to theoretical curves assuming a final metal to ligand stoichiometry of 2:1; the dissociation constants and chemical shift values were determined by non-linear least squares curve fitting procedures. Note that in this analysis one obtains a  $K_d$  and a LIS shift value for each of the two species LM and LM<sub>2</sub>, where L is the peptide ligand and M is the lanthanide metal ion. The determination of the  $K_d$  values in this case was much more difficult due to the multiparameter nature of the program. Good fits were obtained for all four protons of the Dy<sup>3+</sup> titration (one of the  $\beta$ CH<sub>2</sub> proton plots is shown in Figure IV.2B) and for the  $\alpha$ CH proton in the Yb<sup>3+</sup> titration. Since these five values were very close, and since previous work has indicated that the values of dissociation constants for simple ligands do not vary significantly across the lanthanide series (75, 104, 134), they were averaged and the resulting values  $K_{d1} = 0.16$  mM and  $K_{d2} = 7.56$  mM were inserted as constants into the same program to derive the values of the paramagnetic shift<sup>1</sup>

<sup>1</sup> Correction for the diamagnetic shift was carried out as stated previously for all the observed protons except the  $\beta$ CH<sub>2</sub> protons, which shifted so little in the presence of Lu<sup>3+</sup> that their separate shifting patterns could not be

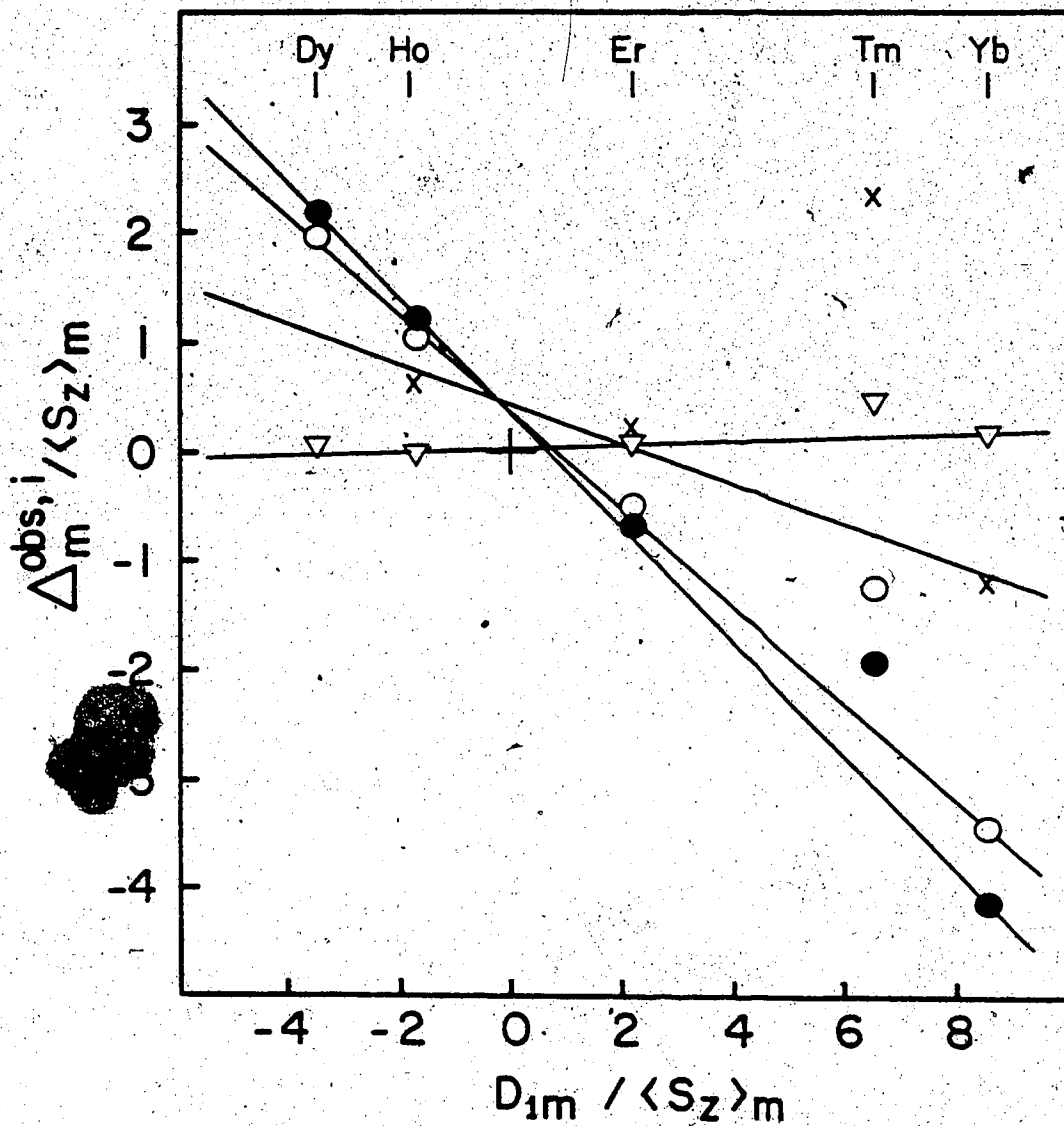


Figure IV.3 Plots of  $\Delta_m^{obs,i} / \langle S_z \rangle_m$  vs  $D_{1m} / \langle S_z \rangle_m$  for the four observable  $^1\text{H}$  NMR resonances of Ac-Asp. The shifted resonances are defined by the symbols x,  $\alpha\text{CH}$ ;  $\nabla$ ,  $\text{CH}_3$ ;  $\bullet$ ,  $\beta\text{A}$ ; and  $\circ$ ,  $\beta\text{B}$ . The titration solution consisted of 2 mM Ac-Asp in  $\text{D}_2\text{O}$ , pH 6.5.

for LM and LM<sub>2</sub> for the rest of the lanthanides studied. These values are shown in Table IV.2.

For both Ac-Asp and Ac-DGD-amide, the maximum LIS values thus obtained for the metal-ligand complex were then used in equation 2 to generate the plots shown in Figures IV.3, IV.4, and IV.5, using the  $\langle S_i \rangle_m$  and  $D_{i,m}$  values given in Table IV.1 (135). From the slopes and intercepts, the corresponding contact ( $\Delta_m^{c,i}$ ) and dipolar ( $\Delta_m^{d,i}$ ) values were calculated. Also, an agreement factor

$$AF = \sqrt{\frac{\sum_i (\delta_m^{obs,i} - \delta_m^{calc,i})^2}{\sum_i (\delta_m^{obs,i})^2}}$$

was calculated (133), where  $m$  is the rare earth metal ion and  $\delta_m^{calc,i}$  is the calculated chemical shift ( $\Delta_m^{c,i} + \Delta_m^{d,i}$ ). The observed and calculated parameters are given in Tables IV.2 to IV.6.

#### D. Discussion

Before looking at the final  $\Delta_m^{c,i}$  and  $\Delta_m^{d,i}$  values, it is necessary to cover the nature of the experiment and the subsequent  $K_d$  and LIS values derived from the data.

-----  
 (cont'd)isolated; the maximum possible shifts for Lu<sup>3+</sup> were, however, negligible compared to the shifts observed for the other lanthanides.

Table IV.3

Calculated Values for the Slopes and Intercepts  
of the plots  $\Delta_m^{obs.}/\langle S_z \rangle_m$  versus  $D_{1m}/\langle S_z \rangle_m$ .

Ligand	Proton	Slope	Intercept ( $A_m$ )
Ac-Asp <sup>a</sup>	$\alpha$ CH <sup>b</sup>	-0.18±0.03	0.43±0.17
	acetyl <sup>c</sup>	0.02±0.00	0.02±0.02
	$\beta$ A	-0.52±0.01	0.34±0.04
	$\beta$ B	-0.44±0.01	0.35±0.05
Ac-DGD <sup>d</sup> amide (LM)	$\alpha$ CH <sup>d,e</sup>	-0.14±0.00	0.00±0.00
	acetyl	0.02±0.00	0.00±0.01
	$\beta$ A	-0.25±0.03	0.18±0.14
	$\beta$ B	-0.06±0.01	0.23±0.05
Ac-DGD <sup>d</sup> amide (LM <sub>2</sub> )	$\alpha$ CH <sup>d,e</sup>	-0.19±0.00	0.08±0.00
	acetyl	0.03±0.00	0.01±0.01
	$\beta$ A	-0.35±0.03	0.32±0.14
	$\beta$ B <sup>e</sup>	-0.10±0.02	0.37±0.08

<sup>a</sup>The Tm<sup>3+</sup> data was excluded in the analysis.

<sup>b</sup>The  $\alpha$ CH proton was obscured by the HDO resonance during the Dy<sup>3+</sup> titration and was excluded from observation and analysis.

<sup>c</sup>The Dy<sup>3+</sup> titration of the acetyl peak was excluded from analysis as it was difficult to monitor this resonance due to the magnitude of the HDO peak and the large sweep width employed.

<sup>d</sup>The  $\alpha$ CH protons were obscured by the HDO resonance during the Er<sup>3+</sup> titration and were excluded from analysis.

<sup>e</sup>The Tm<sup>3+</sup> spectra became very complex towards the end of the titration and the  $\beta$ B proton became very difficult to monitor accurately, so it was excluded from analysis.

Table IV.4

The Calculated Contact and Dipolar Values for Ac-Asp

Ln <sup>3+</sup>	Proton	$\Delta_{m}^{c,i}$ (ppm)	$\Delta_{m}^{d,i}$ (ppm)	$\Delta_{m}^{c,i} + \Delta_{m}^{d,i}$ (ppm)	$\Delta_{m}^{c,i} / \Delta_{m}^{d,i}$	AF
Yb	$\alpha$ CH	1.1	- 4.0	- 2.9	-0.3	0.08
Tm	$\alpha$ CH	3.6	- 9.5	- 6.0	-0.4	
Er	$\alpha$ CH	6.7	- 5.9	+ 0.7	-1.1	
Ho	$\alpha$ CH	9.8	+ 7.0	+16.8	+1.4	
Dy	$\alpha$ CH	12.4	+18.0	+30.4	+0.7	
Yb	acetyl	0.1	+ 0.4	+ 0.5	+0.1	0.03
Tm	acetyl	0.2	+ 1.1	+ 1.2	+0.2	
Er	acetyl	0.3	+ 0.7	+ 1.9	+0.5	
Ho	acetyl	0.5	- 0.8	- 0.6	-0.6	
Dy	acetyl	0.6	- 2.0	- 1.4	-0.3	
Yb	$\beta$ A	0.9	-11.4	-10.5	-0.1	0.01
Tm	$\beta$ A	2.8	-27.6	-24.8	-0.1	
Er	$\beta$ A	5.2	-17.8	-12.6	-0.3	
Ho	$\beta$ A	7.7	+21.1	+28.8	+0.4	
Dy	$\beta$ A	10.8	+54.0	+64.8	+0.2	
Yb	$\beta$ B	0.9	- 9.7	- 8.8	-0.1	0.01
Tm	$\beta$ B	3.0	-23.3	-20.3	-0.1	
Dy	$\beta$ B	5.5	-14.5	- 9.0	-0.4	
Ho	$\beta$ B	8.1	+17.2	+25.3	+0.5	
Dy	$\beta$ B	11.5	+44.0	+55.5	+0.3	

Table IV.5

The Calculated Contact and Dipolar Values  
for the LM Species of Ac-DGD-amide

Ln <sup>3+</sup>	Proton	$\Delta_m^{c,i}$ (ppm)	$\Delta_m^{d,i}$ (ppm)	$\Delta_m^{c,i} + \Delta_m^{d,i}$ (ppm)	$\Delta_m^{c,i} / \Delta_m^{d,i}$	AF
Yb	$\alpha$ CH	0.0	- 3.1	- 3.1	-0.0	0.05
Tm	$\alpha$ CH	0.0	- 7.4	- 7.4	-0.0	
Er	$\alpha$ CH	0.0	- 4.6	- 4.6	-0.0	
Ho	$\alpha$ CH	0.0	+ 5.5	+ 5.5	+0.0	
Dy	$\alpha$ CH	0.0	+14.0	+14.0	+0.0	
Yb	acetyl	0.0	+ 0.5	+ 0.5	+0.0	0.07
Tm	acetyl	0.0	+ 1.3	+ 1.3	+0.0	
Er	acetyl	0.1	+ 0.8	+ 0.9	+0.1	
Ho	acetyl	0.1	- 0.9	- 0.9	-0.1	
Dy	acetyl	0.1	- 2.4	- 2.3	-0.1	
Yb	$\beta$ A	0.5	- 5.5	- 5.1	-0.1	0.02
Tm	$\beta$ A	1.5	-13.3	-11.9	-0.1	
Er	$\beta$ A	2.7	- 8.3	- 5.6	-0.3	
Ho	$\beta$ A	4.0	+ 9.8	+13.8	+0.4	
Dy	$\beta$ A	5.6	+25.1	+30.7	+0.2	
Yb	$\beta$ B	0.6	- 1.3	- 0.7	-0.5	0.05
Tm	$\beta$ B	1.9	- 3.1	- 1.3	-0.6	
Dy	$\beta$ B	3.5	- 2.0	- 1.6	-1.8	
Ho	$\beta$ B	5.2	+ 2.3	+ 7.5	+2.2	
Dy	$\beta$ B	7.3	+ 5.9	+13.2	+1.2	



Table IV.6

The Calculated Contact and Dipolar Values for the LM<sub>2</sub> Species of Ac-DGD-amide

Ln <sup>3+</sup>	Proton	$\Delta_{m}^{c,i}$ (ppm)	$\Delta_{m}^{d,i}$ (ppm)	$\Delta_{m}^{c,i} + \Delta_{m}^{d,i}$ (ppm)	$\Delta_{m}^{c,i} / \Delta_{m}^{d,i}$	<sup>a</sup> AF
Yb	$\alpha$ CH	0.2	- 4.2	- 4.0	-0.1	0.04
Tm	$\alpha$ CH	0.7	-10.0	- 9.3	-0.1	
Er	$\alpha$ CH	1.3	- 6.2	- 5.0	-0.2	
Ho	$\alpha$ CH	1.9	+ 7.4	+ 9.2	+0.3	
Dy	$\alpha$ CH	2.3	+18.9	+21.2	+0.1	
Yb	acetyl	0.0	+ 0.7	+ 0.7	+0.0	0.05
Tm	acetyl	0.1	+ 1.8	+ 1.8	+0.0	
Er	acetyl	0.1	+ 1.1	+ 1.2	+0.1	
Ho	acetyl	0.1	- 1.3	- 1.2	-0.1	
Dy	acetyl	0.2	- 3.3	- 3.1	-0.1	
Yb	$\beta$ A	0.8	- 7.7	- 6.9	-0.1	0.01
Tm	$\beta$ A	2.6	-18.6	-16.0	-0.1	
Er	$\beta$ A	4.9	-11.6	- 6.7	+0.4	
Ho	$\beta$ A	7.2	+13.7	+20.9	+0.5	
Dy	$\beta$ A	9.1	+35.1	+44.2	+0.3	
Yb	$\beta$ B	0.9	- 2.3	- 1.4	-0.4	0.02
Tm	$\beta$ B	2.9	- 5.5	- 2.6	-0.5	
Dy	$\beta$ B	5.5	- 3.4	- 2.0	-1.6	
Ho	$\beta$ B	8.0	+ 4.1	+12.1	+2.0	
Dy	$\beta$ B	11.3	+10.4	+21.7	+1.1	

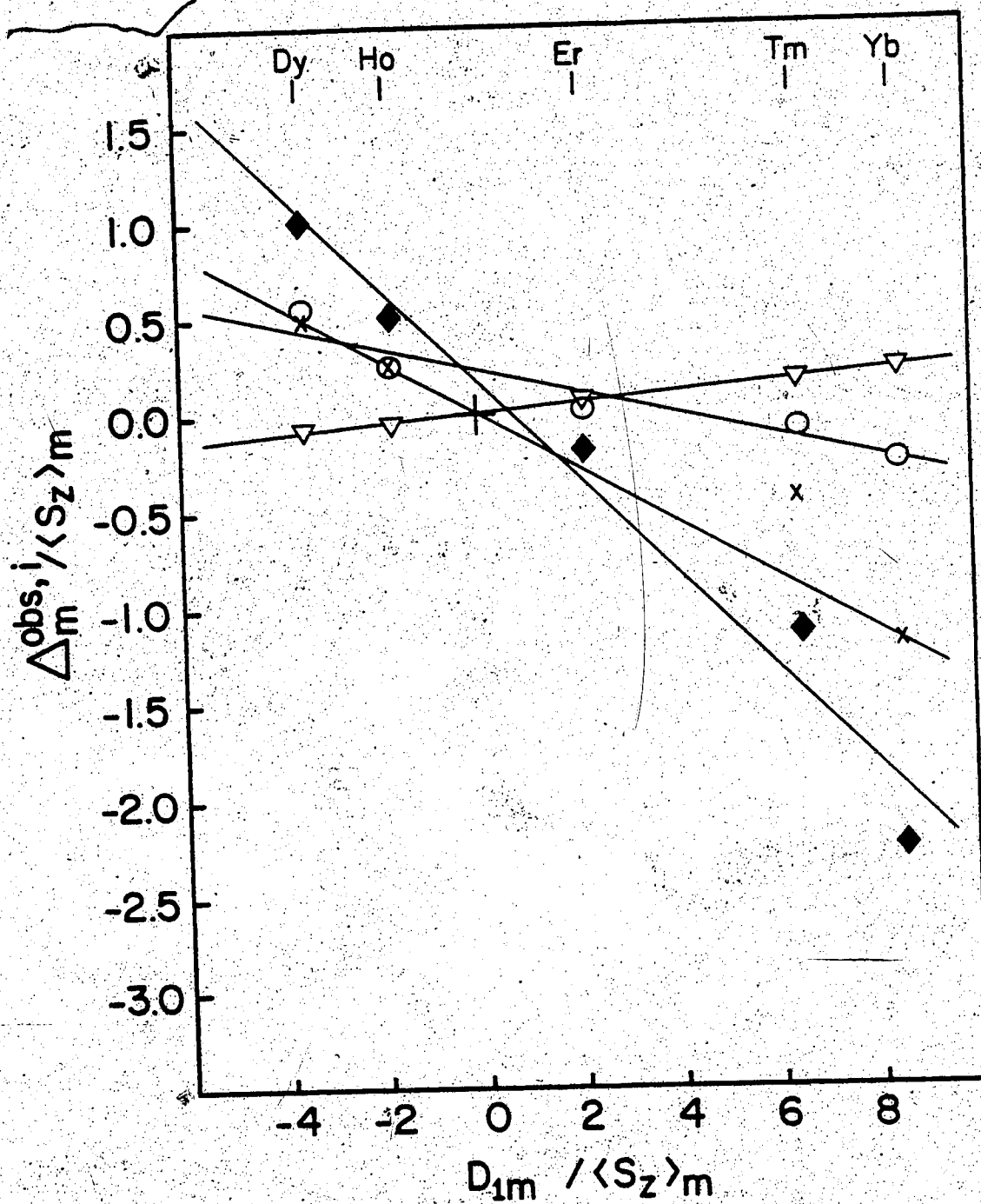


Figure IV.4 The plot of  $\Delta_m^{obs,i} / \langle S_z \rangle_m$  vs  $D_{1m} / \langle S_z \rangle_m$  for the four observable  $^1\text{H}$  NMR resonances of the LM species of Ac-DGD-amide. The LIS were derived using  $K_{s1} = 0.16$  mM. The shifted resonances are defined by the symbols x,  $\alpha\text{CH}$ ;  $\nabla$ ,  $\text{CH}_3$ ;  $\blacklozenge$ ,  $\beta\text{A}$ ; and o,  $\beta\text{B}$ . The titration solution consisted of 2 mM Ac-DGD-amide, in 30 mM Imidazole- $d_4$ , 20 mM KCL, pH 6.5.

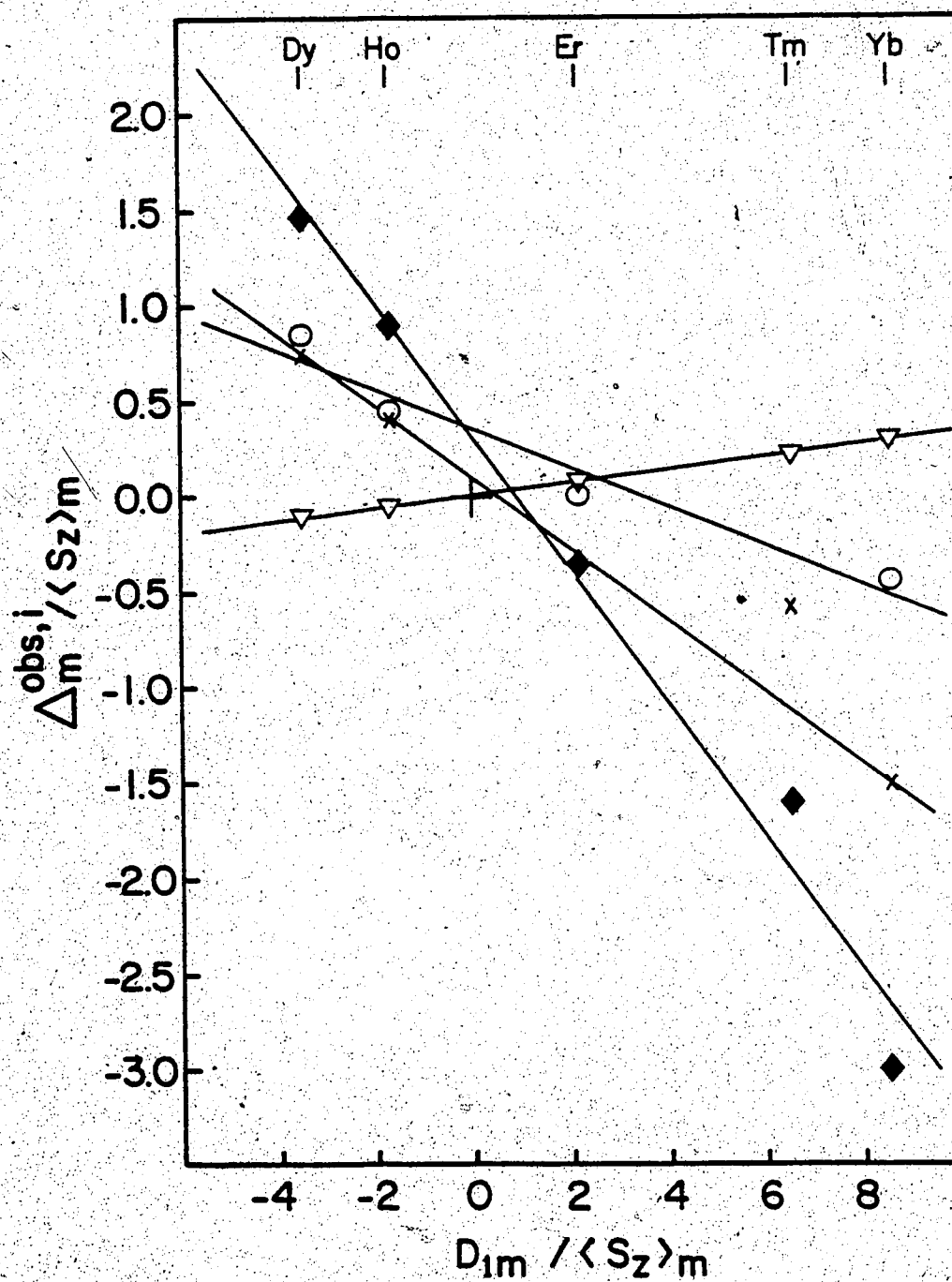


Figure IV.5 Plots of  $\Delta_m^{obs.} / \langle S_z \rangle_m$  VS  $D_{1m} / \langle S_z \rangle_m$  for the four observable  $^1\text{H}$  NMR resonances the LM<sub>2</sub> species of Ac-DGD-amide. The LIS were derived using  $K_{d2} = 7.56$  mM. The shifted resonances are defined by the symbols x,  $\alpha\text{CH}$ ;  $\nabla$ ,  $\text{CH}_3$ ;  $\blacklozenge$ ,  $\beta\text{A}$ ; and o,  $\beta\text{B}$ . The titration solution consisted of 2 mM Ac-DGD-amide, in 30 mM Imidazole- $d_4$ , 20 mM KCL, pH 6.5.

Since the titrations in this study were carried out at pH 6.5, one would expect both of the carboxy groups in the two peptides titrated to be deprotonated. Previous amino acid binding studies at pH 7 indicate that the primary mode of metal coordination by a single aspartic acid residue should be bidentate, involving coordination of both carboxyl groups to the metal ion (140-145). The Ac-Asp molecule has the two carboxyl groups of aspartic acid as well as the carbonyl of the acetate group available for coordination. Ac-DGD-amide has the two carboxyl groups of its two aspartic acid residues and four carbonyl groups available, two from the peptide backbone and one each from the acetate and acetamide group. Note that the acetyl substituents of both molecules serve to neutralize the N-terminus while the C-terminal amide of Ac-DGD-amide neutralizes the free carboxy end-terminal of that molecule; charge effects on the  $K_d$  values and/or modes of ligand coordination (104) were thus eliminated. The titrations take place over a  $Ln^{3+}$ /peptide ratio of 0 to 12 and thus there is a possibility of more than one ligand binding per metal ion ( $ML_n$ ) at low metal/ligand ratios (75, 141, 143, 144, 146-148), as well as a possibility of more than one metal binding per ligand molecule ( $M_nL$ ) at high metal/ligand ratios (28).

*Ac-Asp*: The  $K_d$  varied somewhat for each nucleus during titration with one particular lanthanide but the average values given in Table IV.2 indicate that they were fairly constant over the lanthanide series observed; this supports the

assumption that the species were isostructural. No correction in the  $K_f$  values was made for the effect of increasing ionic strength due to the amount of lanthanide ion added (59,140,148) or for the occurrence of hydrolysis (142,143,148). Although only one binding mode was apparent from the data and was subsequently assumed in the analysis, previous studies of lanthanide binding to aspartic acid have, in fact, shown that two to three stability constants can be observed, depending on the lanthanide used (149); the additional constants arise from the presence of polymeric species ( $ML_n$ ) at low metal:ligand ratios. The differences between the stability constants for aspartic acid given in the literature were so small (149) that any possible differences in our Ac-Asp data would likely not have been apparent even with more titration points. In the Ac-Asp case, therefore, we have assumed a single distinct species ( $ML$ ) existed at the end of the titration and have analyzed the data on that basis. The resultant  $K_f$  values may thus be a composite of the two or three possible values which were not differentiated, but one would expect these values to be so similar that the total effect on the calculated LIS value would be minimal.

The plots of  $\Delta_m^{obs.}/\langle S_2 \rangle_m$  vs  $D_{1m}/\langle S_2 \rangle_m$  for the four observable protons of Ac-Asp are shown in Figure IV.3. The linearity of these plots supports the assumption that only a single geometric isomer of any complex was present along the series of lanthanides studied and that the value of  $A_m^1$  was

independent of the lanthanide used (135). The slopes of the  $\alpha$ CH and acetyl proton plots are small, thus the accuracy is less than for the corresponding  $\beta$ CH<sub>2</sub> protons, but the fits are fairly good, as evidenced by the agreement factors (133) in Table IV.4. The Tm<sup>3+</sup> data was abnormal in all of the plots, and thus was excluded from the final determinations of A<sub>m</sub><sup>1</sup> and the slope; abnormalities in Tm<sup>3+</sup> data have been reported previously (73,134).

The relative  $\Delta_m^{c,i}$  values given in Table IV.4 increase in the order of CH<sub>3</sub> <  $\beta$ A ≈  $\beta$ B ≈  $\alpha$ CH. The acetyl group has a small contact contribution, as expected, since it should be quite far removed from the metal centre. The fact that the relative  $\Delta_m^{c,i}$  is as great for  $\alpha$ CH protons as for the  $\beta$  protons (all of these protons are  $\alpha$  to liganding CO<sub>2</sub><sup>-</sup> groups) suggests that both of the carboxyl groups are coordinating to the metal, as has been observed with other dicarboxylate ligands (140,142-145). The relative  $\Delta_m^{c,i}/\Delta_m^{d,i}$  ratios indicate that one cannot assume that a LIS is primarily dipolar in origin, as all of the protons appear to have a significant contact component.

*Ac-DGD-amide*: Because this titration data appeared to better fit an equation which allowed both LM and LM<sub>2</sub> species to exist, the K<sub>s</sub> and LIS values were derived for both species. One should note here that such a fit was required as the data (i.e., Figure IV.2B) indicated that at least two separate binding modes existed, one with a much weaker K<sub>s</sub>.

Not much can be said about the relative  $K_d$  values for each metal as most of them could not be directly determined, but the fits of the data using the derived  $K_d$  values given above were very good, supporting previous studies on different ligands which have shown that the binding constants for one particular small ligand are effectively the same for all the lanthanides (75, 104, 134, 138, 140). No correction was made for the effects of ionic strength (140, 148, 149) or for lanthanide hydrolysis (142, 143, 148).

The plots of  $\Delta_m^{obs.}/\langle S_z \rangle_m$  vs  $D_{1m}/\langle S_z \rangle_m$  for the four observable shifted proton resonances of the LM and LM<sub>2</sub> species of Ac-DGD-amide are shown in Figures IV.4 and IV.5 respectively. The linearity of these plots supports the assumption that only a single geometric isomer of any complex was present along the series of lanthanides studied and that the value of  $A_m^1$  was independent of the lanthanide used (135).

The four shifted proton resonances in these titrations arose from the  $\alpha$ CH and  $\beta$ CH<sub>2</sub> protons of the aspartic acid residues, and the N-terminal CH<sub>3</sub> group. The  $\alpha$ CH protons of the glycine residue were unaffected by the presence of the lanthanide ion, either because they were too far removed from the metal centre to feel its effects, or because of their particular orientation with respect to the principle magnetic axis. The latter interpretation seems more plausible as recent studies on the site III binding loop peptide of skeletal TnC, which has an internal asp-gly sequence, showed

that the  $\alpha$ CH glycine resonances of this peptide were perturbed by the addition of both  $\text{La}^{3+}$  and  $\text{Lu}^{3+}$  (193).

The slopes of the  $\beta$ B and acetyl plots were the smallest but again the fits were very good (Table IV.5 and IV.6) and the  $\text{Tm}^{3+}$  data were in much better agreement than for the case of the  $\beta$ A and  $\alpha$ CH protons. The relative  $\Delta_m^{c,i}$  values for the LM species increase in the order of  $\alpha\text{CH}_2 < \beta\text{A} < \beta\text{B}$ . Again one assumes that the metal is bound to both  $\text{CO}_2^-$  groups at pH 6.5. The  $\Delta_m^{c,i} / \Delta_m^{d,i}$  ratios indicate that the observed LIS of the  $\alpha$ CH and  $\text{CH}_3$  protons have little to no contact contribution. This was an expected result as these protons should be quite removed from the metal centre. Note the large  $\Delta_m^{c,i}$  contribution for the  $\beta$ B protons; any structural analysis based on the initial assumption that the LIS observed in  $^1\text{H}$  NMR are primarily dipolar in origin would obviously lead to a large degree of error for such protons, and such effects have previously been observed with  $^1\text{H}$  NMR (102, 104).

The slope and  $\Delta_m^i$  values increase by ca. 60-70% for the  $\text{LM}_2$  species (Table IV.3), except for the  $\Delta_m^i$  value of the  $\alpha\text{CH}_2$  protons which increases dramatically by comparison. Changes in both of these parameters are to be expected when one goes from two liganding groups (aspartic acid side chain carboxyl groups) coordinating to the same metal ion to both liganding groups each coordinating to a metal ion, thus experiencing a greater electron spin density. The fact that  $\Delta_m^i$  changes significantly for the  $\alpha\text{CH}_2$  protons indicates that a



different coordination mode is present in the LM<sub>2</sub> species, such that the αCH protons are exposed to the effects of the lanthanide spin to a much greater degree. The net result in the final parameters is a significant increase in the  $\Delta_m^{c,i}$  and  $\Delta_m^{c,i}/\Delta_m^{d,i}$  values of the α-CH protons upon going from the LM species (Table IV.5) to the LM<sub>2</sub> species (Table IV.6). By comparison, the changes in these parameters for the other observable protons are very small. Much further work would be needed to interpret these results accurately in terms of structural information.

One interesting observation in these titrations is that although Ac-DGD-amide has two distinct aspartic acid residues, their αCH and βB protons remain magnetically equivalent throughout the titrations as only one resonance is observed. The βA protons did separate towards the ends of the Yb<sup>3+</sup>, Tm<sup>3+</sup>, and Dy<sup>3+</sup> titrations but remained very close together. This separation became obvious at [M]<sub>0</sub>/[L]<sub>0</sub> ratios of approximately 1:1 for Yb<sup>3+</sup> and Tm<sup>3+</sup>, but not until the ratio was 2.7 in the Dy<sup>3+</sup> case, likely due to the greater amount of line broadening displayed in the presence of that lanthanide. These observations suggest that the two aspartic acid groups in the LM species must coordinate to the lanthanide ion in such a manner that they are symmetrically placed about the central metal ion, and that the mode of binding by these separate residues in the LM<sub>2</sub> species should also be similar. However, the fact that separation of the βA protons is observed for Yb<sup>3+</sup>, Tm<sup>3+</sup> and Dy<sup>3+</sup> does indicate

that these residues in the LM<sub>2</sub> species are in slightly different environments. The lack of such an observation for Ho<sup>3+</sup> and Er<sup>3+</sup> was likely due to the magnitude of the line-broadening in the resonances.

### E. Conclusions

This method successfully separates the contact and dipolar contributions of the LIS without prior knowledge of the symmetry of the complex or the orientation of the principle magnetic axis. The analysis shown works well for this particular system but relies heavily on the value of  $G_2/G_1$  being small (i.e., the non-axial term in equation 1 is small compared to the axial term). There is, of course, also the possibility that the complex is axially symmetric, although this seems unlikely in light of the studies previously mentioned (78,96,150), and the fact that the ratios of the shifts for the different assignable protons were not the same for each lanthanide studied (104,133).

It is obvious that the assumption that the value of  $\Delta_m^{c,i}$  is much less than that of  $\Delta_m^{d,i}$  in the case of <sup>1</sup>H NMR is not always a valid one and that great care must be taken to choose a suitable lanthanide as a probe. It is also apparent that the method employed in this study works best where the dipolar contribution of the LIS observed is large, such that the slope of the plots shown in Figures IV.3 to IV.5 are large (133,135).

From the  $\Delta_m^{c,i} / \Delta_m^{d,i}$  values obtained, it is apparent that either  $Tm^{3+}$  or  $Yb^{3+}$  is the best lanthanide probe for structural studies of nuclei very near to or within the metal binding site because their LIS were relatively large and also displayed the smallest contact components. The  $Tm^{3+}$  data, unfortunately, did not fit well for any of the shifted protons of Ac-Asp or for the larger shifting  $\beta A$  and  $\alpha CH_2$  protons of Ac-DGD-amide. These observations, together with the results of previous studies on the relative linebroadening properties of the lanthanides (96), leads us to conclude that, where LIS are used for structural studies of calcium binding sites,  $Yb^{3+}$  is the preferred lanthanide.

## V. THE INTERACTION OF THE DTNB LIGHT CHAIN OF RABBIT SKELETAL MYOSIN WITH LANTHANIDE IONS

### A. Introduction

Vertebrate skeletal muscle has a striated appearance when examined under the light microscope, which arises from the presence of many parallel myofibrils in the muscle cells. There are two kinds of interacting protein filaments in a myofibril; the thick filament, which is composed primarily of myosin, and the thin filament, which is composed primarily of actin, troponin, and tropomyosin. These proteins form the basic contractile unit of the skeletal muscle of vertebrates. Contraction is brought about by the relative movement of these filaments via the attachment of the cross-bridges of myosin in the thick filament to actin in the thin filament (151-154). The following discussion will concentrate specifically on the role of myosin in vertebrate skeletal muscle and on the properties and subunits of the well-characterized rabbit white skeletal muscle contractile system. There will also be some discussion of the contractile system of invertebrate and smooth muscle myosin.

Rabbit skeletal myosin has been shown to consist of two high molecular weight proteins called the heavy chains, each with a mass of ca. 200,000 daltons, and four low molecular weight proteins known as the light chains (121, 122, 155). Electron micrographs show that myosin consists of a double-headed globular region joined to a very long rod

(156)(Figure V.1A). At physiological ionic strength, the rods aggregate to form the backbone of the myosin thick filament.

Myosin is an ATPase, and it is the hydrolysis of ATP which is the immediate source of the free energy that drives muscle contraction. A very simple and very early model of the relationship between ATP hydrolysis and contraction is outlined in Figure V.2, but the exact mechanism is much more sophisticated and is by no means firmly established (153, 154, 157, 158, and references therein). In the relaxed state of the muscle, the intracellular  $\text{Ca}^{+2}$  concentration is low and the myosin heads are detached from the thin filaments. ADP and  $\text{P}_i$  are bound to the myosin heads, which are currently believed to lie at various angles with respect to the thin filament axis, as indicated in Figure V.2A. When the muscle is stimulated, the intracellular  $\text{Ca}^{+2}$  concentration increases and the myosin heads move away from the thick filaments and attach to actin units on the thin filaments, such that the heads lie at an angle of about  $90^\circ$  relative to the thin filament (Figure V.2B). When this attachment takes place, ADP and  $\text{P}_i$  are released and the orientation of the myosin heads is altered so that their long axis is at an angle of about  $45^\circ$  to  $75^\circ$  to the thin filament axis (Figure V.2C). Consequently, the thick filament is pulled a distance of some 75 Å relative to the thin filament. The actomyosin complex then binds ATP, which weakens the interaction between actin and myosin and results in the

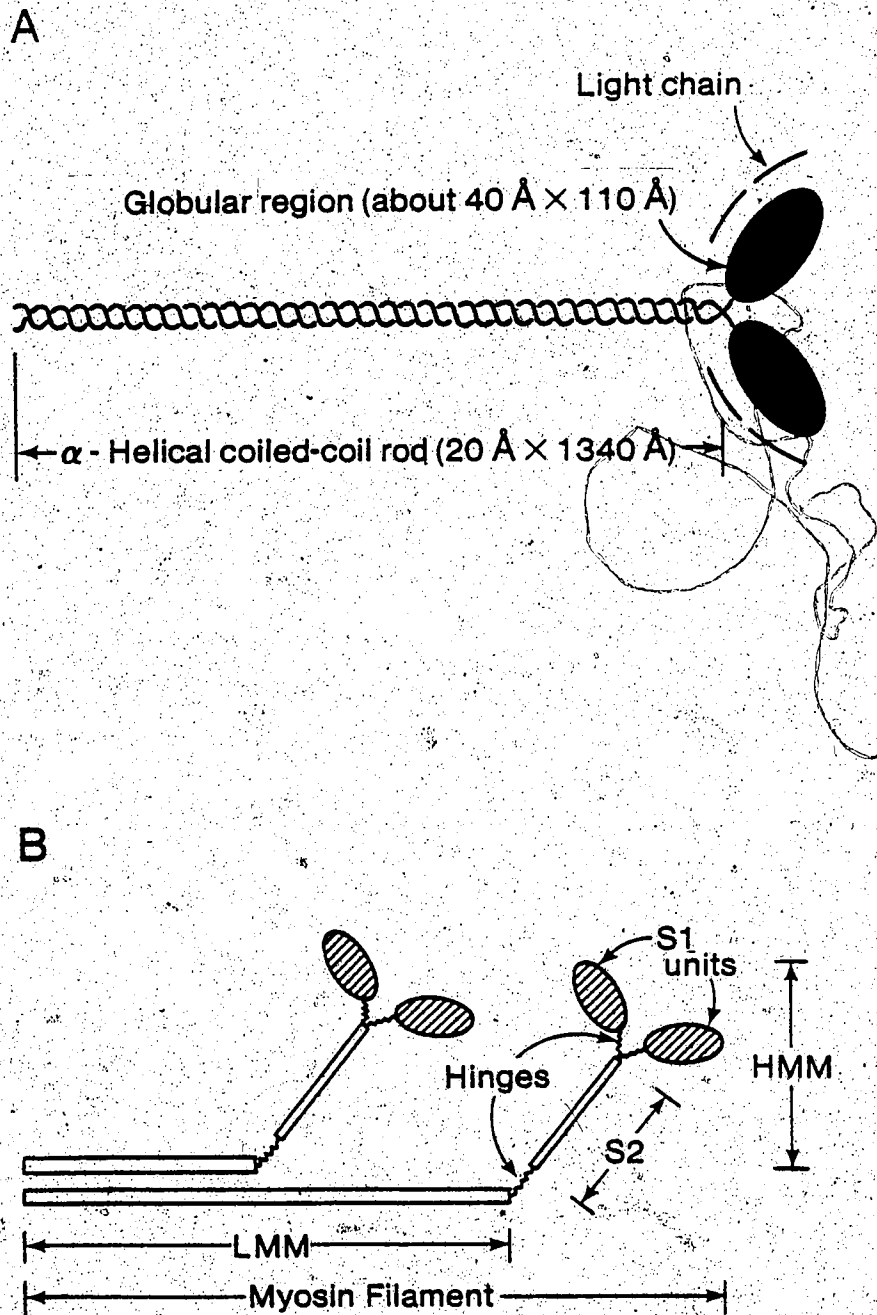


Figure V.1. A. Schematic diagram of a myosin molecule, from Figure 34-8 of reference 159.  
 B. Subfragments resulting from enzymatic cleavage of myosin; adapted from Figure 34-9 of reference 159.

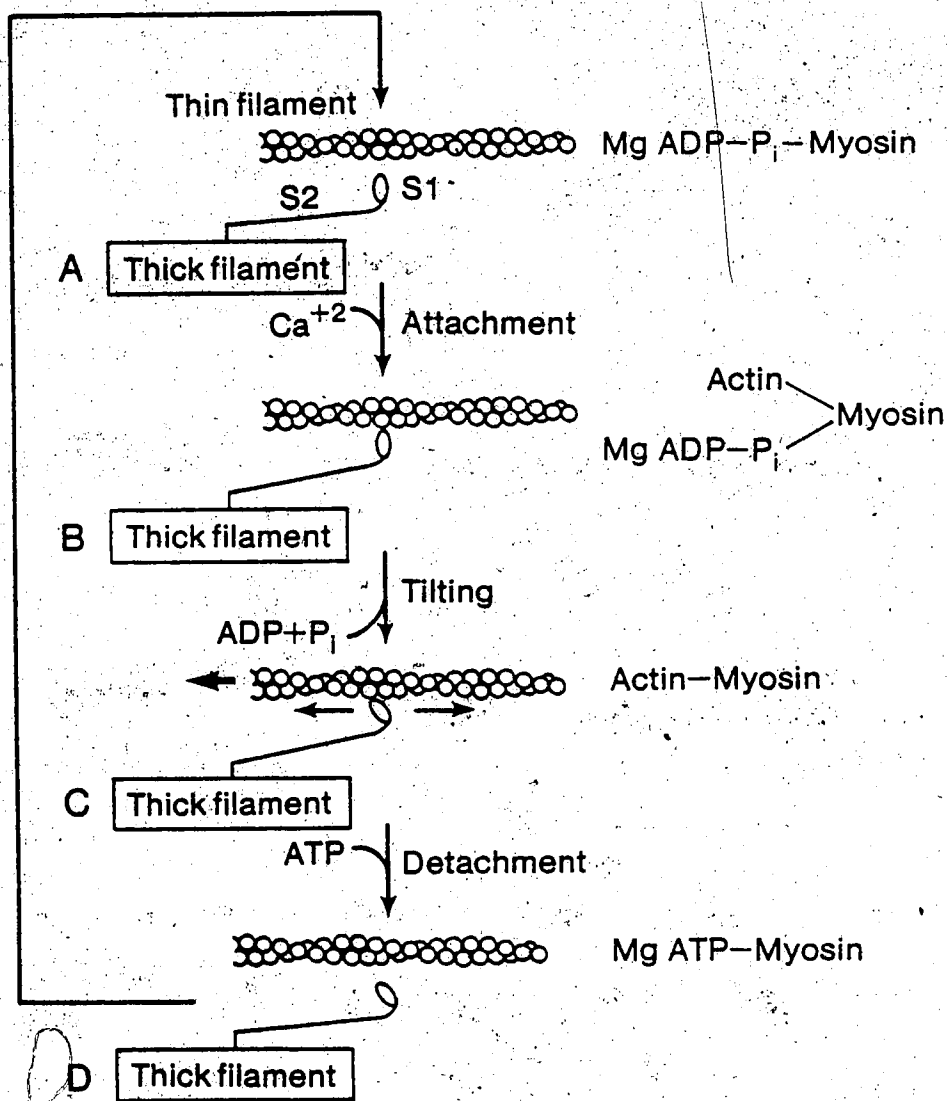


Figure V.2. A - D. Proposed mechanism for the generation of force by the interaction of the S1 units of a myosin filament (for simplicity only one S1 unit is shown; see Figure V.1B) with the actin filament. The thick filament moves relative to the thin filament when the S1 unit bound to actin changes its tilt (in the transition from B to C). MgATP, MgADP, and P<sub>i</sub> are bound to and released from the S1 heads of myosin as indicated; adapted from Figure 34-17 in reference 159.

conversion of ATP to ADP and Pi. When the myosin heads become detached (Figure V.2D), they may either realign themselves at an angle of about 90° to the thin filament axis and repeat the cycle (Figure V.2B), or they may return to the fully relaxed state (Figure V.2A). Under normal physiological conditions (0.1 M to 0.15 M KCl,  $[Mg^{+2}]_0 > 1.0$  mM,  $[Ca^{+2}]_0 = 10^{-7}$  M), the substrate for this catalysis is MgATP (159,160). Myosin can hydrolyze ATP in the absence of actin, but the rate of hydrolysis is much slower due to a decrease in the off rate of ADP and Pi from the enzyme. Myosin ATPase is therefore often referred to as being "actin-activated".

The simple model presented above was first proposed by Huxley in 1969 (151), and was later elaborated upon by both Lynn and Taylor (162) and by Mannherz (163). It should be noted here that the cycle described above remains conjectural. Although some of the biochemical aspects are well documented, the nature, and even the occurrence of conformational changes in the cross bridge cycle have not been established. A thorough discussion of the subject is outside the scope of the present text, but has been reviewed elsewhere (153-155). Although the notion that contraction is achieved by the change in angle of the cross bridges when they are attached to actin is not now generally held to be true, this early model provided a basis for a great deal of the subsequent work on the DTNB LC, which will be outlined below.



Myosin can be enzymatically split by trypsin (161), chymotrypsin (51), and papain (121) into fragments that retain some of the properties and activities of the intact molecule, the two main fragments being heavy meromyosin and light meromyosin (Figure V.1B). Light meromyosin forms filaments like myosin but it lacks ATPase activity and does not combine with actin. Heavy meromyosin, on the other hand, catalyzes the hydrolysis of ATP and binds to actin, but it does not form filaments. HMM consists of a rod attached to a double-headed globular region, and it is this region of the molecule which makes up the cross-bridge of myosin, and which contains the elements required for ATPase activity. It can be split further into two globular subfragments, each called S1, and into one rod-shaped subfragment called S2 (Figure V.1B). The light chains of myosin are highly susceptible to enzymatic cleavage but, under carefully controlled conditions, they are found to be associated with the S1 fragments (see later text). The enzymatic splitting of myosin into LMM, S2, and S1 fragments is an expression of the fact that myosin is constructed of three domains which are joined by two *hinges* (Figure V.1B). Since these products can be obtained by digestion with a number of proteolytic enzymes of differing specificity, it is thought that these regions represent the position of flexible joints in the myosin filament. These hinges enable the S1 heads to span the interfilament distance so that they can reversibly attach and detach from actin and to change their orientation

when bound (151, 153). The hinge between S1 and S2, generally known as the "swivel", may enable S1 to interact with actin in one way when ADP and Pi are bound and in a different way with bound ATP (i.e. Figure V.2B,C). The postulated tilting of the S1 head, as outlined in the simple model above, was thought to be the power stroke of muscle contraction, where the change in angle of the S1 domain was transmitted by the S2 unit of myosin to the thick filament, although little direct evidence exists for this supposition. It is also possible that the swivel may simply reduce the geometric constraint of the system such that suitably oriented actin monomers may be equally available to all myosin heads. The other hinge, between S2 and LMM, also allows considerable variation in the position of the myosin heads relative to the thick filament, and may also be involved in the development of tension in the stimulated muscle.

The interaction of the myosin cross-bridges with actin units in the thin filaments is controlled by the levels of calcium in these tissues. One of the three subunits of troponin, TnC, is the regulatory calcium binding site of this system. Upon activation, the calcium concentration within the interfilament space rises abruptly from  $\approx 10^{-7}$  to  $\approx 10^{-5}$  M, and the binding of this calcium by TnC induces a change in conformation in that subunit which is transmitted over the troponin complex. This conformational change in turn allows the actin and myosin to interact and the subsequent development of tension (38). In the presence of pure actin

(i.e. actin which is devoid of Tn and Tm), skeletal myosin ATPase is not  $Ca^{2+}$ -sensitive.

Although contraction in vertebrate skeletal muscle is regulated by the interaction of calcium ions with the TnC subunit of troponin (thin filament regulation)(38,159) in molluscan muscles and in some other primitive invertebrates contraction is regulated by the interaction of calcium with myosin (thick filament regulation)(38,159). Molluscan myosin preparations bind calcium and their ATPase activity in the presence of pure actin is calcium-dependent. The calcium dependence of the actin-activated ATPase activity of scallop myosin requires the presence of a specific light chain, which is called the EDTA light chain because one mole of it is released from invertebrate myosin if the divalent cation concentration of the medium is lowered by the addition of EDTA. There are two EDTA LC associated with invertebrate myosin, and the release of one mole of this light chain results in a loss of calcium sensitivity. The myosin is 'desensitized' in that the calcium requirement for the actin-activated ATPase activity is abolished and there is a loss of one of the two  $Ca^{2+}$  binding sites on the intact molecule (165).

Comparative studies on the calcium regulatory systems of a wide variety of species have revealed that the muscles of some invertebrate species contain both myosin-linked and actin-linked calcium regulation (164). Although vertebrate

skeletal muscle displays only actin-linked calcium regulation, the myosin itself also binds calcium (166,167), and one of the light chains of skeletal myosin is involved in  $Ca^{2+}$  binding. There are three distinct types of light chain in skeletal myosin, two of which are dissociated from myosin at high pH and are known as the alkali light chains A1 and A2, or as LC-1 and LC-3 respectively; the latter designation arose from their relative mobilities on SDS PAGE. Myosin exists as two isoenzymes, one of which has two moles of A1 per myosin molecule and the other which has two moles of A2. It was originally thought that these light chains could not be removed without total loss of ATPase activity, but more recent work has shown that the ATPase site resides solely on the heavy chain (168-170). The sequence of A2 (17kD) is very similar to that of A1 (21kD) except for an additional 41 residue segment at the amino-terminus of A1. The alkali light chains have a great amount of sequence homology with TnC and parvalbumin (18,171) (Figure 1.3), but there are deletions and substitutions in the appropriate binding site locations and neither isolated LC is able to bind calcium under physiologically significant conditions (40,172).

Treatment of rabbit skeletal myosin with DTNB leads to the selective release of 50-80% of the third type of LC, which is known as the DTNB light chain, LC-2, LMP-II, L<sub>2</sub>, the regulatory light chain, and the P- or phosphorylatable light chain. This LC has two thiol groups, a molecular weight of 19kD, and it is chemically distinct from A1 and A2

(18,121,173). LC-2 has some sequence homology with TnC and parvalbumin (18)(Figure I.3), and there are two moles of LC-2 per myosin molecule. In the isolated state, a sizeable portion of the residues are in a defined, stable environment (45,174) and the DTNB LC can bind calcium in both the native and isolated states; the binding of calcium has been reported for the thick filaments of muscle (175), isolated native thick filaments (166), S1 (176), and the isolated DTNB LC (30). Calcium binds non-cooperatively to two types of sites on myosin which display different affinities; there are two high affinity sites with  $K_d$  values of  $K_{d1} = 10^{-6}$  to  $10^{-8}$  M (51,166,167) and several low affinity sites with  $K_{d2} = 10^{-3}$  to  $10^{-4}$  M (166,167). The isolated light chain has also been reported to bind calcium at two different types of sites; one high affinity site with  $K_{d1} = 10^{-6}$  to  $10^{-7}$  M (40,45,166) and one low affinity site with  $K_{d2} = 10^{-4}$  M (40); it is the high affinity site on the DTNB LC which is the high affinity site of myosin (40,166,176). By sequence homology with TnC and parvalbumin, the high affinity  $Ca^{+2}$  binding loop region of LC-2 should be located within residues 37-48 (Figure I.3), with this site containing only three acidic liganding groups instead of four (18).

$Ca^{+2}$ ,  $Mg^{+2}$  and other divalent metal ions bind to the isolated skeletal light chain (40) as well as to myosin (167). These ions bind competitively and so the calcium binding sites are relatively non-specific. There is essentially a single dissociation constant for  $Mg^{+2}$  which is  $10^{-3}$

to  $10^{-4}$  M (40,45) for the isolated LC and  $\leq 10^{-7}$  M for myosin (167). Obviously the isolation of LC-2 has a significant effect on its affinity for  $Mg^{+2}$  but not for  $Ca^{+2}$ . The fact that the affinities of myosin and the isolated LC for calcium are similar indicates that the binding of  $Ca^{+2}$  by the DTNB LC is not significantly influenced by the association of this light chain with the residual (DTNB LC-free) myosin. Other results indicated that the DTNB LC is in the same conformation in the isolated state as in the intact system. The EPR spectra of rabbit skeletal glycerinated psoas muscle (176), myofibrils (47), HMM, myosin (51,160,176), S1 (176), and the isolated light chain (47,51) showed the presence of a  $Mn^{+2}$  ion binding site which was invariant for the sources above, and which competed with  $Ca^{+2}$  and  $Mg^{+2}$  (47). In addition, there was no difference in the extent of the reaction of antibodies to the DTNB LC against the associated or dissociated protein (174).

The loss of one mole of DTNB light chain does not significantly alter the properties of the residual myosin; it has little effect on the ATPase activity (121,155,177) or on the ability of the myosin to interact with actin. The DTNB LC does not then appear to be a part of the active centre of the myosin head. The loss of either all of this LC, or a great portion of it during S1 preparation using papain (121,166,178), trypsin (161) or chymotrypsin (51) indicates that it is likely localized on the hinge region of the myosin molecule that connects S1 to S2. Image reconstruction

studies comparing intact myosin to myosin without the DTNB light chains also locate this light chain at this region of the myosin head (179). Previous work has shown that the binding of divalent metal ions to myosin and myofibrils inhibits the formation of S2 and S1 upon proteolytic attack by these enzymes, as well as limiting the extent of the degradation of the DTNB LC to a 17kD fragment which is still able to bind divalent metal ions (51, 178, 180). These results strongly suggest that alkaline earth metal ions bind to the S1-S2 "hinge" and change its conformation.

The studies outlined above, and the observation that the binding of calcium by myosin results in significant alterations in sedimentation and other properties (166), led to speculation that these hinges might be "switched on" when muscle is stimulated, but there are several factors which argue against such a control mechanism. Purified vertebrate myosins bind rather small amounts of calcium in the presence of physiological levels of free magnesium, such that under the physiological conditions of living muscle the DTNB LC binding site would always be saturated by magnesium and thus retain the same structure irrespective of contraction or relaxation (166). In addition, kinetic evidence argues against this hypothesis as the effective rate of  $\text{Ca}^{2+}$  binding to the DTNB LC, controlled by the slow rate of  $\text{Mg}^{2+}$  dissociation, is several orders of magnitude too slow to participate in the activation of muscle contraction, which is complete within 100 msec (176). The observation that the addition of

one mole of DTNB-LC to "desensitized" scallop myosin in the presence of actin restored the calcium sensitivity of the scallop actomyosin ATPase (40) initially suggested that the DTNB-LC could functionally replace the scallop EDTA-LC, and indicated a possible role for these light chains in rabbit muscle. However, later work has shown that this reinstated  $Ca^{2+}$  sensitivity was mediated through the remaining scallop regulatory LC (165), since although  $Ca^{2+}$  regulation was restored, there was no effect on  $Ca^{2+}$  binding. To date, the physiological significance of the binding of  $Ca^{2+}$  to the DTNB-LC has not been definitely established.

The DTNB-LC can be readily phosphorylated and dephosphorylated during the extraction of myosin from whole muscle, as well as *in vitro* (181). The site of phosphorylation is a single serine residue (ser 14 or 15) located at the N-terminus, which is very close to the proposed metal binding site (18), and the ability of the light chain to bind  $Ca^{2+}$  (but not  $Mg^{2+}$ ) is affected by the state of phosphorylation of the LC (45). The enzymes which are believed to be involved in this process are called *myosin light chain kinase*, which requires  $Ca^{2+}$  for full activity (182, 183), and *myosin light chain phosphatase* (184). These same enzymes are present in both cardiac and smooth muscle, and are capable of phosphorylating the light chain of these myosins. In smooth muscle, the phosphorylation of this light chain is thought to be the essential triggering action for the stimulation of contraction, as it modulates the actin-myosin



interaction (153,185) However, in skeletal muscle, the *in vitro* enzyme activities indicate that the amounts of these two enzymes present are such that a phosphorylation--dephosphorylation cycle could not occur during single twitch in skeletal muscle (182). It is unlikely that the hydrolysis of ATP by myosin goes via a phospho-enzyme intermediate, as partial removal of LC-2 has no effect on the ATPase activity of the molecule. The extent of enzymatic cleavage of myosin is affected by phosphorylation in much the same manner as by the presence of  $Mg^{+2}$ , in that the LC is cleaved only to a 17kD fragment, and the formation of S1 is suppressed and HMM formation is increased (186). In light of these facts, under physiological  $Mg^{+2}$  concentrations, it seems unlikely that any functionally significant structural changes are accompanied by phosphorylation. At the present time there is no clear indication of the role of the phosphorylation-dephosphorylation process in striated muscle myosin (153), although recent work indicates that the phosphorylation of LC-2 influences both the actomyosin ATPase activity and the calcium sensitivity (186). Other results have suggested that the phosphorylation of LC-2 may modulate the actin-myosin interaction, as it does in smooth muscle (183).

In the following study, the DTNB light chains of rabbit skeletal myosin were isolated and the effects of the binding of calcium, lanthanum, gadolinium, and ytterbium on the far ultraviolet circular dichroism spectra were observed. The changes in ellipticity upon metal binding were different for

all three lanthanides, with only lanthanum displaying an effect which was similar to that shown by calcium. Therefore, the binding of metal ions to LC-2 may not be completely non-specific, in the sense that all metal ions will not induce the same types of conformational changes upon binding. Preliminary  $^1\text{H}$  NMR results for the DTNB light chain are also presented.

## B. Results

The isolated DTNB LC gave a single band on SDS PAGE, with a  $R_f$  value of 0.674. A calibration plot using lysozyme (14.3 kDalton), soybean trypsin inhibitor (21 kDalton), and cardiac Tm (33 kDalton) as standards indicated that the isolated LC had a molecular weight of 17.3 kD (Figure V.3). The molecular weight of this protein as determined by gel electrophoresis has been cited to be 17 to 19kD in the literature (121,122,187). The protein was subjected to amino acid analysis to determine whether we had isolated the intact 19 kDalton protein or a 17 kDalton fragment (Table V.1); the results indicated that the protein was intact and that the gel results were anomolous. The UV spectrum was characteristic of a protein with a high phe/tyrosine ratio (phe/tyr = 6/1)(181,187), showing four phenylalanine maxima in the 250 to 270 nm region (Figure V.4).

The CD spectra for all four samples in the presence and absence of metal ions are shown in Figure V.5. Only the ellipticity values in the range of 210 to 255 nm are shown

Table V.1

## Amino Acid Analysis of the Isolated DTNB LC

---

amino acid	number <sup>a</sup>	sequence
lys	14.1 <sup>b</sup>	17
his	1.1	1
arg	6.6	6
asp + asn	18.6 <sup>b</sup>	23
thr	10.1	10
ser	4.6	5
glu + gln	23.0	23
pro	6.2	6
gly	14.3	13
ala	14.6	14
met	6.0	6
leu	9.7	9
tyr	2.1	2
phe	12.3	12

---

<sup>a</sup>these results are the average of four separate determinations: a typical sample contained 4.3 nmoles of histidine.

<sup>b</sup>The values determined for lys and asp+asn are 83% and 81% respectively of the expected values, due to sample overloading.

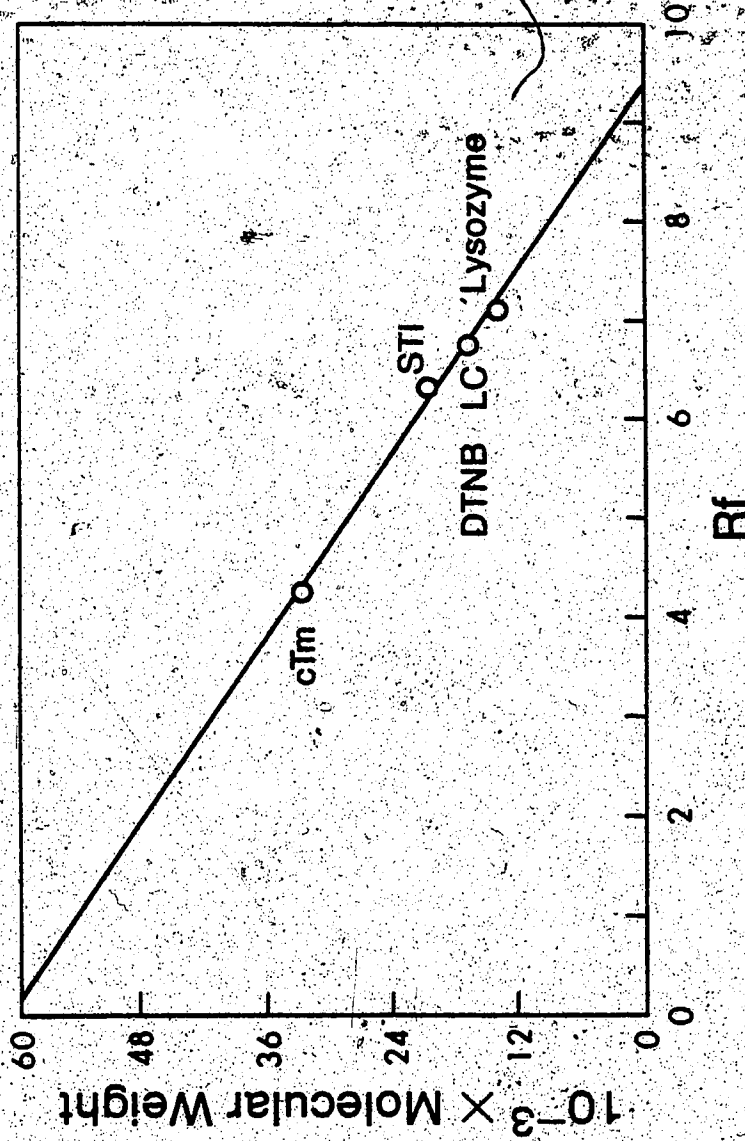


Figure V.3 Plot of  $10^{-3} \times$  Molecular weight vs Rf for one of the SDS gels of the DTNB LC. The three standard proteins were cardiolipin (cTm), soybean trypsin inhibitor (STI), and lysozyme. The best fit for the DTNB LC gave a molecular weight of 17.3 on this gel, corresponding to an Rf value of 0.674.

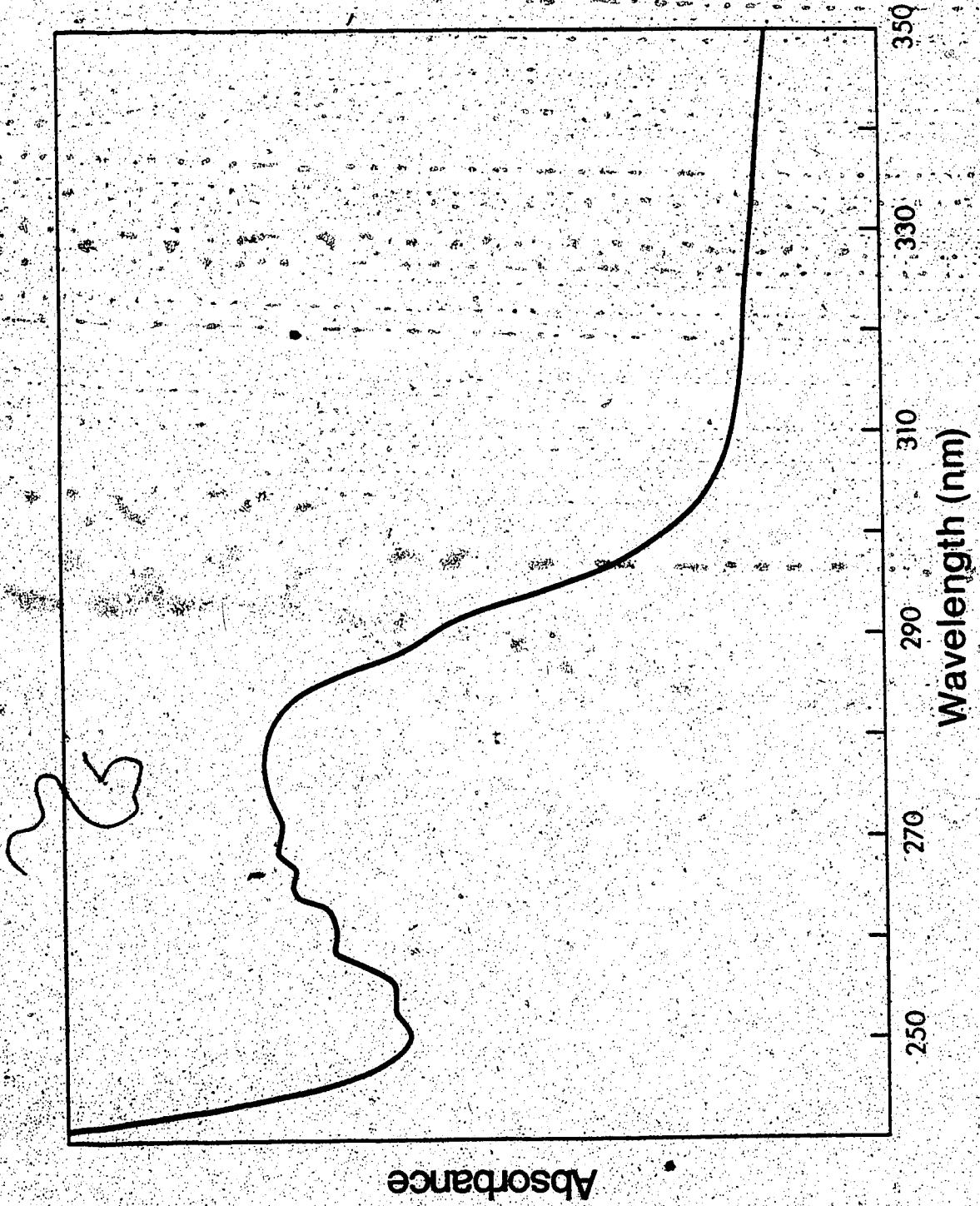


Figure V.4 The UV spectrum of the DTNB LC in 100 mM MDPS, 50 mM KCl, 1 mM EGTA, pH 7.25.

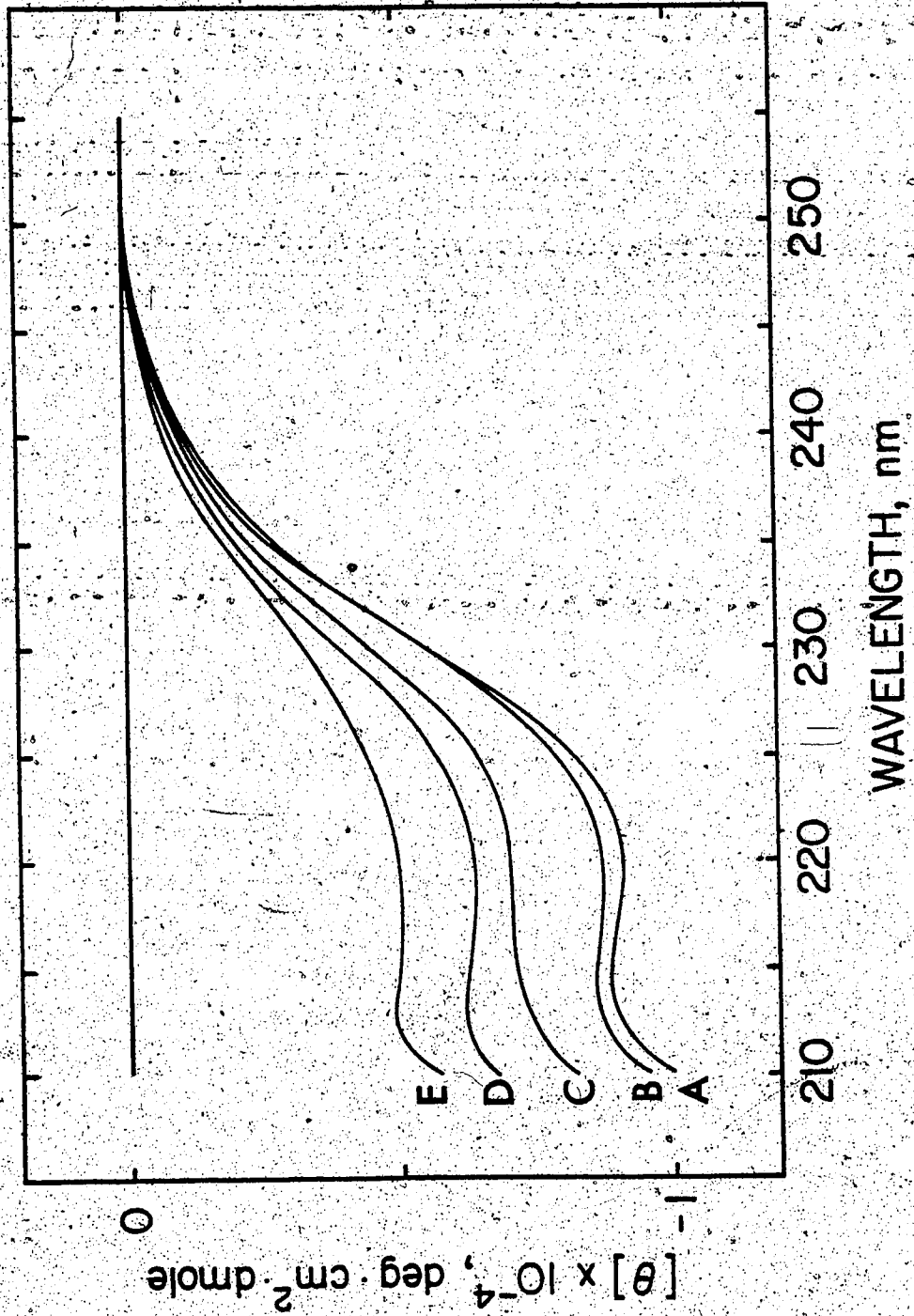


Figure V.5 Plot of  $10^{-4} \times [\theta]$  in  $\text{deg} \cdot \text{cm}^2 \cdot \text{dmole}^{-1}$  versus wavelength in nanometres. The  $[\theta]_{220}$  values for each curve are as follows: A. LC + calcium, 9023; B. LC + lanthanum, 8694; C. averaged apo. protein, 6894; D. LC + gadolinium, 6268; and E. LC + ytterbium, 4778.

as accurate ellipticity measurements at wavelengths less than 220 nm were difficult due to the noise arising from the absorption of chloride ions in the sample buffer (188). The apo spectra of each of the four samples was taken prior to the addition of metal ions. To each of three separate samples were added 5  $\mu$ l of stock lanthanide solution, while the fourth sample was titrated with various aliquots of the three stock calcium solutions (a total of 37  $\mu$ l of solution was added). The ellipticity values from 210 to 255 nm were measured from a baseline (buffer only) spectrum for both the apo and metal-bound CD spectra and were used to calculate  $[\theta]$  values for the same wavelength range. The observed ellipticity values as a function of total calcium concentration were used to determine a dissociation constant for calcium (Figure V.6). The value was  $K_d = 4 \times 10^{-4}$  M and was determined by a nonlinear curve-fitting iterative procedure which has been previously discussed (119); it was *ca.* two orders of magnitude less than the values cited in the literature (Table I.2).

An average apo protein spectrum (calculated from the four samples run in the apo state prior to metal ion addition) is shown in figure V.5, along with the corresponding metal-saturated CD spectra. Our ellipticity values (Figure V.5) for the apo- and calcium-saturated LC were compatible with those cited in the literature (45,188). The final metal/LC ratios were: calcium, 225; lanthanum, 118; gadolinium, 127;  $\text{Yb}^{3+}$ , 127. The  $\alpha$ -helical contents were: LC + apo

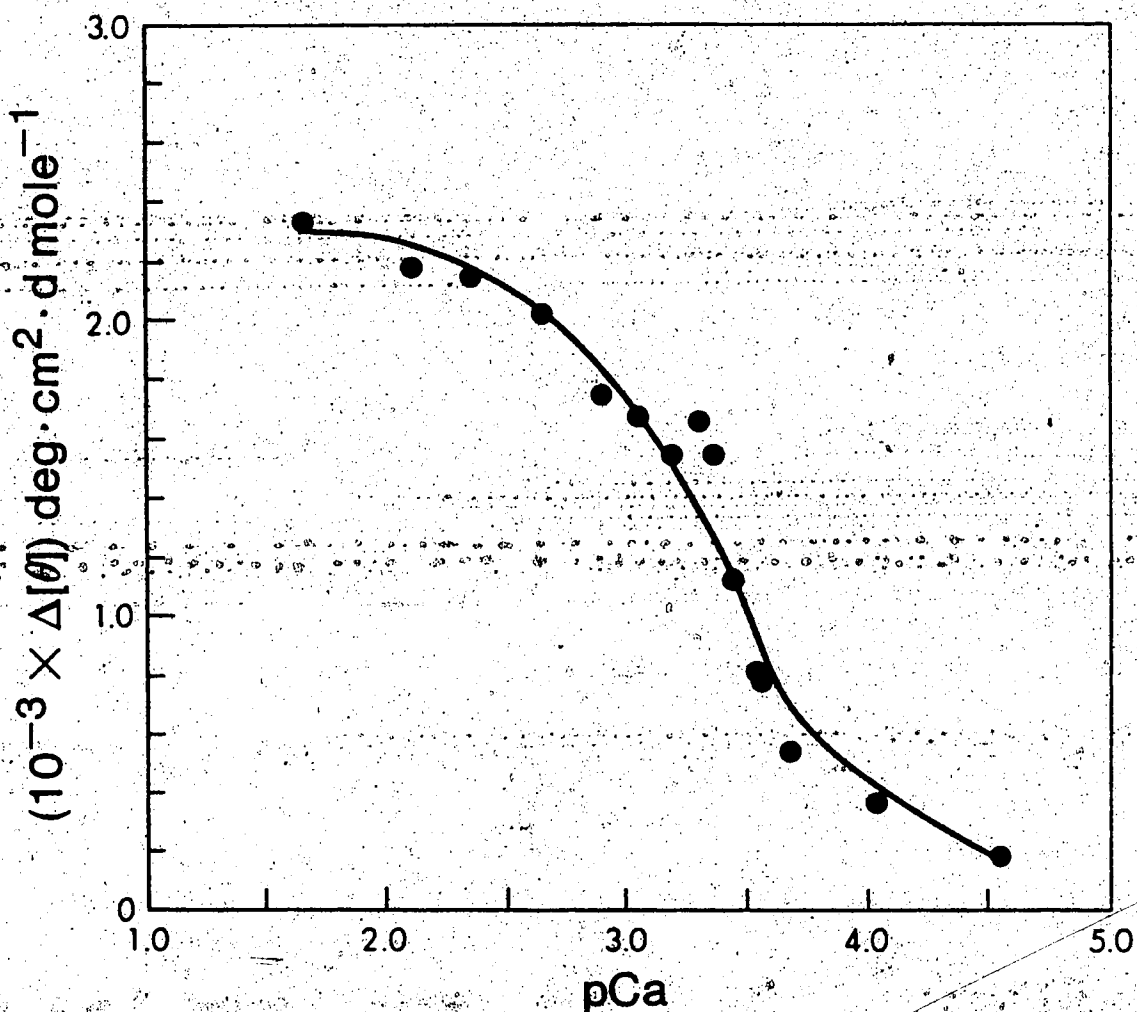


Figure V.6. A plot of  $10^{-3} \times [\theta]$  in  $\text{deg} \cdot \text{cm}^2 \cdot \text{dmole}^{-1}$  vs  $\text{pCa}$  for the  $\text{Ca}^{2+}$  titration of the DTNB LC. The symbols are as follows: •, the observed values; solid line; the best fit values for the data using the BCON1 programme (1.19) which assumes that the protein has one  $\text{Ca}^{2+}$  binding site.



protein, 24%; LC + calcium, 30% LC + lanthanum, 29%; LC + gadolinium, 21%; LC + ytterbium, 17%. It is readily apparent that the three lanthanides have quite different effects on the overall conformation of the isolated DTNB LC, with lanthanum producing a net effect which was the most similar to that of calcium. The amount of  $\alpha$ -helical content determined for the apoprotein indicated that the isolated light chain contains a sizeable proportion of its residues in a defined, static environment. Analysis of the sequence for a theoretical  $\alpha$ -helical content yielded a minimum value of 33% and a maximum value of 41%.

$^1\text{H}$  NMR spectra were taken on an aliquot of this protein in both the presence and absence of calcium (Figure V.7) and they were very similar to those of the phosphorylated and dephosphorylated protein in the literature (45). The  $^1\text{H}$  NMR spectra of the two states are extremely similar, with only a few slight differences apparent in the aliphatic region (45). There were only minor changes in the spectrum upon the binding of calcium, even in the presence of a large excess of calcium ions; the type and magnitude of these changes were consistent with previously published results (45). It was immediately evident from the NMR spectra that there was EDTA in the sample, which likely contributed to the fact that a fairly large excess of calcium ions was needed to observe any spectral differences between the apo- and  $\text{Ca}^{2+}$ -saturated protein. It proved to be very difficult to remove all of the EDTA from the protein, even with

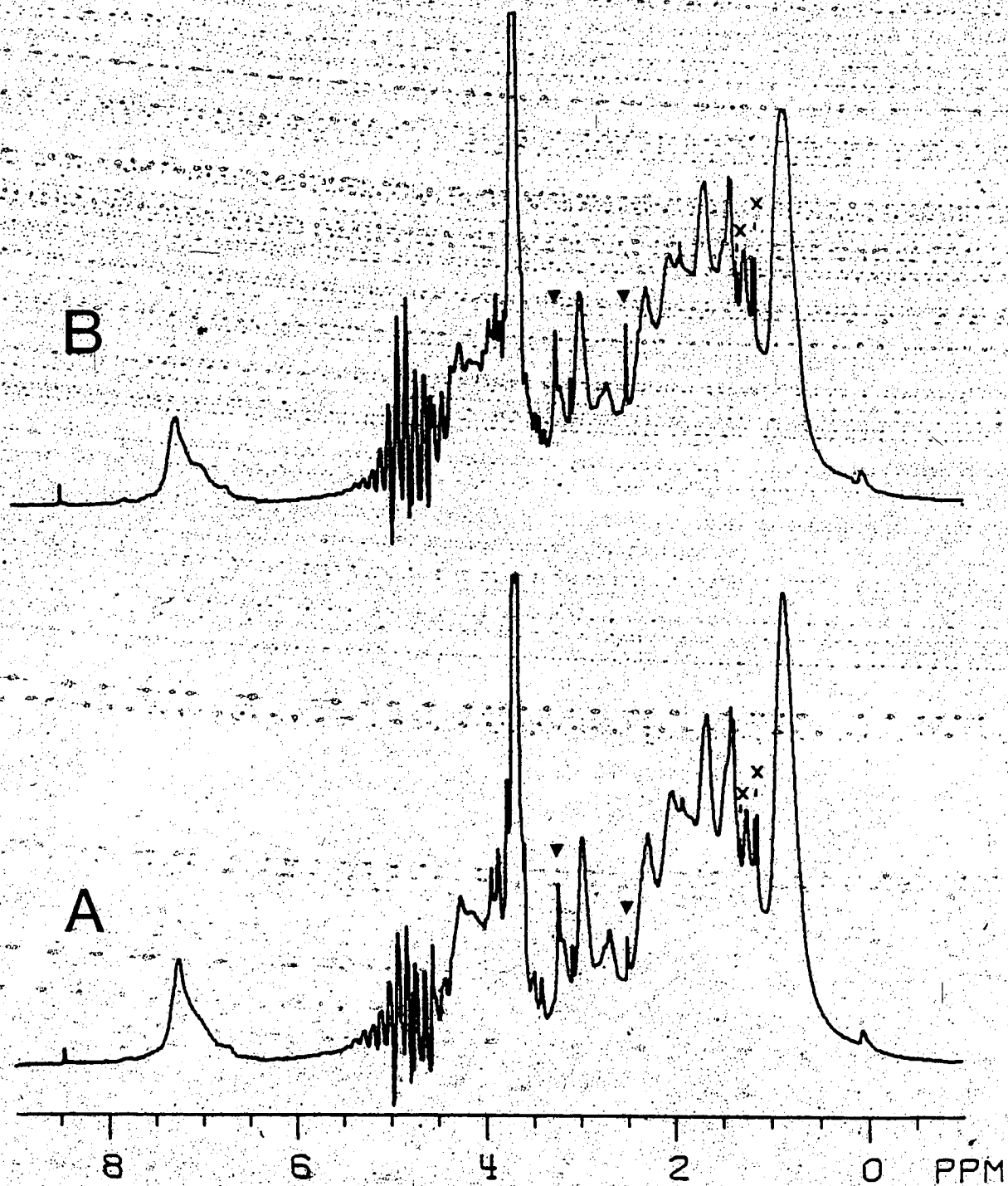


Figure V.7 <sup>1</sup>H NMR spectrum of 0.31 mM apo-DTNB LC in 10 mM Tris, 50 mM KCl, pH 7.8 in the presence of a trace amount of EDTA. The symbols are: x, resonances not seen in published spectra (45); v; metal-bound EDTA resonances.

A. The apo protein spectrum.

B. The spectrum in the presence of excess calcium.

The calcium to DTNB LC ratio was 4.98.

exhaustive dialysis at high salt concentrations.

### C. Discussion

The nature of the CD change observed upon the addition of calcium and the ellipticity values observed for the apo- and calcium-saturated protein in this study (Figure V.5) were consistent with previously published results (45, 188). The value of 24%  $\alpha$ -helix determined by CD was smaller than previously cited values of 33% (188) and 40-50% (174), which may in part have been due to inaccuracies in our analysis, since we used only a limited portion of the spectrum, or which may have been indicative of the presence of small amounts of oxidized protein in the samples. A previous determination of the  $\alpha$ -helical content of the DTNB LC based on its sequence gave a value of 41% (188), using the method and parameters of Chou and Fasman (189). This value agreed fairly well with our determination but both of these theoretical values appear to overestimate the  $\alpha$ -helical contents determined by CD.

The affinity of the isolated DTNB LC for calcium, as measured by CD, is ca. two orders of magnitude below that of the values given in the literature (Table VI.2). The possibility of a significant change in calcium binding affinity due to disulphide formation seemed unlikely since previous workers have found normal binding affinities in the absence of DTT or 2-mercaptoethanol (40), although the effects of aging have, in part, shown to be removed by incubation with

2-mercaptoethanol (161). We were thus achieving a similar type of CD effect upon the addition of calcium, but at a higher metal ion concentration: this result implies that calcium binding was still specific (*i.e.* the calcium was binding to the metal-binding site). The low value of  $K_d$  which we observed may have been due to the effects of age (183) (the protein used in the the CD studies had been stored as the freeze-dried isolated LC for one month prior to use), a preparative or storage technique (*i.e.* lyophilization), or to the presence of EDTA in the samples, which had been immediately obvious in the NMR spectra. Phosphorylation of the light chain would also decrease its affinity for calcium (45,190), but the appearance of the  $^1\text{H}$  NMR spectra indicated that the majority of the protein was in the dephosphorylated state, as will be outlined shortly.

It is readily apparent that each of the lanthanides had quite a different effect on the overall ellipticity of the isolated light chain. One would not intuitively expect to observe such a large difference as the lanthanides are chemically and physically very similar (Chapter II). The effect of the lanthanides seems to vary across the series, with lanthanum having a positive effect, gadolinium having a negative effect, and ytterbium having an even greater negative effect on the ellipticity of the apoprotein, although a more thorough investigation involving many other lanthanide ions would have to be carried out before a definite statement of this type could be made. Due to the large excess of

metal ions employed, it is unlikely that the results reflect a difference in the protein's affinity for the different lanthanide ions, as had been shown for parvalbumin (191) or in the differing affinities of EDTA for these lanthanides (192). Similar studies on a  $\text{Ca}^{2+}$ -binding peptide, which was homologous to the helix-loop-helix regions of the CaBP, have shown that different conformations of the peptide were adopted for the  $\text{La}^{3+}$ -peptide and  $\text{Lu}^{3+}$ -peptide complexes (193). These studies, as well as ours, may indicate that a flexible binding site adopts a conformation which is dependent upon the size (*i.e.* ionic radius) of the lanthanide employed.

The  $^1\text{H}$  NMR spectra of the DTNB LC (Figure V.7) were virtually identical to previously published results, and appeared to most closely resemble the dephosphorylated protein spectrum (45). The state of phosphorylation found in the isolated LC is a function of the extraction buffer content and extraction buffer/muscle volume (184); the conditions that we employed should have resulted in a mixture of the two states, although the protein has been shown to become dephosphorylated with time (181). The spectrum of LC-2 (the protein has 1 his, 1 trp, 2 tyr, and 12 phe residues) bore little superficial resemblance to that of TnC (32), intestinal CaBP (26), parvalbumin (77), or the A1 and A2 light chains (45) in that it lacks the characteristic upfield-shifted methyl and phenyl groups. Also, the addition of calcium ions (Figure V.7B) does not bring about the large

changes in linewidth and chemical shifts reported for these latter proteins (except in the case of A1 and A2, which do not bind calcium): Considering that the amount of change in the  $\alpha$ -helical content of the light chain upon the addition of  $\text{Ca}^{+2}$  was 6%, it seems unusual that a more significant change is not observed in the NMR spectra, as was observed for the titration of bovine brain S100b at pH 7.5 (Chapter VI). In our spectra, it appeared that the affinity of the LC was such that we were observing calcium binding in the slow exchange limit, as the height of some resonances decreased upon the addition of calcium, while the heights of others increased, and no broadening was apparent. The appearance of EDTA in the spectrum has led us to suspect that the affinity of the LC for  $\text{Ca}^{+2}$ , as determined by CD, was probably lowered by contaminating EDTA. The sample which was used in the NMR experiments had been stored for some time in the lyophilized form, and thus the NMR results are preliminary and speculative. It is apparent from our CD work that one should be careful in choosing which lanthanide to use as a calcium analogue; this supports the results of previous studies where lanthanides have been observed to have both very similar and very different effects to those of calcium in a variety of enzymatically active muscle systems (194, 195) and other active enzymes (67, 68). One should be particularly careful when studying structural changes in a system like the isolated DTNB LC which has no enzymatic activity, as such differences in the binding modes of the lanthanides and

calcium may not be as readily apparent. This is particularly true when working with the DTNB LC, since the  $^1\text{H}$  NMR spectrum is little perturbed by the addition of calcium. This study supports growing evidence that one can not simply assume that lanthanide and calcium ions bind to proteins in an identical manner, and that more than one approach, such as X-ray, fluorescence, CD, NMR, and other spectroscopic techniques should be used to probe for the existence and magnitudes of such differences for any one system.

## VI. <sup>1</sup>H NUCLEAR MAGNETIC RESONANCE STUDIES OF BOVINE BRAIN S100b PROTEIN

### A. Introduction

The characterization of proteins specific to nervous tissue is essential for studying the structure and the function of the nervous system at the molecular level. The brain specific S100 protein is localized in multiple sites such as glial cells, neurons, and synaptosomal membranes (196-198, and references therein). This protein is present in a fairly high concentration relative to other soluble brain proteins, suggesting that it plays a major physiological role. The results of previous studies on this protein suggest that it may play a role in the function and development of the nervous system (198-200). S100 protein is a ~~water~~ soluble, highly acidic calcium binding protein (201), which is actually a mixture of two components, S100a and S100b, with a subunit composition of  $\alpha\beta$  and  $\beta_2$  respectively (21,201).

The amino acid sequences of the S-100 proteins have been determined (7,21). The S100b protein polypeptide chain ( $\beta$ -subunit) consists of 91 amino acid residues, whose sequence reveals four clusters of chemically similar residues in the order  $\text{NH}_2$ -hydrophobic-basic-acidic-hydrophobic-COOH, where the four respective sequence residue numbers are: hydrophobic, 4-14; basic, 20-33; acidic, 58-72; hydrophobic, 73-88. Within the cluster of basic and acidic amino acids



there are two regions which have a high sequence homology with the calcium-binding proteins (Figure 1.3). The  $\alpha$ -subunit in S100a consists of 93 amino acid residues and possesses an extensive sequence homology (58 percent) with that of the  $\beta$ -subunit, including the cluster of acidic amino acid residues in the C-terminal half of the molecule, implying a close evolutionary relationship between these subunits. The studies and discussions outlined below will concentrate on the S100b species. This work was undertaken in collaboration with Dr. R. S. Mani and Dr. C. M. Kay at the University of Alberta, who carried out concurrent CD and UV difference spectrophotometric studies on this protein under similar conditions. Their results will be presented in the introduction and discussion, along with those of several other groups who have studied this protein system.

Brain specific S100b protein is unusual in certain aspects compared to other calcium binding proteins like ICaBP, calmodulin and TnC. S100b exists as a non-covalently linked (123) dimer of 21000 daltons in native solvents, whereas the above listed calcium binding proteins exist as monomers. S100b also differs from many other CaBP in that the binding of calcium by the S100b protein results in a conformational change which is accompanied by a loss of secondary structure, rather than an increase, and the structure of S100b is significantly perturbed by monovalent as well as divalent cations (27,123). The far UV CD spectra of S100b at pH 8.5 in the absence and presence of  $Ca^{+2}$  showed

128

that the addition of  $\text{Ca}^{+2}$  caused a conformational change in the protein, resulting in decrease of  $\approx 10\%$  in the  $[\theta]_{222}$  value at 222 nm (27). This represented a larger change than that which had been previously observed ( $\approx 7\%$ ) for this same protein at pH 7.5 (123). The additional decrease in ellipticity at pH 8.5 may be attributed to the higher affinity calcium binding site which is exposed at this pH. Analysis of the CD data indicated a decrease in apparent  $\alpha$ -helical content from 55 to 47 percent (27). The effect of  $\text{Ca}^{+2}$  on the conformation of this protein was very different from its effect on other calcium binding proteins such as TnC and calmodulin (202,203), where an increase in apparent  $\alpha$ -helix content was observed upon calcium addition.

At pH values of ca. 7, skeletal and cardiac TnC have been shown to lose nearly 54 to 60% of their secondary structure in the absence of  $\text{Ca}^{+2}$  and 30 to 52% in the presence of  $\text{Ca}^{+2}$  as the temperature is raised from 5° to 75°C (204). Concurrent CD melt experiments at pH 7.0 showed that S100b is considerably more stable (27); there was a 17% loss in secondary structure in the apoprotein upon raising the temperature from 10° to 70°C, while in the presence of  $\text{Ca}^{+2}$ , there was only a 10% loss in secondary structure. The observed thermal unfolding of the protein was reversible in both states. In this sense S100b behaves more like ICaBP, which is very stable in the same temperature range and which is, in fact, isolated at 65 to 70°C (124). These latter two properties will be discussed below in greater detail.

Several studies have shown that the conformational change induced when  $\text{Ca}^{+2}$  binds to the high affinity site on S100 protein mixture (S100a + S100b) results in the exposure of a discrete hydrophobic portion of the molecule to the solvent (205-207), which may be involved in the physiological function of this protein. The binding of the S100 protein mixture to synaptosomal particles (208,209), liposomes (205,206), myelin basic protein (210), hydrophobic probes (205-207) and chlorpromazine (211) is dependent upon such factors as time, temperature, pH, and the concentration of various mono- and divalent cations. In an earlier study on the mixture of S100 proteins, it was shown that S100 binds 4 moles of  $\text{Ca}^{+2}$  per mole of protein at pH 8.3, while only 2 moles of  $\text{Ca}^{+2}$  were bound at pH 7.6 (205,206). These properties of the protein mixture, as well as those of the isolated S100a and S100b proteins have been shown to also be affected by  $\text{Sr}^{+2}$ ,  $\text{Zn}^{+2}$ ,  $\text{Mn}^{+2}$ ,  $\text{Ba}^{+2}$ ,  $\text{K}^+$ ,  $\text{Na}^+$ ,  $\text{Li}^+$ , and  $\text{Rb}^+$  under various conditions (123,206,212,213).  $\text{Mg}^{+2}$  does not appear to have any effect (27,123,206,208,213). Far UV CD measurements, which were carried out concurrently, indicated a loss of secondary structure when purified S100b, in the absence of  $\text{Ca}^{+2}$ , was titrated from pH 8.6 to 6.0 (27). However, the loss in secondary structure was much smaller when the protein was titrated in the presence of  $\text{Ca}^{+2}$ , so the protein was more susceptible to pH changes in the absence of  $\text{Ca}^{+2}$ , over the range of pH values observed. Earlier studies by our collaborators showed that, at pH 7.5, purified S100b

protein demonstrated a conformational change upon binding  $\text{Ca}^{+2}$ , which resulted in a loss of secondary structure (123). In these same studies, the S100b was shown to bind one calcium ion per monomer with a  $K_d$  value of  $2 \times 10^{-4}$  M. The effect of  $\text{K}^+$  on the protein was antagonistic to  $\text{Ca}^{+2}$ , in that the affinity of the protein for calcium was lowered to  $8 \times 10^{-4}$  M in the presence of 90 mM KCl. The presence of 1.62 mM  $\text{MgCl}_2$  had no significant effect on the conformation of S100b, suggesting some sort of specificity with regard to divalent ions. The interaction of  $\text{Ca}^{+2}$  with purified S100b at pH 8.5 was studied concurrently by aromatic and far UV CD (27). It was evident that two sets of  $\text{Ca}^{+2}$  binding sites per monomer existed at this pH. The calcium affinity of these two sites was  $K_{d1} = 6 \times 10^{-5}$  M and  $K_{d2} = 2 \times 10^{-4}$  M. However, in the presence of 60 mM KCl there was evidence for only one binding site per monomer with  $K_d = 8.5 \times 10^{-4}$  M, and  $\text{Mg}^{+2}$  again had no effect on the conformation of the protein. From the results outlined above (27,123), it was concluded that S100b does not bind  $\text{Mg}^{+2}$  at either pH and that the binding of  $\text{Ca}^{+2}$  to the higher affinity site at pH 8.5 was either inhibited by the presence of KCl, or else the binding of  $\text{K}^+$  caused an increase in  $K_d$  for the tight  $\text{Ca}^{+2}$  binding site.

From sequence analogy with other CaBP, there are two "EF hand" sites in the protein which are shown in regions III and IV in Figure 1.3. The C-terminal site is closely analogous to the EF hand site of the other proteins shown in that figure. If one compares the EF hand sequence for the

N-terminal site in S100b to that of the corresponding region of ICaBP, it is apparent that both sites contain a single amino acid insertion, and that S100b contains the three basic side chains lys-his-lys in positions corresponding to the pro-asn-gln sequence in the calcium binding loop of ICaBP. Previous workers have suggested (8) that titration of the his 25 (his 121 in Figure I.3) residue in the calcium binding loop region may be responsible for exposing the additional calcium binding site ( $K_{d2} = 6 \times 10^{-5}$  M) at pH 8.5, by inducing a pH dependent conformational change in the protein.

The far UV spectrum of S100b is characteristic of a protein with a high phenylalanine to tyrosine ratio (phe/tyr = 7), as shown in Figure VI.1. UV difference spectroscopic results from experiments which were carried out concurrently indicated that the single tyrosine residue was perturbed upon the addition of  $Ca^{+2}$  at pH 8.5 (27). The tyrosyl difference peak was red-shifted, indicating that it was in a less polar environment in the presence of calcium. The magnitude of this shift was smaller than that observed at pH 7.5 (123), suggesting that the tyrosine residue in the apoprotein is in a relatively less nonpolar environment at pH 8.5. It was also evident that one or more phenylalanine chromophores are also perturbed when calcium was bound. The magnitude of these perturbations was greater than those observed at pH 7.5 (123). Therefore, comparison of the difference spectra generated at pH 8.5 (27) with those taken at pH

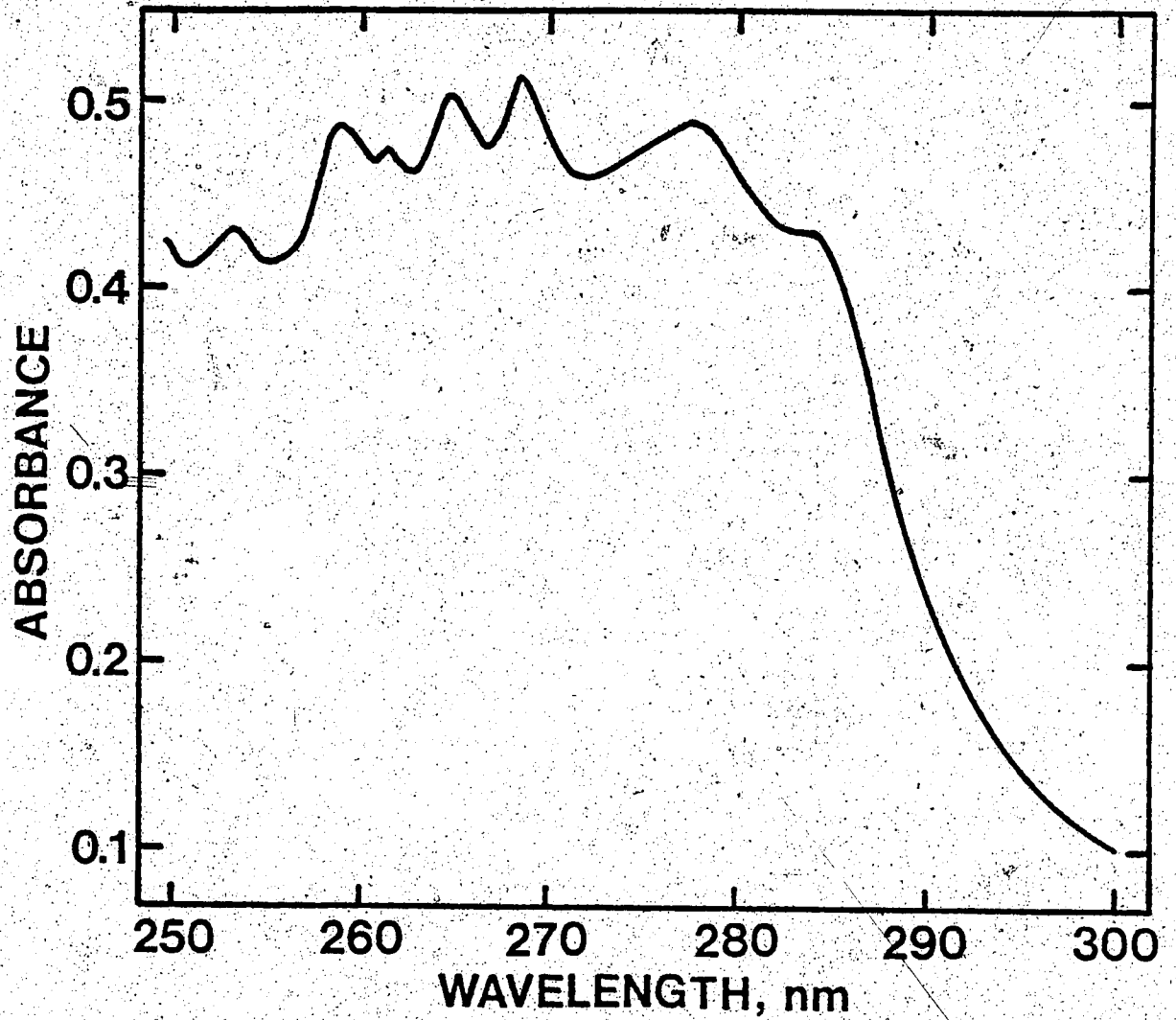


Figure VI.1 The UV spectrum of S100b in 0.1 M Tris-HCl, pH 7.5. Taken from reference 12<sup>B</sup>, with permission.

7.5, (123), indicated that the the microenvironment of the tyrosine and phenylalanine residues were different at these two pH values, and were thus are further perturbed by the binding of a second calcium ion to the protein. These perturbations may be the direct result of structural changes in these residues due to the binding of calcium, or they may be indirectly, due to local charge effects, in that the free negative charge on the carboxyl groups would be reduced by  $\text{Ca}^{+2}$  binding, resulting in changes in the geometry of the binding site and reorientation of the phenolic groups. Observations to this effect have been noted in the past with skeletal and cardiac TnC (214) and porcine intestinal calcium binding protein (39).

Fluorescence studies at pH 7.5 have suggested that S100b possesses one abnormal tyrosine per dimer (123). In an attempt to determine the  $\text{pK}_a$  of this residue, our collaborators performed alkaline pH titrations on S100b. These concurrent far UV and CD studies (27) indicated that apo S100b loses more than 50% of its secondary structure once pH 11.0 is exceeded, and that neither of the the tyrosine residues (one per monomer) titrated below this pH. These results implied that the tyrosine residues in the native S100b dimer were not exposed to the solvent, and that they titrate only after the protein is denatured. In the presence of  $\text{Ca}^{+2}$ , S100b retained its secondary structure up to pH 11.5, indicating that  $\text{Ca}^{+2}$  stabilized the protein somewhat at alkaline pH; the denaturation was irreversible above pH 11 in both

cases (27). These results were supported by other spectrophotometric studies (27).

In the present study we have employed  $^1\text{H}$  NMR to study the binding of  $\text{Ca}^{+2}$  to purified S100b protein, in order to compare these results with earlier CD and UV difference spectroscopic results at pH 7.5 (123), and with similar studies at pH 8.5 which were carried out concurrently (27). These include a  $\text{Ca}^{+2}$  and  $\text{K}^+$  titration of the apoprotein at pH 7.5, followed by the addition of  $\text{K}^+$  and  $\text{Ca}^{+2}$  respectively; a  $\text{Ca}^{+2}$  titration was also carried out at pH 8.23. Both the apo- and  $\text{Ca}^{+2}$ -saturated protein were titrated from ca. pH 5.6 to 8.6 in order to observe the effects of pH on the histidine residues. The ionization characteristics of the single tyrosine residue of the protein in both the presence and absence of calcium were observed by a spectroscopic titration carried out in the alkaline pH range. The heat stability of the protein at pH 7.8 was probed over a temperature range of  $10^\circ$  to  $70^\circ\text{C}$ .

## B. Results

Figure VI.2 shows the complete  $^1\text{H}$  NMR spectra of both the apo- and calcium-saturated forms of S100b at pH 7.5. It is readily apparent that the apoprotein resembles other CaBP's in that it contains upfield shifted methyl and phenylalanine resonances (Figure VI.2A). The number of these resonances was significantly diminished in the presence of



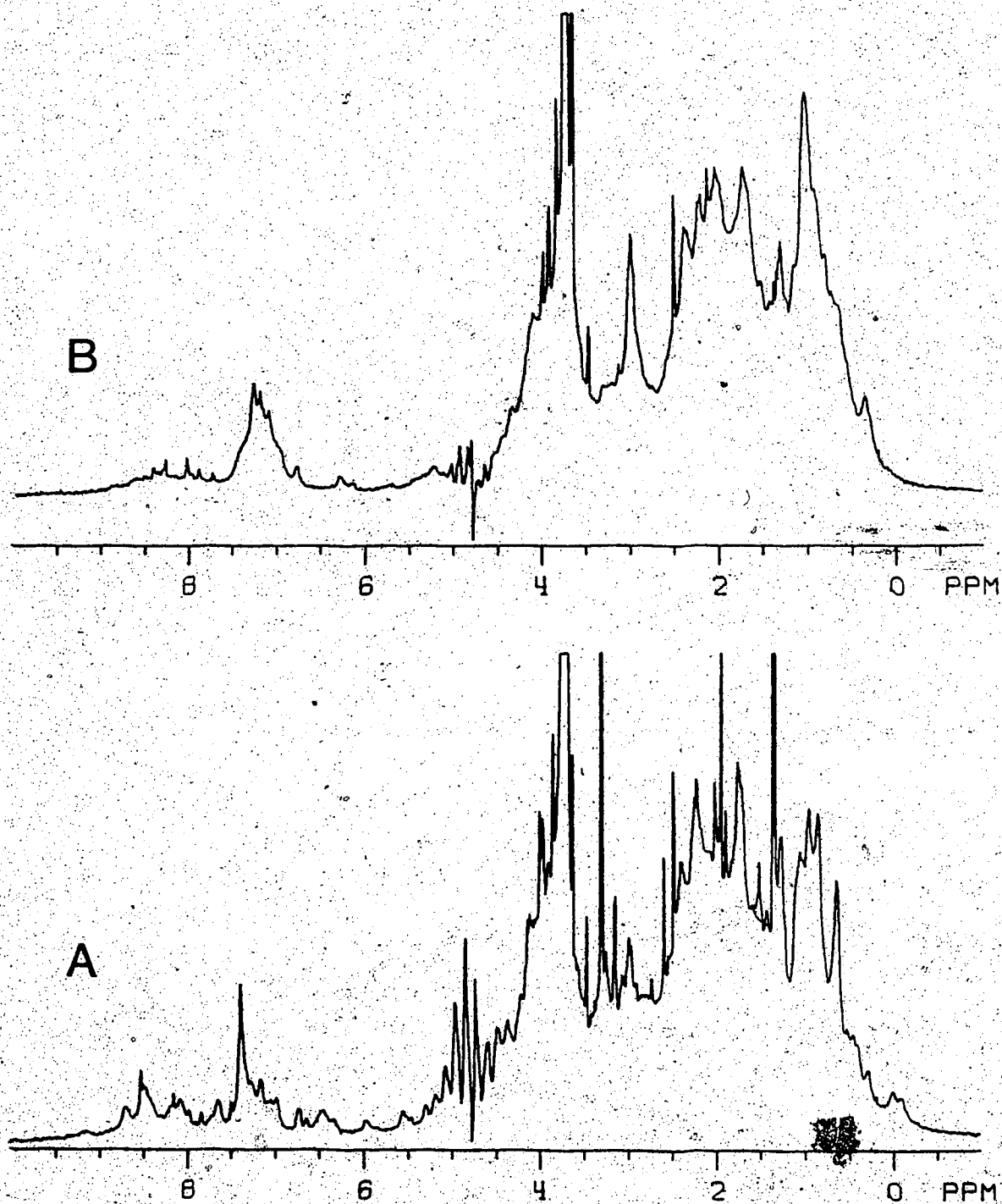


Figure VI.2 The complete 270 MHz <sup>1</sup>H NMR spectrum of 0.4 to 0.5 mM S100b.  
A. The spectrum of apo S100b. The samples had been dialyzed exhaustively against 10 mM Tris, 1 mM EDTA, pH 7.5 prior to lyophilization.  
B. The spectrum of calcium-saturated S100b. The sample had been dialyzed exhaustively against 10 mM Tris, 1 mM CaCl<sub>2</sub>, pH 7.5 prior to lyophilization.

$\text{Ca}^{2+}$  (Figure VI.2B). The rest of the spectra concentrate on the aromatic region of the protein spectrum, which contains the resonances of the aromatic ring protons of seven phenylalanines, five histidines, one tyrosine, and an undetermined number of backbone amide proton resonances which do not exchange rapidly with the deuterated buffer at room temperature. From comparison of these spectra with those of other calcium binding proteins (26,28,29,43), one can attribute the prominent resonance at 7.3 ppm, as corresponding to the majority of the phenylalanine nuclei, the resonance in the range 6.8 to 7.4 ppm to histidine C4 and phenylalanine nuclei, the resonance at 6.7 ppm to the 3,5 protons of two tyrosines, the upfield shifted resonances in the range of 6.2 to 6.6 ppm to phenylalanine protons, and the resonances in the range of 7.5 to 9.0 ppm to histidine C2 protons and amide NH's (with the exception of the contaminating formic acid resonance at 8.44 ppm).

Figure VI.3 shows the results of titration of the apo-protein at pH 7.5 with calcium, and the effect of the subsequent addition of KCl. The addition of calcium up to a  $\text{Ca}^{2+}/\text{S100b}$  ratio of 5:1 causes striking perturbation of the broad phenylalanine envelope, as well as the upfield-shifted phenylalanine resonances, and appears to broaden out many other spectral peaks. The upfield-shifted methyl resonances were also perturbed in that they decreased in number and shifted downfield, as shown in Figure VI.2. The stoichiometry of calcium binding could not be determined directly

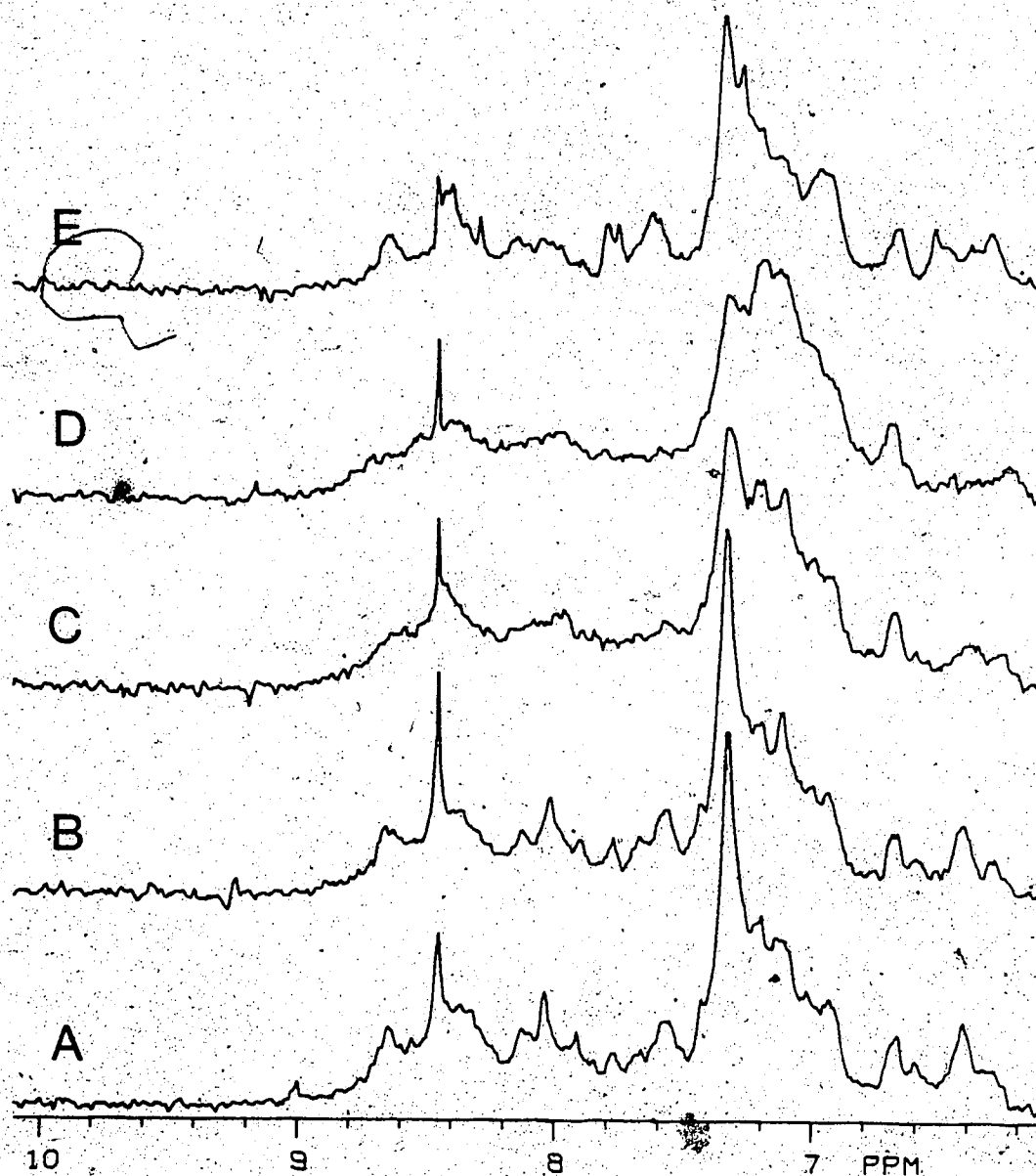


Figure VI.3 Titration of 70 uM apo S-100b in 10 mM Tris, pH 7.5 with calcium, followed by the addition of KCl. The  $\text{Ca}^{2+}$ /S-100b ratios are: A. 0.00, B. 3.08, C. 4.08, D. to E. 5.09. The KCl concentrations are: A. to D. 0, E. 62 mM. The pH of the  $\text{CaCl}_2$  and KCl stock solutions were 7.48 and 6.5 to 7.0, respectively.

from this data as the  $[S100b]=K_d$ , so that a large excess of calcium was needed to maximize the effects of this cation on the  $^1H$  NMR spectra. The addition of KCl was antagonistic, resulting in the resonances becoming sharper again and more clearly resolved, as well as the reappearance of the upfield-shifted phenylalanine resonances. At a slightly higher concentration of S100b (Figure 7, ref. 27), a least squares analysis of the change in intensity of the phenylalanyl resonance at 7.33 ppm versus added calcium, assuming one metal binding site per monomer, gave a dissociation constant of  $2 \times 10^{-4}$  M (Figure VI.4).

Figure VI.5 outlines the results of the titration of the apoprotein at pH 7.5 with KCl, and the effects of subsequent addition of calcium. The initial addition of KCl resulted in some broadening and splitting of the resonance at 7.3 ppm, as well as other changes in the appearance of the spectrum, particularly in the upfield shifted phenylalanines and in the histidine/backbone amide region from 9.0 to 7.5 ppm but the changes are much smaller than those induced by the addition of calcium first. Further addition of calcium caused only minor changes in the spectrum. The final spectra, irrespective of which cation was added first (Figure VI.3E and VI.5E), were very similar.

Figure VI.6 shows the titration of the five histidines of apo S100b in 60 mM NaCl. The pH was adjusted by the addition of small aliquots of NaOD and DCl. The original sample,

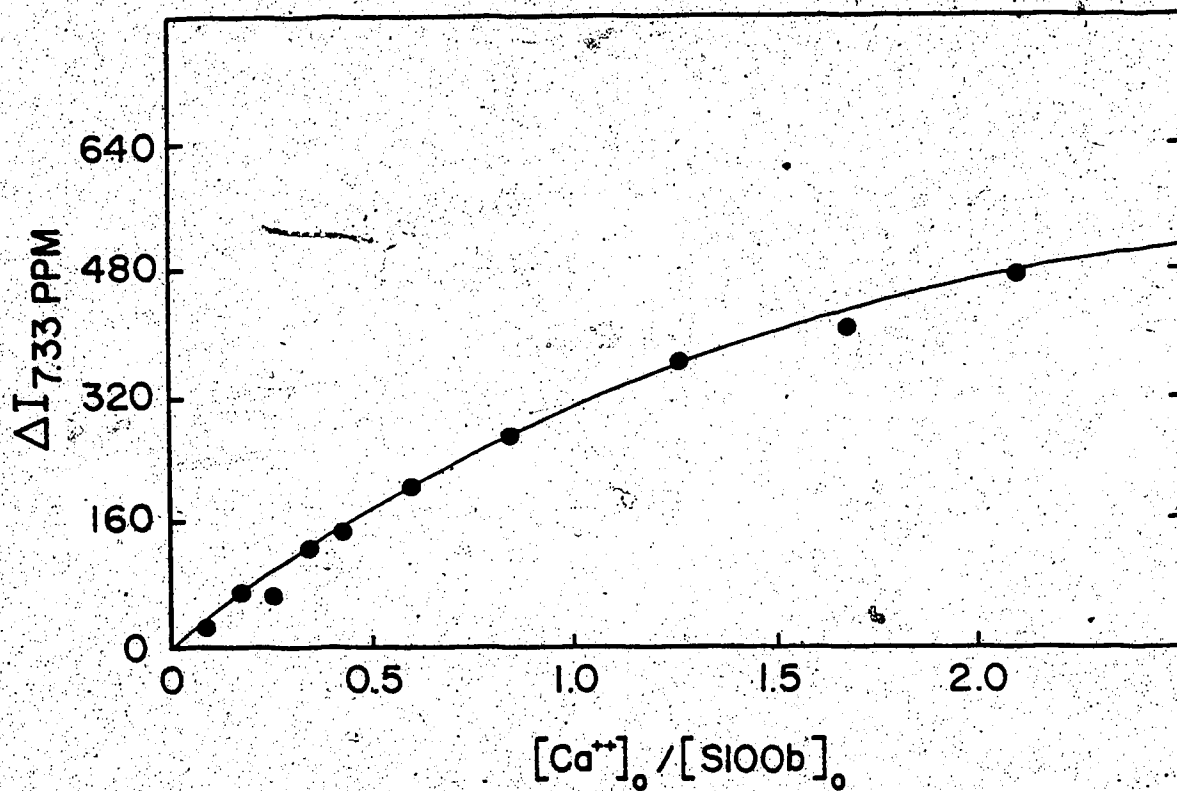


Figure VI.4 The plot of the change in intensity (in arbitrary units) of the 7.33 ppm phenylalanine resonance at pH 7.5 as a function of  $[Ca^{2+}]_0/[S100b]_0$ . The sample was 0.21 mM S100b in 10 mM Tris, pH 7.5. The pH of the  $CaCl_2$  stock solution was 7.48. The spectra are shown in Figure 7, Reference 27.

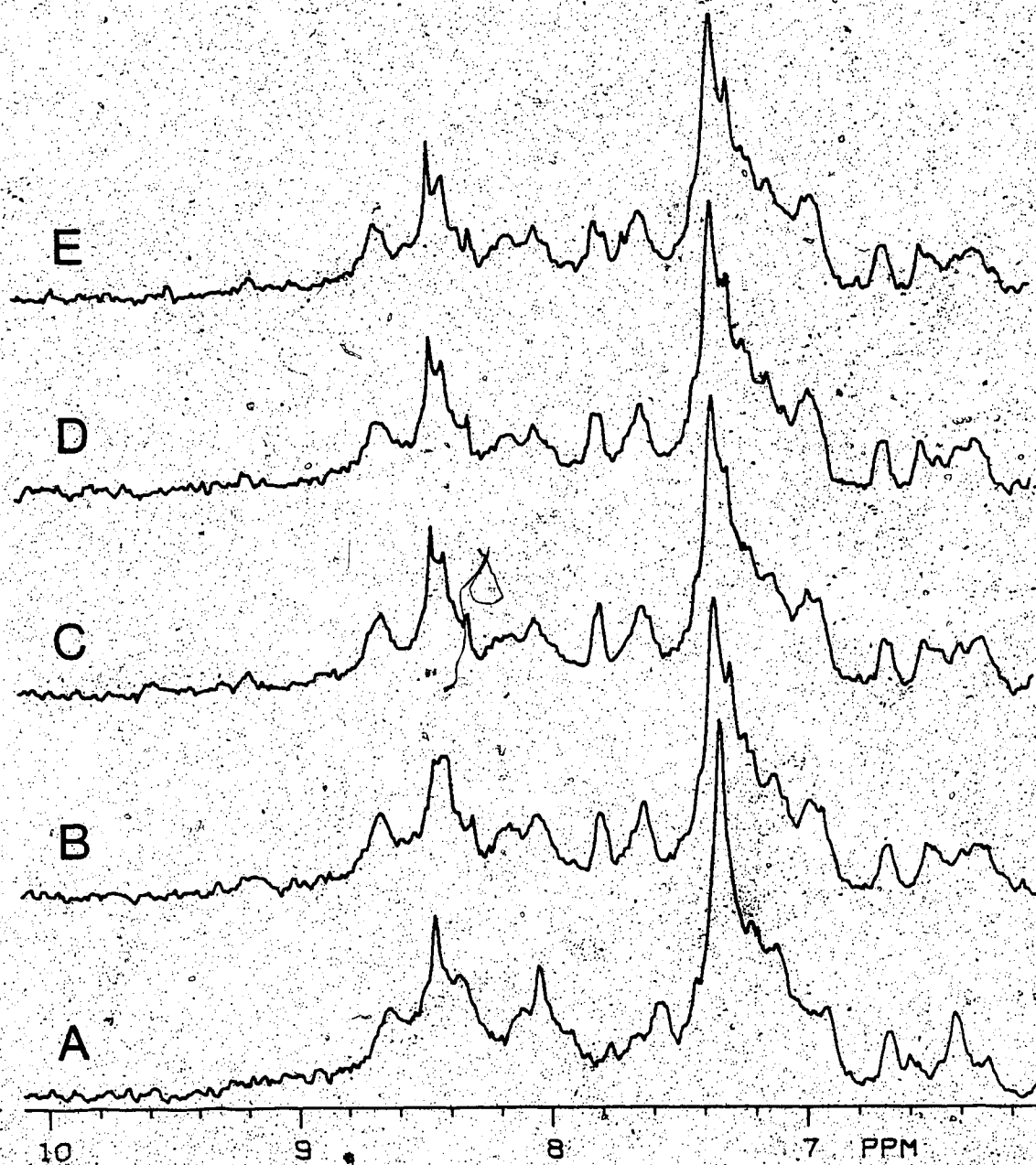


Figure VI.5 Titration of 70  $\mu\text{M}$  apo S-100b in 10 mM Tris, pH 7.5 with KCl, followed by the addition of calcium. The KCl concentrations are: A. 0, B. to E. 63 mM. The  $\text{Ca}^{2+}$ /S-100b ratios are: A. to B. 0, C. 3.05, D. 4.08, E. 5.09. The original sample was identical to that outlined in Figure VI.3 and the same  $\text{CaCl}_2$  and KCl stock solutions were employed.

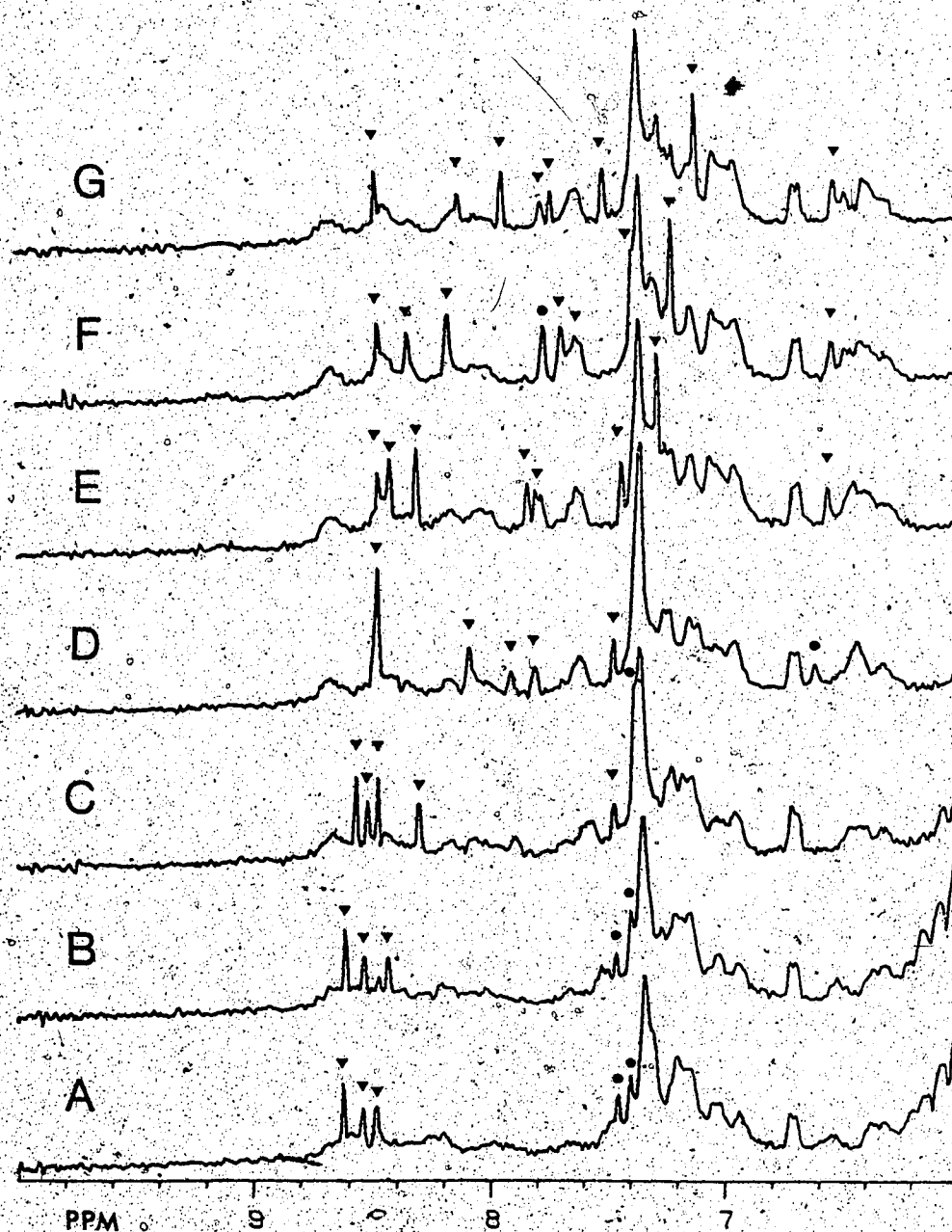


Figure VI.6. The pH titration of the histidine residues of apo S100b. The buffer was 10 mM Pipes and the sample was made up to 60 mM NaCl through the addition of dithionite NaCl in  $D_2O$ . The protein concentration was 0.2 mM. The pH values are: A. 5.58, B. 5.92, C. 6.55, D. 7.09, E. 7.62, F. 7.94, G. 8.49. The resonances marked ▼ were isolated by the T2HSE Pulse technique; those marked ● were not so clearly resolved by that technique but appear to follow the logical shift pattern of the ▼ resonances. For the T2HSE series,  $P1=18\mu\text{sec}$ ,  $P2=9\mu\text{sec}$ , and  $D1=20\text{msec}$ .

prior to any adjustments, was pH 7.09. This sample was first taken up to pH 8.5, then back to 7.09, down to 5.6, and back up to 7.09. The final concentration of Na<sup>+</sup> added was 7 mM. After the samples at pH 5.6 and 8.5 were run, and the pH was restored to 7.09, new spectra were taken. These spectra were very similar to the spectra of the original sample, so that the effects of the small amount of added Na<sup>+</sup> were negligible and the titrations were reversible. The experiment was initiated in 60 mM NaCl as the resonances tend to be more clearly resolved in the presence of salt, and several of the histidine C2 resonances were resolved more clearly using the Hahn Spin Echo Pulse sequence (129). The histidine resonances continue to shift over the entire pH range of 5.6 to 8.5, titrating slowly up to about pH 6.8, then shifting to a much larger degree as one goes to higher pH. The magnitude of these shifts can most easily be observed in Figure VI.7. These results suggest that the influence of pH is more than expected from a simple one proton titration curve, and most likely that a structural change was being felt by these residues.

Figure VI.8 shows the titration of the five histidines in calcium-saturated S100b in 60 mM NaCl. The sample pH was adjusted in the same manner as outlined for the apoprotein and again the effect of the small amount of Na<sup>+</sup> was negligible and the titrations were reversible. It was apparent in this case that one gets the same type of sensitivity to pH over the range 5.7 to 8.6 that was observed for the apo



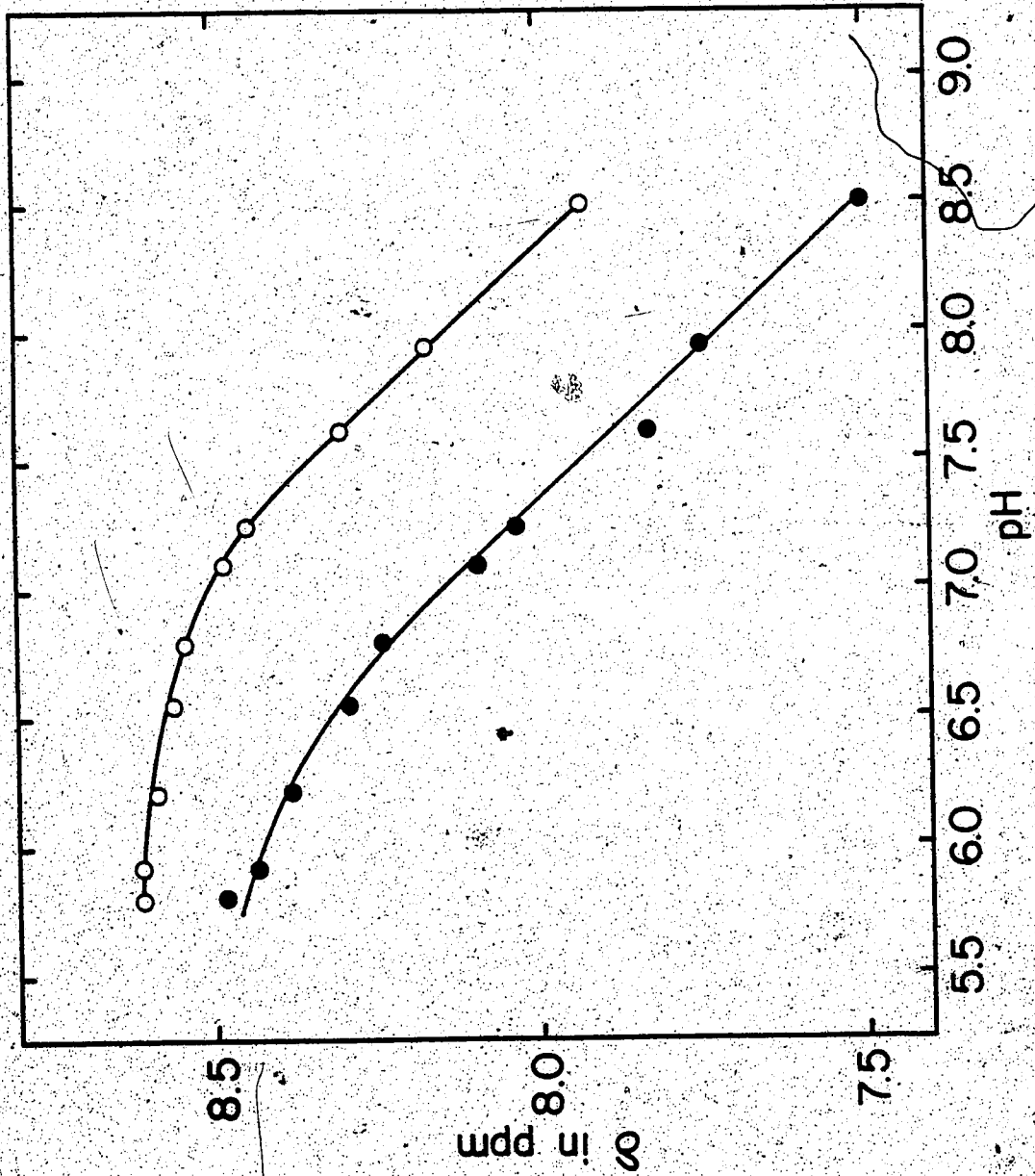


Figure VI.7. The plot of the chemical shift of two of the histidine resonances of apo S100b as a function of increasing pH. The values of the chemical shifts at pH 7.09 were:  $\circ$ , 8.48 ppm;  $\bullet$ , 8.10 ppm.

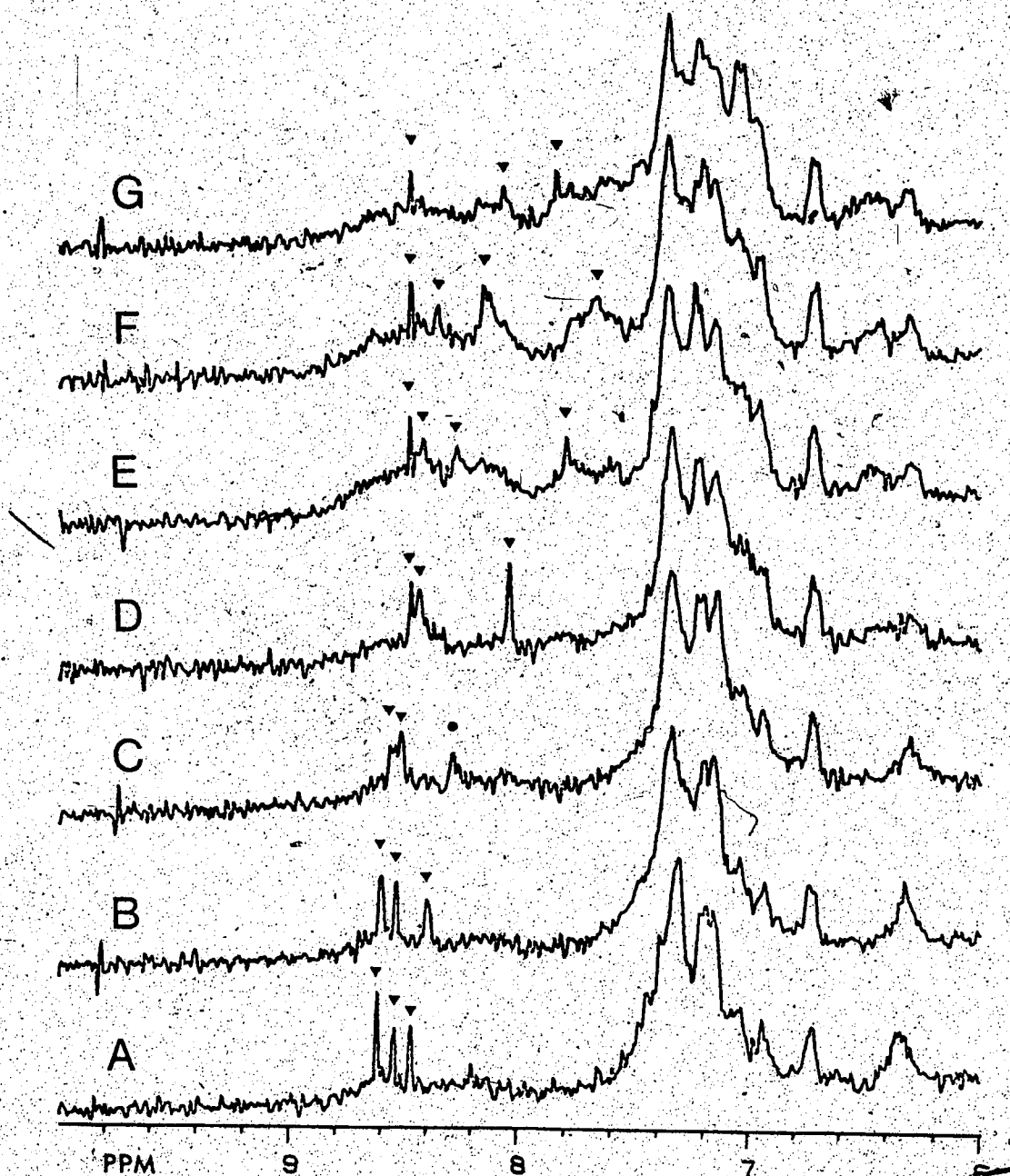


Figure VI.8. The pH titration of the histidine residues of calcium-saturated S100b. The sample was identical to that outlined in Figure VI.4, excepts that a small aliquot of calcium in the same buffer system was added to a final  $\text{Ca}^{2+}$ /S100b ratio of 6:1. The pH values are: A. 5.66, B. 6.02, C. 6.47, D. 7.09, E. 7.62, F. 7.89, G. 8.59. The  $T_2$  Hahn spin echo pulse experimental parameters and the ▼ and ● labelling are as outlined in Figure VI.6.

protein, which is again indicative of the influence of more than a simple one proton titration of the histidine resonances. A plot of the chemical shift of two of the histidine resonances in the calcium-saturated protein as a function of pH is shown in Figure VI.9. These are the same two histidines which were plotted in Figure VI.7, and the spectral changes did not appear to be as large as those observed in the absence of calcium.

Figure VI.10 illustrates the titration of apo S100b with calcium at pH 8.23. The broad phenylalanine/histidine C4 envelope is significantly perturbed by the addition of calcium, and the magnitude of this perturbation is maximized at a  $\text{Ca}^{+2}/\text{S100b}$  ratio of 2:1, indicating that two moles of  $\text{Ca}^{+2}$  are bound per S100b dimer. As observed in Figure IV.3, the addition of calcium at this pH also results in a general broadening of resonances throughout the spectrum. The resulting plot of intensity of the phenylalanine envelope as a function of  $[\text{Ca}^{+2}]_0/[\text{S100b}]_0$  is shown in Figure VI.11. The data lacked sufficient points in the critical region to accurately and independently determine the two binding constants observed in the CD studies, but a calculated binding curve using the two  $K_d$  values determined from concurrent CD and UV difference spectrophotometric titrations (27) fit the observed data well.

The spectra accumulated during the alkaline pH titration of S100b are illustrated in Figures VI.12 and VI.13.

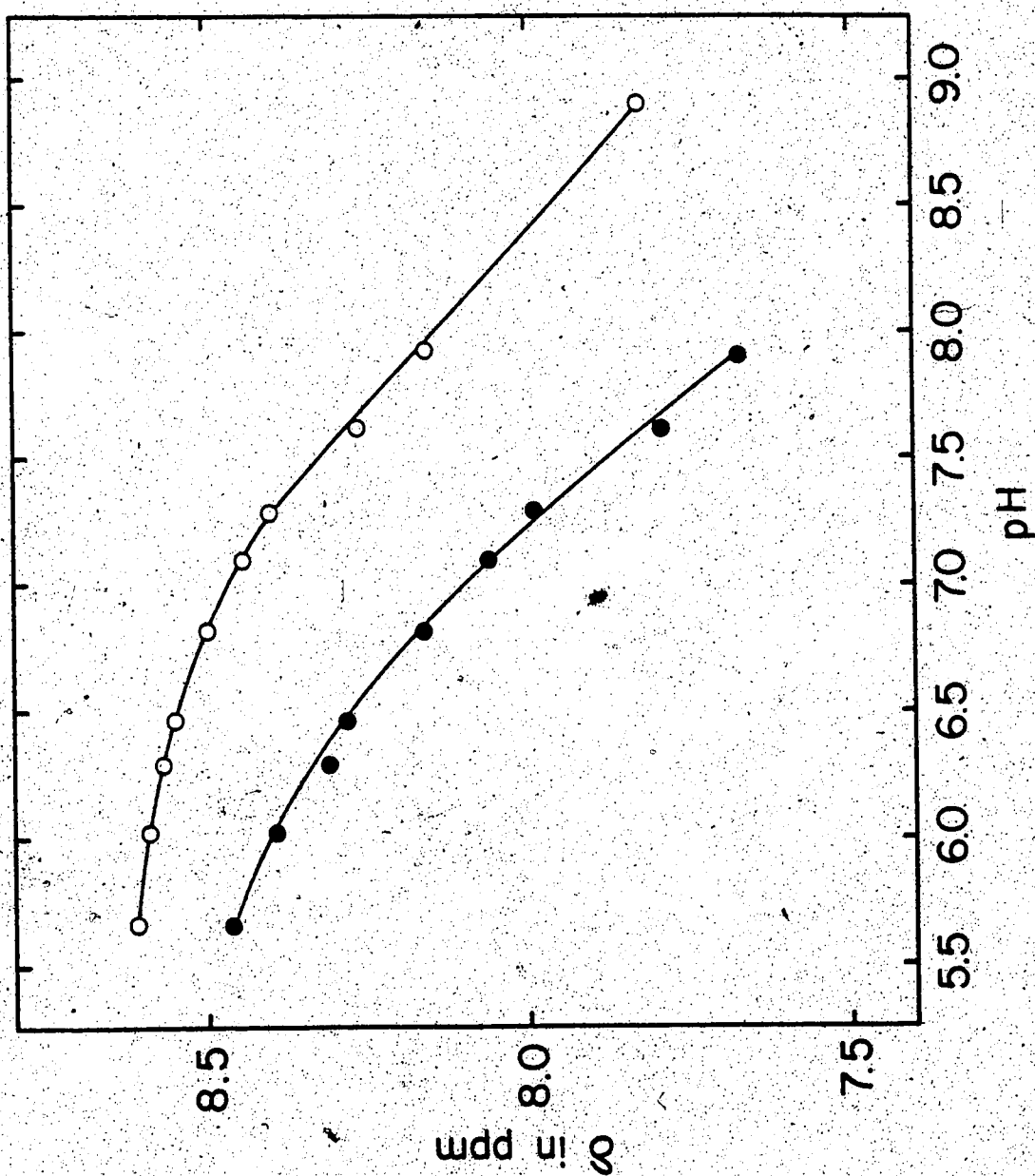


Figure VI.9 The plot of the chemical shifts of two of the histidine resonances of calcium-saturated S100b as a function of increasing pH. The values of the chemical shifts at pH 7.09 were: o, 8.44 ppm; •, 8.06 ppm.

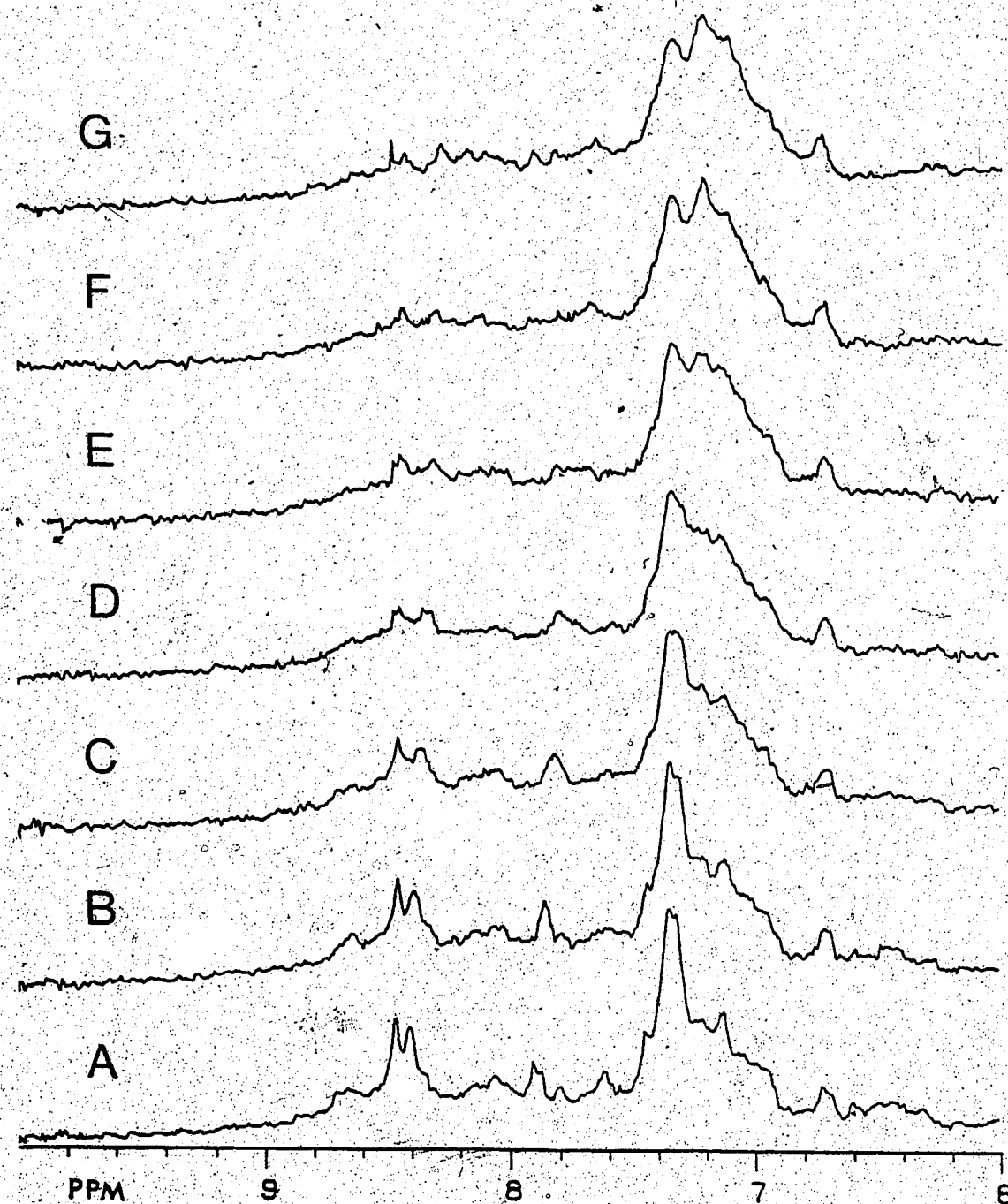


Figure VI.10. Titration of apo S-100b with calcium at pH 8.23. The buffer was 10 mM Tris and the protein concentration was 0.12 mM. The  $\text{Ca}^{2+}/\text{S-100b}$  ratios were: A. 0.00, B. 0.53, C. 1.04, D. 1.58, E. 2.10, F. 3.21, G. 4.37. The stock calcium solution was made up in the same buffer at pH 7.45.

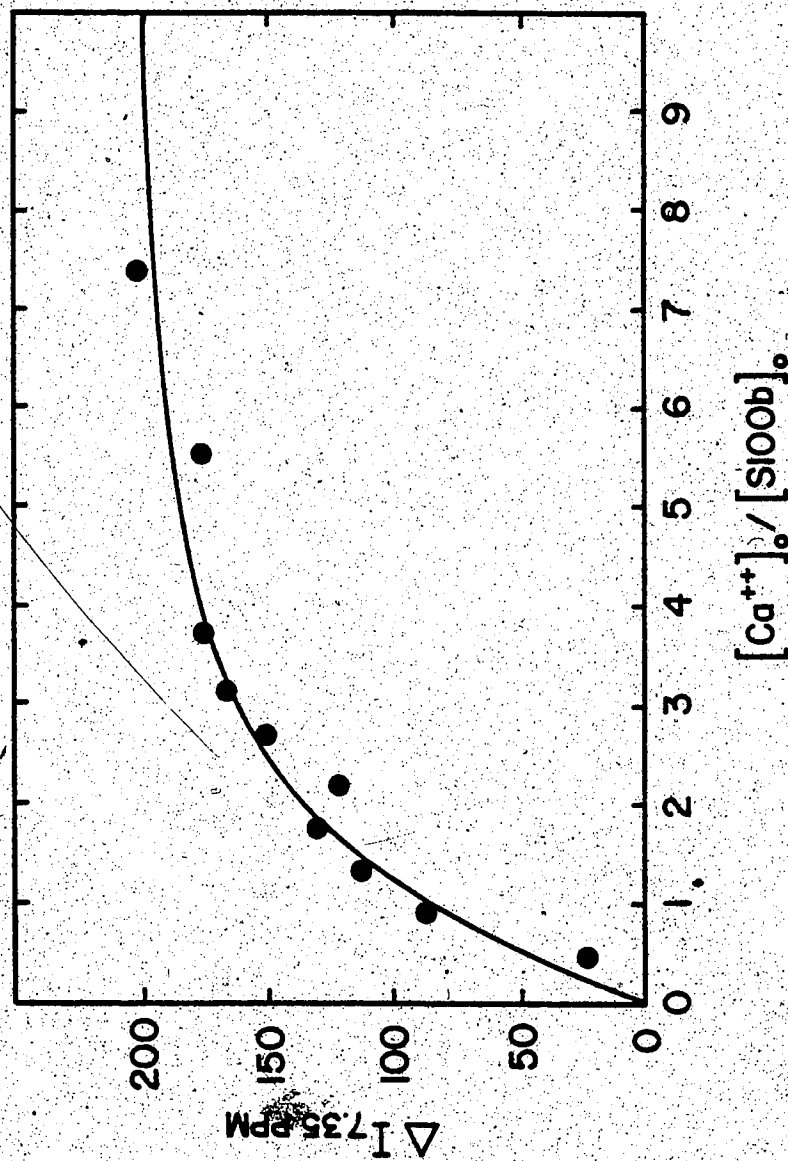


Figure VI. 11 The plot of the change in intensity (in arbitrary units) of the 7.35 ppm phenylalanine resonance at pH 8.23 as a function of  $[Ca^{++}]_0/[S100b]_0$ . The data was taken from the spectra shown in Figure VI. 10.

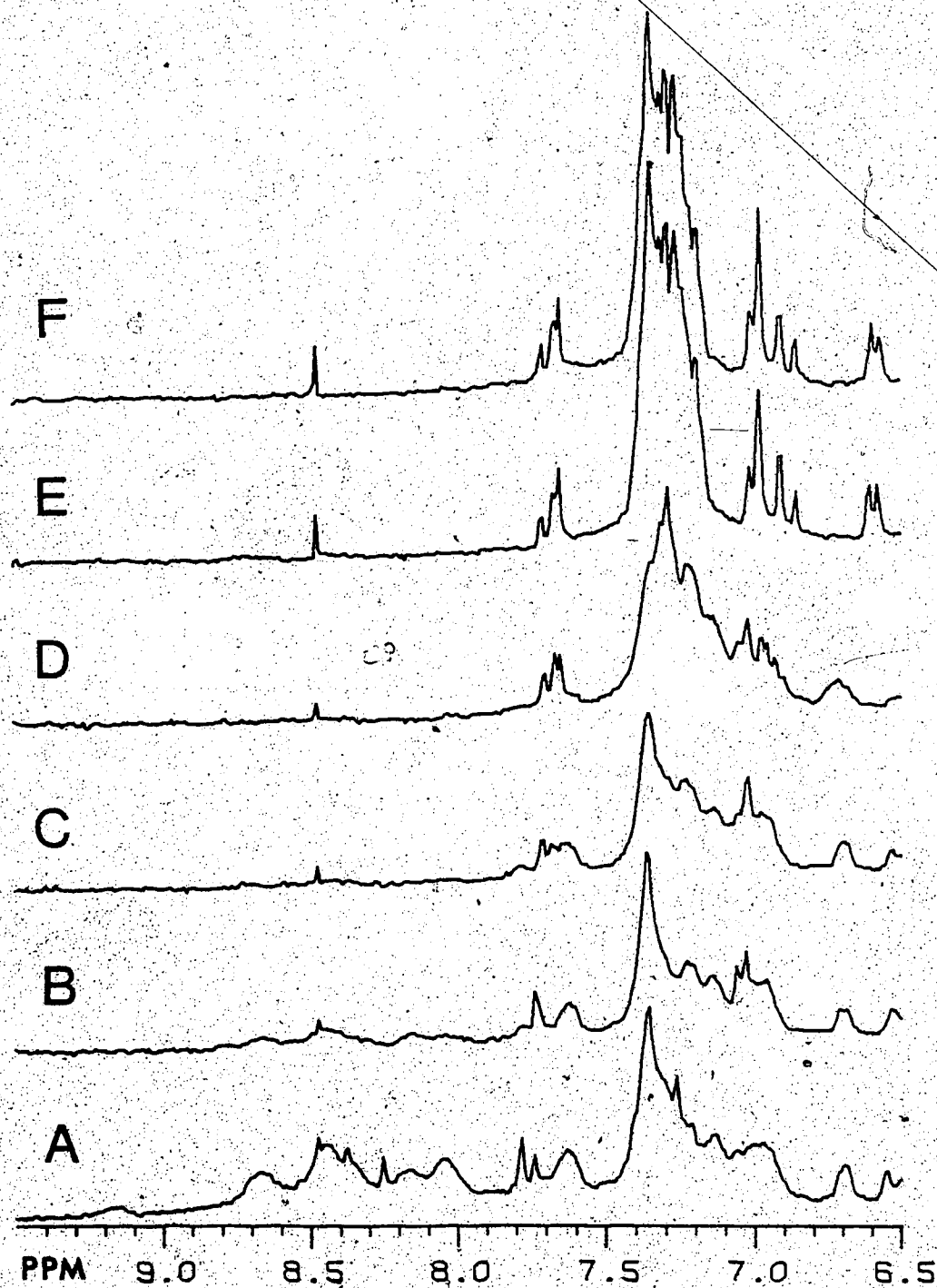


Figure VI.12 Alkaline pH titration of apo S100b in the absence of calcium. The sample conditions were as outlined in Figure VI.2A. The pH values are: A, 8.35; B, 10.12; C, 10.91; D, 11.16; E, 12.08, F, 12.58.

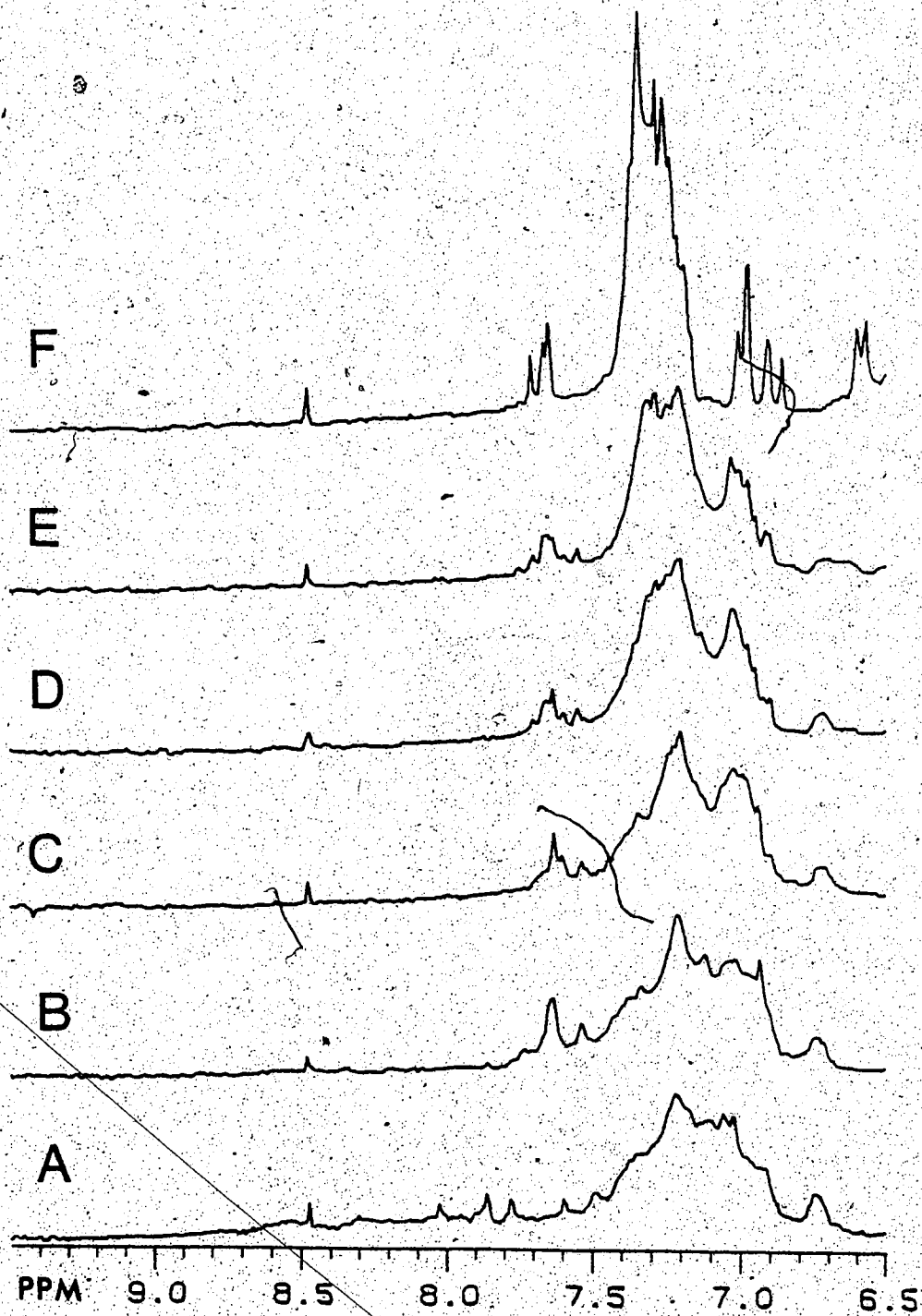


Figure VI.13 Alkaline pH titration of S100b in the presence of calcium. The sample conditions were as outlined in Figure VI.2B. The pH values are: A, 8.35; B, 9.94; C, 10.99; D, 11.41; E, 11.55; F, 12.58.



The concurrent CD measurements indicated that S100b lost more than fifty percent of its secondary structure once pH 11.0 was exceeded, which implied that the tyrosine residue in the native protein is not exposed to the solvent and titrated only after the protein was denatured. In the presence of  $\text{Ca}^{+2}$  the protein began to lose its secondary structure at  $\text{pH} > 11.4$  (Figure VI.13) as opposed to pH 10.9 in the absence of  $\text{Ca}^{+2}$  state (Fig. VI.12). In neither case was the denaturation reversible from the end point (pH 12.6) of the titration. As can be appreciated from the spectra shown in Figures VI.12 and VI.13, it was not possible to plot the chemical shift of the tyrosine resonances as a function of increasing pH due to the overlap of the phenylalanine resonances. The inherent stability gained by the protein upon the binding of  $\text{Ca}^{+2}$  was also reflected by the observation that there were only minor effects upon the spectrum of  $\text{Ca}^{+2}$ -saturated S100b protein as a function of temperature when the temperature was raised from 26°C to 70°C.

Since we were not able to titrate the tyrosine, and therefore definitely assign the tyrosine proton resonances, an attempt was made to assign the tyrosine 3,5 proton resonances using the laser photochemical induced dynamic nuclear polarization method. This attempt was unsuccessful for S100b in both the presence and absence of  $\text{Ca}^{+2}$  because the results, which depend upon exposure of the amino acid, were negative.

### C. Discussion

The data presented in this study support the near and far UV CD measurements carried out concurrently (27), in that they indicate the existence of two sets of calcium binding sites at pH 8.23 with  $K_d$  values of  $6 \times 10^{-5}$  M and  $2 \times 10^{-4}$  M, whereas at pH 7.5 the protein binds only one  $\text{Ca}^{2+}$  per monomer with  $K_d = 2 \times 10^{-4}$  M. It was apparent from the aromatic CD and UV difference spectra at both pH values that binding of  $\text{Ca}^{2+}$  to S100b resulted in the perturbation of the single tyrosine and one or more of the 7 phenylalanine residues (27), and this was supported by the NMR spectra. Both the NMR and far UV CD experiments suggest that S100b undergoes a conformational change when the protein is titrated from pH 8.0 to 6.0, the magnitude of which appeared to be smaller in the absence of calcium. This result was not unexpected in view of the different number of  $\text{Ca}^{2+}$  binding sites observed for S100b at pH 7.5 and pH 8.23. The decrease in secondary structure upon  $\text{Ca}^{2+}$  binding observed in the collaborative studies (27) manifests itself in the NMR spectra as a loss of the upfield-shifted phenylalanine and methyl resonances. Both of these observations are consistent with the explanation put forward for the exposure of the extra calcium binding site at pH 8.5, via deprotonation of his 25 (his 121 in Figure 1.3)(8). The overall affinity of this site for calcium is lower than that of the ICaBP, likely due to the presence of the additional basic side chains in the C-terminal loop region of the protein molecule.

(region III, Figure I.3).

It is noteworthy that the extra site exposed at pH 8.5 was specific for calcium, since the concurrent studies showed that  $Mg^{+2}$  had no effect on S100b protein conformation and  $Ca^{+2}$  was able to induce a conformational change in the protein in the presence of  $Mg^{+2}$  (27). However, the presence of  $K^+$  resulted in a decrease in the binding of  $Ca^{+2}$  to the higher affinity site exposed at pH 8.5. In the presence of  $K^+$  the binding affinity for  $Ca^{+2}$  is virtually the same at both pH 7.5 and 8.5, hence it is the low affinity  $Ca^{+2}$  binding site which operates in the presence of  $K^+$  that is the one of physiological significance. Similarly, in the case of the TnC molecule it is the  $Ca^{+2}$  specific low affinity calcium binding site that is important from the physiological standpoint. However, differences do exist between these two systems, as  $Mg^{+2}$  can compete with  $Ca^{+2}$  for the high affinity site in TnC, whereas  $K^+$  has no effect. Both the CD (27) and NMR work indicated that  $Ca^{+2}$  and  $K^+$  display "antagonistic" effects with respect to their perturbation of the structure of S100b. This is shown in the NMR spectra by the fact that the effects of  $Ca^{+2}$  binding could be reversed by  $K^+$ , and *vice versa*, which would be essential if these two cations are involved in controlling the function of S100b. At this time it is not clear whether  $Ca^{+2}$  and  $K^+$  bind to the same site, or to different sites on S100b.

The single tyrosine residue of the S100b monomer appeared to give rise to only a single pair of doublets in the  $^1\text{H}$  NMR spectra, suggesting that the two tyrosines which are present in the dimer (one per monomer) are in similar environments. Therefore we cannot correlate any particular spectral characteristics of this tyrosine residue to the previous fluorescence studies at pH 7.5 which suggested that the S100b dimer possesses one abnormal tyrosine (123). The tyrosine resonance in the  $^1\text{H}$  NMR work indicates that the tyrosines in the dimer ionize at alkaline pH only after the protein undergoes denaturation, and they appear to ionize in an identical fashion. The NMR results showed clearly that the protein unfolds as one tries to titrate tyrosine in either the presence or absence of  $\text{Ca}^{2+}$ . This was evidenced by the shifting of the phenylalanine and tyrosine proton resonances to those chemical shift values typical of the free amino acids in solution. For the apoprotein, this was observed as we titrated above pH 10.9, while in the presence of calcium, one needs to go to a higher pH ( $>11.4$ ) to get denaturation. These results agree well with the concurrent spectrophotometric pH titration data (27), and indicate that  $\text{Ca}^{2+}$  confers some stability to the protein at high pH. Because of the denaturation of the protein, it was not possible to obtain a  $\text{pK}_a$  value for the tyrosine, but these results suggest that the tyrosine residue is either buried in the interior of the protein molecule, or that intramolecular interactions exist between the phenolic hydroxyl group of

the tyrosine residue and a carboxyl group of either an aspartic acid or glutamic acid, as suggested by recent fluorescence studies with the homologous intestinal calcium binding protein (125). Moreover, recently Morero and Weber (207) have proposed that a hydrogen bond between the tyrosine residue and a carboxyl ion acceptor group might exist in the case of the native mixture of S-100 proteins, based on the UV difference spectrum generated between pH 7.3 and 3.5. The fact that no CIDNP was observed for the protein in either the presence or absence of  $\text{Ca}^{++}$  suggests that it is buried in both forms of the protein, but this conclusion is suspect as there are five histidines in the protein which are also susceptible to polarization by this technique. It is possible that the tyrosine effect was swamped out due to competition with one or more of the five histidines of the protein.

The concurrent CD melt experiments showed that with S100b the loss of secondary structure at 70°C was only 17 percent in the absence of calcium and 10 percent in its presence, and the studies outlined above indicated that the protein was more stable in the presence of  $\text{Ca}^{++}$  at alkaline pH (27). The NMR spectra of  $\text{Ca}^{++}$ -saturated S100b in 60 mM KCl, pH 7.8 showed only small structural changes upon heating this sample to 70°C and that these were completely reversible, aside from the loss of the histidine and most of the backbone NH resonances which was due to exchange with the deuterated buffer (results not shown). This property

could, in future work, be a means of simplifying the aromatic region of the spectrum.

Understanding the structure and function of the central nervous system at the molecular level involves studying the chemistry and physiological behaviour of its constituent proteins. Bovine brain S100b is a unique and very interesting CaBP. The additional spectral data obtained in the NMR, CD, and UV difference studies has enabled us to compare the behaviour of S100b with the other CaBP more fully, which hopefully has given us some insights as to how it might function physiologically in the brain.

VII. <sup>1</sup>H NUCLEAR MAGNETIC RESONANCE STUDIES OF PORCINE  
INTESTINAL CALCIUM BINDING PROTEIN: TYROSINE RESONANCE  
ASSIGNMENTS

A. Introduction

High affinity calcium-binding proteins with molecular weights near 10,000 have been found in the small intestines of several mammalian species (215-218). The synthesis of these proteins is dependent upon Vitamin D, and the protein is probably indirectly involved in the transport of calcium across the intestine (218,219). Porcine intestinal calcium binding protein (ICaBP) is a compact, globular protein (MW 8799), whose amino-acid sequence of 78 residues has been determined (14)(Figure I.3). Porcine ICaBP is highly homologous to the bovine ICaBP (87%)(220,221); the X-ray crystal structure of the minor A form of the bovine protein is known (8) and is shown in Figure VII-1. An examination of the evolutionary relationships among various CaBP's show that the porcine intestinal CaBP is distantly related to parvalbumin and troponin-C (222). The amino acid composition is unique in that there is a lack of his, met, cys, and trp residues, but it is typical of CaBP's in that it contains a high concentration of acidic residues (22%) and contains a sequence (residues 55-69) which is very similar to the EF calcium binding site of carp muscle parvalbumin. A second portion of the sequence (residues 15-30) shows a limited homology to the CD site of carp parvalbumin which includes

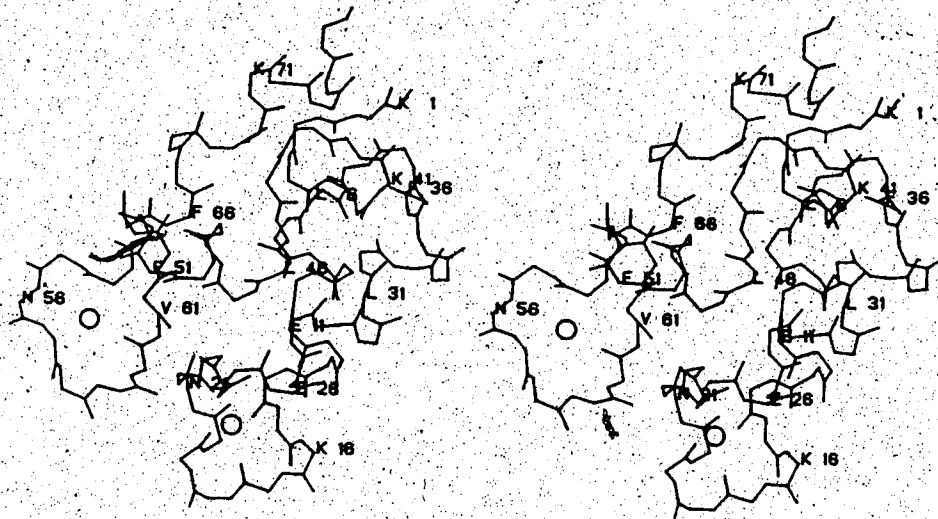


Figure VII.1 A protein-backbone stereo drawing of the X-ray crystal structure of the minor A form of bovine intestinal calcium binding protein. Atomic coordinates available from Brookhaven Protein Data Bank were used to prepare this figure.



an insertion of Pro at residue 23. (Figure I.3).

The porcine ICaBP binds 2 moles of  $\text{Ca}^{+2}$  per mole of protein, with  $K_{d1} = K_{d2} = 5 \times 10^{-7}$  M (39,229), and both the porcine (227) and the bovine (223) protein appear to bind  $\text{Ca}^{+2}$  randomly to these two sites. The UV spectrum of porcine ICaBP, shown in Figure VII.2, is characteristic of a protein with a high phenylalanine to tyrosine ratio (phe/tyr = 5), and is very similar to that of bovine brain S100b (Figure VI.1). Both the tyrosine and one or more of the phenylalanine residues have been shown to be perturbed when porcine ICaBP binds metal ions, but there is little effect on the overall conformation of the protein, suggesting that the dramatic changes in aromatic optical activity arise from local effects near the binding sites (39). This chapter describes the assignment of the tyr resonances in the  $^1\text{H}$  NMR spectrum of the protein and the use of  $^1\text{H}$  NMR to study the environment of aromatic residues within the protein, conformational changes in the protein caused by calcium binding and the calcium binding stoichiometry.

## B. Results

The complete  $^1\text{H}$  NMR spectrum of the apo protein is shown in figure VII.3, along with an expanded view of the aromatic region. Of particular interest in the aliphatic region of the spectrum are the upfield shifted methyl groups at 0.49 and 0.12. The resonances in the expanded aromatic region are derived from several sources. No backbone amine

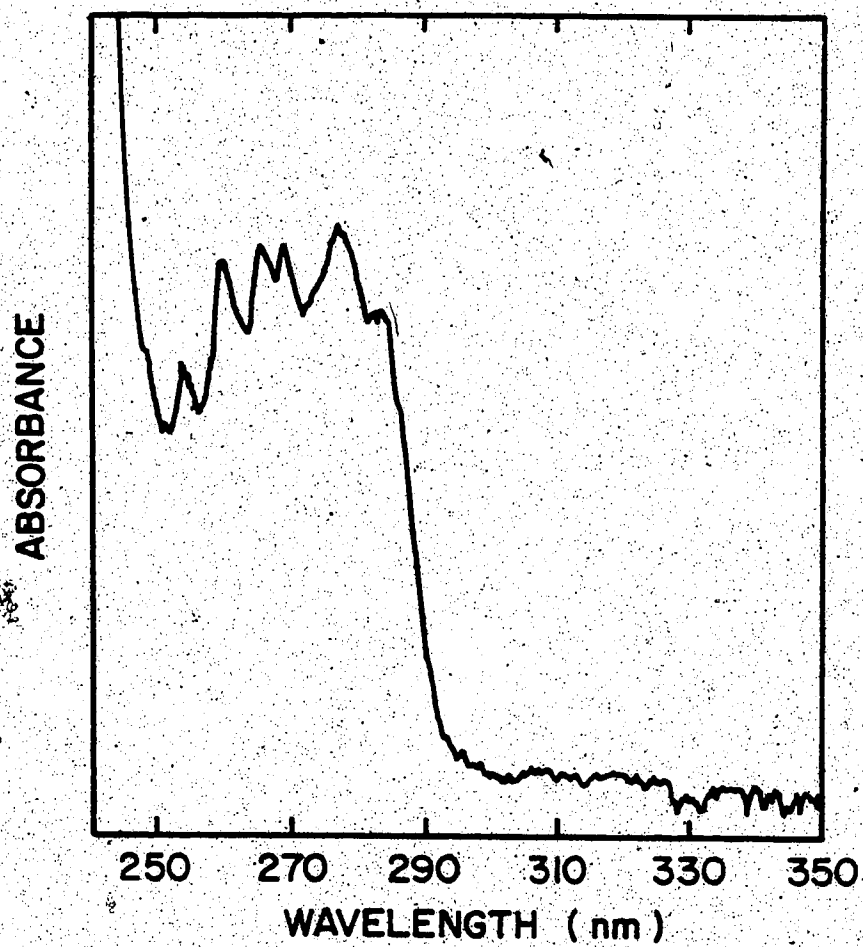


Figure VII.2 The UV spectrum of porcine ICaBP in D<sub>2</sub>O.

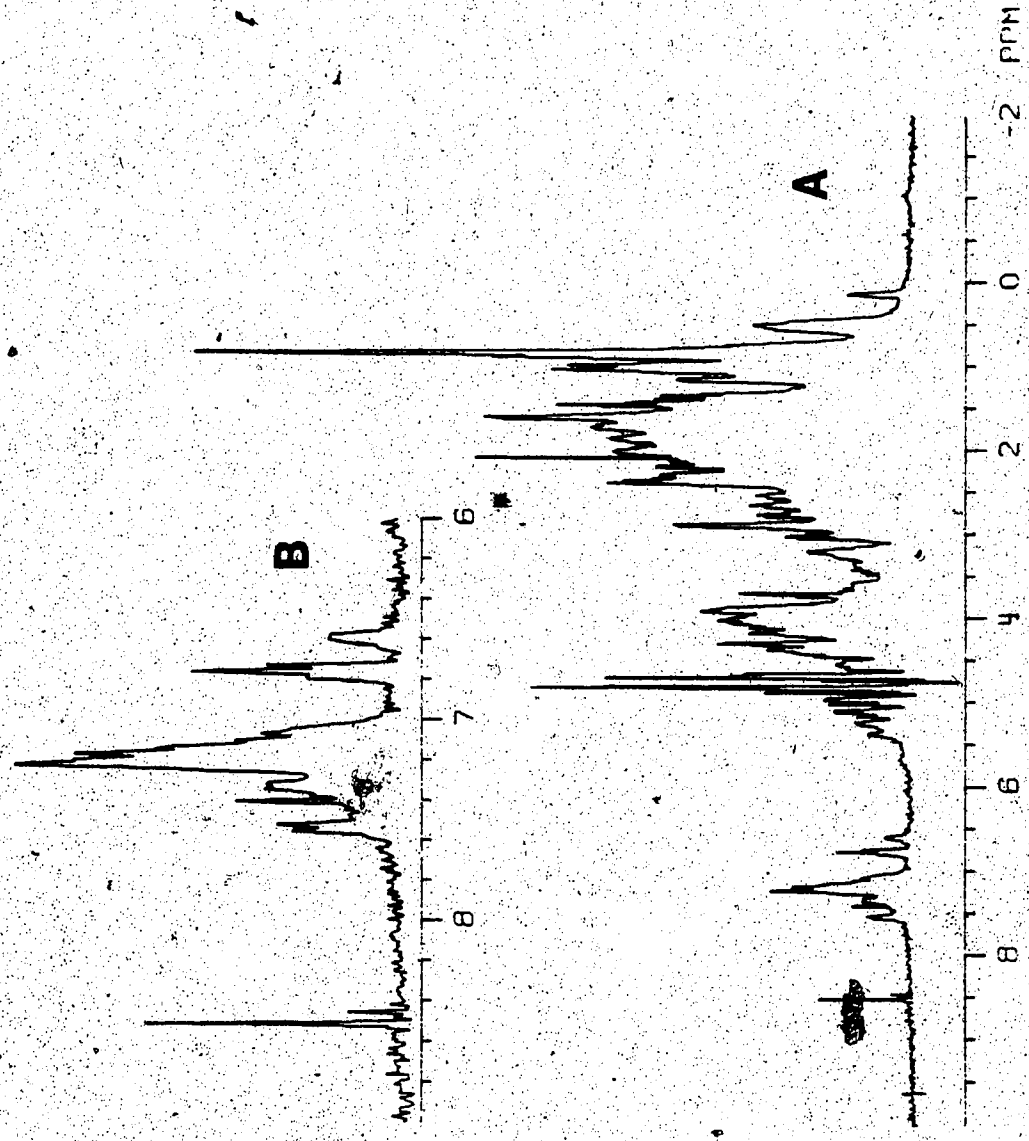


Figure VII The complete 270 MHz <sup>1</sup>H NMR spectrum of the apo ICaBP (A) The sample was pre-exchanged in the presence of 30 mM imidazole-d<sub>5</sub>, 20 mM KCl, pH 6.5 buffer in D<sub>2</sub>O for several hours prior to acquisition. The inset (B) shows the expanded spectrum of the aromatic region. The spectra are resolution enhanced with a Lorentzian to Gaussian conversion and represent 2000 acquisitions.

(NH) proton resonances are apparent. The narrow resonances at 8.50 and 7.40 ppm are from the imidazole of the buffer, which is not completely deuterated. These peaks were useful as an internal pH indicator as, in the pH range used in these experiments, their chemical shift is very sensitive to pH. The small resonance at 8.44 ppm is from formate ion, and the remainder of the resonances are derived from the one tyrosine and five phenylalanines. The spectrum in the region 7.0 to 6.4 ppm is typical of and similar to that of other CaBP's such as skeletal TnC (30,32) and cardiac TnC (28) in that it contains a number of upfield shifted phenylalanine resonances at ca. 6.77 ppm and at 6.58 ppm, in addition to tyrosine (6.74) protons. The spectrum is also sensitive to the addition of  $Ca^{++}$  as will be discussed below.

The laser photo chemical induced dynamic nuclear polarization (CIDNP) experimental results are shown in Figure VII.4 for the apo and  $Ca^{++}$  saturated ICaBP. These experiments allowed the assignment of the tyrosine doublet resonance of the 3,5 protons for both forms of the protein (117); it is readily apparent that the chemical shift of these protons are essentially unaffected by the addition of calcium. The fact that one observes a CIDNP effect in both the presence and absence of calcium indicates that the tyrosine is on the surface of the molecule as it must be accessible to the flavin dye in the solvent (29,117). This is in good agreement with earlier solvent perturbation studies (39) and with the recently published crystal structure of the highly

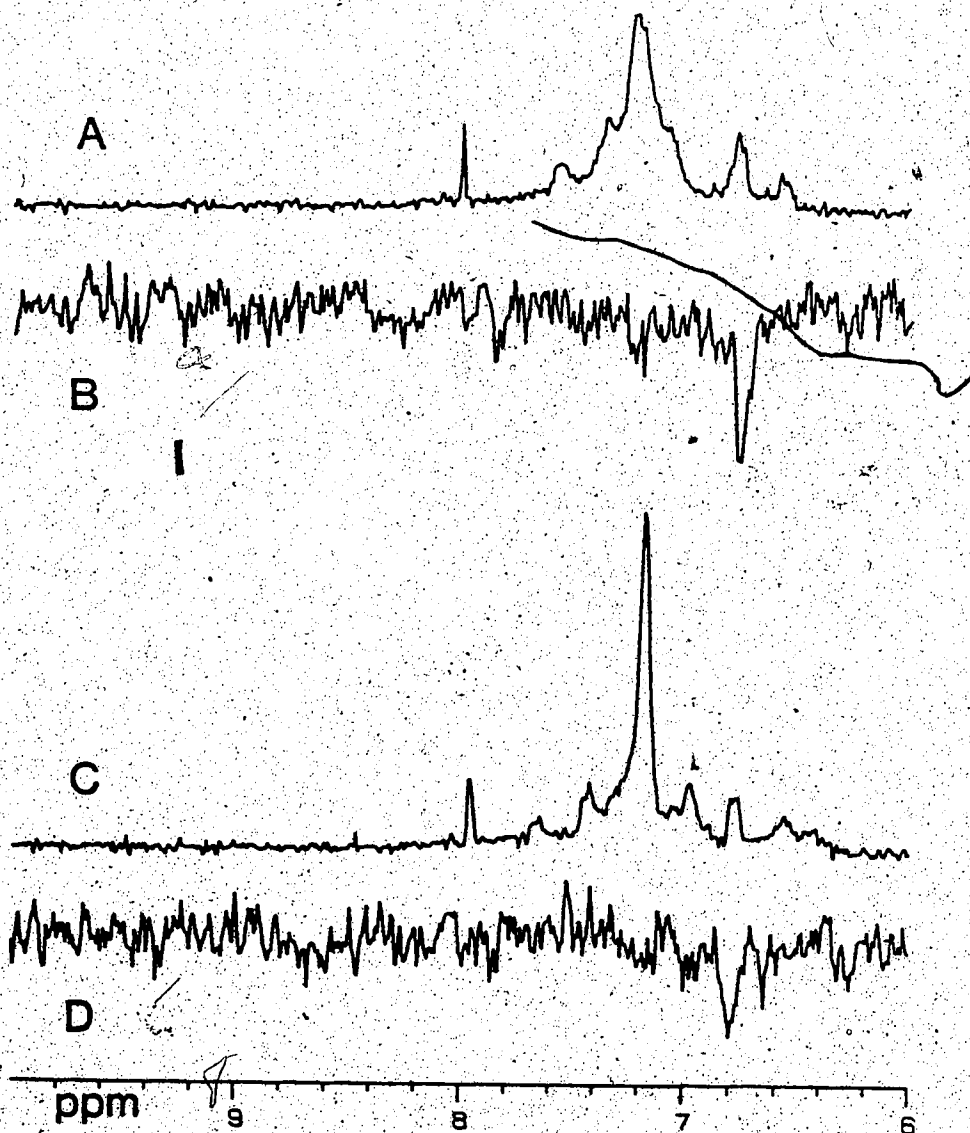


Figure VII.4  $^1\text{H}$  NMR laser photo CIDNP spectra for apo- and calcium-saturated ICaBP. The spectra were taken at ambient temperature.

(A) A "dark" spectrum of apo ICaBP. The spectrum is resolution enhanced with a Lorentzian to Gaussian conversion and represents 2048 acquisitions.

(B) The difference spectrum for apo ICaBP which is a "light" spectrum subtracted from a "dark" spectrum. The spectrum has a line broadening of 2.5 Hz and represents 16 acquisitions.

(C) A "dark" spectrum of the laser CIDNP sample shown in figure A after the addition of excess calcium; the  $[\text{Ca}^{2+}]_0/[\text{ICaBP}]_0 = 4.9$ . The spectrum is resolution enhanced with a Lorentzian to Gaussian conversion and represents 2048 acquisitions.

(D) The difference spectrum ("light" - "dark") for the calcium saturated sample shown in C. The spectrum has a line broadening of 2.5 Hz and represents 16 acquisitions.

homologous bovine ICaBP (8).

The homonuclear decoupling experiments, shown in figure VII.5 for the apo and calcium saturated ICaBP, allow for the assignment of the 2,6 protons of tyrosine 16 in both forms of the protein. Irradiation at 7.53 ppm in the apo protein (figure VII.5B) and at 7.39 ppm in the calcium-saturated protein (figure VII.5D) produced a collapse in the multiplicity of the 3,5 proton resonance at 6.73 and 6.76 ppm respectively, indicating that these respective pairs were the spin coupled protons of the tyrosine in the two states of the protein. The environment of the 2,6 protons, therefore, is slightly perturbed by the addition of calcium. The decoupling experiment in the presence of calcium (figure VII.5C and D) was done at a higher temperature (333°K), but there was no change in the spectrum of the calcium-saturated protein as a function of temperature beyond the narrowing of resonances and the loss of some of the intensity of the slowly exchangeable NH resonances (these are the additional resonances observed in the range of c.a 7.4 to 9.0 ppm). Even at these high temperatures and also at high salt (0.5M KCl) concentrations, intensity in the NH resonances remains for days. These resonances exchange readily (within hours) for the apo protein. The backbone NH resonances of bovine ICaBP were also found to be resistant to exchange at high temperature (224) and high concentrations (up to 1 M) of K<sup>+</sup> and Na<sup>+</sup> had no effect on the CD spectra of the porcine protein (39).

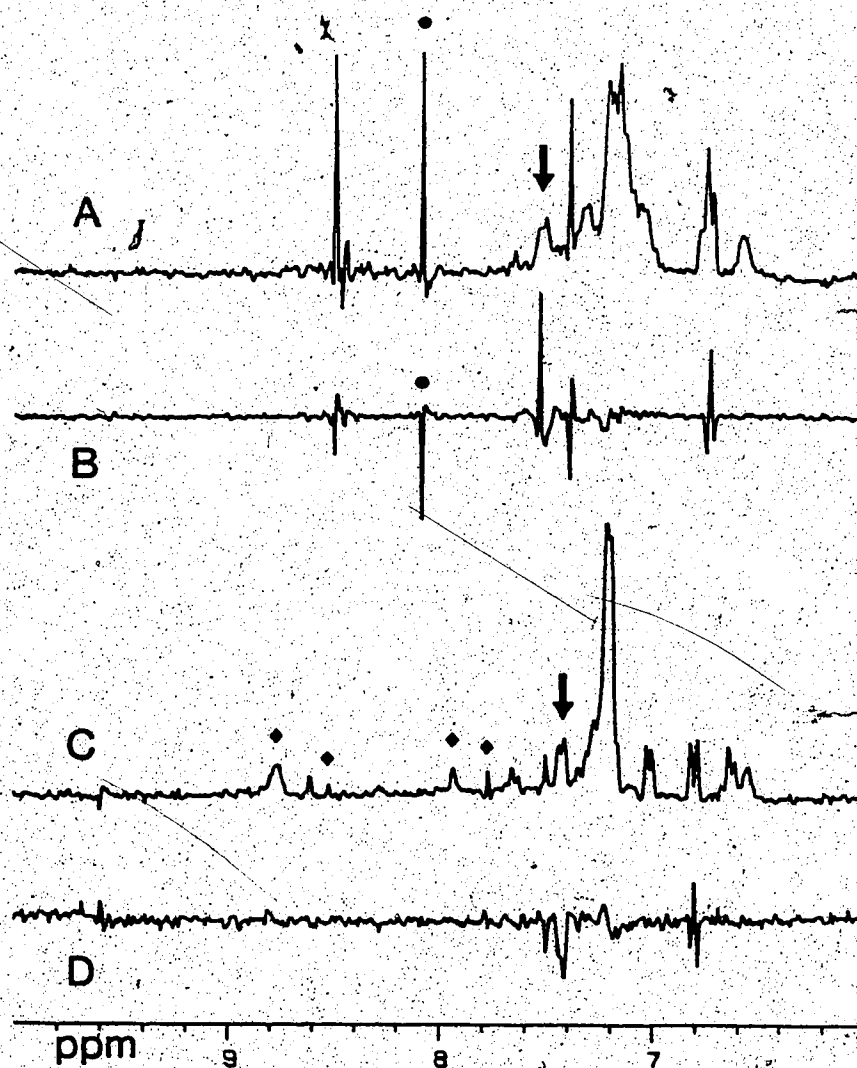


Figure VII.5  $^1\text{H}$  NMR homonuclear decoupling spectra for apo- and calcium-saturated ICaBP. The spectra were taken at ambient temperature. The spectra are resolution enhanced with a Lorentzian to Gaussian conversion.

(A) The undecoupled apo ICaBP spectrum.

(B) A difference spectrum with the decoupler set at 7.53 ppm. The frequency of the decoupling  $\gamma\text{H}_2$  rf field is indicated by  $\downarrow$ . The resonance marked by a  $\bullet$  is the frequency of the decoupling ( $\gamma\text{H}_2$ ) rf field in the blank. The spectra represent 2000 acquisitions.

(C) The undecoupled calcium-saturated ICaBP spectrum.

(D) The difference spectrum with the decoupler set at 7.39 ppm. The frequency of the decoupling  $\gamma\text{H}_2$  rf field is indicated by  $\downarrow$ . The N-H backbone resonances are marked by a  $\blacklozenge$ . The spectra represent 4000 acquisitions.

The pH titration of the apo protein is shown in Figure VII.6. One can see that the tyrosine protons (7.58 and 6.75 ppm) shift upfield as the pH increases, but the shifts are small compared with those observed for other CaBP's (28) and are not apparent until one is above pH 10.3. Thus the tyrosine has a very high  $pK_a$ , even though it is on the surface of the protein. The titration was not taken above pH 12 as this protein has been observed to irreversibly denature under such conditions (125). For this reason one can not obtain a complete titration curve, as shown in Figure VII.7, and it is thus difficult to determine the  $pK_a$ ; it is sufficient to indicate, however, that it is unusually high. One also notes that there are significant shifts in two phenylalanine resonances, one which shifts downfield from 6.78 ppm; it comes out from underneath the 3,5 protons of the tyrosine, the latter of which can then clearly be seen as a well-resolved doublet. The other, at 7.34 ppm, shifts upfield. These effects can be clearly seen in figure VII.5.

In the presence of calcium, there is no significant effect on the aromatic region of the spectrum throughout the pH titration (Figure VII.8); the tyrosine  $pK_a$  therefore is further increased. These titration results are in excellent agreement with spectroscopic studies (125), where a  $pK_a$  for tyrosine in the calcium saturated protein was determined to be 12.9. Readjustment of the pH 12 spectrum for both protein states to pH 6.5 resulted in the original spectrum, thus no



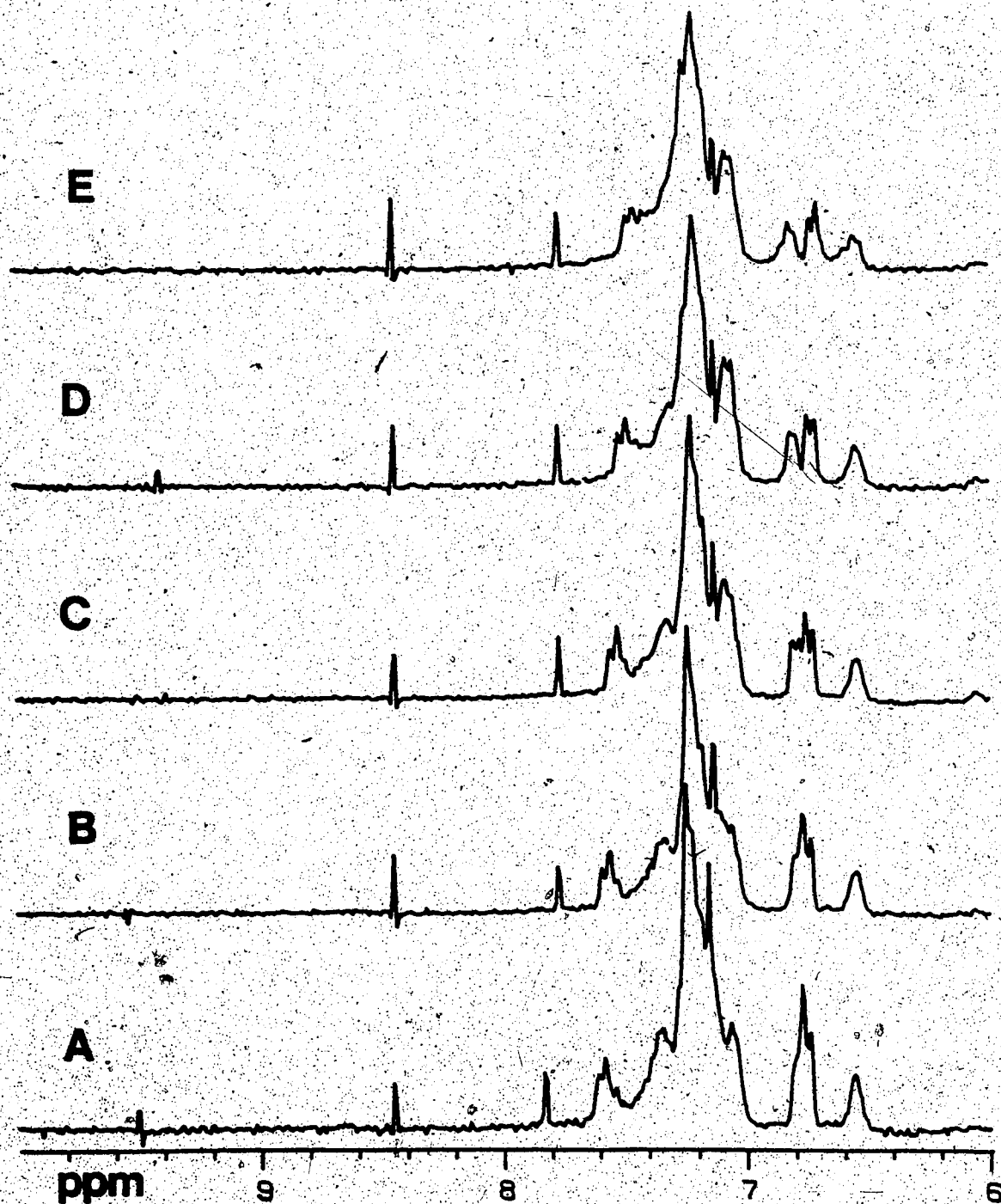


Figure VII.6 The pH titration of ICaBP in the presence of excess EDTA. The pH values are A. 8.48, B. 10.29, C. 10.98, D. 11.52, E. 11.92. The EDTA/ICaBP ratio was 3.25, except for A., where it was 0.81. The spectra represent 4000 acquisitions and are resolution enhanced with a Lorentzian to Gaussian conversion.

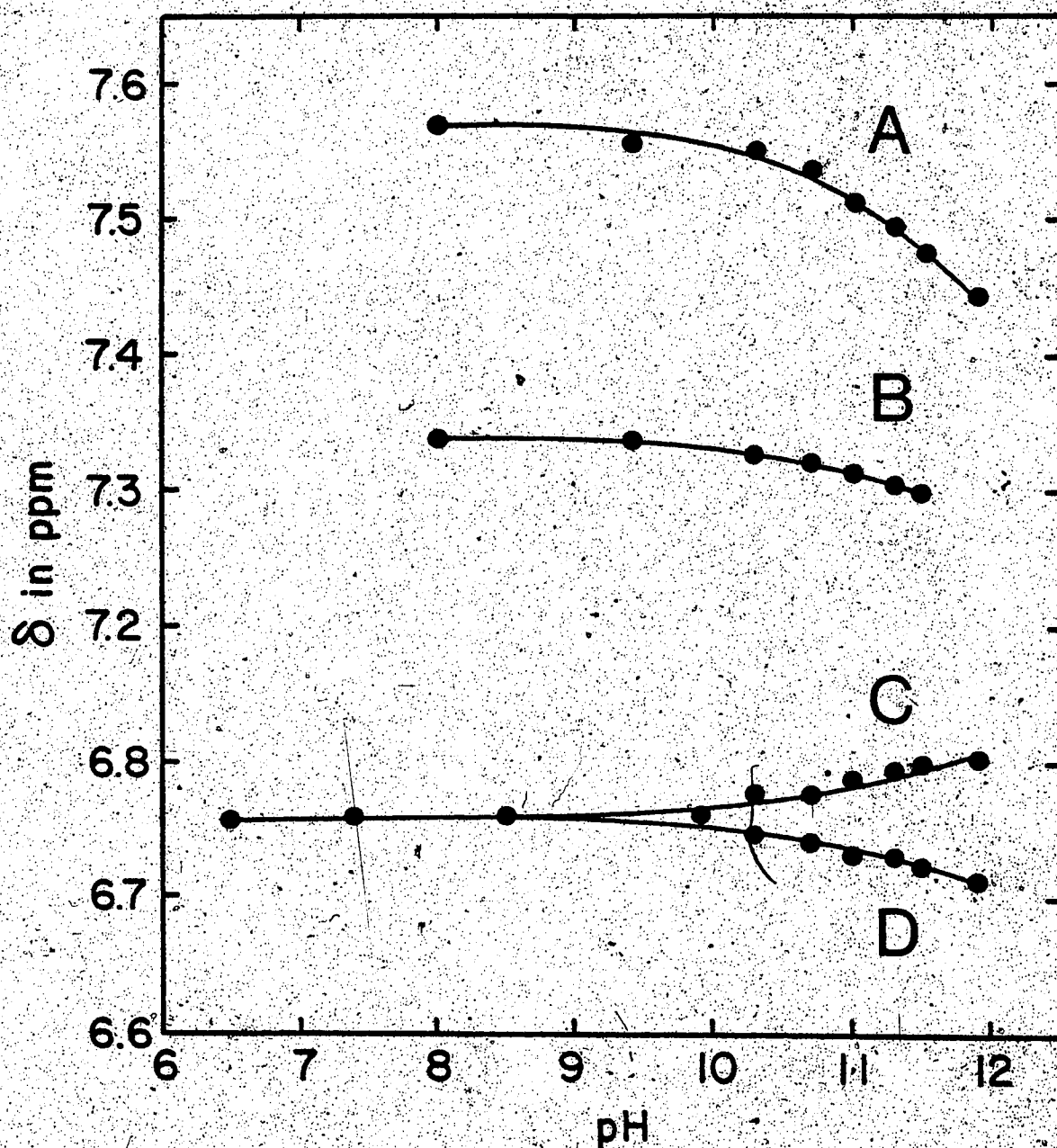


Figure VII.7 The plot of the chemical shifts of the phenylalanine and tyrosine resonances of apo porcine ICaBP as a function of increasing pH. The data was taken from the spectra shown in Figure VII.6, and the chemical shifts of the resonances in ppm at pH 6.5 were: A, 7.57; B, 7.34; C and D, 6.76.

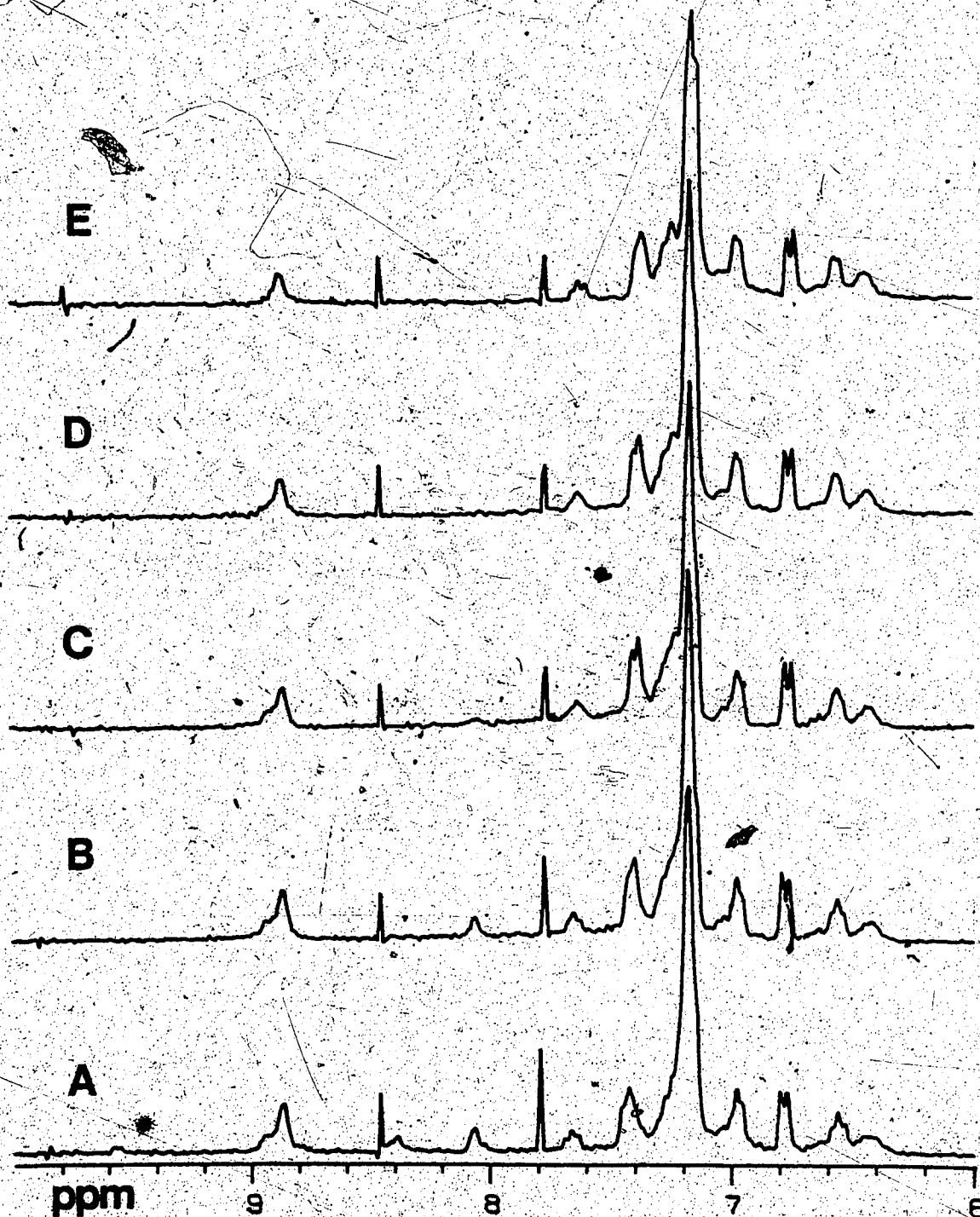


Figure VII.8 The pH titration of ICaBP in the presence of excess calcium. The pH values are A, 9.00, B, 10.44, C, 11.06, D, 11.38, E, 11.85. The  $\text{Ca}^{2+}/\text{ICaBP}$  ratio was 3.98. The spectra represent 4000 acquisitions and are resolution enhanced with a Lorentzian to Gaussian conversion.

denaturation had occurred; the backbone NH resonance at 8.86 ppm is resistant to exchange even at pH 12, which further demonstrates structural integrity of the protein in the presence of  $\text{Ca}^{+2}$ . This has also been observed for bovine ICaBP (224). There were no significant spectral changes in the aliphatic region throughout either of these titrations.

Figures VII.9 and VII.10 show the results of titration of the apo ICaBP with calcium. It is readily apparent in Figure VII.9 that the binding of calcium causes perturbations in the aromatic spectrum, most strikingly in the broad envelope of phenylalanine resonances from 7.0 to 7.4 ppm; this envelope sharpens up and increases in intensity as the calcium/ICaBP ratio increases. The intensity of the apo ICaBP tyr 2,6 proton resonance at 7.56 ppm decreases and the increase of the ICaBP calcium saturated 2,6 tyrosine protons at 7.39 ppm increases, indicating that calcium binding is in the NMR slow exchange limit. The 3,5 tyrosine protons appear to become resolved into a clear doublet at 6.76 ppm as calcium is added because the overlapping phenylalanine resonance in the free form decreases in intensity; the other upfield shifted phenylalanines (6.4 to 6.7 ppm) undergo a significant change as well. The upfield shifted methyl groups are also significantly perturbed, as shown in Figure VII.9. Taking the intensity change in the broad phenylalanine envelope, and plotting it as a function of  $[\text{Ca}^{+2}]_0/[\text{ICaBP}]_0$ , the results of Figure VII.10 show a 2:1 stoichiometry. In this plot we have taken into account the fact that the "apo"

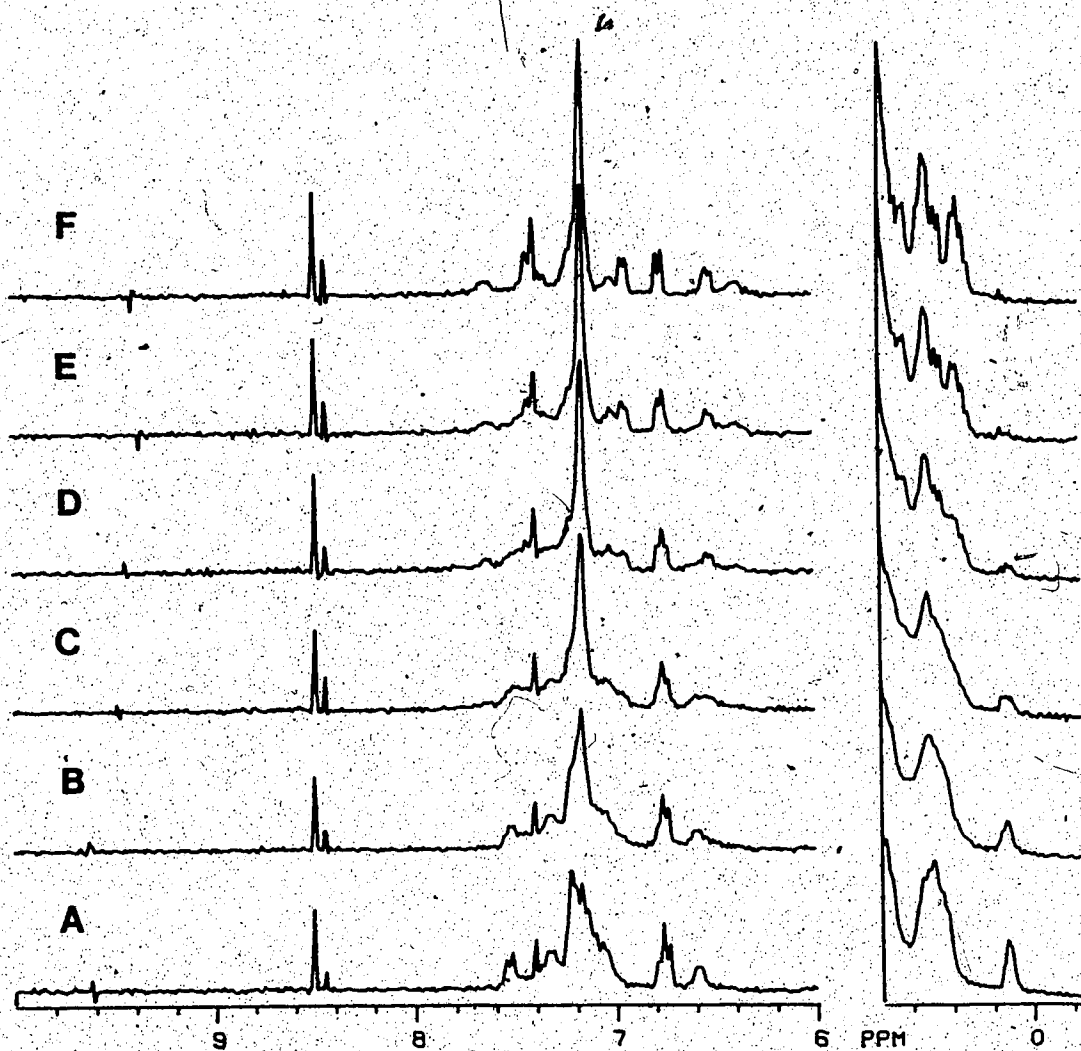


Figure VII.9 The titration of apo porcine ICaBP with  $\text{Ca}^{2+}$ . Both the low and high field portions of the  $^1\text{H}$  NMR spectrum are shown. The  $[\text{Ca}^{2+}]_0/[\text{ICaBP}]_0$  ratios are A. 0.28, B. 0.74, C. 1.16, D. 1.59, E. 2.04, F. 3.33. The spectra are resolution enhanced with a Lorentzian to Gaussian conversion and represent 2000 acquisitions.

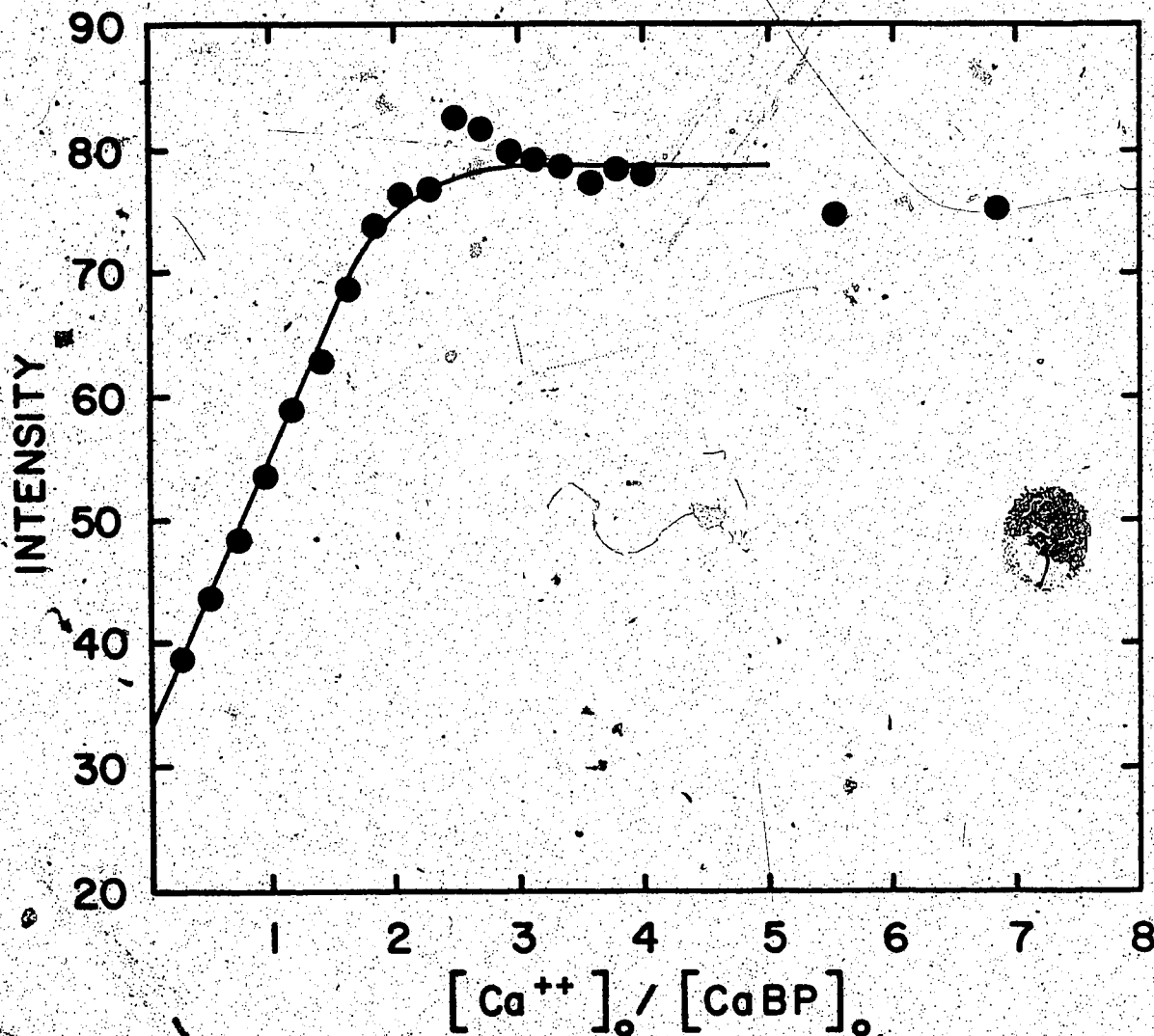


Figure VII.10. A plot of the intensity (in arbitrary units) of the 7.16 ppm resonances of phenylalanine as a function of  $[Ca^{++}]_o/[CaBP]_o$ . The protein was found to have 28% of the two sites saturated with calcium after desalting (see text), and this curve has been corrected for this initial  $Ca^{++}$  contamination.

protein was not completely calcium free. We determined the extent of the calcium content in the apo protein by CD, as shown in Figure VII.11. The CD spectra were run on protein sample that was identical to the desalted protein sample used in the calcium titration. These protein samples were pre-treated as outlined in the experimental section, but differed from subsequent preparations (which produced true apo protein) in that neither the column buffers nor the deuterated NMR sample buffers were pretreated with chelex, and the eluted column fractions were not handled with, collected in, or stored in plasticized glassware. The difference in ellipticity at 275 nm between the CD spectrum of the parallel protein sample at pH 8.00 in the presence of excess EDTA and calcium was assumed to be the maximum change in ellipticity between totally apo- and calcium-saturated ICaBP. The difference between the initial ellipticity value of the parallel protein sample and that of the same sample in excess EDTA was then used to calculate the initial amount (14%) of calcium-saturated protein. Assuming there are two moles of calcium bound per mole of ICaBP, the initial point in the titration thus corresponds to a  $[Ca^{2+}]_0/[ICaBP]_0$  ratio of 0.28. It was readily apparent that the degree of negative ellipticity in Figure VII.11A was much less than that observed in other studies (39). Using the published molar ellipticity value for the apo protein of  $-180 \text{ deg}\cdot\text{cm}^2\cdot\text{dmole}^{-1}$  at 275 nm, along with our own values for the ----- the deuterated NMR sample buffer had been pre-treated with dithizone.

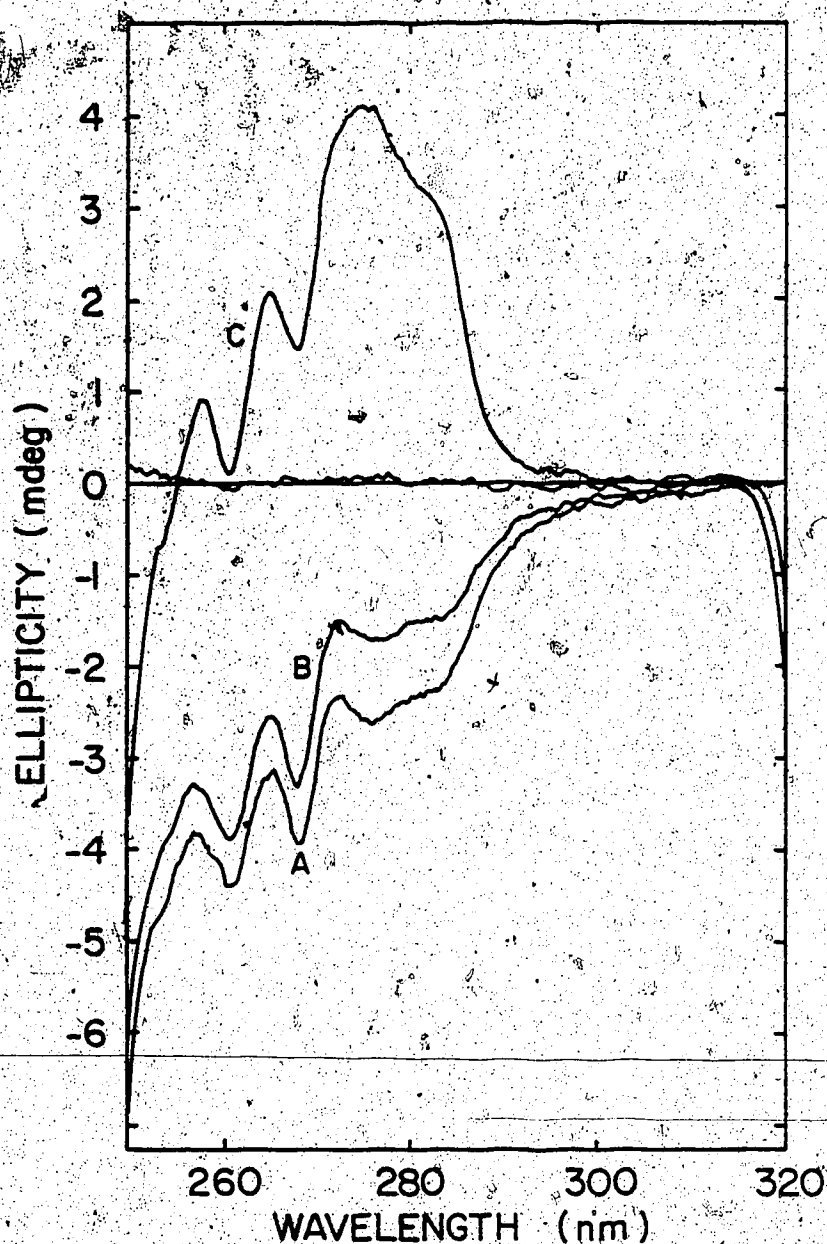


Figure VII.11 The CD spectra for ICaBP in the presence of excess EDTA and  $\text{Ca}^{2+}$ . The respective molar ellipticity values at 275 nm were  $-1771$  and  $+2928 \text{ deg}\cdot\text{cm}^2\cdot\text{dmol}^{-1}$ . The samples were  $0.14 \text{ mM}$  ICaBP,  $30 \text{ mM}$  imidazole,  $20 \text{ mM}$  KCl, pH 8.00 and the path length was  $1 \text{ cm}$ .

A. The "apo protein" spectrum in the presence of excess EDTA. The sample size was  $602 \text{ ul}$  and the EDTA/ICaBP ratio was  $5/1$ .

B. The "apo protein" spectrum. The sample size was  $600 \text{ ul}$ .

C. The "apo protein" spectrum in the presence of excess calcium. The sample size was  $101 \text{ ul}$  and the  $\text{Ca}^{2+}$ /ICaBP ratio was  $67/1$ .



apo and  $\text{Ca}^{2+}$ -saturated ICaBP, we derived a 68% level of saturation for their sample.

### C. Discussion

In this discussion we concentrate primarily on the assigned tyr 16 (tyr 113 in Figure 1.3) aromatic ring resonances, and their use as probes of the effects of  $\text{Ca}^{2+}$  binding to porcine ICaBP. If the aromatic ring of the tyrosine is free to undergo at least a  $180^\circ$  flipping motion, then one would expect to observe doublets for both the 2,6 and 3,5 pairs of protons, and they should titrate upfield with the loss of the tyr phenolic proton (127,225). The CIDNP and homonuclear decoupling experiments provide a definite assignment for the 2,6 and 3,5 resonances of the single tyrosine of the porcine ICaBP in both the presence and absence of calcium.

The 3,5 protons of tyr 16 (tyr 113 in Figure 1.3) in the apo protein appear initially as a triplet as they are superimposed on phenylalanine resonance, and are resolved into a clear doublet only by the addition of calcium or an increase in pH. Note that the difference  $^1\text{H}$  decoupling pattern is appropriate for a doublet. In the apo protein above pH 10 this doublet resonance titrates upfield with a  $\text{pK}_a \geq 11-12$ . The CIDNP experiments indicate that the tyrosine is exposed to the solvent in both the apo and calcium saturated form. This agreed with solvent perturbation studies on porcine ICaBP (39) and with fluorescent studies on the

homologous bovine protein (226). The recent publication of the X-ray structure of the highly homologous bovine minor A ICaBP indicates that this tyrosine is exposed and lies on the surface of the molecule in a fairly hydrophobic pocket (8). A model for the existence of such a high pK<sub>a</sub> for a surface tyrosine has been proposed in which the hydroxyl group of the tyrosine is hydrogen bonded to glutamic acid residue 38; this model is consistent with the X-ray crystal structure of bovine ICaBP (8). These authors also indicate that the hydrophobic depression in which the tyrosine lies provides an unfavourable environment for unhindered tyrosine ionization (125).

The phenylalanine resonances which shift as a function of increasing pH have not yet been assigned. Our pH titration spectra were similar to those achieved when calcium-saturated cardiac TnC was titrated, in that the tyrosine doublets began to titrate upfield at pH 10.7, while one of the overlapping phenylalanine doublets shifted downfield towards resonance frequencies more typical of phenylalanine ring protons (7.4 to 7.0 ppm) (28). This was attributed to a loss of the specific environments which produced the upfield-shifted phenylalanine resonances and yet, as they observed, both the 2,6 and 3,5 tyrosine resonances titrated upfield and remained distinct from the random coil phenolate resonances observed for more exposed tyrosine residues.

In the presence of calcium the resonance at 6.76 ppm is simplified into a clear tyrosine-like doublet which is spin coupled to the doublet at 7.39 ppm. That no resonances, however, shift with pH in the calcium-saturated protein implies that the tyrosine has a very high  $pK_a$  when calcium is bound. This is in agreement with a UV spectrophotometric titration from which a tyrosine  $pK_a = 12.9$  was derived (125). The lack of observation of any significant changes in the aliphatic region of the protein from pH 6.5 to 12, in either the absence or presence of calcium, indicates that there is no large change in protein conformation over this pH range. The chemical shift of 6.76 ppm for the 3,5 protons of the single tyr is the same as for the apo protein, and is similar to the values observed for skeletal and cardiac TnC, and calmodulin (28,32,43). The addition of calcium to the apo protein causes changes in the resonance attributed to the 2,6 (meta) protons of tyr and changes in several resonances associated with phe residues. This is consistent with the previous spectral work (39). The aromatic region of the spectra for the apo and calcium-saturated states are similar to those of bovine ICaBP (224).

Under the conditions of these experiments (ICaBP concentration=0.5 mM), the stoichiometry of calcium binding was 2:1. All of the  $Ca^{+2}$  titrations showed some decrease in intensity beyond a  $Ca^{+2}/ICaBP$  ratio of  $\approx 2/1$ , which may indicate weak third site binding and/or non-specific binding of excess  $Ca^{+2}$ ; the decrease in intensity was due to shifting

within and/or broadening of the phe envelope. Analysis of the X-ray crystal structure of the bovine ICaBP, using the data supplied by the Brookhaven Data bank (8), showed that there were three  $\text{Ca}^{2+}$  ions bound to the crystal determined, two were in the binding sites and one was bound non-specifically on the surface of the protein.

The  $\text{Ca}^{2+}$  stoichiometry of 2:1 for porcine ICaBP is in disagreement with some of the earlier published CD results, which showed that this protein bound only one calcium at high (0.5 mM) protein concentrations whereas, at lower concentrations of porcine intestinal CaBP, (0.141 mM) the titration as observed by CD tended towards a stoichiometry of 2:1 (39). However, a recent repeat of the titration of this protein with calcium, also monitored by CD, has confirmed that it has two high affinity calcium binding sites (227). In addition, analysis of the  $\text{Ca}^{2+}$ -saturated protein by atomic absorption spectrophotometry showed 2 calcium atoms per protein molecule (228), and so it is now generally believed that porcine ICaBP binds two calciums per molecule of protein, as has been observed for the highly homologous bovine ICaBP (221). The apparent saturation level value of 68% which can be derived for the earlier published spectra (39) indicated that one mole of calcium was already present in their protein, which could explain why they observed the protein to bind calcium with a stoichiometry of 1 at  $\approx$  0.5 mM concentration of protein. Since the dissociation constant of ICaBP is in the micromolar range and the protein concentration

employed in these studies was in the millimolar range, it was not possible to determine an accurate  $K_d$  value for  $\text{Ca}^{2+}$ , as outlined in Chapter VIII.

There were no specific perturbations in the spectra which allowed us to differentiate between the two sites. Therefore the protein either has two binding sites with approximately the same affinity for calcium, as was suggested by other studies (227,229), or the binding shows complete positive cooperativity. From the results outlined in this chapter, one can not determine if the binding of calcium by the porcine ICaBP is cooperative or not, but we have presented evidence in Chapter VIII which indicates that the binding is non-cooperative, in agreement with other recent studies on both the porcine (227) and bovine (223) ICaBP. Even in the case of two independent binding sites with equal calcium affinities, there are two possible modes of  $\text{Ca}^{2+}$  binding which can explain our results. The first is that the binding of calcium to each site results in specific perturbations which differ between the two sites, but because  $\text{Ca}^{2+}$  binds equally to both sites, we see only an average of these two sets of perturbations. The second possibility is that all or most of the perturbations arise when calcium binds to one of the sites, and that the binding of calcium to the second site is spectroscopically "silent". The results which we achieved by titrating the protein with the lanthanide ion  $\text{Lu}^{3+}$  support the latter possibility, as outlined in Chapter IX.

That the rate of calcium binding is slow enough to result in NMR spectra in the slow exchange limit is in agreement with the results for the high affinity sites of TnC and calmodulin (28,32,43). It is interesting that, as the  $[Ca^{2+}]_0/[ICaBP]_0$  ratio increases, the broad phenylalanine envelope sharpens up and narrows to a distinct resonance centered at 7.16 ppm, and some phenylalanine intensity appears even further upfield in the spectrum of the calcium-saturated protein from where it appears in the apoprotein spectrum. This has also been observed for bovine ICaBP (223). With the tightening of the overall protein structure as it binds more calcium, as evidenced by the lack of backbone NH exchange, it is likely that each of the five phenylalanine residues would be in a more rigid environment. Because they are spread out over almost the entire ICaBP sequence, one would expect that one or more of these phenylalanine residues would be in a fairly unique environment. Contrary to these initial expectations, the range in phenylalanine chemical shifts for most of the phe resonances decreases in the calcium-saturated protein; this implies that these residues experience a similar environment in the calcium-bound protein.

The presence of upfield shifted phenylalanine resonances in the aromatic region, and upfield shifted methyl groups in the aliphatic region (Figure VII.2) in the apo protein indicates that a well-defined tertiary structure exists in the protein even in the absence of calcium, as was

observed for apo cTnC (28,32). Previous CD work suggests that ca. 30% of the apo protein is in an  $\alpha$ -helical conformation, although this estimate is now in question due to the disparity between our apo aromatic CD spectrum and theirs (39). Increasing the temperature of the protein sample to 333°K showed no change in chemical shift of the aromatic resonances in the calcium-saturated protein and no apparent change in the shape or intensity of these resonances. This result shows the inherent thermal stability of porcine ICaBP under such conditions. It is, in fact, isolated as a soluble protein at 70°C (124). The calcium-saturated protein spectrum was also virtually insensitive to increasing salt concentration ( $\leq 0.5$  M KCl), again indicating the structural stability of the calcium bound protein. This agrees well with previous studies on bovine ICaBP which indicated that KCl exerted minimal effects on  $\text{Ca}^{2+}$  binding over the range of 0.01 to 0.2M (221).

VIII. THE DETERMINATION OF THE  $K_d$  OF PORCINE ICaBP FOR  
CALCIUM IN THE PRESENCE OF EDTA AND ANALYSIS OF THE RESULTS  
TO DETERMINE IF THE  $Ca^{+2}$  SITES ARE COOPERATIVE

A. Introduction

The use of  $^1H$  NMR to determine the dissociation constants for various metal ions binding to proteins in solution has some limitations, particularly when these dissociation constants are in the micromolar range. The reasons for these difficulties will be outlined below, and we will demonstrate a method of overcoming these difficulties, and a means of determining if the coordination of  $Ca^{+2}$  by the porcine ICaBP is cooperative.

Due to the extended time periods needed to get good protein spectra, one usually tries to obtain FID's on proteins at a minimum concentration of 0.5 mM. The problem with using a concentration of chelating ligand which is so much greater than the dissociation constant can most easily be explained by the example shown in Figure VIII.1. This plot represents the data obtained from a  $Ca^{+2}$  titration of 0.6 mM EDTA, which has a  $K_d$  for calcium of  $2 \times 10^{-7}$  at pH 6.5 (230). The value of the dissociation constant derived from the data shown was  $K_d = 1.2 \pm 1.7 \times 10^{-6}$  M. The accuracy of this fit is poor as the calculated value of  $K_d$  spans a range of 0 to  $2.9 \times 10^{-6}$  M. The source of this inaccuracy can be outlined by looking at the data in terms of how the dissociation constant is determined. There are three regions to



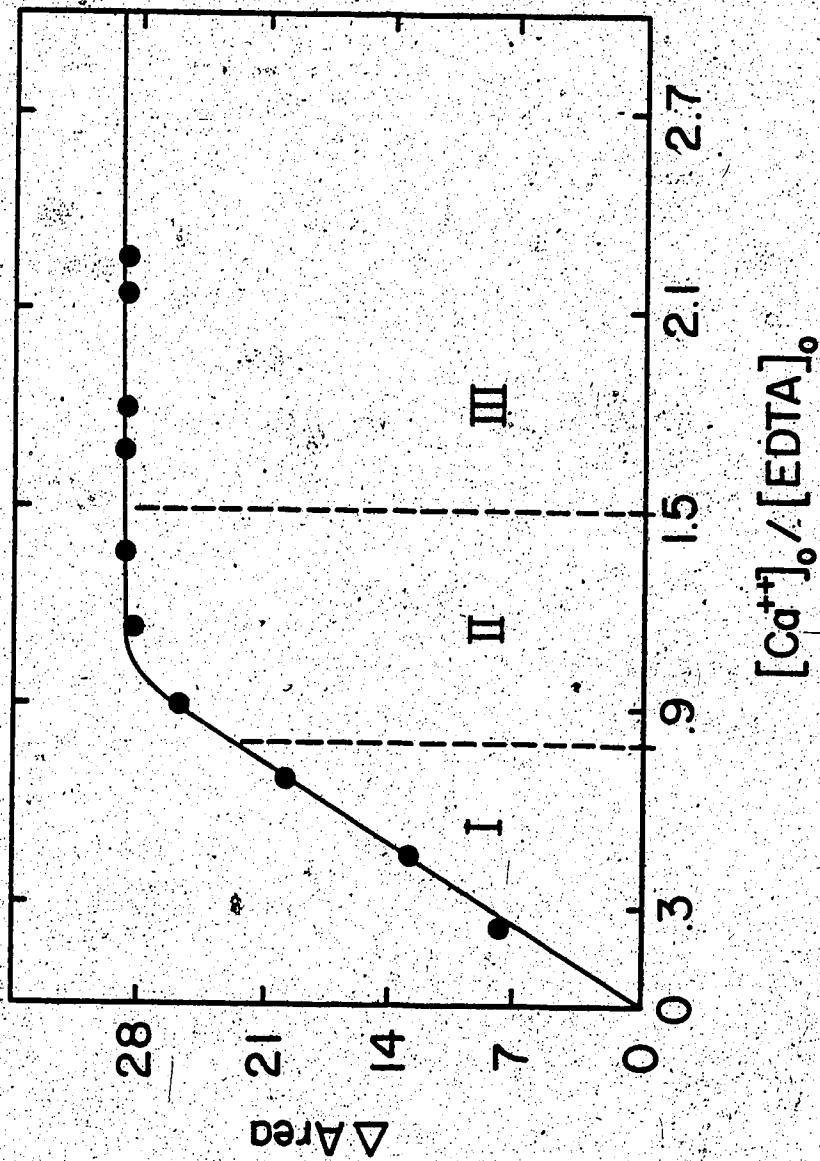


Figure VIII.1. A plot of the change in the area under the EDTA resonance at 2.5 ppm as a function of  $[Ca^{++}]_0/[EDTA]_0$ . The sample consisted of 0.61 mM EDTA in 30 mM imidazole-d, 20 mM KCl, pH 6.5, and the fit is shown assuming a single binding constant. The areas were taken by integrating the spectrum over 2.7 to 2.3 ppm. (Figure VIII.2) and are in arbitrary units.

consider in this plot shown in Figure VIII.1;

- I the initial region with a linear slope,
- II the curved portion of the plot where the slope decreases rapidly, and
- III the plateau region where the slope is effectively zero.

In region I, essentially all of the calcium exists as the EDTA-Ca<sup>2+</sup> complex, while in region III there is free metal ion present but the ligand is saturated. The curved portion of the plot, shown in region II, is very small, and it is this portion of the plot which is critical in the determination of the dissociation constant since significant amounts of both free metal ions and free ligand molecules exist only in this region. The large amount of deviation in the value determined for the data shown in Figure VIII.1 was due to the lack of definition in region II. Data obtained in this region represents very small changes in the observed intensity and is difficult to fit, even with more data points, due to errors in the measurement of the intensities over a very small range of [Ca<sup>2+</sup>]. The data presented in Figure VIII.1 can be compared with the Ca<sup>2+</sup> titration of the S100b protein shown in Figure VI.4 ([S100b] = 0.21 mM, K<sub>d</sub> = 1.95 ± 0.06 × 10<sup>-4</sup> M), where one can see that the curved portion of the plot is much more extensive when the ligand concentration and the K<sub>d</sub> values are similar. The resulting

$K_d$  value is much more accurate in this case as the majority of the data points lie within the curved region, where the intensity changes are much more extensive and occur over a greater range of metal ion concentration.

For the calcium titration of apo porcine ICaBP, the limitations outlined above were augmented by the fact that region II displayed a pronounced curvature due to non-specific  $\text{Ca}^{2+}$  binding (Figure VII.10). To alleviate these problems in the determination of the  $K_d$  for  $\text{Ca}^{2+}$ , we titrated the protein with calcium in the presence of EDTA, so that, by obtaining a dissociation constant for the protein which was relative to a known dissociation constant, our determination of that value would become more accurate. Porcine ICaBP is known to have two calcium binding sites which have equal affinity for  $\text{Ca}^{2+}$ , the  $K_d$  values of which are  $(1.81 \text{ to } 5) \times 10^{-7}$  (39,217,229). It is not known whether this is the result of two sites which are cooperative, or if the binding of calcium to these sites is random and of equal affinity, although there is evidence which supports the latter mechanism (227). By measuring the dissociation constants of this protein relative to that of EDTA and analysing the resulting data, we have shown that there is no cooperativity between the two sites on the protein.

We chose to use EDTA because it has a dissociation constant in the micromolar range which is compatible with that of ICaBP. We initially attempted to titrate EDTA in the

micromolar range, in order to obtain an accurate  $K_d$  for calcium for that ligand. Although these attempts were not really successful, some interesting and valuable information came out of these studies, which will be discussed below.

## B. Results

A spectrum of EDTA in the presence of a non-saturating concentration of  $\text{Ca}^{+2}$  is shown in Figure VIII.2. EDTA binds calcium in the slow exchange limit, with the resonances at 3.7 ppm and 3.5 ppm arising from the free EDTA, while those at 3.1 and 2.5 ppm correspond to bound EDTA. Our initial studies showed that one can not simply use the intensities of these peaks to determine the fractions of free and bound EDTA accurately. Rather, it is necessary to measure the areas under the resonances by integration, and then the relative amounts of free and bound EDTA can be determined as outlined below,

$$f_L = \frac{A_L}{A_L + A_{LM}} \quad \text{and} \quad f_{LM} = \frac{A_{LM}}{A_L + A_{LM}} \quad (1)$$

$$[L] = f_L [L]_0 \quad \text{and} \quad [LM] = f_{LM} [L]_0 \quad (2)$$

where  $f_L$  is the fraction of free ligand,  $f_{LM}$  is the fraction of the ligand-metal complex,  $A_L$  is the area under the free ligand resonance,  $A_{LM}$  is the area under the bound ligand resonance,  $[L]$  is the concentration of free ligand,  $[LM]$  is the concentration of the ligand-metal complex, and  $[L]_0$  is the total ligand concentration. The values of the fractions

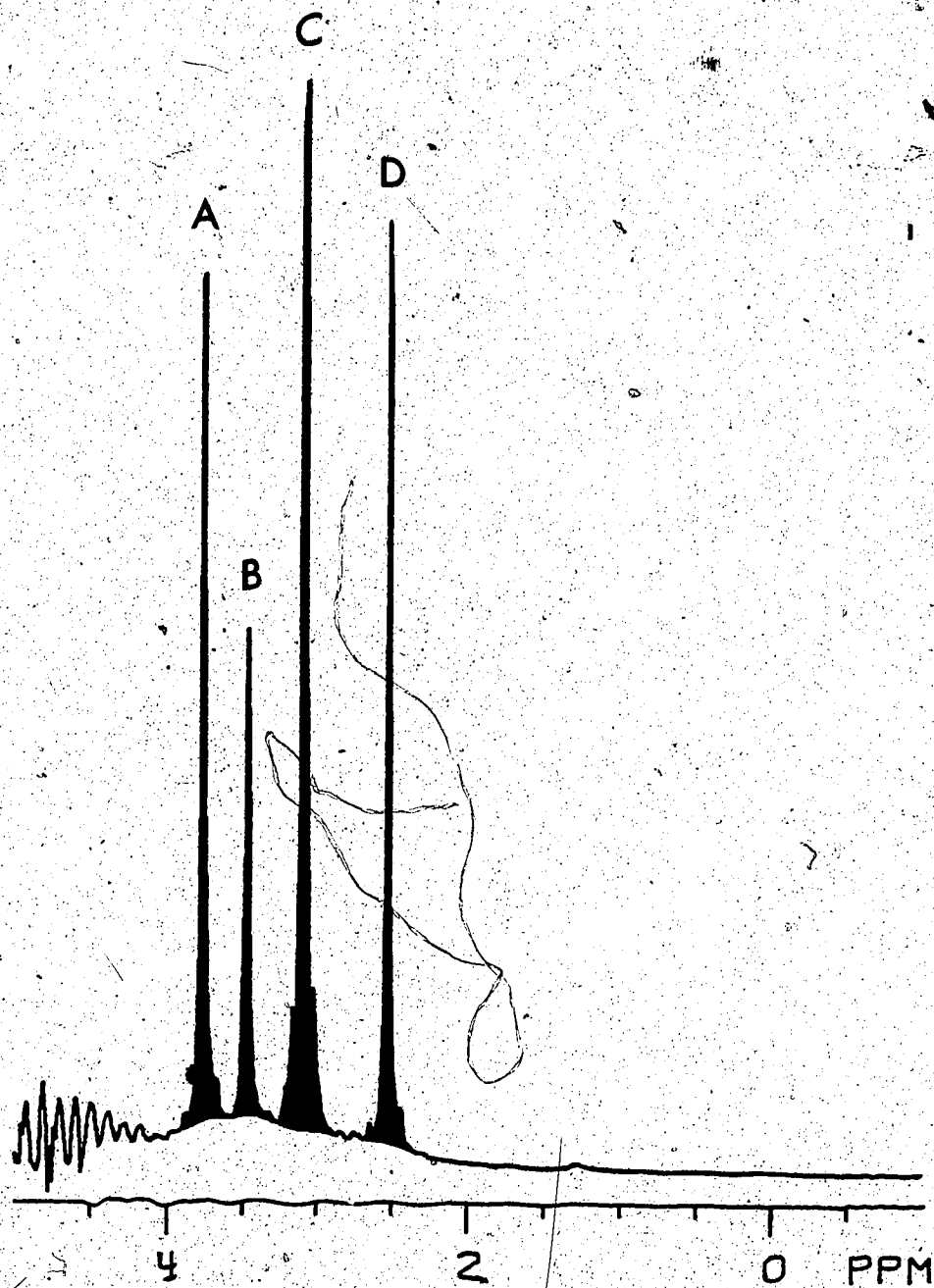


Figure VIII.2 The complete 270 MHz  $^1\text{H}$  NMR spectrum of EDTA in the presence of a non-saturating concentration of calcium. The sample contained 4.05 mM EDTA and 1.98 mM calcium in 18.9 mM imidazole- $d_6$ , pH 6.3. The typical integration ranges for the resonances were: A, 3.8 to 3.6 ppm; B, 3.6 to 3.4 ppm; C, 3.2 to 2.9 ppm; D, 2.7 to 2.3 ppm. These regions are indicated in the spectrum by shading. The A,C and B,D resonance pairs represent the free, bound form of the two proton resonances of EDTA.

outlined in equation 1 can easily be checked as their sum should be unity. In this way we could establish the correct regions over which to integrate. The EDTA was not tightly bound to the protein as the  $T_1$  relaxation times of the EDTA resonances in the presence of protein (A, 0.39; B, 0.23; C, 0.21; D, 0.22 sec) did not differ appreciably from those observed in the absence of protein (A, 0.38; B, 0.28; C, 0.33; D, 0.44 sec), and so we have assumed that the presence of EDTA has no appreciable effect on the  $Ca^{2+}$  affinity of porcine ICaBP; such effects have been observed previously with parvalbumin in the presence of EGTA (244).

The spectra of the protein in the presence of EDTA are shown in Figure VIII.3 as a function of increasing  $Ca^{2+}$  concentration. In these spectra it is obvious that, as the  $[Ca^{2+}]_0$  increases, the intensity of the free EDTA resonances decreases, while the intensity of the bound EDTA resonances increases. The change in the intensities of the resonances in the aromatic region of porcine ICaBP as a function of increasing calcium concentration have been observed previously in Figure VII.9.

We initially assumed that the two  $Ca^{2+}$  binding sites of ICaBP had the same affinity. In this system  $K_{d1} = K_{d2} = K_p$ , where  $K_p$  is the dissociation constant of the protein for  $Ca^{2+}$ . In the presence of EDTA there is a second dissociation constant  $K_e$ , which is the dissociation constant of  $Ca^{2+}$  for EDTA. In this experiment we used the areas of the A (free)

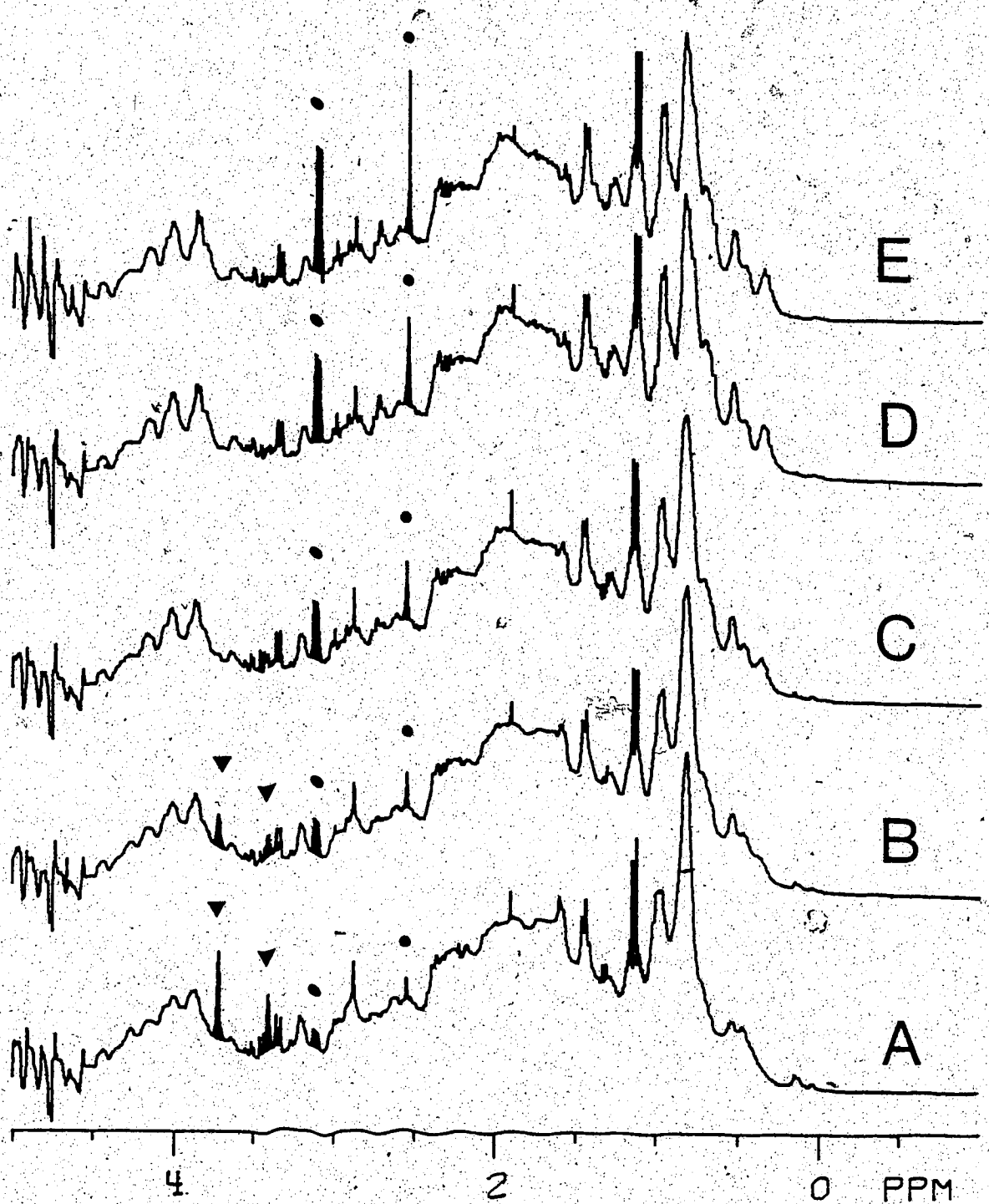


Figure VIII.3 The titration of porcine ICaBP with  $\text{Ca}^{2+}$  in the presence of EDTA. The samples contained 0.61 mM ICaBP, 0.31 mM EDTA (shaded resonances) in 30 mM imidazole- $d_6$ , 20 mM KCl, pH 6.5. The total calcium concentrations in mM were: A, 0.56; B, 0.78; C, 1.00; D, 1.21; E, 1.42. The symbols are: ▼, free EDTA resonances; ●, bound EDTA resonances.

and C (bound) resonances of EDTA (Figure VIII:2) and the area under the 7.0 ppm (integrated over 7.05 to 6.95 ppm) resonance of ICaBP to determine the extent of metal ion bound to each chelator. We have derived an equation which we can use to measure the ratio  $k_p/k_c$  by the following means:

$$K_p = \frac{[P][M]}{[PM]} \qquad K_c = \frac{[C][M]}{[CM]} \qquad (3)$$

$$\frac{[PM]}{[P]_0} = f_{PM} = \frac{A_p^{obs}}{A_p^{max}} \qquad \frac{[CM]}{[C]_0} = f_{CM} = \frac{A_c^{obs}}{A_c^{max}} \qquad (4)$$

$$[P]_0 = [P] + [PM] \qquad [C]_0 = [C] + [CM]$$

where  $[P]_0$  and  $[C]_0$  are the total protein and EDTA concentrations,  $[P]$ ,  $[M]$  and  $[C]$  are the concentrations of free (apo) protein,  $Ca^{2+}$ , and EDTA respectively,  $[PM]$  and  $[CM]$  are the concentrations of the calcium-protein and calcium-EDTA complexes respectively,  $A_p^{obs}$  and  $A_p^{max}$  are the observed and maximum areas under the resonances of the protein,  $A_c^{obs}$  and  $A_c^{max}$  are the observed and maximum areas of the bound EDTA resonances, and  $f_{PM}$  and  $f_{CM}$  are the fractions of the PM and CM species respectively. By appropriate rearrangement of these relationships, one can arrive at the following equation

$$\left\{ \left[ \frac{A_c^{max}}{A_c^{obs}} \right] - 1 \right\} \left( \frac{K_p}{K_c} \right) = \left[ \frac{A_p^{max}}{A_p^{obs}} \right] - 1 \qquad (5)$$

so that a plot of  $\left[ \frac{A_c^{max}}{A_c^{obs}} \right] - 1$  versus  $\left[ \frac{A_p^{max}}{A_p^{obs}} \right] - 1$  should yield a slope of  $K_p/K_c$  and an intercept of zero.



The analysis of the resulting data according to equation 5 is shown in Figure VIII.4. It is readily apparent that the intercept is zero and, although there is some scatter in the points, there is reasonable agreement in the data. The resulting value for  $K_p/K_c$  was  $0.47 \pm 0.04$ . Using a published value of the  $K_a$  of EDTA for calcium, after appropriate modification for the pH used in this study (230)', the value of  $K_a$  determined for the ICaBP was  $9.4 \pm 0.8 \times 10^{-8}$  M which agrees fairly well with the values given in the literature (39,217,229).

In order to determine if the protein binds calcium cooperatively, it is necessary to analyze the data in a slightly different manner, by taking into account the interaction between the two  $Ca^{+2}$  binding sites of the protein. The inherent assumption in this analysis was that  $[PM] = C \times [PM_2]$ , such that the value of C would be 0 if the calcium ions bound in a 100% cooperative manner while a value of  $C > 0$  would indicate that the sites bound  $Ca^{+2}$  with a lesser degree of cooperativity. Derivation of the resulting equation using the parameters outlined above yields the following relationship.

$$\log \left\{ \frac{A_c^{max}}{A_c^{obs}} - 1 \right\} = 2x \log \left( \frac{k_p}{k_c} \right) + \log C + 2x \log \left\{ \frac{A_p^{max}}{A_p^{obs}} - 1 \right\} \quad (6)$$

-----  
 'In this modification we used the  $pK_a$  values cited for the association of EDTA with hydrogen, not deuterium.

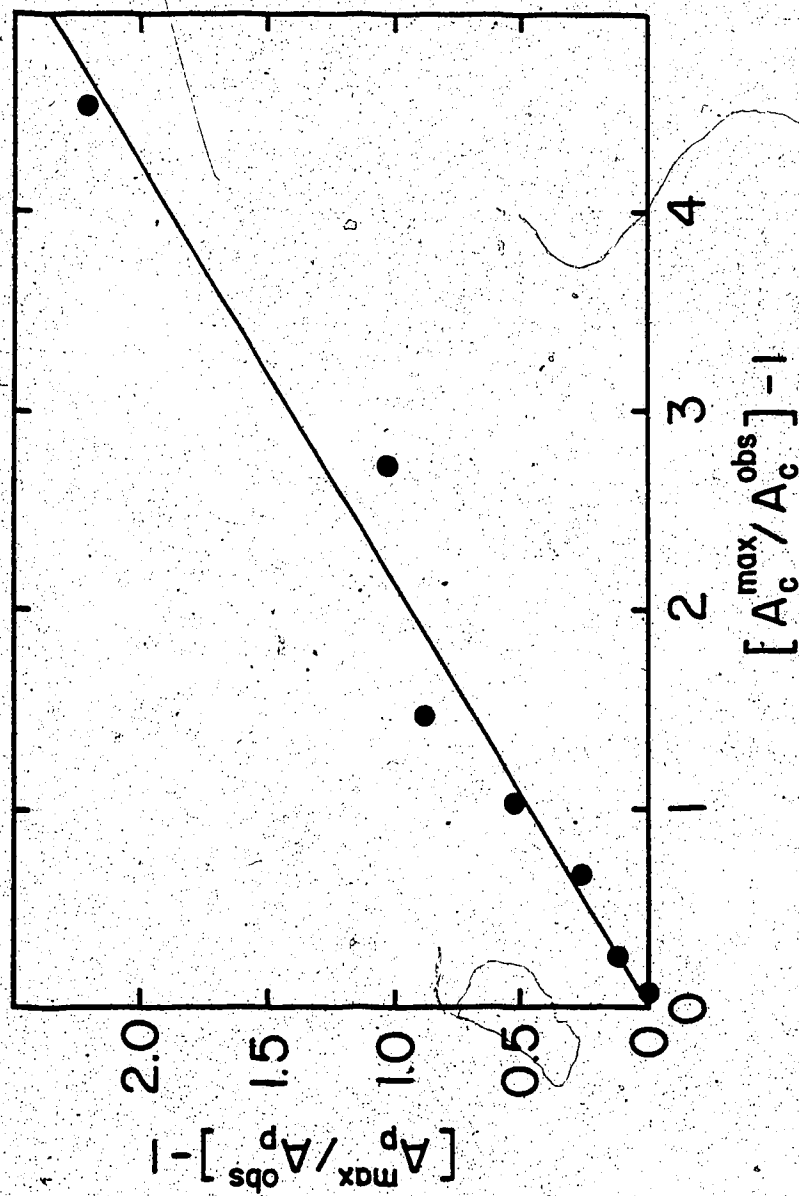


Figure VIII.4 The plot of  $[(A_c^{\max, \text{obs}} / A_c^{\text{obs}}) - 1]$  versus  $[(A_p^{\max, \text{obs}} / A_p^{\text{obs}}) - 1]$  for the data shown in Figure VIII.3

The plot of the  $\log [(A_p^{max}/A_p^{obs}) - 1]$  versus  $\log [(A_c^{max}/A_c^{obs}) - 1]$  should yield a slope of 2 and an intercept of  $2 \times \log (k_p/k_c)$ , where  $K_p = K_{d1} \times K_{d2}$ . The resulting plot is shown in Figure VIII.5.

For the data shown, the fit yielded a slope of 1 indicating by comparison with equation 5 that no cooperativity was present. The intercept of this plot was  $-0.31 \pm .03$ . This yields a  $k_p/k_c$  ratio of 0.49, which determines a value of  $k_p = 9.8 \pm 0.6 \times 10^{-4}$  M, which agrees with the results shown in Figure VIII.4, as expected.

The results of this study make use of a published parameter, the  $K_d$  value of EDTA for  $Ca^{+2}$ . No correction was made for the ionic strength of the medium, but the  $K_d$  value of this chelator has been shown to be only slightly affected by a change in the ionic strength over the range of 0.0 to 0.1 M (192). We did attempt to lower the concentration of EDTA to the micromolar range and to titrate it ourselves under the experimental conditions used in the above studies. Even at these low concentrations, however, the resulting plot was of the type shown in Figure VIII.1, and there was a great deal of trouble with contaminating metal ions. Though these attempts were unsuccessful, some valuable information was derived from them, and will be outlined below.

We initially tried to make up 6 to 10  $\mu$ M samples of EDTA for our titrations. In our first attempts to do so, it was readily apparent that there was a significant amount of

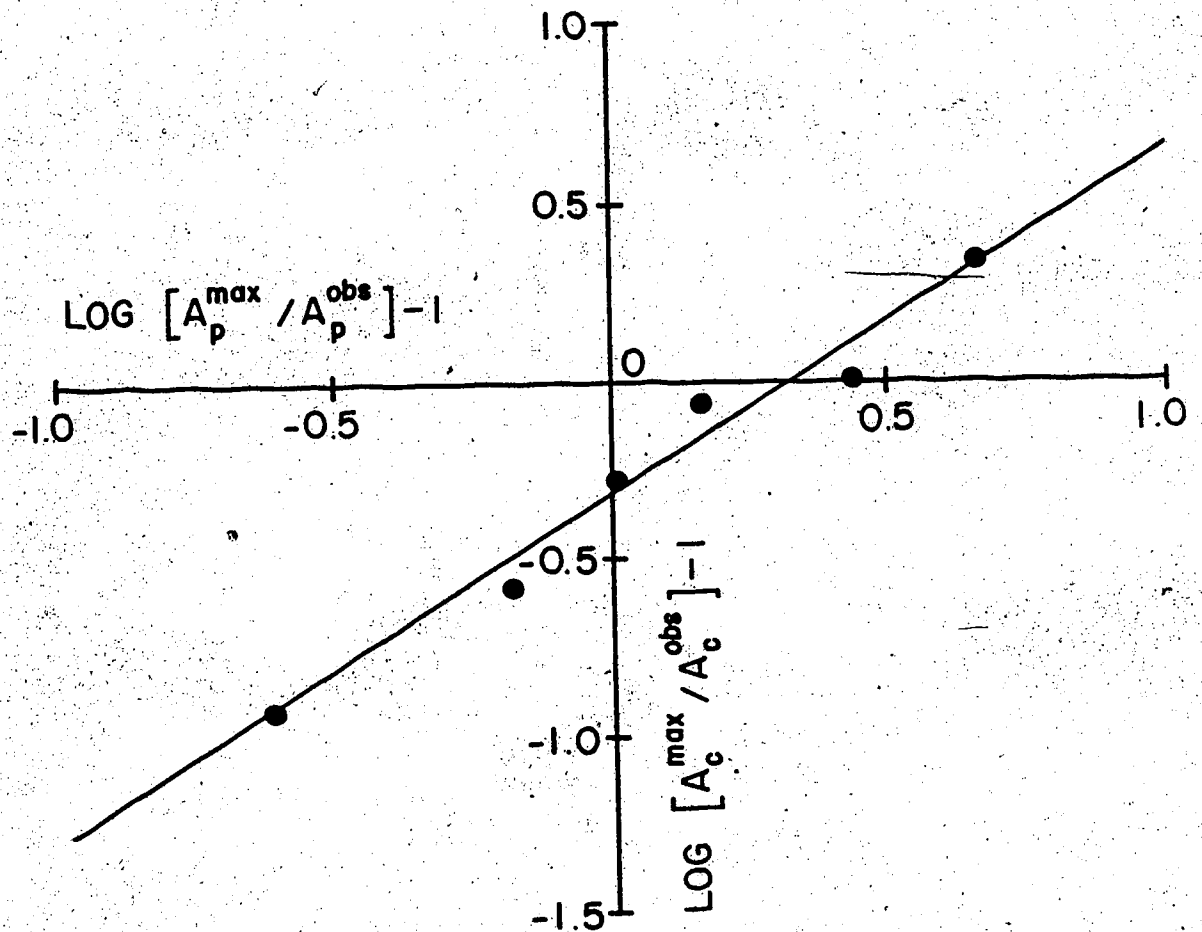


Figure VIII.5 The plot of  $\log [(A_c^{\text{max}}/A_c^{\text{obs}})-1]$  versus  $\log [(A_p^{\text{max}}/A_p^{\text{obs}})-1]$  for the data shown in Figure VIII.3.

metal ion contamination present in both  $D_2O$  and in the deuterated buffers, even after pretreatment with dithizone. Dithizone is an organic chelating agent which had been used extensively in our lab to remove metal ion from these solutions, primarily because it undergoes a colour change (green to pink) when chelated and so it is visually easy to tell when the metal ions have been extracted. The problem with dithizone is that it has a low affinity for many divalent and trivalent cations, notably  $Ca^{+2}$ ,  $Mg^{+2}$ , and the lanthanides (231), which in many studies on CaBP are the metals of primary interest. After treatment with dithizone, a NMR sample was made up to a final EDTA concentration of 6 to 50  $\mu M$  and the ratio of the areas under the free/bound (A + B/C + D) resonances were measured. A typical 360  $\mu l$   $^1H$  NMR sample of 49  $\mu M$  EDTA in  $D_2O$  was found to contain ca. 9  $\mu M$  contamination, while the same sample of deuterated imidazole-d<sub>4</sub> buffer contained 18  $\mu M$  contamination. We have no way of knowing what the contaminating metal ions were, but atomic absorption analysis of the  $D_2O$  samples showed that they contained 4  $\mu M$  calcium contamination. When the samples were stored for several days in plastic vials, this same type of analysis indicated that an additional 4  $\mu M$  contamination was present. It was this result which led us to store and collect further protein, buffer, and EDTA samples in plasticized glassware, rather than in plastic containers.

We attempted to use EDTA which was immobilized on either glass beads (CGA-EDTA, Pierce) or on agarose (supplied by

Dr. E. Birnbaum) to remove these contaminating metal ions, but these attempts were not completely successful. We finally arrived at a suitable procedure using chelex. Chelex also has a low affinity for  $\text{Ca}^{+2}$  and  $\text{Mg}^{+2}$  (232) and so it was used in excess. After several attempts, the method outlined in Chapter III was shown to use a minimal amount of chelex with virtually 100% efficiency. This technique worked very well for  $\text{D}_2\text{O}$ , as micromolar EDTA samples made up in both  $\text{D}_2\text{O}$  and deuterated buffer immediately after pretreatment with chelex showed virtually no metal ion contamination. This result also showed that the EDTA itself was not significantly contaminated, and additional studies at mM concentrations of EDTA indicated that there was < 1% contamination in this reagent. However, it was necessary to readjust the pH of the buffer after chelex treatment and this resulted in ca. 4  $\mu\text{M}$  metal ion contamination. It was likely that the NaOD or the DCl used to adjust the pH, or simple contact of the solution with the electrode were the sources of this contamination. Note that this level of contamination is not significant at mM ligand concentrations, only at  $\mu\text{M}$  ligand concentrations. Since we were not able to achieve essentially metal-free buffer solutions at the micromolar level, and the binding curves of titrations of EDTA at this concentration level were still not well defined, this precluded any attempts to titrate EDTA with  $\text{Ca}^{+2}$  at lower than micromolar concentrations.

### C. Discussion

The use of the procedures outlined above enabled us to obtain a dissociation constant for  $\text{Ca}^{+2}$  in the case of the porcine ICaBP when we titrated the protein in the presence of EDTA. This method allows for the determination of dissociation constants of proteins for metal ions at concentrations which are high enough to make the accumulation of  $^1\text{H}$  NMR spectra time efficient. In these studies we used a sample which was contaminated with EDTA (see Chapter I) and we estimated the EDTA concentration in this sample by comparing the areas of each resonance to those of several different standard EDTA solutions of known concentration. Although some error would arise from such a determination, the methods outlined above do not require any knowledge of the EDTA concentration, although it must be at a suitable level for this type of analysis. We were also able to demonstrate that the two  $\text{Ca}^{+2}$ -binding sites of ICaBP bind calcium independently, not cooperatively. We hope to repeat this work with other proteins such as parvalbumin and TnC, which are believed to bind  $\text{Ca}^{+2}$  cooperatively, and to determine the overall usefulness of this approach in studying the calcium-binding modes of other CaBP. The levels of contaminating metal ions found in  $\text{D}_2\text{O}$  and deuterated buffer has led us to use chelex, rather than dithizone, to remove traces of metal ions in all of our working solutions, and to avoid contact of the treated solutions with glass or plastic containers.

## IX. <sup>1</sup>H NUCLEAR MAGNETIC RESONANCE STUDIES OF THE INTERACTION OF LANTHANIDE IONS WITH PORCINE INTESTINAL CALCIUM BINDING PROTEIN

### A. Introduction

There have been several studies of the interaction of porcine ICaBP with lanthanide ions. Dorrington *et. al.* observed that  $Ca^{+2}$ , several other divalent cations, and several of the lanthanides all produced the same overall effect on the CD spectrum above 250 nm, in that they indicated there was no change in the overall conformation of the protein upon metal binding (39). These authors stated that the porcine protein displayed about the same affinity for calcium and the lanthanides, although no data was shown to this effect. Subsequent  $Tb^{+3}$  luminescence studies have shown that  $Tb^{+3}$  binds sequentially to two sites on the protein, with  $K_{d1} \leq 10^{-7}$  M and  $K_{d2} = 10^{-5}$  M (227). The first mole of  $Tb^{+3}$  fills the C-terminal site and the second mole fills the N-terminal site (regions IV and III respectively in Figure I.3). The binding of  $Tb^{+3}$  to the second site was found to be less effective as the salt concentration was raised. At  $Tb^{+3}$ /ICaBP ratios greater than one there is a significant quenching of the tyrosine fluorescence, suggesting that self-association of the protein was occurring.

The binding of several divalent cations and the lanthanides to the highly homologous bovine ICaBP has also been



studied (221). The addition of various ions to bovine ICaBP in the presence of calcium indicated that the displacement of bound calcium decreased with the divergence of the charge density (charge/ionic radius in Å) of the added cation from that of  $\text{Ca}^{+2}$ . Similar trends were shown for the protection of the protein against cleavage by trypsin as a function of added cations. For the lanthanide series in the presence of calcium,  $\text{La}^{+3}$  showed the largest degree of calcium displacement and protection against trypsin cleavage and  $\text{Yb}^{+3}$  displayed the smallest. In the absence of any bound calcium,  $\text{La}^{+3}$  was the only lanthanide ion which afforded any protection against trypsin cleavage. Similarly, recent work has shown that the differences in the affinities of the lanthanides and calcium for the two metal ions sites of parvalbumin are also proportional to the charge density ratio of these ions. These differences were shown to be the result of variation in the  $k_i^n$  and  $k_i^{off}$  rate constants across the lanthanide series (233). These results suggest that metal ions other than  $\text{Ca}^{+2}$  may have different effects on the local structure of the protein, as was observed in Chapter V for the DTNB LC of rabbit skeletal muscle.

Fluorescence studies on the bovine ICaBP have shown that  $\text{Tb}^{+3}$  binds to two sites on the apo protein with high affinity (226). The  $K_d$  values differed by at least a factor of 20, with both values being  $< 8.5 \times 10^{-5}$  M. In the presence of excess calcium ( $\text{Ca}^{+2}/\text{ICaBP} \geq 2$ ),  $\text{Tb}^{+3}$  was still able to bind to the protein (226). X-ray crystallographic

studies have shown that the addition of  $\text{Nd}^{3+}$  and  $\text{Tb}^{3+}$  to the calcium-saturated crystal resulted in the displacement of only the C-terminal calcium ion. These results indicate that the N-terminal site was not available to the solvent (8,226). These authors suggest that this latter site may be a structural site which remains saturated with calcium, while the C-terminal site is a regulatory site which binds or releases  $\text{Ca}^{2+}$  as the intracellular levels of calcium vary.

In the work outlined in this section, the addition of ytterbium to the calcium-saturated protein resulted in the appearance of lanthanide-shifted resonances in the  $^1\text{H}$  NMR spectra which were in the slow exchange limit. The lanthanide-shifted resonances were very broad, and it appeared that this broadening was the result of the close proximity of the lanthanide ion to residues on the protein. Titration of the calcium-saturated protein with  $\text{Yb}^{3+}$  suggested that significant structural changes occurred only when the first mole of the lanthanide was bound. Titration of the apo protein with  $\text{Lu}^{3+}$  showed that 2 equivalents of  $\text{Lu}^{3+}$  bound sequentially to the protein in the absence of  $\text{Ca}^{2+}$ , with the binding of the second mole of this lanthanide producing little effect on the conformation of porcine ICaBP. At a  $\text{Lu}^{3+}/\text{ICaBP}$  ratio greater than two, it was apparent that the protein began to aggregate as all of the resonances became significantly broadened and the solution became more viscous. From a ratio of 1 to 2, there was

evidence of only slight aggregation. The two dissociation constants of the apo protein for  $\text{Lu}^{3+}$  were determined to be  $K_{d1} = 4.9 \pm 6.7 \times 10^{-6} \text{ M}$  and  $K_{d2} = 2.3 \pm 1.2 \times 10^{-6} \text{ M}$ .

## B. Results

Figure IX.1 shows the two  $^1\text{H}$  NMR spectra of calcium-saturated porcine ICaBP in the presence of excess ytterbium. The lanthanide shifted resonances (LSR) which will be discussed in the following text are labelled a to z. The a,b resonance appeared to be a doublet under higher magnification and was analyzed as such. The c,d and x,y regions contain overlapping resonances, as will be outlined shortly. The lanthanide-induced shifts are large and the resonances are broad compared with those of carp muscle parvalbumin (97). This result was somewhat surprising in view of the fact that the correlation time  $\tau_R$  of ICaBP is slightly smaller than that of parvalbumin and, since the linewidths are proportional to  $\tau_R$ , one would expect the linewidths of the ICaBP to be either comparable to or smaller than those of parvalbumin. There were three most likely possibilities which could have lead to such broadening;

- 1) the close proximity of the protons to the lanthanide,
- 2) aggregation of the protein, and
- 3) chemical exchange broadening.

The first possibility was that the LIS observed for ICaBP were derived from protons on residues which were closer to

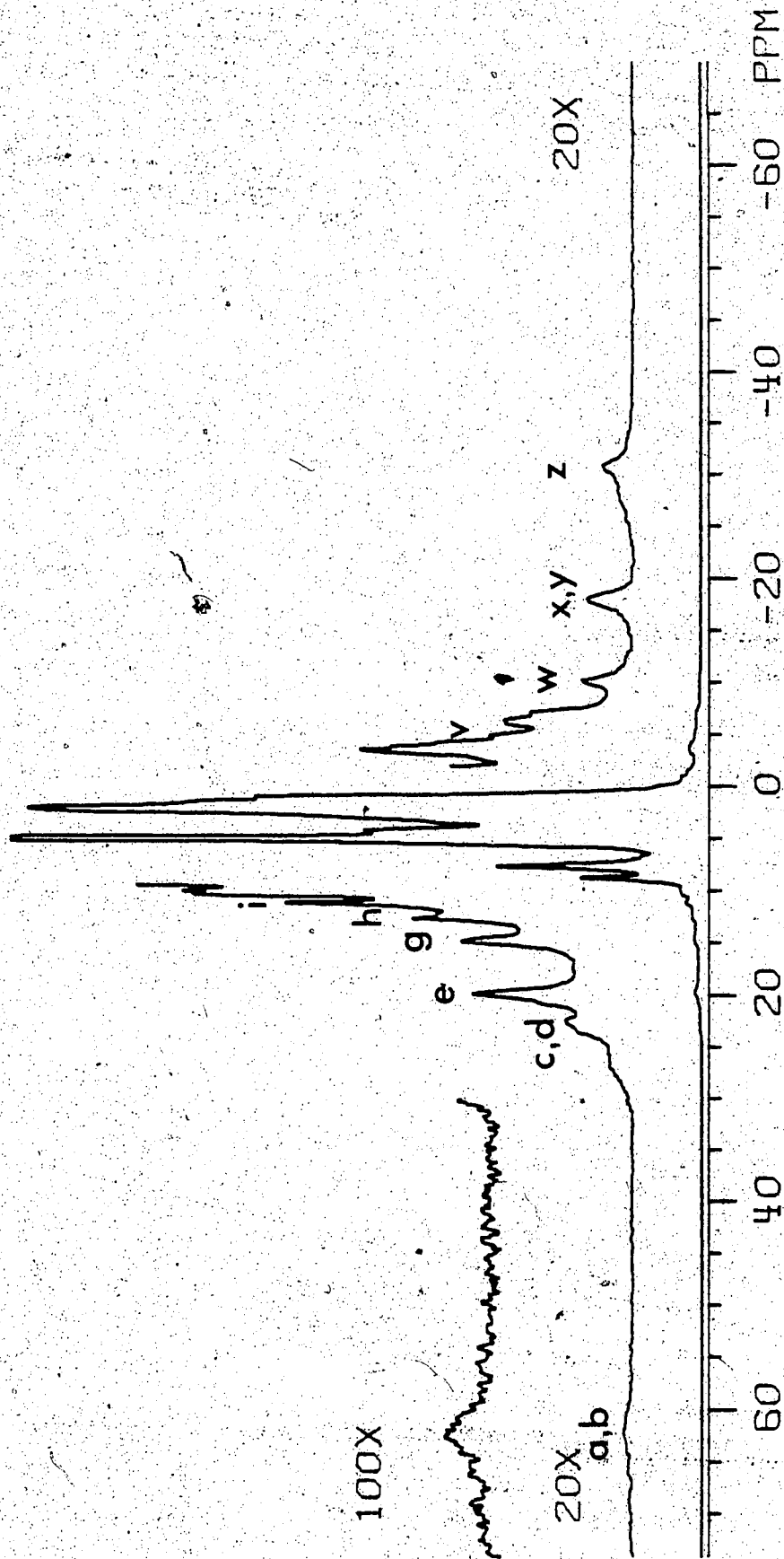


Figure IX.1 The complete 270 MHz  $^1\text{H}$  NMR spectrum of initially calcium-saturated porcine ICaBP in the presence of excess  $\text{Yb}^{3+}$ . The sample was 1.01 mM ICaBP, 30 mM imidazole-d<sub>3</sub>, 20 mM KCl, pH 6.5. The  $\text{Yb}^{3+}/\text{ICaBP}$  ratio was 2.04. The spectrum was taken at 299 K. The vertical expansions shown are 20x and 50x. The LSR which will be discussed in the following text are labelled a through z.

the metal ion than those of the LIS observed for parv-albumin, and thus were broadened much more due to a greater effect of the paramagnetic metal on their relaxation times. The resonances of protons which are in close proximity to a  $\text{Yb}^{3+}$  ion would experience broadening as well as well as lanthanide-induced shifts, and this broadening is related to the correlation time of the protein in the following manner (58,97):

$$\pi \Delta\nu_{\chi} = \frac{1}{T_{2\chi}} = \left( \frac{1}{5} \right) \frac{\omega_I^2 g_L^2 \beta^4 J^2 (J+1)^2}{r^6 (3kT)^2} \left[ 4\tau_R + \frac{3\tau_R}{1 + (\omega_I \tau_R)^2} \right] \quad (1)$$

where  $\Delta\nu_{\chi}$  is the linewidth of the resonance in Hz assuming the primary relaxation mechanism is susceptibility relaxation (97),  $\omega_I = (270)(2\pi \times 10^6)$  rad·sec<sup>-1</sup> is the resonant frequency,  $g_L = 8/7$  is the Lande  $g$  factor,  $\beta = 9.273 \times 10^{-21}$  erg·gauss<sup>-1</sup>, is the Bohr magneton,  $J = 7/2$  is the spin angular momentum number,  $k = 1.3805 \times 10^{-16}$  erg·°K<sup>-1</sup>, is the Boltzmann constant,  $T$  is the temperature in degrees Kelvin, and  $r$  is the distance in cm between the shifted proton the the lanthanide ion. From this relationship, one can calculate  $r$ . Before one can assume that the broadening resulted solely from proximity to the metal ion, however, the other two possible source of broadening must be probed.

The second possibility was that the protein was aggregated. Previous sedimentation equilibrium studies (234,235) had shown that aggregation does occur at high protein concentrations. In order to probe this system for the likelihood of aggregation, we chose to tackle this aspect by increasing the ionic strength of the solution via increasing the concentration of KCl, as shown in Figure IX.2. Both KCl and NaCl have been shown to exert minimal effects on the ability of bovine ICaBP to bind calcium over the range 0.01 to 0.2 M (221). The spectra indicated that there were only very small chemical shift changes in the LSR as the ionic strength increased. The resonances *c*, *e*, *g*, *h*, *y*, and *z* shifted upfield, while resonances *v* and *x* shifted downfield. The remaining labelled resonance *d*, *i*, and *w* were not affected. It was apparent that the single resonance *g* and the *c,d* and *x,y* resonance pairs separate into a doublet and into two separate resonances respectively upon increasing the KCl concentration. These slight shifts indicated that only very small structural variations occurred as the KCl concentration increased, and there was no general decrease in the linebroadening. It must be noted here that lanthanide-shifted resonances are very sensitive to even the slightest alterations in the structure of the protein; changes less than an Å in magnitude would perturb these shifts to a very large extent. These results implied that no aggregation of the protein had occurred, at least of the type which could be reversed at a high concentration of salt. The absence of

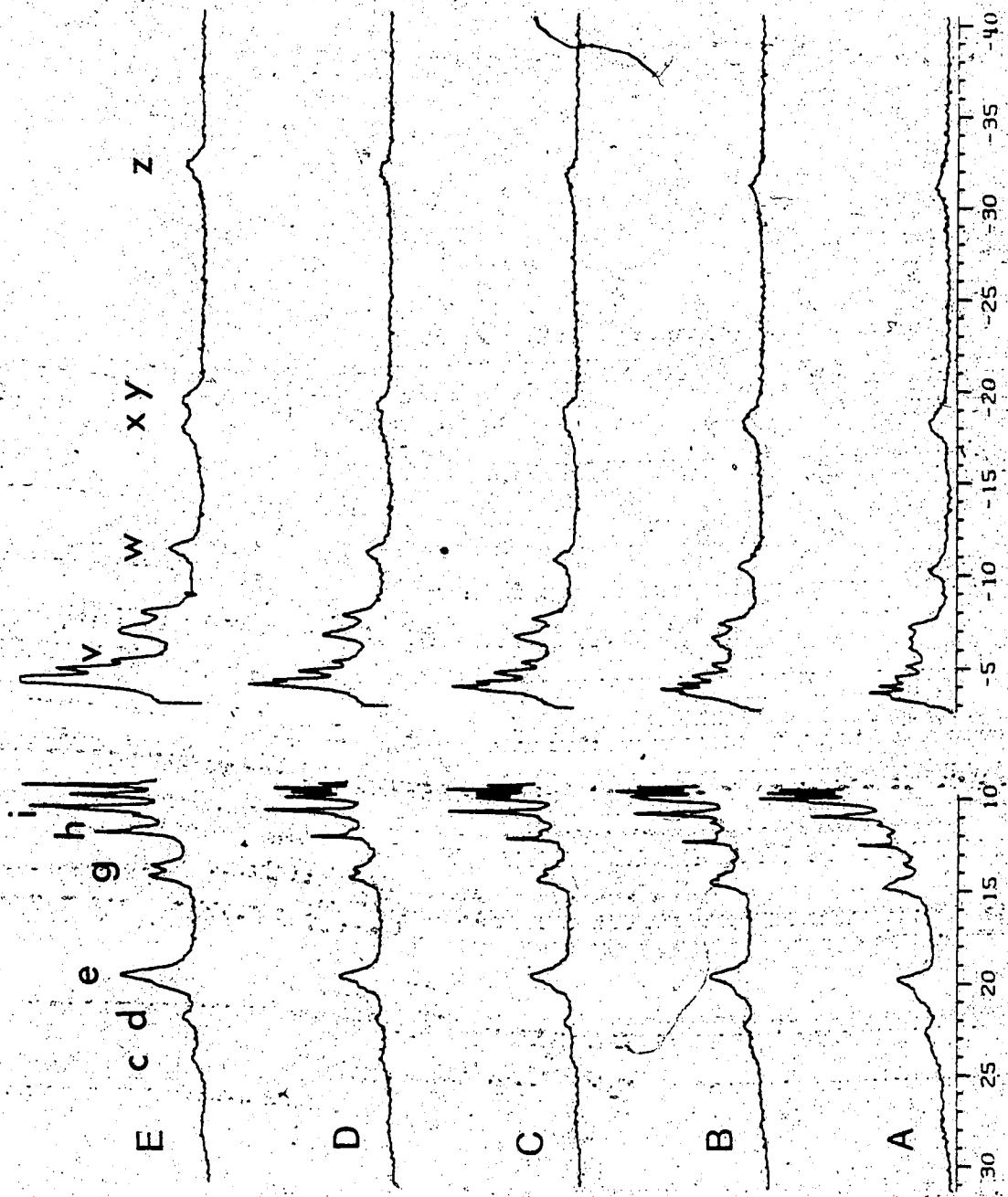


Figure IX.2 The titration of Yb<sup>3+</sup>-substituted ICaBP with KCl. The sample was 0.89 mM ICaBP in 30 mM imidazole-d<sub>6</sub>, 20 mM KCl, pH 6.5. The Yb<sup>3+</sup>/ICaBP ratio was 0.91 for A to D, and was 2:1 for E. The KCl concentrations were: A, 0.02 M; B, 0.1 M; C, 0.3 M; D and E, 0.5 M. The LSR are labelled as in Figure IX.1

such shifts indicates that the affinity of ICaBP for  $\text{Yb}^{+3}$  was not affected by the increase in ionic strength. Note that the addition of a second equivalent of  $\text{Yb}^{+3}$  at high salt concentration (Figure IX, 2E) did not appear to significantly affect the LLS, except that the c, d, g, x, and y resonances appeared to be more clearly resolved. By analogy with the  $\text{Tb}^{+3}$  binding studies on porcine ICaBP (227), this suggests that the high salt concentration hindered the binding of the second equivalent of  $\text{Yb}^{+3}$  to the protein. These results suggest that either the coordination of the lanthanide to the second binding site of the protein resulted in no further change in the overall structure of the protein or, more likely, that the presence of calcium (8,22) and/or KCl (227) prevented the coordination of the second equivalent of  $\text{Yb}^{+3}$ .

The third possibility was that the system was subject to chemical exchange broadening, whereby the process



is not in the slow exchange limit. This possibility seemed unlikely in view of the fact that ICaBP had previously been shown to bind calcium in the slow exchange limit, and one would expect ytterbium, which has an ionic radius similar to calcium and yet has a valency of +3, to bind more tightly to the protein and thus also bind in the slow exchange limit; this situation was previously observed with parvalbumin



(97). In addition, if chemical exchange broadening were present, one would expect all of the lanthanide-shifted resonances to be broadened to the same extent and it was apparent from the spectra (Figure IX.1) that they were not. To probe the possibility of chemical exchange broadening, spectra were acquired as a function of increasing temperature, as shown in Figure IX.3. Fortunately, as was the case with parvalbumin (98), this protein is stable at high temperatures (26,124). As one increases the temperature the exchange rate increases, as outlined in Chapter II. The rotational correlation time  $\tau_R$  also increases, as indicated by the Stokes-Einstein equation,

$$\tau_R = \frac{4\pi\eta r^3}{3kt} \quad (2)$$

where  $T$  is the temperature,  $k$  is the Boltzmann constant,  $\eta$  is the viscosity coefficient, and  $r$  is the radius of the protein. In the case of Yb<sup>3+</sup>-substituted porcine ICaBP, the increase in the temperature caused the lanthanide-shifted resonances to shift upfield towards the diamagnetic position, which indicated that we were initially in the slow exchange limit. The large shift of the resonances as a function of temperature is due either to averaging of the 4f electrons over the spin states of the metal ion, or to the motional averaging of residues in the protein. The c,d and x,y resonance pairs again were separated, as was observed in the case of increasing ionic strength (Figure IX.2). This increase in

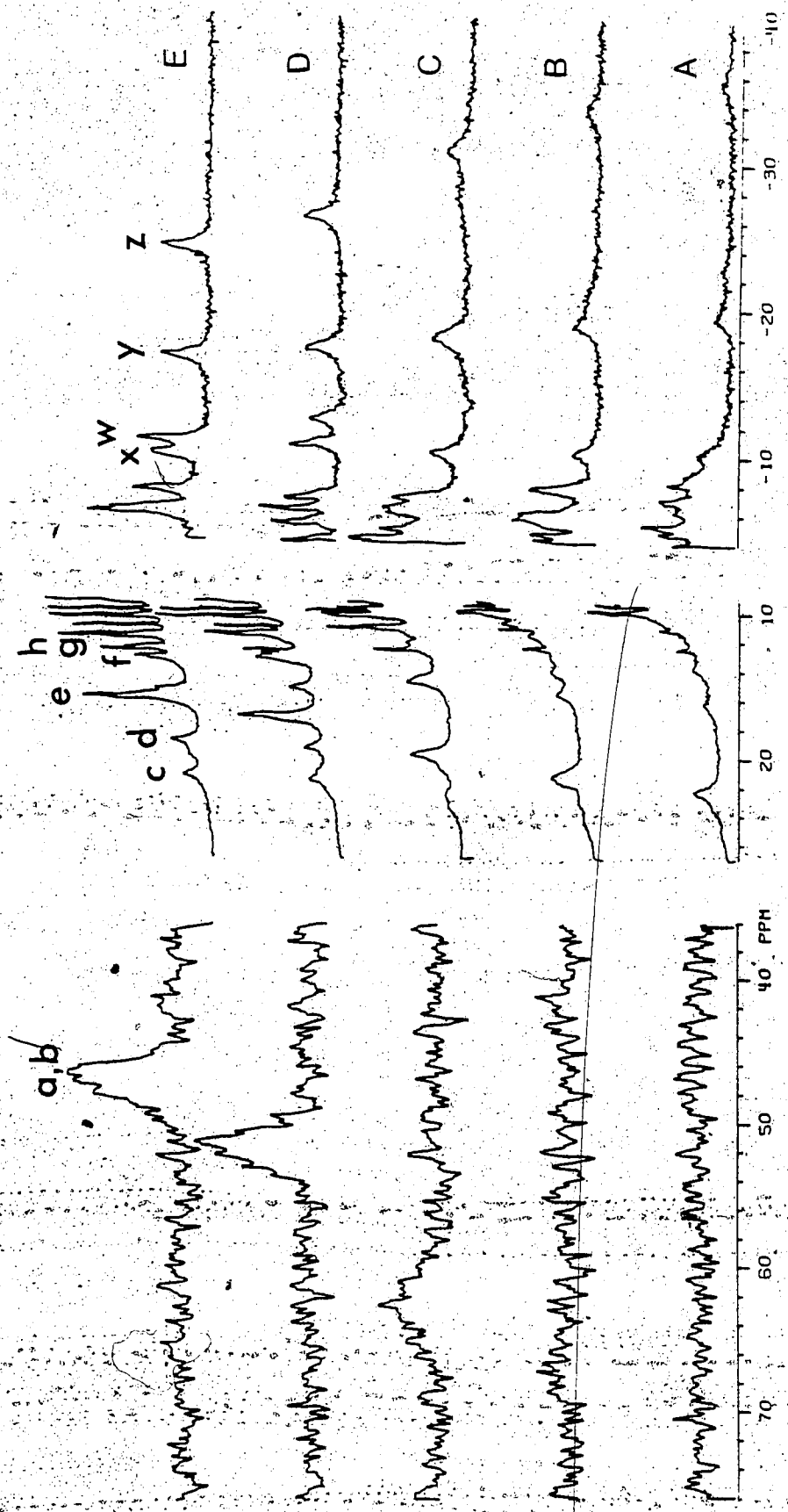


Figure IX.3. The effect of increasing temperature on the LIS of Yb<sup>3+</sup>-substituted ICaBP. The sample was 1.01 mM, in the same buffer as putlined in Figure VIII.2, and the Yb<sup>3+</sup>/ICaBP ratio was 2.04. The temperatures for each spectra, in degrees Kelvin, were: A, 277; B, 287; C, 299; D, 329; E, 329. These three sets of spectra were scaled to different values for clarity; the relative peak heights are shown in Figure IX.1.

temperature did not, however, result in further broadening of the lines, as outlined in Chapter II, but the resonances became much sharper. This was due to the decrease in the correlation time, as outlined in equation 2. It was apparent from these results that the lines were not broadened due to chemical exchange broadening. The temperature dependence of these shifts is shown in Figure IX.4 and in Table IX.1. One unusual result obtained from this data was that two of the resonances ( $h,w$ ) were essentially unaffected by increasing the temperature.

Since the second and third possible sources of line broadening appeared to be ruled out by the studies above, the line widths of the lanthanide-shifted resonances were analyzed according to equation 1 in order to obtain  $r$  values for the protons which give rise to these shifts. Table IX.2 shows the calculated values of the distances between some of the protons indicated in Figures IX.2B and IX.3C and the  $Yb^{3+}$  ion. These were identical samples except for the KCl concentration and these spectra displayed very similar line widths for the resonances indicated above. There were two assumptions made in this calculation. The first that the correlation time of ICaBP was  $10 \times 10^{-9}$  sec. This value was derived from the known correlation times of parvalbumin ( $12 \times 10^{-9}$  sec) (236,237) and actin ( $1.15 \times 10^{-9}$  sec) (238), and the knowledge that  $\tau_R$  is proportional to the size (molecular weight) of the protein, as outlined in equation 2. The second assumption was that the primary relaxation mechanism

Table IX.1

The Chemical Shift Values for the LSR of  $\text{Yb}^{3+}$ -substituted Porcine ICaBP as a Function of Temperature

T (°K)	chemical shift (ppm)						
	A	B	F	W	X	Y	Z
277	-*	-*	22.5	-10.2	-22.5	-19.6	-35.5
282	-	-	22.0	-10.1	-22.0	-19.2	-34.8
287	-	-	21.5	-10.2	-21.0	-19.0	-33.6
292	-	-	20.5	-10.1	-18.7	-18.7	-32.2
299	66.5	64.0	20.0	-10.0	-18.0	-18.0	-30.8
309	59.5	58.0	19.4	-10.2	-15.0	-17.5	-28.5
319	52.5	52.5	18.4	-10.2	-12.0	-17.0	-26.0
329	47.5	47.5	18.0	-10.2	-9.5	-16.0	-24.0

\* These resonances were not observed at the lower temperatures.

Table IX.2

The Observed Linewidths and Calculated Distances  
for the LSR of Yb<sup>3+</sup>-substituted Porcine rCaBP

LIS	linewidth (Hz)		r Å	
A	546 <sup>a</sup>	--- <sup>b</sup>	3.7 <sup>a</sup>	--- <sup>b</sup>
B	775	---	3.5	---
Z	375	356	4.0	4.0
X,Y	375	260	4.0	4.2
W	261	193	4.2	4.5

<sup>a</sup>Values derived from the spectra shown in Figure IX.3C; the KCl concentration was 20 mM.

<sup>b</sup>Values derived from the spectra shown in Figure IX.2B; the KCl concentration was 100 mM.

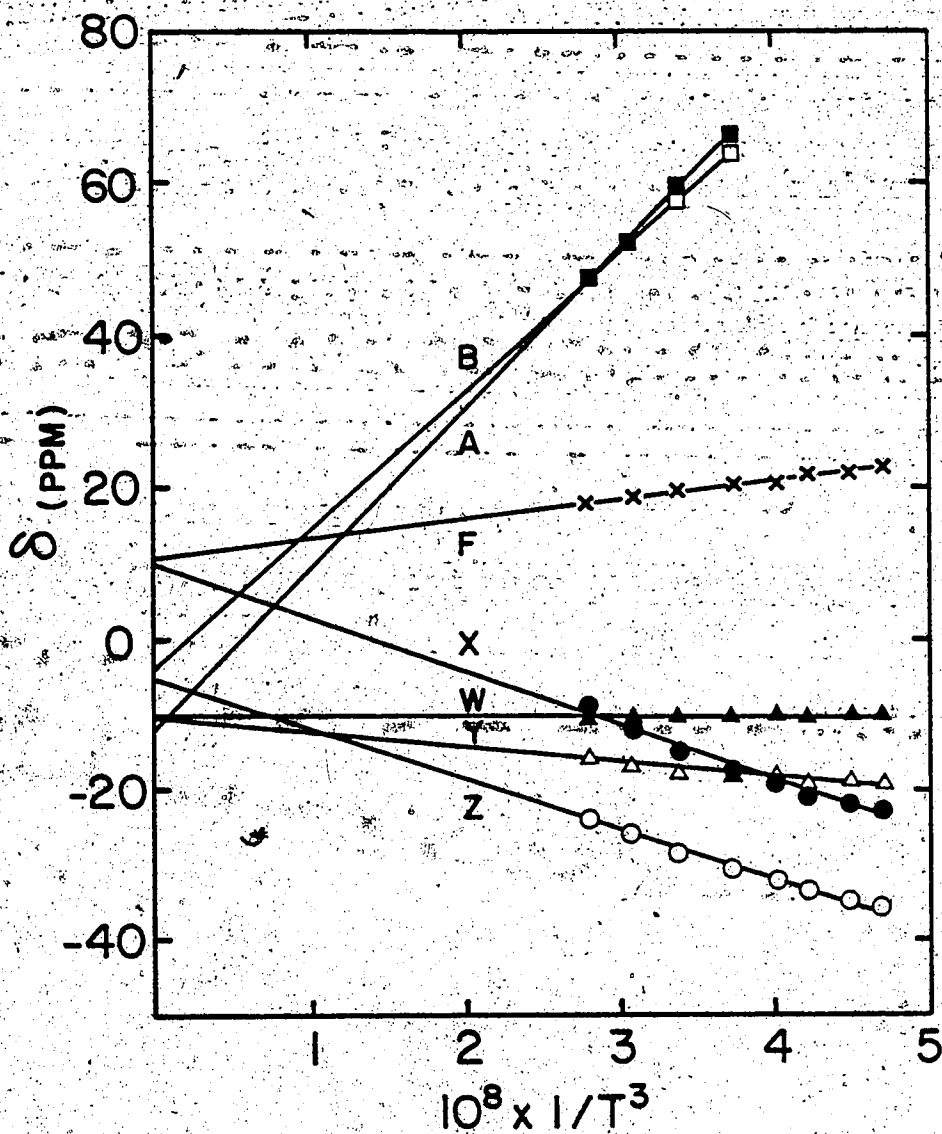


Figure IX.4 The plot of the chemical shifts of the LSR of  $\text{Yb}^{3+}$ -substituted porcine ICaBP as a function of  $1/T^3$ . The data was taken from the spectra shown in Figure IX.3.

was susceptibility relaxation, given that  $\tau_R > \tau_c$  (97), where  $\tau_c$  is the electron correlation time. The line widths were measured directly from the spectra, so that although the calculations above are rough, it appears from these results that these shifted protons were very close to the metal ion. This was further supported by other studies where  $Gd^{3+}$  was added to the apo form of porcine ICaBP. In this case the broadening resulting from the presence of this isotropic lanthanide was very severe, even at  $[Gd^{3+}]_0/[ICaBP]_0$  ratios much less than 1. In these studies also the lanthanide bound in the slow exchange limit.

Figure IX.5 shows a portion of the spectrum of ICaBP as a function of the concentration of  $Yb^{3+}$ . What we observe here is an increase in the intensity of the *e, g, h, i* and *j* resonances and of the *c, d* resonance pair as a function of increasing ytterbium concentration, with the *g* and *h* resonances becoming clearly resolved into doublets. These resonances could be saturated without any observable change in their chemical shift value, indicating again that we were in the slow exchange limit. The effects of proceeding from a  $Yb^{3+}/ICaBP$  ratio of 1.57 to 2.37 appeared to be negligible, again suggesting that the protein bound only one equivalent of ytterbium in the presence of excess calcium, since the binding of the second ytterbium ion had no significant effect on the resonances of the protein. A plot of the intensity of the 19.9 ppm resonance as a function of  $[Yb^{3+}]_0/[Ca^{2+}-ICaBP]_0$  is shown in Figure IX.6, and a

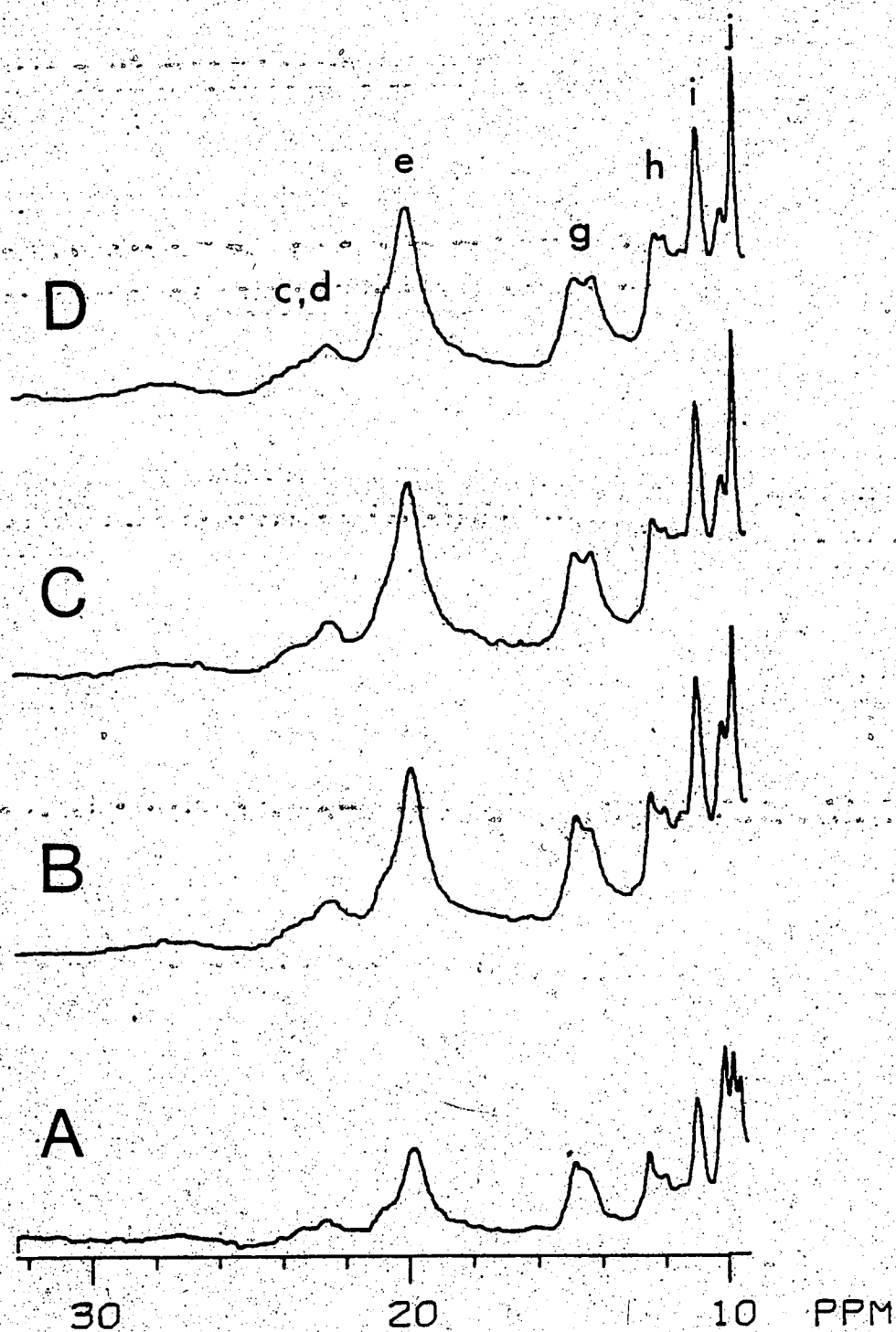


Figure IX.5 The titration of  $\text{Ca}^{2+}$ -saturated ICaBP with  $\text{Yb}^{3+}$ . The LIS in the range of 30 ppm to 10 ppm are shown. The  $\text{Yb}^{3+}/\text{ICaBP}$  ratios were: A, 0.79; B, 1.57; C, 2.37; and D, 3.15. The sample was 0.84 mM ICaBP, 30 mM imidazole- $d_4$ , 20 mM KCl, pH 6.5. The spectra represent 50,000 acquisitions.



computed value for the relative dissociation constant  $K_d\text{-Yb}^{3+}/K_d\text{-Ca}^{2+} = 0.18 \pm 0.31$  was determined. The inaccuracy in this value likely arises from the lack of points used in the determination, as well as the low  $K_d$  values involved.

The apo protein was also titrated with the diamagnetic lanthanide ion  $\text{Lu}^{3+}$ , as shown in Figure IX.7. The spectra indicate that  $\text{Lu}^{3+}$  binds to porcine ICaBP in the slow exchange limit. Up to a  $\text{Lu}^{3+}/\text{ICaBP}$  ratio of 1, the change in the spectrum of the apo protein was like that observed for  $\text{Ca}^{2+}$  (Figure VII.9). At  $\text{Lu}^{3+}/\text{ICaBP}$  ratios of  $\geq 1$  there was no further change in the spectrum, aside from a general broadening of all of the resonances, resulting in a net decrease in their intensity. This was apparent in both the aromatic region and the aliphatic region, as can be seen in the upfield-shifted methyl resonances. This broadening was very small from 1 to 2, but at larger ratios the entire spectrum began to broaden significantly, and the sample itself became quite viscous, although it remained clear. The decrease in the intensity of the phenylalanine envelope as a result of the broadening in these resonances can be most easily observed in Figure IX.8. These results agreed with those obtained from the KCl titration of  $\text{Yb}^{3+}$ -substituted ICaBP in that they indicate that no significant aggregation occurred when one equivalent of lanthanide ion is bound to the protein. A plot of the change in the area under the upfield-shifted phenylalanine resonance at 7.01 ppm as a function of  $[\text{Lu}^{3+}]_0/[\text{ICaBP}]_0$  yields the data shown in Figure IX.9.

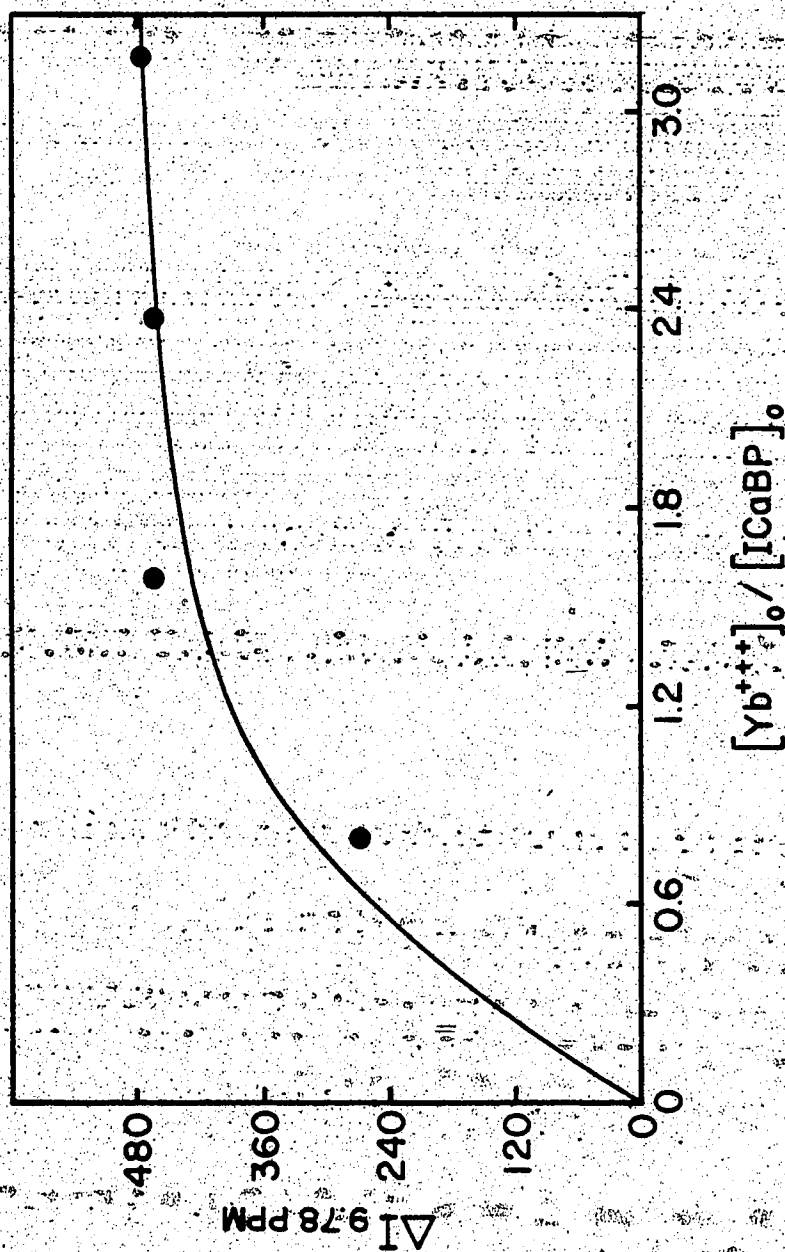


Figure IX.6 The plot of the change in intensity (in arbitrary units) of resonance  $\Delta I$  at 9.78 ppm versus  $[Yb^{3+}]_0/[CaBP]_0$  for the  $Yb^{3+}$  titration of  $Ca^{2+}$ -saturated porcine IcaBP. The data was taken from the spectra shown in Figure IX.5.

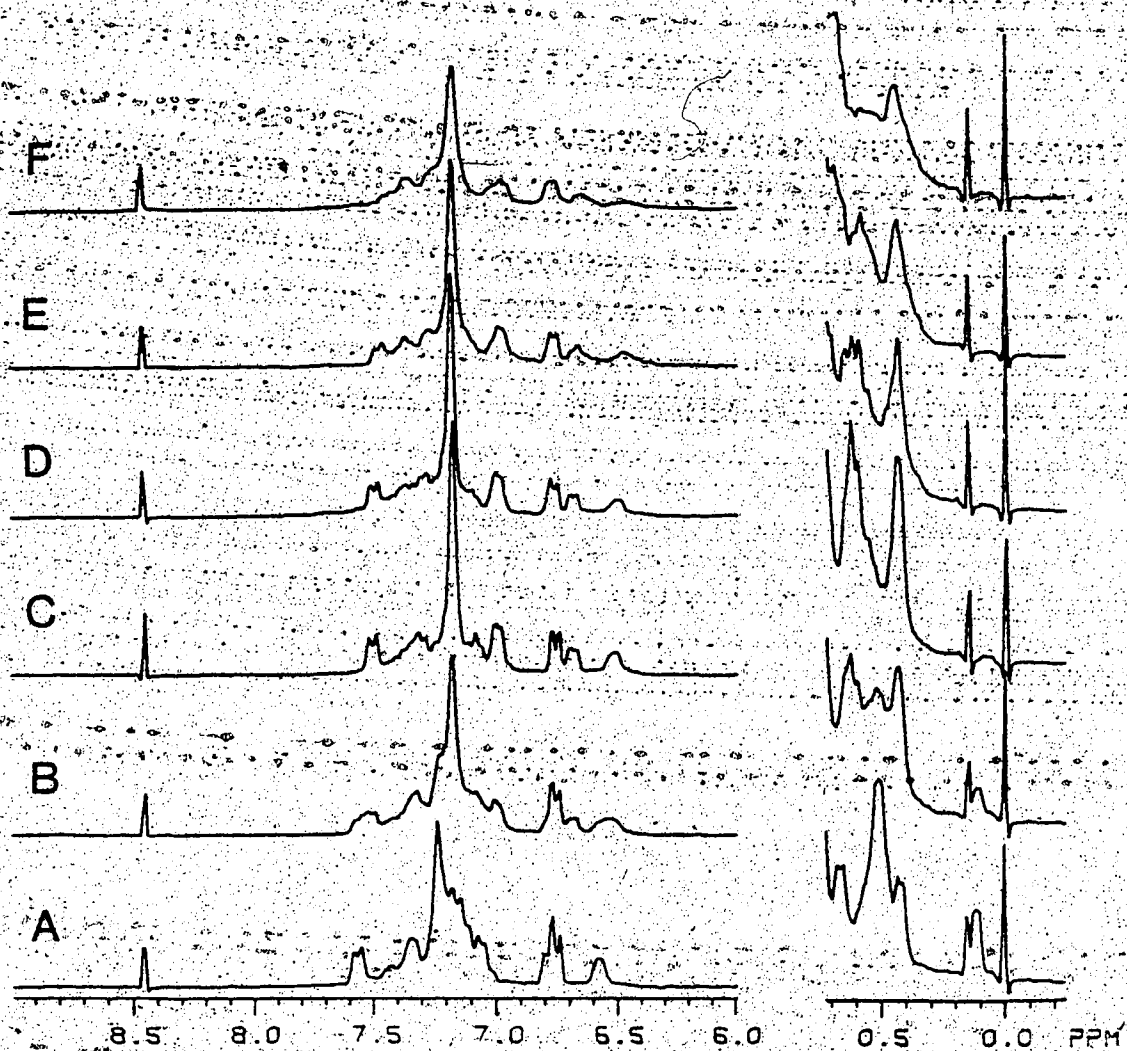


Figure IX.7 Titration of apo ICaBP with  $\text{Lu}^{3+}$ . The sample was 0.54 mM ICaBP, 15 mM Pipes, 20 mM KCl, pH 6.5. The  $[\text{Lu}^{3+}]_0/[\text{ICaBP}]_0$  values were: A, 0.00; B, 0.54; C, 0.98; D, 1.52; E, 1.98; F, 4.85. The spectra represent 8320 acquisitions and are resolution enhanced with a Lorentzian to Gaussian conversion.

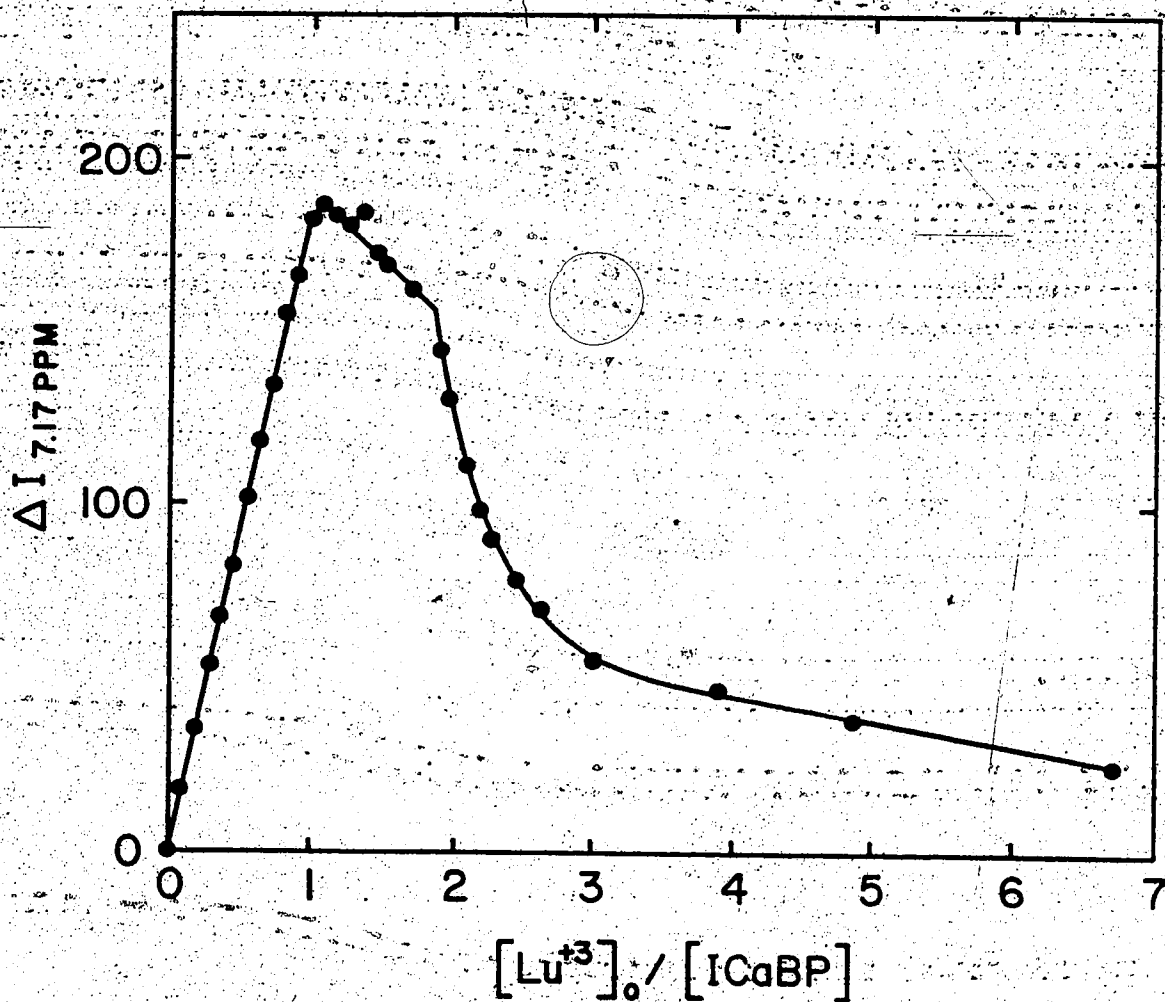


Figure IX.8 A plot of the intensity (in arbitrary units) of the 7.17 ppm resonance of phenylalanine as a function of  $[\text{Lu}^{3+}]_0 / [\text{CaBP}]_0$ . The data was taken from the spectra shown in Figure IX.7.

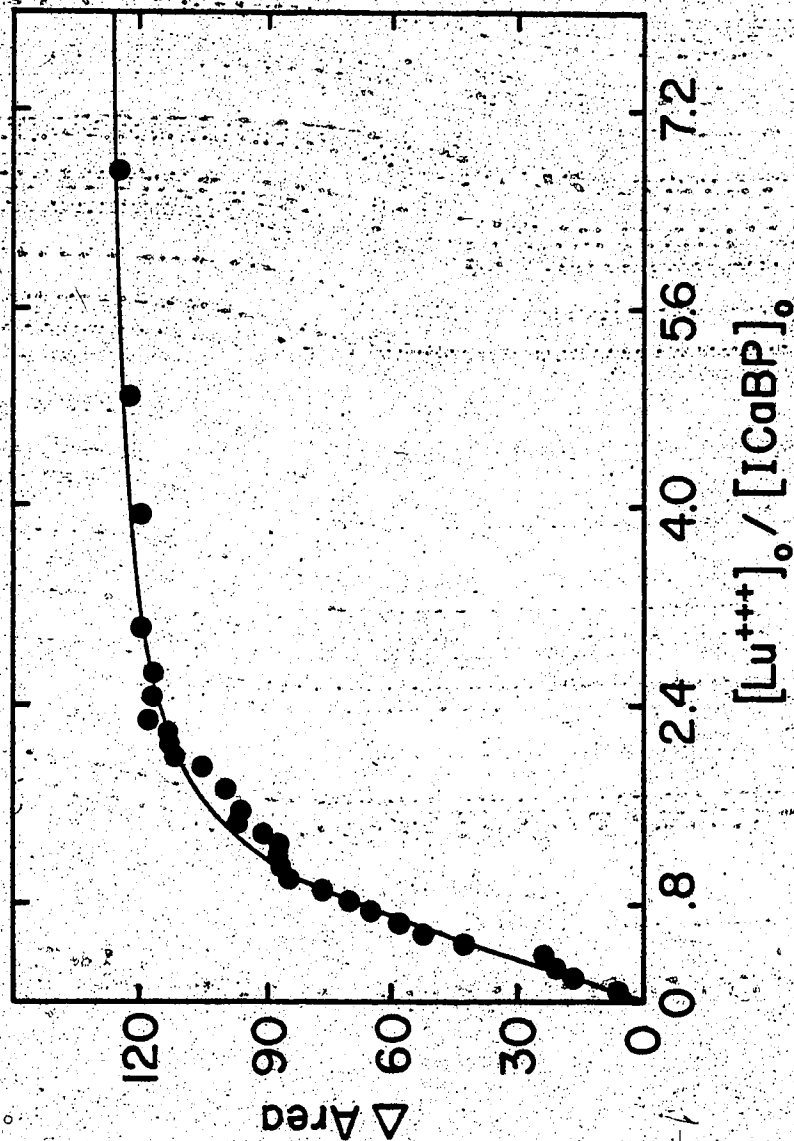


Figure IX.9 A plot of the change in area (in arbitrary units) of the 7.01 ppm resonance of phenylalanine as a function of  $[Lu^{+++}]_0/[ICaBP]_0$ . The resonance was integrated over the range of 7.04 to 6.93 ppm. The change in area was calculated as  $A_{max} - A_{obs}$  where  $A_{max}$  corresponded to the spectrum with a  $Lu^{+++}/ICaBP$  ratio of 1.34, which had the maximum observed intensity.

The fit of this data, assuming the apo protein binds two moles of lutetium per mole of protein and  $K_{d1} < K_{d2}$  is also shown. The resulting computed values were  $K_{d1} = 4.9 \pm 6.7 \times 10^{-6}$  M and  $K_{d2} = 2.3 \pm 1.2 \times 10^{-6}$  M. The value of  $K_{d2}$  agrees fairly well with the results of other studies (227), but it was apparent that  $K_{d1}$  was too small to be accurately determined by  $^1\text{H}$  NMR in this manner, as outlined in Chapter VIII.

### C. Discussion

Porcine ICaBP binds lanthanide ions, as displayed above for both  $\text{Yb}^{3+}$  and  $\text{Lu}^{3+}$ . The temperature studies on  $\text{Yb}^{3+}$ -substituted ICaBP studies verified that the binding of lanthanide ions is in the slow exchange limit.

The results of the addition of  $\text{Lu}^{3+}$  to the apo protein showed clearly that apo porcine ICaBP binds two moles of lanthanide. In addition, the first mole equivalent of  $\text{Lu}^{3+}$  affected the  $^1\text{H}$  NMR spectra in virtually the same manner as that observed for the addition of 2 equivalents of  $\text{Ca}^{2+}$ , indicating that the binding of metal ions by one site on the protein is responsible for the majority of the spectral changes observed. The similarity in these two effects also shows that these two ions bind to the protein in a similar manner. This situation differs sharply with the CD results shown for the binding of  $\text{Ca}^{2+}$  and  $\text{Yb}^{3+}$  to rabbit skeletal DTNB LC, as outlined in Chapter V. It was readily apparent that the binding of  $\text{Lu}^{3+}$  to ICaBP does not result in significant broadening of the spectra until the ratio of

lanthanide/ICaBP is greater than two. The overall broadening of the spectrum after this point is likely due to aggregation, as evidenced by the fact that the sample became fairly viscous after this point. In addition, it appeared that the binding of the second  $\text{Lu}^{3+}$  ion did not perturb the system further, but it did seem to stabilize it towards aggregation, likely by simply binding the excess lanthanide. It is interesting to note that several investigations have shown that, for the apo protein, the presence of greater than or ca. equal to stoichiometric levels of  $\text{Tb}^{3+}$  results in anomalous data and/or aggregation of both porcine ICaBP (227) and other CaBP's such as calmodulin (239) and parvalbumin (240). It is possible that aggregation is the source of the anomalous data, or it could be due to non-specific binding of excess lanthanide, as was observed for calcium in Chapter VII. The value of  $K_{d2}$  determined for the  $\text{Lu}^{3+}$  titration was larger than that of  $\text{Ca}^{2+}$  ( $k_p$ , Chapter VIII), while the value of  $K_{d1}$  appeared to be  $\leq k_p$ . These observations differ from the results reported for the apo bovine protein (39). Such a discrepancy would appear to be unlikely in view of the high sequence homology between these two proteins. Our values do, however, agree fairly well with the recently determined values for the binding of  $\text{Tb}^{3+}$  to porcine ICaBP (227).

The results of the addition of  $\text{Yb}^{3+}$  to the calcium-saturated protein indicated that the presence of a second mole equivalent of this lanthanide had no effect on the spectrum.

From the apo protein  $K_{d2}$  value determined for  $\text{Lu}^{3+}$ , it is likely that this second equivalent of lanthanide would not be able to bind to the protein in the presence of stoichiometric amounts of calcium, such that the lanthanide-shifted resonances which we studied were due solely to the replacement of the calcium at the first site. This conclusion is also supported by the studies where the second mole equivalent of  $\text{Yb}^{3+}$  added to the calcium-saturated protein at both high (0.5 M) (Figure IX.2) and low (20 mM) (Figure IX.3) concentrations of KCl had little effect on the spectra, particularly in light of the fact that an increase in the salt concentration has been shown to decrease the affinity of the second site for  $\text{Tb}^{3+}$  in the apo protein (227). In addition, there was no evidence of aggregation in the presence of excess  $\text{Yb}^{3+}$ , which was evident in the apo protein results when the  $[\text{Lu}^{3+}]_0/[\text{ICaBP}]_0$  was greater than 1. As outlined previously, the chemical shifts and line widths of LSR are extremely susceptible to changes in the environment, and aggregation would perturb these resonances to a much larger degree than would be observed in the case of a diamagnetic metal-protein complex. It appears that the presence of  $\text{Ca}^{2+}$  in the second site of the protein (and/or non-specifically bound  $\text{Ca}^{2+}$ ) stabilized the protein against aggregation. From the relative dissociation constants determined, it was apparent that  $\text{Yb}^{3+}$  has a higher affinity than  $\text{Ca}^{2+}$  for the first site.



The temperature dependence of the lanthanide-shifted resonances is peculiar, but not unique in that it has also been observed for parvalbumin (98). There has been considerable controversy over the form of the temperature dependence of lanthanide-induced dipolar shifts (98, and references therein) and they centre on which terms dominate the series

$$\delta_{obs} - \delta_D = \sum_n a_n/T^n \quad (3)$$

where  $\delta_{obs}$  is the observed chemical shift of the resonance in the presence of the lanthanide ion,  $\delta_D$  is the corresponding diamagnetic shift for that resonance, and  $a$  is a constant. Figure IX.4 plots the change in chemical shift of the LSR versus  $1/T^3$  since, for the majority of the resonances, similar plots versus  $1/T$  and  $1/T^2$  had intercepts which were outside of the diamagnetic frequency spectrum for the protein. However, due to the close proximity of the protein residues to the lanthanide ion in this study, we can not rule out the influence of contact components of the observed LSR, which could greatly influence their temperature dependence. Such a compensating factor could explain the lack of a temperature dependence of  $h$  and  $w$ .

It appears from the  $Yb^{3+}$  and  $Lu^{3+}$  titrations that there is no great conformational change when lanthanides bind to porcine ICaBP, but that several of the protons of the protein may be brought into very close proximity to the lanthanide ion when it binds, as indicated by the broadening of

the  $\text{Yb}^{3+}$ -shifted resonances. The results above have led us to conclude that the LIS were likely broadened more than those of parvalbumin because they were closer to the metal ion. By comparison of the  $\text{Yb}^{3+}$  and  $\text{Lu}^{3+}$  spectra, it appeared to be unlikely that the broadening of the resonances observed in the former case arose from aggregation as broadening in the apo protein spectrum was only apparent at  $[\text{Lu}^{3+}]_0/[\text{ICaBP}]_0$  ratios greater than 1, and it has been shown that only one equivalent of  $\text{Yb}^{3+}$  was bound to the calcium-saturated protein. In addition, increasing the KCl concentration had no significant effects upon the spectra of the LIS, indicating that the protein did not aggregate in the presence of excess  $\text{Yb}^{3+}$ .

The use of the LIS and line widths of the LSR in probing the structure of the protein will have to await further residue assignments and clarification of the present X-ray crystal structure.

## CONCLUDING DISCUSSION

The scope of the work outlined in this thesis is quite diverse and, since each section carries a fairly thorough discussion of the salient points for that particular system, there will be no further conclusions made here. Rather, I will attempt to compare some of the similarities and differences between these systems and outline several proposals for future work.

### A. Highlights of the Studies on CaBP and Peptides

The results of the lanthanide titrations of Ac-asp and Ac-DGD-amide highlight the fact that the magnitude of contact shifts may not always be assumed to be negligible for  $^1\text{H}$  NMR, so that one must be careful when analysing LIS in terms of structural aspects. This was particularly true for these studies as the peptides are small ligands and so most of the protons were very close to the paramagnetic metal ion centre in the lanthanide-peptide complexes. The peculiar temperature dependencies of the LSR of  $\text{Yb}^{3+}$ -substituted porcine ICaBP may reflect the presence of a sizeable contact shift contribution to these shifts, which we have shown to arise from protons which were in close proximity to the metal centre.

The peptide studies indicated that  $\text{Yb}^{3+}$  was the best calcium analogue for structural studies of calcium binding sites on the basis of the  $^1\text{H}$  NMR spectral characteristics of

the LIS. However, the CD work on the DTNB LC indicated that  $\text{Yb}^{3+}$  is not the best calcium analogue for this particular protein because it has a far different effect on the overall conformation of the protein than does  $\text{Ca}^{2+}$ . By comparison, the diamagnetic lanthanide  $\text{Lu}^{3+}$  had a very similar effect to calcium on the  $^1\text{H}$  NMR spectrum of porcine ICaBP. These two results indicate that it is advisable to study the effect of the diamagnetic lanthanides on the NMR spectra of CaBP and to use other methods in conjunction with NMR to assess the effects of the paramagnetic and diamagnetic lanthanides on the overall conformation of the protein being studied, in order to compare the effects of these analogues to those induced by calcium.

The studies on the S100b protein have pointed out that if the protein concentration is similar to the  $K_d$ , then an excess of calcium is needed to saturate the protein and stoichiometry can not be determined directly. In addition, one must be aware of the possibility of protein denaturation when a tyrosine ionizes at an unusually high  $\text{pK}_a$  value, and that abnormalities in the pH titration results of other protein residues such as his are indicative of more than a simple deprotonation of these residues.

The ICaBP results have indicated that an unusually high  $\text{pK}$  for a tyrosine does not necessarily mean that the residue is buried within the protein core. The  $\text{Lu}^{3+}$  and  $\text{Yb}^{3+}$  studies have shown that, although lanthanides can still bind

to ICaBP in the presence of  $\text{Ca}^{2+}$ , they will substitute for only one of the bound calcium ions in this protein. The  $\text{Lu}^{3+}$  studies have shown, as previously outlined, that it is essential to obtain diamagnetic lanthanide spectra on the protein of interest prior to analyzing any paramagnetic spectra, in order to compare the spectral changes with those induced by calcium. It is also important to obtain these spectra in order to observe any anomalous effects due to lanthanide coordination, such as aggregation. The aggregation observed for CaBP in the presence of lanthanides is reminiscent of the problems that we encountered when protein precipitation was evident upon the addition of  $\text{Yb}^{3+}$  to the S1 subfragment of rabbit skeletal myosin (Chapter I). The calcium titration of porcine ICaBP in the presence of EDTA has yielded information about the mode of calcium binding (*i.e.* non-cooperative) in this protein, which has been a very controversial subject for the calcium coordination of other CaBP.

#### B. Possible Future Studies

The binding of lanthanides by peptides could be expanded to include  $^{13}\text{C}$  NMR in order to obtain additional information on the magnitudes of the contact and dipolar shifts induced by the coordination of lanthanides by these peptides.

The DTNB light chain CD results could be further probed by using  $^1\text{H}$  NMR to monitor the titration of the protein with

the diamagnetic lanthanides  $\text{La}^{3+}$  and  $\text{Lu}^{3+}$  in order to compare the spectral changes observed by the addition of the two lanthanides which are at the extreme ends of the lanthanide series and to probe for the possibility of aggregation arising from the presence of one or both of these lanthanides. It would be beneficial to carry out these studies on fresh protein which has a normal  $K_d$  for calcium as well as a known phosphorylation state, and to do them in both the presence and absence of a sulfhydryl reducing agent such as  $\beta$ -mercaptoethanol or DTT.

With a protein like S100b, which responds to so many external stimuli, there is virtually an unlimited number of experiments which can be proposed to probe the nature of these responses. For example, the effect of KCl upon the binding of  $\text{Ca}^{2+}$  at pH our initial work in the absence of KCl, since  $\text{Ca}^{2+}$ ,  $\text{K}^+$ , and pH all modify the properties of the protein. It would be particularly interesting to look at the effect of hydrophobic probes such as TNS and/or ANS and drugs such as chlorpromazine on the conformation of this protein, as well as the effects of sulfhydryl reducing reagents on the response of the protein to metal ions and other stimuli. Along with the studies on purified S100b protein, there could be analogous  $^1\text{H}$  NMR studies on purified S100a, which have already been initiated. There is also the possibility of carrying out some similar studies on the S100a + S100b mixture, thus there is a great deal of work which needs to be done on both the isolated components of

this system and on the protein mixture before a general outline of the function of this protein could be proposed.

The porcine ICaBP will shortly be titrated with  $\text{Yb}^{3+}$  in both the presence and absence of  $\text{Ca}^{2+}$  in order to better define and clarify our present results, and with  $\text{Lu}^{3+}$  in the presence of  $\text{Ca}^{2+}$  to expand upon our apo protein titration results, particularly with regards to the effect of the presence of calcium upon lanthanide-induced aggregation. The sequential binding of lutetium to the two binding sites on the protein, as well as the replacement of only one calcium ion by the lanthanide  $\text{Yb}^{3+}$  could allow one to set up fairly simple conditions under which to look at the binding of other lanthanides, such as  $\text{Gd}^{3+}$ , specifically to either one of these sites. It would be of great interest to titrate this protein with  $^{113}\text{Cd}$  and/or  $^{45}\text{Ca}$  and to use the resulting NMR spectra of these nuclei to determine if the binding of diamagnetic metal ions by this protein is random or sequential. These results could then be compared to those observed for the sequential binding of the trivalent lanthanide  $\text{Lu}^{3+}$  in which it appeared that the binding of the second  $\text{Lu}^{3+}$  equivalent was spectroscopically "silent". Finally, it would be very instructive to carry out a calcium titration in the presence of EDTA on a CaBP which is believed to bind calcium in a cooperative manner, in order to establish if our technique is generally suitable for probing this aspect of metal ion binding by CaBP in general.

There is an abundance of experiments to be done and a wealth of information to be derived from the results of these experiments, which would further the knowledge that we presently hold for both the CaBP outlined in this thesis, and for CaBP in general.



## BIBLIOGRAPHY

1. R.H. Kretsinger, *Ann. Rev. Biochem.* 45 (1976) 239.
2. H. Rasmussen, D.B.P. Goodman, and A. Tenenhouse, *CRC Crit. Rev. Biochem.* 1, (1972) 95.
3. H. J. Vogel, T. Drakenberg, and S. Forsén, in *NMR of Newly Accessible Nuclei*, P. Laslo, ed., Academic Press, N. Y. (1984) *in press*.
4. B. W. Matthews, L. H. Weaver, and W. R. Kester *J. Biol. Chem.* 249 (1974) 8030.
5. P. C. Moews and R. H. Kretsinger *J. Mol. Biol.* 91 (1975) 201.
6. W. Bode and P. Schwager *FEBS Letters* 56 (1975) 139.
7. M. Verheij, J. J. Volwerk, E. H. J. M. Janse, W. C. Puyk, B. W. Dijkstra, J. Drenth, and G. H. de Haas *Biochemistry* 19 (1980) 743.
8. D. M. E. Szebenyi, S. K. Obendorf, and K. Moffatt *Nature* 294 (1981) 327.
9. J. Gariépy, *Ph.D. Thesis*, University of Alberta (1983).
10. C. J. Coffee, R. A. Bradshaw, and R. H. Kretsinger, in *Advances in Experimental Medical Biology*, M. Friedman, ed., Plenum Press, N. Y. 48 (1973) 211.
11. R. H. Kretsinger and C. E. Nockolds *J. Biol. Chem.* 248 (1973) 3313.

12. L. Lee, *Ph.D. Thesis*, University of Alberta (1980).
13. A.G. Weeds and A.D. McLachlan, *Nature* 252 (1974) 646.
14. T. Hofmann, M. Kawakami, A.J.W. Hitchman, J.E. Harrison, and K.J. Dorrington *Can. J. Biochem.* 57 (1979) 737.
15. T.C. Vanaman, F. Sharief, and D.M. Watterson, in *Calcium Binding Proteins and Calcium Function*, R. H. Wasserman, R. A. Corradino, E. Carafoli, R. H. Kretsinger, D. H. MacLennan, and F. L. Siegel, eds., Elsevier North Holland, Inc., N.Y. (1977) 107.
16. W. C. Barker and M. O. Dayhoff, *Comp. Biochem. Physiol.* 62B (1979) 1.
17. R. H. Kretsinger *CRC Crit. Rev. Biochem.* 8 (1980) 119.
18. J. H. Collins *Nature* 259 (1976) 699.
19. G. Henry, The University of Alberta, *personal communication*.
20. D. M. Watterson, F. Sharief, and T. C. Vanaman *J. Biol. Chem.* 255 (1980) 962.
21. T. Isobe and T. Okuyama *Eur. J. Biochem.* 89 (1978) 379.
22. R. M. Tufty and R. H. Kretsinger *Science* 187 (1975) 167.
23. M. Goodman, in *Calcium Binding Proteins: Structure and Function*, F. L. Siegel, E. Carafoli, R. H. Kretsinger, D. H. MacLennan, and R. H. Wasserman, eds., Elsevier North Holland Inc., N. Y. (1980) 347.

24. H. P. Vogt, W. Strassburger, A. Wollmer, J. Fleischhauer, B. Bullard, and D. Mercola *J. Theor. Biol.* 76 (1979) 297.
25. C. J. Coffee and C. Solano *Biochim. Biophys. Acta.* 453 (1976) 67.
26. J. G. Shelling, B. D. Sykes, J. D. J. O'Neil, and T. Hofmann, *Biochemistry* 22 (1983) 2649.
27. R. S. Mani, J. G. Shelling, B. D. Sykes, and C. M. Kay, *Biochemistry* 22 (1983) 1734.
28. M. T. Hincke, B. D. Sykes, and C. M. Kay, *Biochemistry* 20, (1981) 3286.
29. M. T. Hincke, B. D. Sykes, and C. M. Kay, *Biochemistry* 20, (1981) 4185.
30. B. A. Levine, D. Mercola, D. Coffman, and J. M. Thornton, *J. Mol. Biol.* 115 (1977) 743.
31. J. Krebs and E. Carafoli, *Eur. J. Biochem.* 124 (1982) 619.
32. K. B. Seamon, D. J. Hartshorne, and A. A. Bothner-By, *Biochemistry* 16 (1977) 4039.
33. K. Bose and A. A. Bothner-By, *Biochemistry* 22 (1983) 1342.
34. D. J. Nelson, A. D. Theoharides, A. C. Nieburgs, R. K. Murray, F. Gonzalez-Fernandez, and D. S. Brenner, *Internat. J. Quantum. Chem.* 16, (1979) 159.

35. J. Grandjean, P. Lazlo, and C. Gerday, *FEBS Letters* 81, (1977) 376.
36. T. Andersson, T. Drakenberg, S. Forsén, E. Thulin, and M. Sward, *J. Amer. Chem. Soc.* 104 (1982) 576.
37. J. D. Potter, J. D. Johnson, and F. Mandel *Fed. Proc. Fed. Am. Soc. Exp. Biol.* 37 (1978) 1608.
38. W. D. McCubbin and C. M. Kay *Acc. Chem. Rev.* 13 (1980) 185.
39. K. J. Dorrington, D. I. C. Kells, A. J. W. Hitchman, J. E. Harrison, and T. Hofmann *Can. J. Biochem.* 56 (1978) 492.
40. M. M. Werber, S. L. Gaffin, and A. Oplatka *J. Mechanochem. Cell Motility* 1 (1972) 91.
41. D. J. Wolff, P. G. Poirier, C. O. Brostrom, and M. A. Brostrom *J. Biol. Chem.* 252 (1977) 4108.
42. T. Drakenberg, B. Lindman, A. Cavé, and J. Parello, *FEBS Letters* 92 (1978) 346.
43. K. B. Seamon *Biochemistry* 19 (1980) 207.
44. T. C. Williams, The University of Alberta, *personal communication*.
45. M. N. Alexis and W. B. Gratzer *Biochemistry* 17 (1978) 2319.
46. H. Sternlicht and D. Wilson *Biochemistry* 6 (1967) 2881.
47. C. R. Bagshaw and J. Kendrick-Jones *J. Mol. Biol.* 130 (1979) 317.

48. R. Jakes, F. Northrop, and J. Kendrick-Jones *FEBS Letters* 70 (1976) 229.
49. A. G. Szent-Györgyi, E. M. Szentkiralyi, and J. Kendrick-Jones *J. Mol. Biol.* 74 (1973) 179.
50. R. Cooke, *Biochem. Biophys. Res. Comm.* 49 (1972) 1021.
51. C. R. Bagshaw *Biochemistry* 16 (1977) 59.
52. F. A. Cotton and G. Wilkinson, in *Advanced Inorganic Chemistry*, Interscience Publ., Chapter 24 (1962) 493.
53. C. P. Schlichter, in *Principles of Magnetic Resonance*, Springer-Verlag, N. Y., Chapter 4 (1978) 77.
54. M. Nelkon, in *Electricity*, Edward Arnold Ltd., London, Chapter 8 (1970) 188.
55. M. Nelkon, in *Electricity*, Edward Arnold Ltd., London, Chapter 11 (1970) 287.
56. F. A. Cotton and G. Wilkinson, in *Advanced Inorganic Chemistry*, Interscience Publ., Chapter 31 (1962) 870.
57. R. D. Shannon, *Acta Cryst.* A32 (1976) 751.
58. E. Nieboer, *Structure and Bonding*, 22 (1975) 1.
59. R. S. Kolat and J. E. Powell *Inorg. Chem.*, 1 (1962) 293.
60. S. A. Cotton and F. A. Hart, in *The Heavy Transition Elements*, Macmillan, London, Chapter 10 (1975) 188.
61. T. Moeller, in *MTP International Review of Science, Inorganic Chemistry, Series One*, H. J. Emeleus and K. W. Bagnall, eds., University Park Press, Baltimore, Md., 7 (1972) 275.

62. S. J. S. Wasson, D. E. Sands, and W. F. Wagner *Inorg. Chem.* 12 (1973) 187.
63. W. DeW. Horrocks, J. P. Sipe III, and J. R. Lubner *J. Amer. Chem. Soc.* 93 (1971) 5258.
64. D. J. Hewkin and R. H. Prince, *Coord. Chem. Rev.* 5 (1970) 45.
65. H. Diebler, M. Eigen, G. Ilgenfritz, G. Maab, and R. Winkler, *Pure Appl. Chem.* 20 (1969) 93.
66. E. R. Birnbaum and T. Moeller, *J. Amer. Chem. Soc.* 91 (1969) 7274.
67. D. W. Darnall and E. R. Birnbaum, *J. Biol. Chem.* 245 (1970) 6484.
68. G. E. Smolka, E. R. Birnbaum, and D. W. Darnall, *Biochemistry* 10 (1971) 4556.
69. J. Reuben, *Naturwissenschaften* 62 (1975) 172.
70. R. B. Martin and F. S. Richardson, *Quart. Rev. Biophys.* 12 (1979) 181.
71. M. V. R. Stainer and J. Takats, *J. Amer. Chem. Soc.* 105 (1983) 410.
72. D. J. Raber, G.H. Caines, M.D. Johnston Jr., and N. K. Raber, *J. Mag. Res.* 47 (1982) 38.
73. R. J. P. Williams, *Structure and Bonding* 50 (1982) 79.
74. R. A. Dwek, in *Nuclear Magnetic Resonance in Biochemistry*, Chapters 4 and 9, Clarendon Press, Oxford (1973) 62 and 174.

75. G. A. Elgavish and J. Reuben, *J. Mag. Res.* 42 (1981) 242.
76. L. Lee and B. D. Sykes, *Biophys. J.* 32 (1980) 193.
77. L. Lee and B. D. Sykes, in *Biochemical Structure Determination by NMR*, A. A. Bothner-By, J. D. Glickson, and B. D. Sykes, eds., Chapter 7, Marcel-Dekker Inc., N.Y. (1982) 16.
78. D. G. Agresti, R. E. Lenkinski, and J. D. Glickson, *Biochem. Biophys. Res. Comm.* 76 (1977) 771.
79. R. E. Lenkinski, D. G. Agresti, D. M. Chen, and J. D. Glickson, *Biochemistry* 17 (1978) 1463.
80. F. Abbott, J. E. Gomez, E. R. Birnbaum, and D. W. Darnall *Biochemistry* 14 (1975) 4935.
81. J. L. Dimicoli and J. Bieth *Biochemistry* 16 (1977) 5532.
82. T. D. Marinetti, G. H. Snyder, and B. D. Sykes *Biochemistry* 16 (1977) 647.
83. C. C. Hinckley *J. Amer. Chem. Soc.* 91 (1969) 5160.
84. C. D. Barry, A. C. T. North, J. A. Glasel, R. J. P. Williams, and A. V. Xavier *Nature* 232 (1971) 236.
85. C. F. G. C. Geraldes and R. J. P. Williams *Eur. J. Biochem.* 85 (1978) 463.
86. C. F. G. C. Geraldes *J. Mag. Res.* 36 (1979) 89.
87. C. F. G. C. Geraldes and R. J. P. Williams *Eur. J. Biochem.* 85 (1978) 471.

88. C. F. G. C. Geraldès and R. J. P. Williams *Eur. J. Biochem.* 97 (1979) 93.
89. P. Tanswell, J. M. Thornton, A. V. Korda, and R. J. P. Williams *Eur. J. Biochem.* 57 (1975) 135.
90. C. M. Dobson, C. F. G. C. Geraldès, G. Ratcliffe, and R. J. P. Williams *Eur. J. Biochem.* 88 (1978) 259.
91. R. A. Dwek, R. E. Richards, K. G. Morallee, E. Nieboer, R. J. P. Williams, and A. V. Xavier *Eur. J. Biochem.* 21 (1971) 204.
92. I. D. Campbell, C. M. Dobson, R. J. P. Williams, and A. V. Xavier *J. Mag. Res.* 11 (1973) 172.
93. I. D. Campbell, C. M. Dobson, R. J. P. Williams, and A. V. Xavier *Ann. N. Y. Acad. Sci.* 222 (1973) 163.
94. I. D. Campbell, C. M. Dobson, R. J. P. Williams *Proc. R. Soc. Lond. A.* 345 (1975) 23.
95. I. D. Campbell, C. M. Dobson, R. J. P. Williams *Proc. R. Soc. Lond. A.* 345 (1975) 41.
96. L. Lee and B. D. Sykes, *Adv. Inorg. Chem.* 2 (1980) 183.
97. L. Lee and B. D. Sykes, *Biochemistry* 19 (1980) 3208.
98. L. Lee and B. D. Sykes, *J. Mag. Res.* 41 (1980) 512.
99. L. Lee and B. D. Sykes, *Biochemistry* 20 (1981) 1156.
100. L. Lee and B. D. Sykes, *Biochemistry* 22 (1983) 4366.
101. T. D. Marinetti, *Ph.D. Thesis*, Harvard University, (1975).



102. T. D. Marinetti, G. H. Snyder, and B. D. Sykes *J. Amer. Chem. Soc.* 97 (1975) 6562.
103. T. D. Marinetti, G. H. Snyder, and B. D. Sykes *Biochemistry* 15 (1976) 4600.
104. A. D. Sherry and E. Pascual *J. Amer. Chem. Soc.* 99 (1977) 5871.
105. M. Singh, J. J. Reynolds, and A. D. Sherry *J. Amer. Chem. Soc.* 105 (1983) 4172.
106. J. G. Shelling, M. E. Bjornson, R. S. Hodges, A. K. Taneja, and B. D. Sykes *J. Mag. Res.* 57 (1984) 000.
107. B. A. Levine and R. J. P. Williams *Proc. R. Soc. Lond. A.* 345 (1975) 5.
108. C. C. Hinckley, M. R. Klotz, and F. Patil *J. Amer. Chem. Soc.* 93 (1971) 2417.
109. B. Bleaney, *J. Mag. Res.* 8 (1972) 91.
110. H. M. McConnell and R. E. Robertson, *J. Chem. Phys.*, 29 (1958) 1361.
111. R. J. Kurland and B. McGarvey *J. Mag. Res.* 2 (1970) 286.
112. R. M. Golding and M. P. Halton *Aust. J. Chem.* 25 (1972) 2577.
113. W. DeW. Horrocks, Jr., in *NMR of Paramagnetic Molecules*, G. N. La Mar, W. DeW. Horrocks, Jr., and R. H. Holm, eds., Academic Press, Chapter 4 (1973), 127.

114. C. P. Slichter, in *Principles of Magnetic Resonance*, Chapter 3 (1978) 56.
115. T. J. Swift, in *NMR of Paramagnetic Molecules*, G. N. LaMar, W. DeW. Horrocks, Jr., and R. H. Holm, eds., Academic Press, N. Y., Chapter 2 (1973) 53.
116. E. D. Becker, in *High Resolution NMR*, Academic Press, N. Y., Chapter 10 (1969) 214.
117. R. Kaptein, K. Dijkstr, and K. Nicola *Nature* 274 (1978) 293.
118. R. Kaptein, *Chem. Commun.* (1971) 732.
119. R.E. Reid, J. Gariépy, A. Saund, and R.S. Hodges, *J. Biol. Chem.* 256 (1981) 2742.
120. A. G. Weeds and B. S. Hartley, *Biochem. J.* 107 (1968) 531.
121. A. G. Weeds and S. Lowey, *J. Mol. Biol.* 61 (1971) 701.
122. S. Sarkar, F. A. Sreter, and J. Gergely, *Proc. Natl. Acad. Sci. USA* 68 (1971) 946.
123. R. S. Mani, B. E. Boyes, and C. M. Kay, *Biochemistry* 21 (1982) 2607.
124. A. J. W. Hitchman, M. K. Kerr, and J. E. Harrison, *Arch. Biochem. Biophys.* 155 (1973) 221.
125. J. D. J. O'Neil, K. J. Dorrington, D. I. C. Kells, and T. Hofmann *Biochem. J.* 207 (1982) 389.
126. D.A. Skoog and D.M. West, in *Analytical Chemistry*, Holt, Rinehart, and Winston, N.Y. (1965) 234.

127. G. H. Snyder, R. Rowan, S. Karplus, and B. D. Sykes, *Biochemistry* 14 (1975) 3765.
128. K. Weber and M. Osborn *J. Biol. Chem.* 244 (1969) 4406.
129. I. D. Campbell, *FEBS Letters* 57 (1975) 96.
130. M. Levitt *Biochemistry* 17 (1978) 4277.
131. P. Manavalan and P. K. Ponnuswamy *Nature* 265 (1978) 673.
132. J. T. Yang, G. C. Chen, and B. Jirgensons, in *CRC Handbook of Chemistry and Molecular Biology*, G. D. Fasman, ed., Third edition (1976) 3.
133. C. N. Reilley, B. W. Good and R. D. Allendoerfer, *Anal. Chem.* 48 (1976) 1446.
134. C. M. Dobson, R. J. P. Williams, and A. V. Xavier, *J. Chem. Soc., Dalton Trans.* (1973) 2662.
135. J. Reuben and G. A. Elgavish, *J. Mag. Res.* 39 (1980) 421.
136. W. DeW. Horrocks Jr. and J. P. Sipe III, *Science* 177 (1972) 994.
137. J. Reuben, *J. Mag. Res.* 11 (1973) 103.
138. B. C. Mayo *Chem. Soc. Rev.* 2 (1973) 49.
139. B. Bleaney, C. M. Dobson, B. A. Levine, R. B. Martin, R. J. P. Williams, and A. V. Xavier, *J. Chem. Soc., Chem. Commun.* (1972) 791.
140. A. D. Sherry, C. Yoshida, E. R. Birnbaum, and B. W. Darnall, *J. Amer. Chem. Soc.*, 95 (1973) 3011.

141. J. Legendziewicz, H. Kozlowski, and E. Burzala, *Inorg. Nucl. Chem. Lett.* 14 (1978) 409.
142. R. Prados, L. G. Stadtherr, H. Donato Jr., and R. B. Martin, *J. Inorg. Nucl. Chem.* 36 (1974) 689.
143. H. G. Brittain and F. S. Richardson, *Bioinorg. Chem.* 7 (1977) 233.
144. H. G. Brittain, *Inorg. Chem.* 18 (1979) 1740.
145. J. Legendziewicz, H. Kozlowski, B. Jezowska-Trzebiatowska, and E. Huskowska *Inorg. Nucl. Chem. Lett.* 15 (1979) 349.
146. F. Inagaki, S. Takahashi, M. Tasumi, and T. Miyazawa *Bull. Chem. Soc. Japan* 48 (1975) 853.
147. G. A. Elgavish and J. Reuben, *J. Amer. Chem. Soc.* 100 (1978) 3617.
148. G. A. Elgavish and J. Reuben, *J. Amer. Chem. Soc.* 98 (1976) 4755.
149. M. Cefola, A. S. Tompa, A. V. Celiano, and P. S. Gentile, *Inorg. Chem.* 1 (1962) 290.
150. M. Delepierre, C. M. Dobson, and S. L. Menear, *J. Chem. Soc. Dalton Trans.* (1981) 678.
151. H. E. Huxley *Science* 164 (1969) 1356.
152. F. D. Carlson and D. R. Wilkie, in *Muscle Physiology*, Prentice-Hall, Inc., N. J., Chapter 3 (1974) 52.
153. S. V. Perry *Biochem. Soc. Trans.* 7 (1982) 593.

154. R. S. Goody and K. C. Holmes *Biochim. Biophys. Acta.* 726 (1983) 13.
155. J. Gazith, S. Himmelfarb, and W. F. Harrington *J. Biol. Chem.* 245 (1970) 15.
156. A. Elliot and G. Offer *J. Mol. Biol.* 123 (1978) 505.
157. J. Squire, in *The Structural Basis of Muscular Contraction*, Plenum Press, N. Y. Chapters 10 and 11 (1981) 523 and 617.
158. C. R. Bagshaw, in *Muscle Contraction*, Chapman and Hall, N. Y., Chapter 2 (1982) 11.
159. L. Stryer, in *Biochemistry*, Second edition, W. H. Freeman and Co., San Francisco, Chapter 34 (1981) 815.
160. C. R. Bagshaw and G. H. Reed *J. Biol. Chem.* 251 (1976) 1975.
161. M. Bálint, F. A. Sréter, I. Wolf, B. Nagy, and J. Gergely *J. Biol. Chem.* 250 (1975) 6168.
162. R. W. Lymn and E. W. Taylor *Biochemistry* 10 (1971) 4617.
163. H. G. Mannherz, J. Barrington-Leigh, K. C. Holmes, and G. Rosenbaum *Nature* 241 (1973) 226.
164. W. Lehman, J. Kendrick-Jones, and A. G. Szent-Györgyi *Cold Spring Harbor Symp. Quant. Biol.* 37 (1972) 319.
165. J. Kendrick-Jones, E. M. Szentkiralyi, and A. G. Szent-Györgyi *J. Mol. Biol.* 104 (1976) 747.

166. K. Morimoto and W. F. Harrington *J. Mol. Biol.* 88 (1974) 693.
167. M. C. Beinfeld, D. A. Bryce, D. Kochavy, and A. Martonosi *J. Biol. Chem.* 250 (1975) 6282.
168. P. D. Wagner and E. Giniger *Nature* 292 (1981) 560.
169. M. Sivaramakrishnan and M. Burke *J. Biol. Chem.* 256 (1981) 2607.
170. M. Burke and M. Sivaramakrishnan *J. Biol. Chem.* 256 (1981) 8859.
171. A. G. Weeds and A. D. McLachlan *Nature* 252 (1974) 646.
172. S. L. Gaffin and A. Oplatka *J. Biochem.* 75 (1974) 277.
173. J. Kendrick-Jones *Nature* 249 (1974) 631.
174. S. Lowey and J. C. Holt *Cold Spring Harbor Symp. Quant. Biol.* 7 (1972) 19.
175. H. E. Huxley *Cold Spring Harbor Symp. Quant. Biol.* 37 (1972) 361.
176. C. R. Bagshaw and G. H. Reed *FEBS Letters* 81 (1977) 386.
177. A. G. Weeds *Nature* 223 (1969) 1362.
178. S. S. Margossian, S. Lowey, and B. Barshop *Nature* 258 (1975) 163.
179. E. Katayama and T. Wakabayashi *J. Biochem.* 90 (1980) 703.
180. E. N. A. Biró, R. Coelho, E. Ehrlich, F. Guillain, and C. Dvornic *Eur. J. Biochem.* 40 (1973) 527.

181. W. T. Perrie, L. B. Smillie, and S. V. Perry  
*Biochem. J.* 135 (1973) 151.
182. E. M. V. Pires and S. V. Perry *Biochem. J.* 167 (1977)  
137.
183. N. Frearson and S. V. Perry *Biochem. J.* 151 (1975) 99.
184. M. Morgan, S. V. Perry, and J. Ottaway *Biochem. J.* 157  
(1976) 687.
185. D. L. Pulliam, V. Sawyna, and R. J. C. Levine *Biochemi-  
stry* 22 (1983) 2324.
186. C. J. Ritz-Gold, R. Cooke, D. K. Blumenthal, and J. T.  
Stull *Biochem. Biophys. Res. Comm.* 93 (1980) 209.
187. S. L. Gaffin and S. Watanabe *J. Mechanochem. Cell Moti-  
lity* 1 (1972) 139.
188. C-S. C. Wu and J. T. Yang *Biochemistry* 15 (1976) 3007.
189. P. Y. Chou and G. D. Fasman *Biochemistry* 13 (1974) 222.
190. Y. Okamoto and K. Yagi *J. Biochem.* 80 (1976) 111.
191. D. C. Corson, T. C. Williams, and B. D. Sykes *Biochemi-  
stry* 22 (1983) 5882.
192. A. E. Martell and R. M. Smith, in *Critical Stability  
Constants*, Plenum Press, N. Y., 1 (1974) 204.
193. J. Gariépy, B. D. Sykes, and R. S. Hodges *Biochemistry*  
22 (1983) 1765.
194. P. D. Chantler *J. Biol. Chem.* 258 (1983) 4702.
195. K. Oikawa, W. D. McCubbin, and C. M. Kay *FEBS Letters*  
118 (1980) 137.

196. D. Cocchia *Cell Tissue Res.* 214 (1981) 529.
197. E. Bock *J. Neurochem.* 30 (1978) 7.
198. C. Zomzely-Neurath and A. Keller *Neurochem. Res.* 2 (1977) 353.
199. P. Calissano, and A. D. Bangham *Biochem. Biophys. Res. Comm.* 43 (1971) 504.
200. R. Donato *FEBS Letters* 162 (1983) 310.
201. T. Isobe, N. Ishoika, and T. Okuyama *Eur. J. Biochem.* 115 (1981) 469.
202. M. Walsh, F. C. Stevens, K. Oikawa, and C. M. Kay *Can. J. Biochem.* 57 (1979) 267.
203. A. C. Murray and C. M. Kay *Biochemistry* 11 (1972) 2622.
204. W. D. McCubbin, M. T. Hincke, and C. M. Kay *Can. J. Biochem.* 58 (1980) 683.
205. P. Calissano, S. Alemà, and P. Fasella, *Biochemistry* 13 (1974) 4553.
206. P. Calissano, S. Alemà, and P. Fasella, *Proc. 10th FEBS Meeting* (1975) 207.
207. R. D. Morero, and G. Weber *Biochim. Biophys. Acta.* 703 (1982) 231.
208. R. Donato *J. Neurochem.* 27 (1976) 439.
209. R. Donato *J. Neurochem.* 30 (1978) 1105.
210. S. P. Mahalik, L. Graf, and M. M. Rapport *J. Neurochem.* 27 (1976) 405.



211. R. Donato, in *Calcium-Binding Proteins 1983*, B. De Bernard, G. L. Sottocasa, G. Sandri, E. Carafoli, A. N. Taylor, T. C. Vanaman, and R. J. P. Williams, eds., Elsevier Publishers Inc., N. Y. (1983) 141.
212. R. S. Mani and C. M. Kay *FEBS Letters* 163 (1983) 282.
213. P. Calissano, B. W. Moore, and A. Friesen *Biochemistry* 8 (1969) 4318.
214. M. T. Hincke, W. D. McCubbin, and C. M. Kay *Can. J. Biochem.* 56 (1978) 384.
215. F. A. Kallfelz, A. N. Taylor, and R. H. Wasserman *Proc. Soc. Exp. Biol. Med.* 125 (1967) 54.
216. D. Drescher and H. F. Deluca *Biochemistry* 10 (1971) 2302.
217. A. J. W. Hitchman and J. E. Harrison, *J.E. Can. J. Biochem.* 50 (1972) 758.
218. R. H. Wasserman, C. S. Fullmer, and A. N. Taylor, in *Vitamin D*, D. E. M. Lawson, ed., Academic Press. N. Y., Chapter 4 (1978) 133.
219. R. H. Wasserman, in *Calcium-Binding Proteins: Structure and Function*, F. L. Siegel, E. Carafoli, R. H. Kretsinger, D. H. MacLennan, and R. H. Wasserman, eds., Elsevier North Holland, Inc. (1980) 357.
220. C. S. Fullmer and R. H. Wasserman *J. Biol. Chem.* 256 (1981) 5669.

221. C. S. Fullmer and R. H. Wasserman, in *Calcium-Binding Proteins and Calcium Function*, R. H. Wasserman, R. A. Corradino, E. Carafoli, R. H. Kretsinger, D. H. MacLennan, and F. L. Siegel, eds., Elsevier North Holland, Inc., N. Y. (1977) 303.
222. W. C. Barker, L. K. Ketcham, and M. O. Dayhoff, in *Calcium Binding Proteins and Calcium Function*, R. H. Wasserman, R. A. Corradino, E. Carafoli, R. H. Kretsinger, D. H. MacLennan, and F. L. Siegel, eds., Elsevier North Holland, Inc., N. Y. (1977) 73.
223. D. C. Dalgarno, B. A. Levine, R. J. P. Williams, C. S. Fullmer, and R. H. Wasserman *Eur. J. Biochem.* 137 (1983) 523.
224. B. A. Levine, R. J. P. Williams, C. S. Fullmer, and R. H. Wasserman, in *Calcium-Binding Proteins and Calcium Function*, R. H. Wasserman, R. A. Corradino, E. Carafoli, R. H. Kretsinger, D. H. MacLennan, and F. L. Siegel, eds., Elsevier North Holland, N. Y. (1977) 29.
225. G. H. Snyder, R. Rowan, and B. D. Sykes *Biochemistry* 15 (1976) 2275.
226. A. J. S. Jones, D. M. Szebenyi, and K. Moffat, in *Calcium-Binding Proteins: Structure and Function*, F. L. Siegel, E. Carafoli, R. H. Kretsinger, D. H. MacLennan, and R. H. Wasserman, eds., Elsevier North Holland, Inc., (1980) 413.

227. J. D. J. O'Neil, K. J. Dorrington, and T. Hofmann. *Can. J. Biochem.* (1983) *in press*.
228. J. D. J. O'Neil and T. Hofmann, The University of Toronto, *personal communication*.
229. K. Chiba, T. Ohyashiki, and T. Mohri *J. Biochem.* 93 (1983) 487.
230. W. J. O'Sullivan, in *Data for Biochemical Research*, R. M. C. Dawson, D. C. Elliot, W. H. Elliot, and K. M. Jones, eds., Second Edition, Oxford University Press, London (1969) 423.
231. E. B. Sandell, in *Chemical Analysis*, B. L. Clarke, P. J. Elving, and I. M. Kolthoff, eds., Interscience Publishers Inc., N. Y. III (1959) 137.
232. *Product Information Bulletin*, Bio-Rad Laboratories, #2020 (1976) 1.
233. T. C. Williams, D. C. Corson and B. D. Sykes in, *Calcium Binding Proteins 1983*, B. de Bernard, G. L. Scotocasa, G. Sandri, E. Carafoli, A. N. Taylor, T. C. Vanaman, and R. J. P. Williams, eds., Elsevier Science Publishers B. V., N. Y. (1983) 57.
234. K. J. Dorrington, A. Hui, and T. Hofmann *J. Biol. Chem.* 249 (1974) 199.
235. A. J. W. Hitchman, A. Hui, T. Hofmann, T. M. Murray, B. Arnold, K. J. Dorrington, M. K. Kerr, and J. E. Harrison, in *Calcium Binding Proteins*, W. Drabikowski, H. Strzelecka-Golaszewska, and E. Carafoli, eds, PWN-Polish Scientific Publishers, Warszawa (1974) 721.

236. D. R. Bauer, S. J. Opella, D. J. Nelson, and R. Pecora  
*J. Amer. Chem. Soc.* 97 (1975) 2580.
237. D. J. Nelson, S. J. Opella, and O. Jardetzky *Biochemi-*  
*stry* 15 (1976) 5552.
238. M. Brauer and B. D. Sykes *Biochemistry* 20 (1981) 6767.
239. R. W. Wallace, E. A. Tallant, M. E. Dockter, and W. Y.  
Cheung *J. Biol. Chem.* 257 (1982) 1845.
240. H. Donato Jr. and R. B. Martin *Biochemistry* 13 (1974)  
4575.
241. J. Gariépy and R. S. Hodges, *FEBS Letters* 160 (1983) 1.
242. J. Gariépy, B. D. Sykes, and R. S. Hodges, in  
*Calcium-Binding Proteins 1983*, B. De Bernard, G. L.  
Scottocasa, G. Sandri, E. Carafoli, A. N. Taylor, T. C.  
Vanaman, and R. J. P. Williams, eds., Elsevier Publish-  
ers Inc., N. Y. (1983) 141.
243. T. C. Farrar and E. D. Becker, in *Pulse and Fourier*  
*Transform NMR*, Academic Press, N. Y., Chapter 1 (1971)  
1.
244. J. Parello, P. Reimarsson, E. Thulin, and B. Lindman  
*FEBS Letters* 100 (1979) 153.